Localised excitations in long Josephson junctions with phase-shifts with time-varying drive

Amir Ali, M.Phil.

Thesis submitted to The University of Nottingham
for the degree of Doctor of Philosophy

August 2012

I dedicate this thesis to my wonderful family. Particularly to my understanding and patient wife, Safia, who has put up with these many years of research, and to our precious daughters Mona, Hina and Shifa, who are the joy of our lives. I also thank my loving mother for encouragement. This all becomes possible due to her moral support. Finally, I dedicate this work to my brothers, sisters and friends whom believed in diligence, science, art, and the pursuit of academic excellence.

Abstract

In this project, we consider a variety of ac-driven, inhomogeneous sine-Gordon equations describing an infinitely long Josephson junctions with phase shifts, driven by a microwave field. First, the case of a small driving amplitude and a driving frequency close to the natural (defect) frequency is considered. We construct a perturbative expansion for the breathing mode to obtain equations for the slow time evolution of the oscillation amplitude. We show that, in the absence of an ac-drive, a breathing mode oscillation decays with a rate of at least $\mathcal{O}(t^{-1/4})$ and $\mathcal{O}(t^{-1/2})$ for $\mathbf{0}-\pi-\mathbf{0}$ and $\mathbf{0}-\kappa$ junctions, respectively. Multiple scale expansions are used to determine whether, e.g., an external drive can excite the defect mode of a junction (a breathing mode), to switch the junction into a resistive state. Next, we extend the study to the case of large oscillation amplitude with a high frequency drive. Considering the external driving force to be rapidly oscillating, we apply an asymptotic procedure to derive an averaged nonlinear equation, which describes the slowly varying dynamics of the sine-Gordon field. We discuss the threshold distance of $\mathbf{0}-\pi-\mathbf{0}$ junctions and the critical bias current in $\mathbf{0}-\kappa$ junctions in the presence of ac drives. Then, we consider a spatially inhomogeneous sine-Gordon equation with two regions in which there is a π-phase shift, and a time periodic drive, modelling $\mathbf{0}-\pi-\mathbf{0}-\pi-\mathbf{0}$ long Josephson junctions. We discuss the interactions of symmetric and antisymmetric defect modes in long Josephson junctions. We show that the amplitude of the modes decay in time. In particular, exciting the two modes at the same time will increase the decay rate. The decay is due to the energy transfer from the discrete to the continuous spectrum. For a small drive amplitude, there is an energy balance between the energy input given by the external drive and the energy output due to radiative damping experience by the coupled mode. Finally, we consider spatially inhomogeneous coupled sine-Gordon equations with a time periodic drive, modelling stacked long Josephson junctions with a phase shift. We derive coupled amplitude equations considering weak coupling and strong coupling in the absence of ac-drive. Next, by considering the strong coupling with time periodic drive, we expect that the amplitude of oscillation tends to constant for long times.

Acknowledgements

First of all I would like to praise the almighty Allah, the most merciful, Gracious and Compassionate Lord who has gathered all knowledge in his essence and who is the creator of all knowledge for eternity. I bow my head with all submission and humility by way of gratitude to almighty Allah. I thank to Allah almighty for making my dream come true. The day that I dreamt of to acquire my PhD degree has finally come.

I would like to acknowledge many people for the contribution to my thesis. First, my adviser Dr. Hadi Susanto, whose encouragement, supervision and support from the preliminary to the concluding level enabled me to develop an understanding of the subject. I owe him my deepest gratitude for his continual help and advice about my thesis and more. Dr. Jonathan Wattis, my second adviser has been very helpful, and I thank him for his technical help, suggestion, guidance and advice. I feel proud and honor to be supervised by Dr. Hadi Susanto and Dr. Jonathan Wattis.

I would like to thank the University of Malakand Dir(L), Khyber Pukhtunkhwa, Pakistan and Higher education commission of Pakistan for providing me financial support for my PhD studies. I would also like to express my thanks to the School of Mathematical Sciences University of Nottingham for providing me support and computing facilities to produce and complete my thesis. I would like to offer my sincere gratitude and thanks to the internal examiner Dr. Stephen Cox University of Nottingham and the external examiner Dr. Gianne Derks University of Surrey for their useful comments. Finally, I would like to offer my great regards and blessings to my friends and family who supported me in any respect during the completion of the project.

Amir Ali,
Nottingham, United Kingdom, August 2012.

Contents

CHAPTER 1

Introduction

1.1 Superconductivity and the physics of Josephson junctions

In this section we discuss the basic properties of Josephson junctions. In order to understand Josephson junctions, it is important to consider the microscopic theory behind them. We first present a short review of superconductivity, its history and extra ordinary features. We then discuss Josephson effect and related terminology to Josephson junctions. We also derive the relations which describe the dynamics of the Josephson junctions.

1.1.1 Superconductivity

Superconductivity is one of the most exciting topics in solid state physics. Superconductivity arises due to the formation of Cooper pairs, which are spin zero bosons (subatomic particles), made of two spin $1/2$ electrons. Superconductivity is a phenomenon of exactly zero electrical resistance occurring in certain materials below a characteristic temperature. It was discovered by Dutch physicist Heike Kamerlingh-Onnes in 1911. In the course of investigation of the electrical resistance of different metals at liquid helium temperatures, Kamerlingh-Onnes observed that the resistance of a sample of mercury dropped from 0.08 Ω at above 4^oK to less than $3 \times 10^{-6}\,\Omega$ at about 3^oK and this drop occurs over a temperature interval of $0.010K$.

In 1933 German physicist Walter Meissner and Robert Ochsenfeld discovered a phenomenon now known as the Meissner effect, shown in Fig: 1.1, where lowering the temperature of an object below T_c in the presence of magnetic field, causes the magnetic field to be expelled from the object [1]. The occurrence of the Meissner effect indicates that superconductivity cannot be understood simply as the idealization of perfect conductivity in classical physics. It was a breakthrough for theories of superconductivity

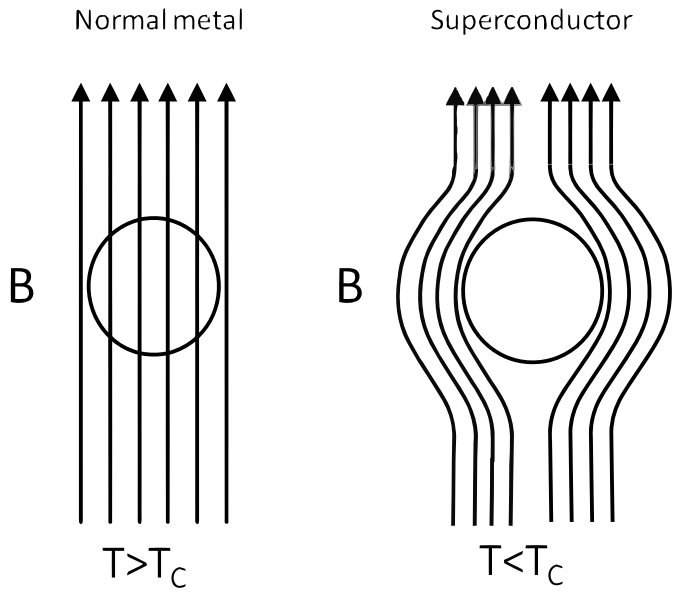

Figure 1.1: The Meissner effect. A superconductor in an external magnetic field is cooled below its superconducting transition temperature T_c, and the magnetic flux, B, is abruptly expelled.

because it allowed superconductivity to be treated thermodynamically and, it helped the development of the London equations.

In 1935 Fritz and Heinz London proposed a theory explaining that the Meissner effect was a consequence of minimization of electromagnetic free energy carried by superconducting current [2]. The London brothers derived the equations

$$\frac{\partial \mathbf{j}}{\partial t} = \frac{n_s e^2}{m}\mathbf{E}, \tag{1.1.1}$$

$$\nabla \times \mathbf{j} = -\frac{n_s e^2}{mc}\mathbf{B}. \tag{1.1.2}$$

Here **E** and **B** are respectively the electric and magnetic fields in the superconductors, e is the elementary charge of an electron, m is the mass of electron and n_s is the density of Cooper pairs. The **j** term in Equations (1.1.1) and (1.1.2) is the quantum mechanical current given by

$$\mathbf{j} = \frac{i\,q\,\hbar}{2\,m}\left(\varphi\nabla\varphi^* - \varphi^*\nabla\varphi\right) - \frac{q^2}{m\,c}\mathbf{A}.\varphi\varphi^*, \tag{1.1.3}$$

with $q = -2\,e$ and vector potential **A**. The total wave function $\varphi = \varphi(t)$ is described by

$$\varphi = \sqrt{n_s}.\exp(i\,\phi), \tag{1.1.4}$$

where ϕ is the phase of the wave function. Equation (1.1.1) describes perfect conductivity, since any electric field accelerates the superconducting electrons rather than sus-

taining their velocity against resistance as described by Ohm's law in a normal conductor. Equation (1.1.2) when combined with Maxwell's equation

$$\nabla \times \mathbf{B} \quad = \quad 4\pi \mathbf{j}/c, \tag{1.1.5}$$

gives

$$\nabla^2 \mathbf{B} = \frac{1}{\lambda_L^2}\mathbf{B}, \tag{1.1.6}$$

with $\lambda_L = \sqrt{mc^2/4\pi n_s e^2}$. This equation describes that the applied magnetic field decays exponentially inside the superconductors with the characteristic decay given by the London penetration depth λ_L.

In 1950, Landau and Ginzburg produced a mathematical theory to model superconductivity. This Ginzburg–Landau theory does not claim to explain the mechanism giving rise to superconductivity, instead it studies the microscopic properties of superconductors with the help of general thermodynamic arguments.

In 1957, the disappearance of electrical resistivity was modelled in terms of electron pairing in the crystal lattice by John Bardeen, Leon Cooper, and Robert Schrieffer in what is commonly called the BCS theory. According to this theory, pairs of electrons can behave very differently from single electrons which are fermions and must obey the Pauli exclusion principle. Pauli exclusion principle is the quantum mechanical principle which states that the total wave function for two identical fermions is antisymmetric with respect to exchange of the particles. Pairs of electrons act more like bosons which can condense into the same energy level. The electron pairs have a slightly lower energy and leave an energy gap above them, of the order of 0.001 eV, which inhibits the kind of collision interactions which lead to ordinary resistivity. For temperatures where the thermal energy is less than the band gap, the material exhibits zero resistivity. Bardeen, Cooper, and Schrieffer received the Nobel Prize in 1972 for the development of the BCS theory.

A new era in the study of superconductivity began in 1986 with the discovery of high critical temperature superconductors. Two IBM scientists Georg Bednorz and Alex Müller claimed that they had discovered a new class of ceramic superconductors in 1986. One of these compounds, containing yttrium, barium, copper and oxygen, became superconducting at the almost balmy 'critical' temperature (T_c), of 90K. In the ensuing frenzy of activity, more members of this layered cuprate superconductor family were identified, with T_c's ranging up to an amazing 133K. These discoveries opened the door to superconductors and devices cooled by much cheaper liquid nitrogen.

Superconductivity occurs in a wide variety of materials, including simple elements like tin and aluminium, various metallic alloys and some heavily-doped semiconductors.

The electrical resistivity of a metallic conductor decreases gradually as temperature is lowered. In ordinary conductors, such as copper or silver, this decrease is limited by impurities and other defects. Even near absolute zero, a real sample of a normal conductor shows some resistance. In a superconductor, the resistance drops rapidly to zero when the material is cooled below its critical temperature. An electric current flowing in a loop of superconducting wire can continue indefinitely with no power source. Superconducting magnets are some of the most powerful electromagnets made of superconducting coils. The idea of making superconducting magnets was proposed by Heike Kamerlingh-Onnes after he discovered superconductivity in 1911, but the first superconducting magnet was built by George Yntema in 1954 using niobium wire and achieved a field of $0.71T$ at $4.2K$. They are used in MRI (Magnetic Resonance Imaging) machines, mass spectrometers, etc. It can also be used for magnetic separation, where weakly magnetic particles are extracted from a background of less or non-magnetic particles, as in the pigment industries.
In past decades, superconductors were used to build experimental digital computers using cryotron switches. The cryotron works on the principle that magnetic fields destroy superconductivity. It consists of two superconducting wires (e.g. tantalum and niobium) with different critical temperatures (T_c). A straight wire of tantalum (having a lower T_c) is covered around with a wire of niobium in a single layer coil. The wires are electrically separated from each other. When this device is dipped in a liquid helium bath, both wires become superconducting and hence offer no resistance to the passage of electric current. In superconducting state, tantalum can carry a large amount of current (compared to its normal state). Now, when current is passed through the niobium coil (wrapped around tantalum) it produces a magnetic field, which in turn reduces the superconductivity of the tantalum wire and hence reduces the amount of the current that can flow through the tantalum wire. Hence one can control the amount of the current that can flow in the straight wire with the help of small current in the coiled wire. We can think of the tantalum straight wire as a "gate" and the coiled niobium as a "control".

More recently, superconductors have been used to make digital circuits based on rapid single flux quantum technology, radio frequency and microwave filters for mobile phone base stations. Superconductors are used to build Josephson junctions which are the building blocks of SQUIDs (superconducting quantum interference devices), the most sensitive magnetometers known. Other markets are arising where the relative efficiency, size and weight advantages of devices based on high-temperature superconductivity outweigh the additional costs involved. Promising future applications include high-performance smart grid, electric power transmission, transformers,

power storage devices, electric motors, magnetic levitation devices, fault current limiters, nanoscopic materials such as buckyballs, nanotubes, composite materials and superconducting magnetic refrigeration.

1.1.2 Josephson effect

The Josephson effect is one of the most important phenomena in superconductivity. It is a stimulating topic of research in both experimental and theoretical physics, and also a source of widely used practical applications. It is a quantum mechanical effect which predicts that the electron belonging to the metal has a small chance of being found of the material. If the two superconducting metals are almost brought together leaving just a small gap containing an insulator, the electrons can jump from one superconductor to the other. If a potential difference is applied, a current can flow from one metal to the other, even in the presence of an insulator as shown in the Fig: 1.2. This phenomenon is called the Josephson effect and the apparatus used is called a Josephson junction.
In 1962 British physicist Brian David Josephson explained the tunnelling processes through a weak link as the quantum mechanical tunnelling of Cooper pairs. He predicted the Josephson effect. Soon afterwards, systems where two superconducting electrodes are coupled via an insulator, were named Josephson junctions. The schematic diagram can be seen in Fig: 1.2. He also predicted the exact form of the current and voltage relations for the junction. Experimental work proved that he was right, and Josephson was awarded the 1973 Nobel Prize in Physics for his work. Since then, the Josephson effect that describes the flow of a supercurrent through a tunnel barrier, have been a subject of considerable research.

The flow of electrons along superconductors in the absence of an applied voltage, is called the Josephson current. The movement of electrons across the barrier is called Josephson tunnelling. Numerous ways of forming such weak links have been explored for both metallic low-temperature superconductors (LTS) and oxide high-temperature superconductors (HTS). In a Josephson junction, the nonsuperconducting barrier separating the two superconductors must be very thin. If the barrier is an insulator, it has to be on the order of 30Å thick or less. When the two superconductors are moved closer to about 30Å separation, quasiparticles can flow from one superconductor to the other by means of single electron tunnelling. When the separation is reduced to 10Å, Cooper pairs can flow from one superconductor to the other. In this case, phase correlation is realised between the two superconductors, and the whole Josephson junction behaves as a single superconductor. This phenomenon is often called weakly supercon-

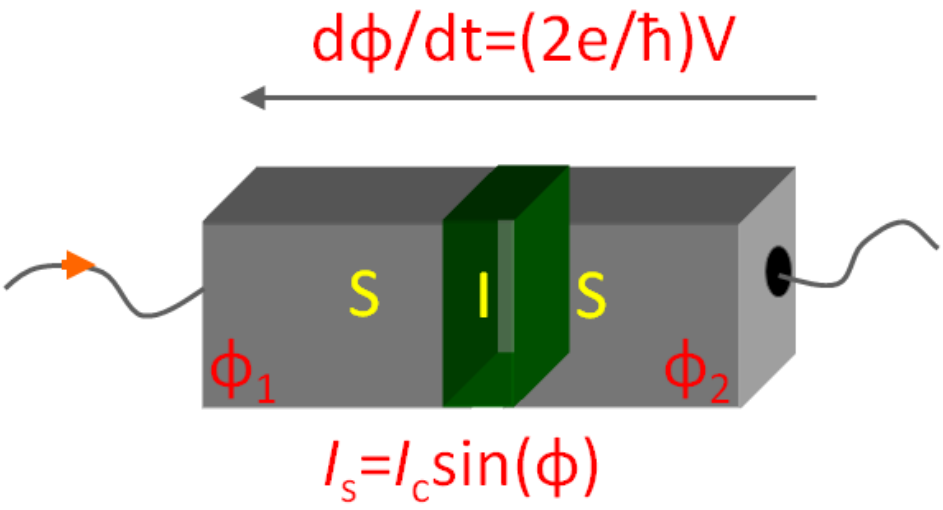

Figure 1.2: Josephson junction Model.

ducting, because of the smaller values of the critical parameter involved. If the barrier is another metal (nonsuperconducting), it can be as much as several microns thick. Josephson junctions can be formed in many ways, such as superconductor-normal metal-superconductor, thin film bridges, grain boundary junctions, point contact, etc.

The difference in phases of the quantum mechanical waves in the two superconductors of the Josephson junction is called the Josephson phase and is denoted by $\phi(x,t)$. If $\psi_1 = Ae^{i\theta_1}$ and $\psi_2 = Ae^{i\theta_2}$ represent the quantum mechanical waves, the Josephson phase ϕ is given by

$$\phi = \theta_2 - \theta_1 + \frac{2\pi}{\Phi_0}\int_1^2 \vec{A}.\vec{dl}, \tag{1.1.7}$$

where $\vec{A}$ is the vector potential, $\vec{dl}$ is the element of line integration from the first superconductor with phase θ_1 to the second superconductor with phase θ_2 in a Josephson junction. Due to the quantisation in superconductors

$$\Phi_0 = \hbar/2\,e \approx 2.07 \times 10^{-15}\,\text{Wb}, \tag{1.1.8}$$

is the magnetic flux quantum. The supercurrent that flows through a conventional Josephson junction (I_s) is given by

$$I_s = I_c \sin(\phi), \tag{1.1.9}$$

where $I_c > 0$ is the critical current, that is, the maximum current that can pass through the junction without dissipation. Until a critical current is reached, electron pairs can tunnel across the barrier without any resistance.

If a direct voltage is applied to the junction terminals, the current of the electron pairs crossing the junction oscillates at a frequency which depends on the applied voltage

V and fundamental constants, that is, the electron charge e and the Planck constant $\hbar$. Conversely, if an AC voltage of frequency is applied to the junction terminals by microwave irradiation, the current of Cooper pairs tends to synchronize with this frequency (and its harmonics) and a direct voltage appears at the junction terminals. Mathematically we write

$$I = I_c \sin\left(\phi + \frac{2eV}{\hbar}t\right),$$

describing an AC-current with frequency

$$\omega = 2\pi v = \left(\frac{2e}{\hbar}\right) V.$$

The relation between the frequency v and the voltage V is given by

$$\frac{v}{V} = 483.6\frac{MHz}{\mu V}. \tag{1.1.10}$$

In most cases, this frequency, v, lies in the microwave regime. μV represent micro volt, i.e. one millionth of a volt in the above relation. The phenomenon of a direct current crossing from the insulator in the absence of electromagnetic field, owing to tunnelling is called the DC Josephson effect, which lies between supercurrent $\pm I$, and depends on the temperature and geometry of the junction.

The technology for fabricating Josephson junctions has come a long way since the 1960's. The first junctions were made of soft materials such as lead. In the early 1970's it became increasingly clear that it was convenient to divide the theory of Josephson junctions into separate parts: solid state physics and dynamics. The objective of solid state physics is to derive general expressions relating the functions $I(t)$, $V(t)$ for superconductivity, while the latter part begins with these expressions, and describe the various phenomena observed in Josephson junctions. The problems of dynamics have proved to have more variety and complexity, mainly due to two reasons. First, the Josephson junction supercurrent has an unusual and highly nonlinear dependence on electromagnetic field. Second, the extremely high sensitivity of the supercurrent to the electromagnetic field leads to its high sensitivity to oscillation. A considerable number of observed properties of the junctions cannot be explained without taking the oscillations into account. As a result of these reasons, the study of some dynamical phenomena, such as chaotic behaviour, classical and quantum dynamics and statics of solitons had begun.

In the early 1980's a more robust technology based on niobium was developed. The discovery of the high-temperature cuprate superconductors in 1986 led many researchers to try and develop Josephson junctions based on these materials.

1.1.3 Josephson relations

There are several different approaches to obtaining the basic Josephson relations (for more explanation, see [3, 4, 5]). Here we discuss a simple derivation due to the American physicist Richard Feynman, based on the two level system shown in Fig: 1.3. This method suggests a powerful tool for understanding of unusual Josephson phenomena.

Let us suppose that ψ_L, ψ_R are the quantum mechanical wave functions shown in the Figure 1.3. These wave function amplitudes represent Cooper pairs and satisfy the Schrödinger equation on each side of insulating barrier,

$$i\hbar\frac{\partial\psi_L}{\partial t} = \mu_1\psi_L + K\psi_R, \tag{1.1.11}$$

$$i\hbar\frac{\partial\psi_R}{\partial t} = \mu_2\psi_R + K\psi_L, \tag{1.1.12}$$

where μ_1, μ_2 are potential energies of superconductor and K is a constant representing the coupling across the barrier. Let us choose the zero level of energy such that $\mu_1 = -\mu_2$ and substitute $\mu_1 - \mu_2 = 2eV$, where $2e$ is the charge of the current carrying particle. Equation (1.1.11), (1.1.12) then become

$$i\hbar\frac{\partial\psi_L}{\partial t} = eV\psi_L + K\psi_R, \tag{1.1.13}$$

$$i\hbar\frac{\partial\psi_R}{\partial t} = -eV\psi_R + K\psi_L, \tag{1.1.14}$$

where wave functions ψ_L, ψ_R are complex valued functions. To solve (1.1.13)-(1.1.14), we take $|\psi_i|^2$ to be the density of pairs in two superconductors

$$\psi_L = \sqrt{n_1}e^{i\theta_1}, \tag{1.1.15}$$

$$\psi_R = \sqrt{n_2}e^{i\theta_2}. \tag{1.1.16}$$

Substituting (1.1.15), (1.1.16) into (1.1.13), (1.1.14) we obtain

$$\hbar\frac{\partial n_1}{\partial t} = 2K\sqrt{n_1 n_2}\sin(\theta_2 - \theta_1), \tag{1.1.17}$$

$$-\hbar\frac{\partial n_2}{\partial t} = 2K\sqrt{n_1 n_2}\sin(\theta_2 - \theta_1), \tag{1.1.18}$$

$$\hbar\frac{\partial\theta_1}{\partial t} = K\sqrt{\frac{n_2}{n_1}}\cos(\theta_2 - \theta_1) - eV, \tag{1.1.19}$$

$$\hbar\frac{\partial\theta_2}{\partial t} = K\sqrt{\frac{n_1}{n_2}}\cos(\theta_2 - \theta_1) + eV. \tag{1.1.20}$$

The current through the junction must be equal to change in the density, i.e.,

$$\frac{\partial n_1}{\partial t} = -\frac{\partial n_2}{\partial t}. \tag{1.1.21}$$

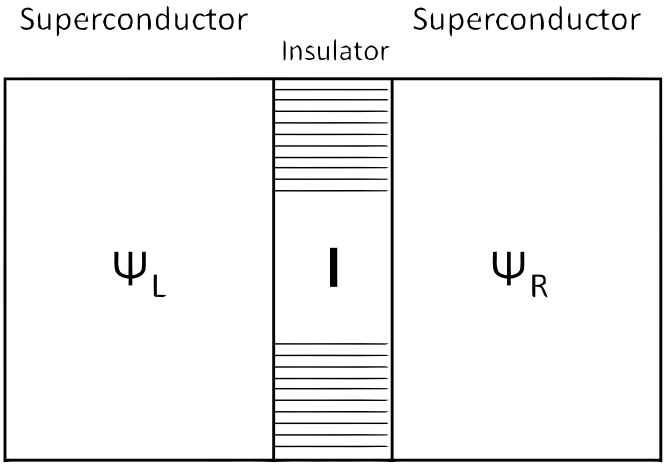

Figure 1.3: Two superconductors separated by a thin insulator, I.

The time derivative of the density of Cooper pairs describes charge transport, so we write

$$\frac{\partial n_1}{\partial t} = I_s. \tag{1.1.22}$$

Writing

$$I_c = 2K\sqrt{n_1 n_2}/\hbar, \qquad \phi = \theta_2 - \theta_1,$$

we obtain

$$I_s = I_c \sin(\phi), \tag{1.1.23}$$

$$\frac{\partial \phi}{\partial t} = \left(\frac{2e}{\hbar}\right) V. \tag{1.1.24}$$

Equations (1.1.23), (1.1.24) represent the general equations governing Josephson junctions. The first Josephson equation shows that the phase difference between order parameters leads supercurrent flow through the junction. The later Josephson equation shows that a voltage across the junction leads to time dependent phase difference. At time $t = 0$, the junction is in the ground state $\phi(0) = 0$, and, at time t, the junction has the phase $\phi(\tau)$. The total free energy of the Josephson junction is given by the integral

$$E_I(\phi) = \int_0^t I_s V \, dt. \tag{1.1.25}$$

Using relations (1.1.23) and (1.1.24) together with (1.1.8), we obtain

$$E_I(\phi) = \frac{\Phi_0}{2\pi} \int_0^t I_c \sin(\phi) \, d\phi = \frac{\Phi_0 I_c}{2\pi}(1 - \cos\phi). \tag{1.1.26}$$

The energy $E_I(\phi)$ is the potential energy accumulated inside the junction and depends only on the current state of the junction. The constant of integration is chosen such that the energy $E_I(\phi)$ is zero for the ground state $\phi = 2k\pi$, $(k \in Z)$.

There are many general properties for the Josephson phase relation.

• Changing the phase across the junction by 2π does not change the physical state of the junction, that is, Equation (1.1.23) is a 2π-periodic function

$$I(\phi) = I(\phi + 2n\pi), \tag{1.1.27}$$

for any $n \in \mathbb{Z}$.

• A *DC* supercurrent can flow if there is a change of the phase of order parameter as one crosses the barrier. That is, in the absence of any current, the phase gradient must be zero and both electrodes form a single superconductor with a common phase. Hence if $\theta_1 = \theta_2$, then

$$I(0) = I(2\,n\,\pi) = 0, \tag{1.1.28}$$

where n is any integer.

• The direction of the flow of supercurrent also changes with the direction of the phase

$$I(\phi) = -I(-\phi). \tag{1.1.29}$$

However this does not hold when the time-reversible symmetry is broken (for explanation, see [6, 7]). There is a characteristic length called the Josephson penetration length λ_J. On the basis of the Josephson penetration depth, λ_J , Josephson junctions are classified into short and long Josephson junctions.

1.2 Josephson junctions and the sine-Gordon equation

In this section, we discuss long Josephson junctions and the sine-Gordon equation as a model for long Josephson junctions. We briefly describe the applications of Josephson junctions. We also study the dynamics of Josephson junctions with an arbitrary phase jump $\theta(x)$, which can be describe by an additional term in the sine-Gordon equation in the nonlinearity.

1.2.1 Modelling long Josephson junctions

A long Josephson junction (or transmission line) is a Josephson junction which has one or more dimensions longer than the Josephson penetration depth $L \geq \lambda_J$ (L is x or

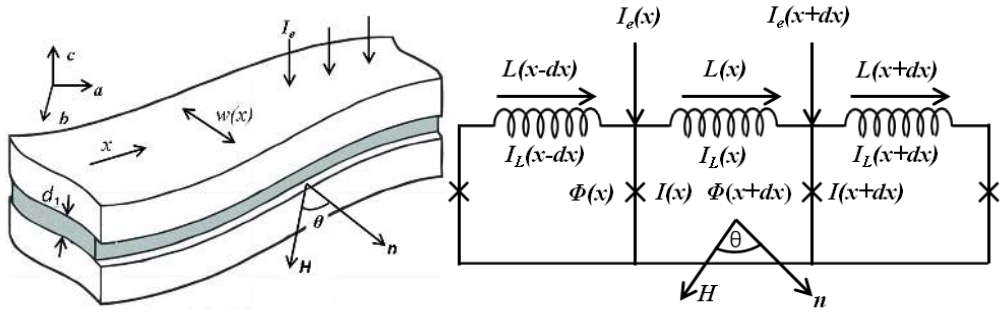

Figure 1.4: Resistively Capacitively Shunted Junction model of Josephson junction. The Josephson channel, denoted by "X" is shunted by a resistance R and capacitance C.

y direction andλ_J is Josephson penetration depth). In a long Josephson junction, the phase ϕ is a function of one or two spatial coordinates, i.e. $\phi(x,t)$, $\phi(x,y,t)$. In a short Josephson junction, phase ϕ is a function of time but not of spatial coordinates, i.e. the junction is assumed to be point-like in space.

A common way of modelling Josephson junctions is to use the so-called Resistively Capacitively Shunted Junction (RCSJ) model shown in Fig. 1.4. The junction is represented by an ideal Josephson junction shunted by a capacitor, C, and a resistor, R. The capacitive channel describes the displacement current due to the geometric shunting capacitance C and the resistive channel describes the dissipation. Here we follow the guidelines presented in [8, 9, 10, 11, 12].

The Josephson phases in an elementary loop [13] between two points with coordinates x and $x+dx$ are

$$\phi(x+dx)-\phi(x) = \frac{2\pi}{\Phi_0}\left(\phi_e(x)-L(x)I_L(x)\right), \tag{1.2.1}$$

and using Kirchhoff equations for current

$$I_L\left(x+dx\right)-I_L(x) = I_e(x)-I(x), \tag{1.2.2}$$

where $\phi(x)$ is the Josephson phase at the point x, $\phi_e(x)$ is the external magnetic flux, $L(x)$ is the inductance, $I_L(x)$ is the total current in the electrodes per unit length along x, $I(x)$ is the AC Josephson current and $I_e(x)$ is the bias current density in the junction. Assuming that the interval dx is infinitesimal

$$I(x) = J(x)w(x)dx, \tag{1.2.3}$$

$$I_e(x) = J_e(x)w(x)dx, \tag{1.2.4}$$

$$L(x) = \frac{u_0 d'}{w(x)}dx, \tag{1.2.5}$$

$$\phi_e(x) = u_0(\overrightarrow{H}.\overrightarrow{n})dx = u_0 H(x)\Lambda dx, \tag{1.2.6}$$

where $w(x)$ is the width of the junction, μ_0 is the vacuum permeability, $d^{'} \approx 2\lambda_1$ is the effective magnetic thickness with λ_1 is the London penetration depth, $H(x)$ is the magnetic field through the bulk superconducting loop is quantized in unit of $\Phi_0 = \pi\hbar/e$, $\overrightarrow{n}$ is the unit normal to the plane of the junction and $\Lambda\mu_0 H$ is the magnetic flux per unit length. Putting Equations (1.2.5)-(1.2.6) into (1.2.1), we obtain

$$\frac{\partial\phi}{\partial x} = \frac{2\pi}{\Phi_0}\left[u_0 H(x)\Lambda - \frac{u_0 d^{'}}{w(x)} I_L(x)\right], \tag{1.2.7}$$

Using relations (1.2.2) with (1.2.3)-(1.2.4)

$$\frac{\partial I_L(x)}{\partial x} = w(x)\left(J_e(x) - J(x)\right), \tag{1.2.8}$$

after simple calculation, from (1.2.7) and (1.2.8) we obtain

$$\frac{\Phi_0}{2\pi u_0 d^{'}}\phi_{xx} - \frac{\Lambda}{d^{'}} H_x(x) = J(x) - J_e(x). \tag{1.2.9}$$

The equation describing RSJ circuit

$$J(x) = J_c \sin(\phi) + \frac{V}{R} + C\frac{dV}{dt}. \tag{1.2.10}$$

Substituting relation (1.2.10) into (1.2.9) and using the Josephson junction relation (1.1.24) together with (1.1.8), we obtain the (1+1)-dimensional partial differential equation

$$\frac{\Phi_0}{2\pi u_0 d^{'} J_c}\phi_{xx} = \sin(\phi) + \frac{\Phi_0}{2\pi R u_0 d^{'}}\phi_t + \frac{\Phi_0 C}{2\pi u_0}\phi_{tt} - \frac{J_e(x)}{J_c} + \frac{\Lambda}{J_c d^{'}} H_x(x). \tag{1.2.11}$$

The governing equation of one-dimensional long Josephson junction is thus

$$\lambda_J^2\phi_{xx} - \omega_p^{-2}\phi_{tt} - \sin\phi = \omega_c^{-1}\phi_t - J_e(x)/j_c + QH_x(x), \tag{1.2.12}$$

with

$$\lambda_J^2 = \frac{\Phi_0}{2\pi u_0 d^{'} J_c}, \quad \omega_c^{-1} = \frac{\Phi_0}{2\pi R u_0 d^{'}}, \quad \omega_p^{-2} = \frac{\Phi_0 C}{2\pi u_0}, \quad Q = \frac{2\pi\mu_0\Lambda\lambda_J^2}{\Phi_0},$$

where subscripts x and t denote partial derivatives with respect to spatial and temporal coordinates, λ_J is the Josephson penetration depth, ω_p is the Josephson plasma frequency, ω_c is the characteristic frequency and $J_e(x)/j_c$ is the bias current density, normalized to the critical current density j_c. One uses the normalised sine-Gordon equation

$$\phi_{\tilde{x}\tilde{x}} - \phi_{\tilde{t}\tilde{t}} - \sin(\phi) = \alpha\phi_{\tilde{t}} - \gamma + h_x(x), \tag{1.2.13}$$

where the spatial coordinate is normalized to the Josephson penetration depth λ_J ($\tilde{x} = x/\lambda_J$) and time is normalised to the inverse plasma frequency ω_p^{-1} ($\tilde{t} = t\omega_p$).

The parameter $\alpha = 1/\sqrt{\beta_c}$ is the dimensionless damping parameter, β_c is McCumber-Stewart parameter, $\gamma = J_e(x)/j_c$ is a normalised bias current and the field h is normalised as $h(x) = 2H(x)/H_{c1}$, where $H_{c1} = \Phi_0/(\pi\mu_0\Lambda\lambda_J)$ is the critical field for long Josephson junction which is equal to the field in the center of fluxon [8]. The applied biased current does not need to be small, but can be taken to be small to be able to perform perturbation analysis. The respective boundary conditions can be adjusted to consider geometrical aspects and experimental conditions. If the right hand side of Equation (1.2.13) is zero, it reduces to the sine-Gordon equation, which is Hamiltonian and is completely integrable. Physically this means that the superconductors are ideal, and there are no quasi-particle currents.

1.2.2 Josephson junctions with phase shift

In a standard long Josephson junction, the ground state of the system is constant, $\phi(x) = \sin^{-1}\gamma$, where γ is an applied constant (dc) bias current. A novel type of Josephson junction was proposed by Bulaevskii *et al.* [14, 15], in which a nontrivial ground-state can be realised, characterised by the spontaneous generation of a fractional fluxon, i.e. a vortex carrying a fraction of magnetic flux quantum. This remarkable property can be invoked by intrinsically building piecewise constant phase-shifts, $\theta(x)$, into the junction. Examples are given in Equation (1.2.14) and (1.2.16) below. Due to the phase-shift, the supercurrent relation then becomes $I \sim \sin(\phi + \theta)$. Due to the nontrivial properties of Josephson junctions with phase shifts, they may have promising applications in information storage and information processing [16, 17].

Josephson phase discontinuities may appear in specially designed long Josephson junctions. A junction containing a region with a phase jump of π is called a $0-\pi$ Josephson junction. The Josephson junctions have a π-discontinuity of the Josephson phase at a point where 0 and π parts join. The phase-shift (jump) in Josephson phase is described by $\theta(x)$, where

$$\theta(x) = \begin{cases} 0, & |x| > 0, \\ \pi, & |x| < 0, \end{cases} \tag{1.2.14}$$

and the Josephson junction is governed by

$$\phi_{xx} - \phi_{tt} - \sin(\phi + \theta(x)) = \alpha\phi_t - \gamma. \tag{1.2.15}$$

A sketch of $0-\pi$ Josephson junction can be seen in Fig: 1.5. The Josephson phase discontinuity was first proposed in [14]. It was suggested that π phase-shifts may occur in the sine-Gordon equation due to magnetic impurities. There are many technologies

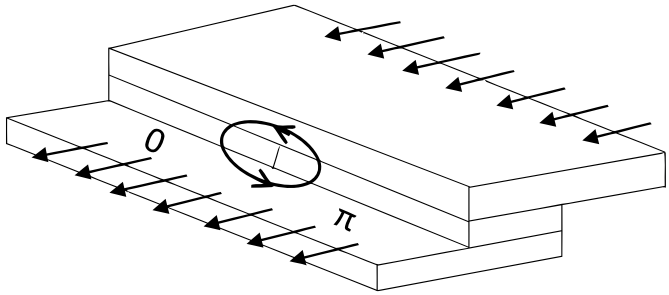

Figure 1.5: Schematic drawing of a $0-\pi$ Josephson junction. The bias current is shown by the left-pointing arrows. The semifluxon is described as a circulating current around the discontinuity point.

available for manufacturing $0-\pi$ Josephson junctions [18, 19]. They were fabricated by using d-wave superconductors [20, 21, 22, 23, 24] or were obtained using a ferromagnetic barrier [25, 26]. Present technological advances can also impose a π phase-shift in a long Josephson junction as they promise important advantages for Josephson junction based electronics. A $0-\pi$ Josephson junction admits a half magnetic flux (semifluxon), sometimes called π-fluxon, at the discontinuity point [23]. A semifluxon is represented by a π-kink solution of the $0-\pi$ sine-Gordon equation [27].

A π-junction defines the situation when the Josephson coupling between the two superconductors becomes real and negative, that is, energy is minimized as the phase difference between the two superconductors is π, in contrast to the case of a normal junction. The occurrence of the π-phase behaviour can be usually due to the magnetic ordering, strong correlation effect near the tunnelling interface [28].

Recently, a long Josephson junction geometry which allows us to create arbitrary discontinuities was suggested and successfully tested [29]. In this long Josephson junction a pair of closely situated current injectors creates an arbitrary κ- discontinuity (not only $\kappa = \pm\pi$) of the Josephson phase, with κ being proportional to the current passing through the injectors [29, 30]. This value of the phase discontinuity is denoted by κ with $0 < \kappa < 2\pi$, because the phase is 2π periodic, and is given by

$$\theta(x) = \begin{cases} 0, & x < 0, \\ -\kappa, & x > 0. \end{cases} \tag{1.2.16}$$

Such systems are called $0-\kappa$ Josephson junctions. The κ-vortex carrying the flux $\phi = -\phi_0\kappa/2\pi$, automatically appears to recompense the κ-discontinuity [29, 31]. Two types of fractional vortices may exist in a $0-\kappa$ long Josephson junction, i.e. $0-\kappa$ and $2\pi-\kappa$ [31]. The κ-vortex is the ground state (presumably only when $\kappa < \pi$), while the latter is the excited state of the system.

Phase discontinuities (1.2.14), and (1.2.16) are the simplest configurations admitting a uniform and a nonuniform ground state, respectively.

The eigenfrequency of fractional vortices plays a vital role in long Josephson junctions. Classical devices which use the fractional Josephson vortices do not operate at frequencies near the eigenfrequency. For example, a low eigenfrequency of the system indicates that the system is close to the instability region. The eigenfrequency of the ground state in the simplest case of Josephson junctions with one or two phase-shifts has been calculated theoretically in [32, 33, 34, 35, 36, 37]. More importantly, the eigenfrequency of the ground state of a $0-\kappa$ junction has recently been confirmed experimentally in [38, 39]. The experimental measurements were performed by applying microwave radiation of fixed frequency and power to the Josephson junction.

1.2.3 Applications of Josephson junctions

Electronic circuits can be built from Josephson junctions, especially digital logic circuitry. Many researchers are working on building ultrafast computers using Josephson logic. Important applications of Josephson junctions include their applicability for logic devices based on the Josephson effect for high-performance computers [40, 41, 42]. Josephson junctions can also be fashioned into circuits called SQUIDs (superconducting quantum interference devices) [43, 44]. These devices are extremely sensitive and useful for constructing extremely sensitive magnetometers and voltmeters. For example, one can make a voltmeter that can measure picovolts, about 1,000 times more sensitive than other available voltmeters.

The achievements in Josephson-junction technology have made it possible to develop a variety of sensors for detecting ultralow magnetic fields and weak electromagnetic radiation. They have also enabled the fabrication, testing, and application of ultrafast digital rapid single flux quantum circuits as well as the design of large-scale integrated circuits for signal processing and general purpose computing. Significant applications of Josephson junctions can also be found in many areas, e.g. in medicine for measurement of small currents in the brain and the heart.

The Josephson junctions are one of most important tool for superconducting electronics, including sensitive superconducting magnetometers [45], superconducting ratchets, amplifiers [46, 47, 48], superconducting terahertz emitters [49], superconducting circuits and quantum information [50]. Recent interest in the studies of dynamics of Josephson junctions was stimulated by proposals [51] and realisations [52] of several novel terahertz devices based on layered superconductors, which can be modelled as a stack of identical intrinsic Josephson junctions. Vortices in long Josephson junctions

[53, 54] or Josephson junction arrays [55, 56], have been investigated.

The investigation of quantum ratchets [57, 58] is a fascinating new field for research. A particle in a periodic potential lacking spatial reflection symmetry, is known as a ratchet potential [59]. A ratchet potential is a periodic potential which lacks reflection symmetry in one dimension. If the kink experiences a ratchet potential, then the current needed to move the kink Josephson junction in one direction is different to that needed to move it in the opposite direction. A ratchet potential exhibits this net unidirectional motion in the absence of a net driving force. Ratchets can produce a direct current when driven by nonequilibrium noise. The rachets have many realisations in nature and in artificial nanodevices, like cold atoms, colloidal magnetic particles, single-molecule optomechanical devices, fluxons in superconductors, and many other systems. In Josephson junction systems, various realisations of ratchet effect have been investigated [48, 56].

Some important advantages of Josephson junction based ratchets are as follows.

• directed motion results in an average dc voltage which is easily detected experimentally.
• Josephson junctions are fast devices which can operate in a broad frequency range from dc to $\sim$100 GHz, capturing a lot of spectral energy.
• by varying junction design and bath temperature, both overdamped and underdamped regimes are accessible.
• one can operate Josephson ratchets in the quantum regime [46, 58].

There are several types of long Josephson junctions. Most notably the in-line, overlap and annular junctions. For both experimental and theoretical studies, the most convenient object to study is an annular circular long Josephson junction, in which the net number of initially trapped fluxons is conserved, hence new solitons may only be created as fluxon-antifluxon pairs [60, 61]. Annular Josephson junctions offer applications in sources of highly coherent microwave radiation [61], radiation detectors [62] and have a potential for designing fluxon qubits [63, 64] and fluxon rachets [53, 54].

1.3 The sine-Gordon equation and its soliton solutions

In this section we discuss the sine-Gordon equation and briefly describe various properties and applications of the equation. We present the general theory of solitons and their applications. We also discuss some particular soliton solutions of the unperturbed sine-Gordon equation called kinks and breathers.

1.3.1 The sine-Gordon equation

The partial differential equation first appeared in differential geometry and relativistic field theory. Its name is wordplay on its more general form the Klein-Gordon equation. The equation, as well as several solution techniques, were known in the 19th century, but the equation gained its great importance in 1970's when it was realized that it led to soliton solutions with elastic collisional properties. The sine-Gordon equation became the focus of research in mathematics and physics because it appears in many systems, for example, pattern formation, period-doubling, stochastic oscillations [65, 66, 67, 68], dislocations in crystals [69], charge density waves [70], information transport in microtubules [71], nonlinear optics [72], the propagation of localised magnetohydrodynamic modes in plasma physics [73], *etc*.

The basic nonlinear localised excitations of sine-Gordon system can be presented as an asymptotic superposition of elementary excitations of three kinds, i.e. the one-soliton (kink), the two-soliton (breather) solution and phonons. The one-soliton (kink) and the two-soliton (breather) solution play important roles in many fields of physics and in particular the influence of various perturbations on the soliton behaviour is of great interest.

There have been many methods developed to approximate analytical solutions to sine-Gordon equations, namely inverse scattering transform [74], variational iteration method [75], homotopy analysis [76], and some numerical methods. Here we discuss the solutions of sine-Gordon equation (1.2.13) with the right hand side vanishes, *i.e.*

$$u_{tt} - u_{xx} + \sin\, u \;\; = \;\; 0, \tag{1.3.1}$$

which is completely integrable and has exact solutions for travelling 2π-kink (antikink) and the breather.

In the low amplitude case where $\sin(u) \approx u$, the completely integrable sine-Gordon Equation (1.3.1) is approximated by wave equation

$$u_{tt} - u_{xx} + u \;\; = \;\; 0. \tag{1.3.2}$$

This is called a (linear) Klein-Gordon equation. It is a linear equation, and so has a superposition principle. However, there are no localized traveling wave solutions. Substitute $u(x,t) = F(\zeta)$ with $\zeta = x - ct$ and by the chain rule obtain

$$u_{tt} = c^2 F''(\zeta), \quad u_{xx} = F''(\zeta),$$

so under the substitution the equation becomes

$$F''(\zeta) - \frac{1}{1-c^2} F(\zeta) \;\; = \;\; 0, \tag{1.3.3}$$

so if $c^2 < 1$ then

$$F(\zeta) \quad = \quad a_+ e^{\zeta/\sqrt{1-c^2}} + a_- e^{-\zeta/\sqrt{1-c^2}}, \tag{1.3.4}$$

which is unbounded and not localized solution. Similarly, if $c^2 > 1$ then

$$F(\zeta) \quad = \quad a\cos\left(\zeta/\sqrt{c^2-1}\right) + b\sin\left(\zeta/\sqrt{c^2-1}\right), \tag{1.3.5}$$

which is bounded and periodic (not pulse-like). A plane wave solution of the form

$$u(x,t) \quad = \quad Ae^{(kx-\omega t)i}, \tag{1.3.6}$$

substituting into the linear Klein-Gordon equation, admits the relation

$$\omega \quad = \quad \sqrt{1+k^2}, \tag{1.3.7}$$

where k is the wave number and ω is the frequency. This formula is called dispersion relation. Equation (1.3.7) shows that for $k \in \mathbb{R}$, ω is real and the equilibrium solution $u = 0$ of (1.3.2) is stable, i.e. perturbations away from $u = 0$ do not grow exponentially. Similarly, if $u = \pi + \widehat{u}$, with $\widehat{u} \leq 1$, Equation (1.3.2) can be linearized to obtain

$$\widehat{u}_{tt} - \widehat{u}_{xx} - \widehat{u} \quad = \quad 0, \tag{1.3.8}$$

which gives the dispersion relation

$$\omega \quad = \quad \sqrt{k^2-1}. \tag{1.3.9}$$

Hence we conclude that if $k^2 < 1$, then $\omega \in \mathbb{C} \setminus \mathbb{R}$ and $\widehat{u}$ and (hence $u(x,t)$) grow exponentially in time, i.e. $u = \pi$ is unstable.

1.3.2 Brief history of solitons

An interesting feature of the sine-Gordon equation is the existence of the so-called soliton-solutions. Before discussing such soliton solutions of the equation, we will briefly discuss the history of solitons.

The theory of solitons is very attractive in the field of mathematics with its deep ideas and amazing aspects. The theory is related to many areas of mathematics and has many applications to physical sciences. The soliton concept has a broad area of research due to significant role in different scientific fields such as fluid dynamics, astrophysics, plasma physics, magneto-acoustics [77, 78, 79, 80], *etc.*

In mathematics and physics, a soliton is a self-reinforcing solitary wave (a wave packet or pulse) that maintains its shape while it travels at constant speed. Solitons are caused

by a balancing of nonlinear and dispersive effects in the medium. Solitons arise as the solutions of a widespread class of weakly nonlinear dispersive partial differential equations describing physical systems. The basic expression of a solitary wave solution is the form

$$u(x,t) = f(x-ct), \tag{1.3.10}$$

where c is the speed of wave propagation. For $c > 0$ the wave moves in the positive direction and for $c < 0$ it moves in the negative direction. Also $f, f', f'' \longrightarrow 0$ as $x - ct \longrightarrow \pm\infty$. However the solutions of nonlinear equations have a variety of shapes, e.g, sech ,sech^2, arctan $\left(e^{r(x-ct)}\right)$. Solitary waves appear in a variety of types such as solitons, kink, peakons and cuspons.

The term "soliton" was introduced in the 1960's, but the scientific research of solitons had started in the 19th century by John Scott Russell (1808-1882) who observed a solitary wave in the Union Canal in Scotland [81]. He then performed some experiments in the laboratory in a small-scale wave tank in order to study the phenomenon more carefully and named it the Wave of Translation. Russell derived the relation

$$c^2 = g(h+a), \tag{1.3.11}$$

which determines the speed of the solitary wave. In the above relation, c is the speed of the solitary wave, a is the amplitude above the water surface, h is finite depth, and g is the acceleration due to gravity. Therefore these solitary waves are also called gravity waves. Russell's observation perplexed physicists for a long time and caused much controversy, because it could not be explained by linear water wave theory. In 1895, Diederik Johannes Korteweg (1848–1941) and Gustav de Vries (1866–1934) derived an equation for water waves in shallow channels, and confirmed the existence of solitons. They noticed that while dispersion causes a water wave to decay, nonlinear effects can cause it to steepen. After detailed theoretical analysis, in 1895 Diederik Korteweg and Gustav de Vries derived the famous nondimensionalized wave equation called the Korteweg-de Vries (KdV) equation [82]

$$\psi_t + \psi_{xxx} + 6\psi\psi_x = 0, \tag{1.3.12}$$

where ψ_t describes the time evolution of water surface, $\psi\,\psi_x$ represent nonlinearity for the steeping of wave, and ψ_{xxx} represents linear dispersion that describes the spreading of wave. This equation admits travelling solitary waves [80, 83]

$$\psi(x,t) = \frac{1}{2}c\,\mathrm{sech}^2\sqrt{c}\,(x-ct), \tag{1.3.13}$$

where c is the wave speed. The KdV equation is a general model for the study of weakly nonlinear waves, including leading order nonlinearity and dispersion. The nonlinear

and dispersive terms in the KdV equation describes the propagation of long waves of small but finite amplitude in a dispersive media. These solitary wave solutions correspond to the wave of translation in Russell's observation.

Until the 1960's the properties of solitons were not well understood. In 1965 Zabusky and Kruskal [84] numerically discovered the elastic collision between KdV solitary waves. A remarkable quality of these waves was that they could collide with each other and yet preserve their shape and speed after collision, and then in 1967, Gardner, Green, Kruskal and Miura [85] introduced the inverse scattering transform to integrate the nonlinear wave equations, and solved the KdV equation analytically. This revolutionary work initiated an exceptional burst of research in soliton theory. In subsequent years, many other nonlinear equations such as the nonlinear Schrödinger (NLS) equation, the sine-Gordon equation, and the Kadomtsev-Petviashvili (KP) equation were solved by this method, and such equations are now called integrable. These equations admit solitonic behaviour and infinite number of exact solutions.

The theory of solitons provides a fascinating insight into nonlinear processes, in which the combination of dispersion and nonlinearity together lead to the appearance of solitons. The mathematical theory of these equations is a broad and highly active field of mathematical research. Solitons are stable solitary wave solutions of these equations. As the term "soliton" suggests, these solitary waves behave like particles. When they are located far apart, each of them is approximately a travelling wave with constant shape and velocity. As two such solitary waves get closer, they gradually deform and finally merge into a single wave packet. This wave packet, however, soon splits into two solitary waves with the same shapes and velocities as before the "collision". During the collision of solitons the solution cannot be represented as a linear combination of two soliton solutions but after the collisions solitons recover their shapes and the only result of collision is a phase shift.

Integrable equations, such as the sine-Gordon equation and the KdV equation can support soliton solutions which travel without change of shape. Perturbations, such as damping, dispersion, and high order nonlinearity can be taken into account, as a physical system is modelled by perturbed equations. In perturbed systems, solitons may not propagate with fixed speeds, and their shape may be slowly distorted overtime. In non-integrable systems, collisions can be more complicated, and the outcome can depend on initial conditions in a sensitive fractal manner.

1.3.3 Soliton solutions

1.3.3.1 Kink (antikink) solution

The 1-soliton solution of the sine-Gordon equation is called a kink and represents a twist in the variable ϕ which takes the system from one solution $\phi = 0$ to an adjacent one with $\phi = 2\pi$. The 1-soliton solution in which ϕ decreases is called an antikink.

It should be noted that a static kink does not emit any radiation, neither does it emit radiation if it is moving at a constant velocity. Sine-Gordon kinks are perfect examples of solitons in the mathematical sense in which when two or more solitons (anti-solitons) collide, they pass through other and the only consequence of the scattering is a phase-shift. Since the colliding solitons recover their velocity and shape, such interactions are called 'elastic'.

To determine the solitary wave solution (kink or antikink) for Equation (1.3.1), we let

$$u(x,t) = f(x-ct),$$

which gives the one solitary wave solution

$$u(x,t) = 4\arctan\left[\exp\left(\pm\frac{x-ct}{\sqrt{1-c^2}}\right)\right], \tag{1.3.14}$$

which represents a localized solitary wave, travelling at any velocity $|c| < 1$. We observe that $u(x,t) \longrightarrow 0$ as $x \longrightarrow \mp\infty$ and $u(x,t) \longrightarrow 2\pi$ as $x \longrightarrow \pm\infty$ as shown in the Fig: 1.6.

The kinks have been used to describe crystal dislocations, domain walls representing structural phase transitions in incommensurate, ferroelectric, and ferromagnetic systems, polymerization mismatches in polyacetyline, spinwaves, charged density waves, and energy transfer along hydrogen-bonded molecular chains. It has been noted that kinks are extremely stable under the influence of external forces, however, the influence of high frequency parametric force may change the dynamics of sine-Gordon system dramatically [86]. It has also been observed that if a kink is accelerated with some external force, or its shape is deformed, it can emit radiation in the form of scalar particles [87, 88].

In the context of long Josephson junctions, the soliton-solution describes Josephson vortices (fluxons). Fluxon is a circulating current across the insulator due to the phase difference between the electron's wave functions in the superconductors. This fluxon can be forced to move along the junction by applying an exterior bias current to the junction's superconductors. Fluxons are highly robust and stable objects. They emerge due to topological reasons. Therefore they are also called topological solitons.

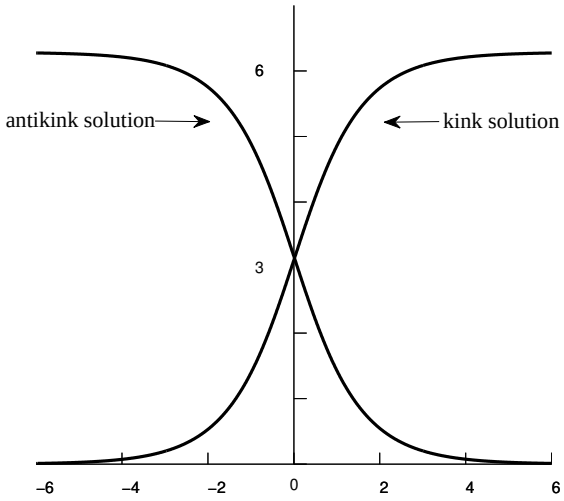

Figure 1.6: kink and antikink solution for sine-Gordon equation.

The solution of the sine-Gordon Equation (1.3.1) represents a fluxon if the total phase difference ϕ along the junction varies from 0 to 2π as x varies from $-\infty$ to ∞. Similarly if the flux quantum makes a phase variation from 2π to 0 along the junction as x varies from $-\infty$ to ∞, then it is called an antifluxon (antikink). This phase variation can be seen in Fig: 1.6, which represents a fluxon (kink) and antifluxon (antikink).

The study of fluxons in Josephson junctions has been the subject of interest over the last few decades due to their nonlinear nature and applications [45, 46, 64, 89].

1.3.3.2 Kink-kink and kink-antikink collisions

The interactions of 2-soliton solutions of sine-Gordon equation can be classified into several distinct cases, like collision of two kinks, collision of two anti-kinks, collision of a kink and anti-kink and the bound kink-antikink state known as the breather. During the collision of solitons the solution cannot be represented as a linear combination of two soliton solutions but after the collision, solitons recover their shapes.

The solutions for the kink-kink collision of sine-Gordon Equation (1.3.1) can be read as

$$u(x,t) \quad = \quad 4\arctan\left[\frac{v\sinh\left(\frac{x}{\sqrt{1-v^2}}\right)}{\cosh\left(\frac{vt}{\sqrt{1-v^2}}\right)}\right]. \tag{1.3.15}$$

In the kink-kink collision, kinks move toward each other with velocities $\pm v$, and approaches towards origin from $t \to -\infty$ and moving away with the same velocities for $t \to \infty$ as shown in the Fig: 1.7.

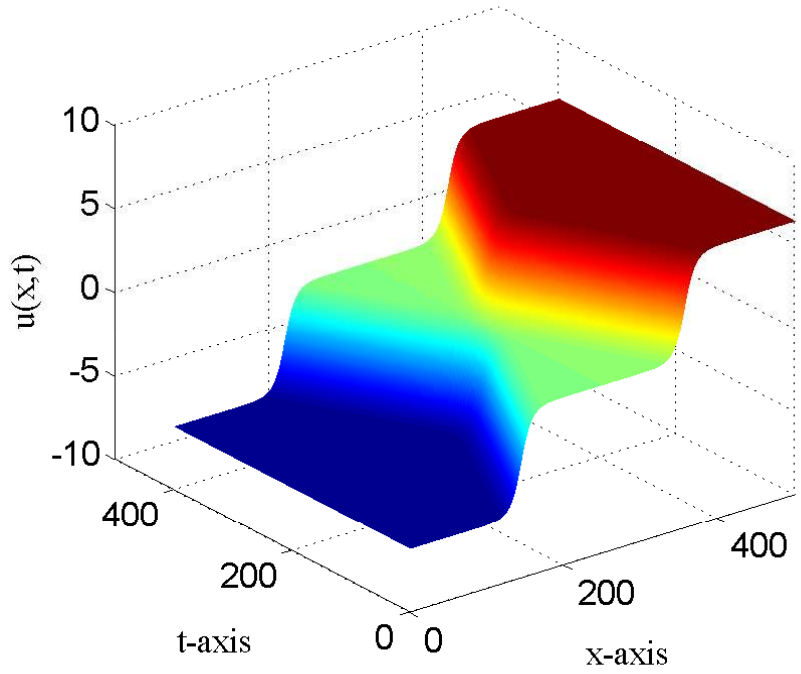

Figure 1.7: Space-time representation of kink-kink collision oscillating with velocity $v = 0.5$.

Similarly the solution for a kink-antikink pair can be obtained in the form [90, 91]

$$u(x,t) = 4\arctan\left[\frac{\sinh\left(\frac{vt}{\sqrt{1-v^2}}\right)}{v\cosh\left(\frac{x}{\sqrt{1-v^2}}\right)}\right]. \tag{1.3.16}$$

Exact kink-kink and kink-antikink solutions of the sine-Gordon equation show that kinks repel each other, while kinks and antikinks attract each other [92, 93] as shown in the Fig: 1.8.

1.3.3.3 Breather solution

The 2-soliton localized periodic solution of the sine-Gordon equation is called a breather. The term breather originates from the characteristic that breathers are localized in space and oscillate (breathe) in time [74]. Breathers may be considered as dynamical bound states of the kink-antikink pair, with a frequency lying below the linear spectrum (1.3.7). The existence of kink-antikink bound states has been interpreted as a resonance phenomenon between the natural excitation frequency of the kink profile and the frequency of oscillation of the bound kink-antikink system.

The exactly integrable sine-Gordon equation [74] and the nonlinear Schrödinger equation [94] are examples of one-dimensional partial differential equations that have breather

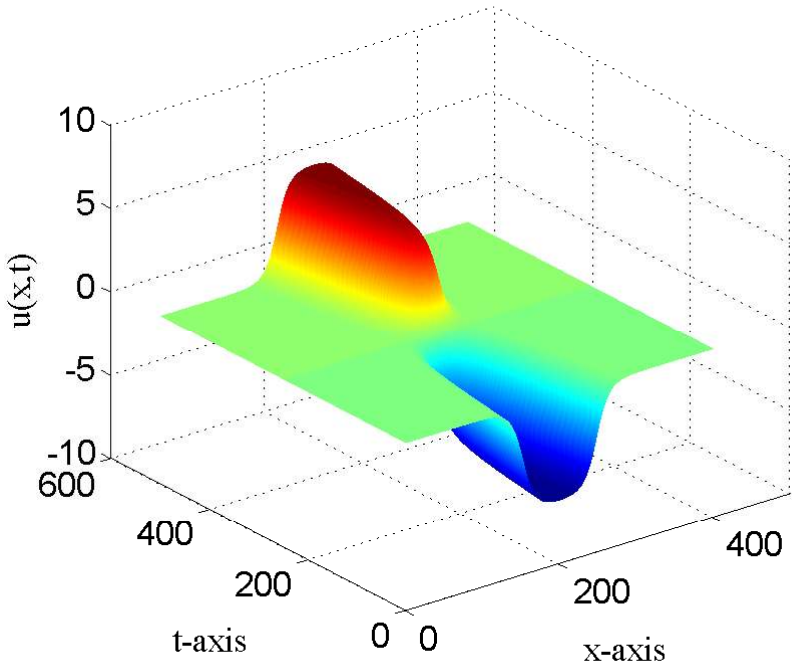

Figure 1.8: Space-time representation of kink-antikink collision oscillating with frequency $v = 0.1$.

solutions. Discrete nonlinear Hamiltonian lattices can have breather solutions, if the breather main frequency and all its multipliers are located outside of the phonon spectrum of the lattice.

There are two types of breathers namely standing or travelling ones. Standing breathers correspond to localized solutions whose amplitude varies in time. They are sometimes called oscillons.

An exact breather solution of Equation (1.3.1) by using inverse scattering transform [74] is

$$u(x,t) \quad = \quad 4\arctan\left[\frac{\sqrt{1-\omega^2}\cos(\omega\, t)}{\omega\cosh(\sqrt{1-\omega^2}x)}\right], \tag{1.3.17}$$

which is periodic in time t for $\omega < 1$ and decays exponentially when moving from $x = 0$.

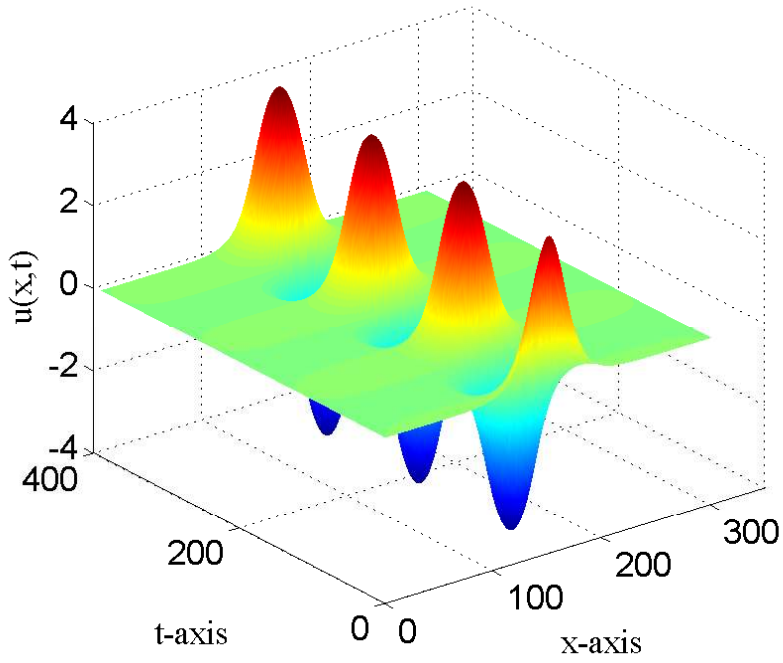

Figure 1.9: Space-time plot of the moving breather solution, oscillating with the frequency $\omega \approx 0.5$.

1.4 Mathematical techniques

In this section, we briefly describe the historical and physical background of asymptotic technique of multiple scale expansions, and the method of averaging used in Chapters 2, 3 and 4.

1.4.1 Perturbation methods

Exact analytical solutions of nonlinear differential equations are only possible for a limited number of special classes of differential equations. To find the general solutions, scientists have devoted considerable time and effort to develop efficient approximate methods. There are two distinct categories of approximation method for analysing nonlinear systems, i.e. numerical methods and asymptotic (perturbation) methods. The main advantages of the asymptotic approach is that it provides analytical approximations for many simple nontrivial problems which are suitable for subsequent discussion and interpretation. Perturbation methods start with a simplified form of the original problem, which can be solved exactly. The solved simplified problem is then "perturbed" by a small term to make the conditions closer to the real problem. The key property is that the solution of the perturbed problem is close to the solution of the simplified problem.

The practical significance of asymptotic methods is in finding useful fundamental structural properties of the original equation. The history of perturbation theory back goes to the seventeenth century, when Euler (1772) dealt with perturbed oscillatory systems in his research on the motion of the moon. The basic perturbation theory for differential equations was enhanced in the 19th century. Charles-Eugene Delaunay (1860) studied the perturbative expansion for the Earth-Moon-Sun system and discovered the method called the problem of small denominators, and this problem led Henri Poincaré to make one of the first deductions of the existence of chaos, called the "butterfly effect", that even a very small perturbation can have a large effect on a system.

Delaunay recognized the major difficulty in the avoidance of the unbounded terms in series solution, and produced the first systematic series, called Floquet's characteristic exponent. Soon after that, Poincáre (1886) produced a systematic averaging procedure for a Hamiltonian system. Brown (1931) illustrated Bohlin's method for nonlinear resonance. Bohlin's method was an improved version of Delaunay's, with the same basic idea but without the inconvenience of numerous changes of variables.

In the late 20th century, broad dissatisfaction with perturbation theory in the quantum physics community, including not only the difficulty of going beyond second order in the expansion, but also questions about whether the perturbative expansion is even convergent, has led to a strong interest in the area of non-perturbative analysis, that is, the study of exactly solvable models. To improve the accuracy of asymptotic expansions by including more terms in expansions is not generally valid, because the asymptotic expansion makes the statement about the series in the limit of $\epsilon \to 0$, where increasing the number of terms means taking the limit $n \to \infty$. Increasing the order of terms, an asymptotic expansion does not necessarilly to converge. However, if it converges, it does not have to converge to the function that was expanded. We end by noting that perturbation approximations are an art rather than science. There are no routine methods appropriate to all problems.

1.4.2 Multiscale methods

The method of multiple scales is a general method applicable to a wide range of problems in science and engineering to approximate nonlinear partial differential equations. Multiscale expansions are a way of solving nonlinear systems which can be applied when there are two or more considerably different scales.

The multiple scales method is able to deal with situations in which parameters introduced in the perturbative construction have a slow dependence on the space and time variables, and allows one to determine this dependence. This slow dependence is a

result of the energy carried away from the internal mode by the radiation waves. Classical perturbation methods generally break down because of resonances that lead to what are called "secular terms". With multiscale methods one obtains new equations, which could be different from the initial one and are sufficient to the given problems. Multiscale expansions can be applied to integrable and non-integrable systems. The result for the non-integrable systems can be both integrable or non-integrable, but for the integrable system, we obtain integrable systems.

In this thesis we used the systematic perturbation methods multiple-scale analysis to study the dynamics of the sine-Gordon equation with perturbations.

1.4.3 The method of averaging

The method of averaging is used to study certain time-varying systems by analyzing easier, time-invariant properties of the original system. The method of averaging is different from the method of multiple scales but is often used in conjunction with it, to analyze perturbations to strongly nonlinear partial differential equations with oscillatory solutions. The effect of rapidly varying perturbations on the dynamics of nonlinear systems's may lead to a strong change of the systems behaviour in the sense of dynamics averaged over the fast timescale. Such an effect may be obtained by applying a direct ac-driving force of large amplitude [95]. The first usage of the method of averaging is attributed to Van der Pol, and it has been used more widely to examine oscillations since the work of Krylov and Bogoliubov [96].

The idea of the method is to determine conditions under which solutions of an autonomous dynamical system which includes high frequencies can be used to approximate solutions of a more complicated (i.e. non-autonomous) time-varying dynamical system [97] which only evolves on the slow time scale. It provides a means to assess the cumulative effect of small terms over a long time interval [98]. Applications of the method of averaging can be found in nonlinear oscillations, stability analysis, bifurcation theory, vibrational control, and many other areas.

1.5 Aim of this thesis

The governing equation we consider in this thesis is

$$\phi_{xx}(x,t) - \phi_{tt}(x,t) = \sin(\phi + \theta(x)) - \alpha\phi_t(x,t) + \gamma + h\cos(\Omega t), \;\; x \in \mathbb{R},\; t > 0, \quad (1.5.1)$$

which describes an infinitely long Josephson junction with phase-shifts $\theta(x)$, damping α, and driven by a microwave field. The applied time periodic (ac) drive has amp-

litude h, which is proportional to the applied microwave power, and frequency Ω. The term γ is the applied dc bias current. Our aim is to analyze the equation, explain its behaviour, and if possible, predict novel characteristics of the system for technological applications.

We begin in Chapter 2, by considering the sine-Gordon equation as a model which describes infinitely long Josephson junctions with phase shifts. We construct a perturbative expansion for the breathing mode to obtain equations for the slow time evolution of the oscillation amplitude from our expansion. A similar approach has been used by Oxtoby and Barashenkov [99, 100] for the ϕ^4 equation. The multiple scales expansion is the best way to introduce the slow dependence on space and time variables, and to determine this dependence. We shall avoid arithmetic unboundedness in radiation functions by using multiscale expansions. We show in Sections 2.2 and 2.4 that, in the absence of an ac-drive, a breathing mode oscillation decays with a rate of at least $\mathcal{O}(t^{-1/4})$ and $\mathcal{O}(t^{-1/2})$ for junction with a uniform and nonuniform ground state, respectively. In Sections 2.3 and 2.5 we extend our multiple scale analysis to the governing equation driven by microwave field. Chapter 2 also covers radiation from a breathing mode.

We confirm our analytical results numerically. Using numerical computations, we show that there is a critical driving amplitude at which the junction switches to the resistive state. Yet, it appears that the switching process is not necessarily caused by the breathing mode. We show a case where a junction switches to a resistive state due to the continuous wave background becoming modulationally unstable.

In Chapter 3, we study the dynamics of a κ-kink in the long Josephson junction in the presence of rapidly varying driving force modelled by the sine-Gordon equation. The ac-drive is assumed to be fast compared to the system's natural frequency. We derive analytically an averaged equation for the slowly-varying dynamics. Our method uses multiscale expansions rather than direct averaging to analyze the dynamics of kink solitons. This averaged equation is a double sine-Gordon equation. This equation describes the kink dynamics in the long time where behaviour depends strongly on the short time-scale dynamics. We also obtain analytically and numerically the critical value of the applied bias current, γ, above which there are no static semifluxons in the presence of ac drive.

In Chapter 4, we consider a spatially inhomogeneous sine-Gordon equation with a double well potential and a time periodic drive modelling $0-\pi-0-\pi-0$ long Josephson junctions. A phase shift formation acting as a double well potential is considered. In Section 4.2, we construct a perturbation expansion to solve the unperturbed

sine-Gordon equation for the coupled mode to obtain equations for the slow time evolution of oscillation amplitude in $0-\pi-0-\pi-0$ junction. In Section 4.3, the method of multiple scales is applied to obtain the amplitude of oscillation in the presence of driving.

We discuss the interactions of symmetric and antisymmetric defect modes in the long Josephson junctions. We show that the modes decay in time. In particular, exciting the two modes at the same time will increase the decay rate. The decay is due to the energy transfer from the discrete to the continuous spectrum. For small drive amplitude, there is an energy balance between the energy input given by the external drive and the energy output due to radiative damping experienced by the coupled mode.

In Chapter 5, we consider a spatially inhomogeneous coupled sine-Gordon equations with a time periodic drive, modelling stacked long Josephson junctions with phase shift. In Section 5.2 and 5.3, we construct the analytical approximation of two stacked long Josephson junctions as coupled sine-Gordon equations with different magnetic inductance. By considering weak coupling we show that amplitude of oscillation decays to steady state as $t \to \infty$. Similarly in the absence of ac-drive for strong coupling the amplitude equations decay at the order $\mathcal{O}(t^{-1/4})$. In Section 5.4, the method of multiple scales is applied to obtain the amplitude of oscillation in the presence of driving. By considering the strong coupling with time periodic drive, we expect that the amplitude of oscillation tends to constant for a long time.

CHAPTER 2

Breathing modes of long Josephson junctions with phase-shifts

The contents of the chapter have been published in SIAM Journal on Applied Mathematics, vol. **71**, *no. 1, pp. 242-269, (2011)* [101].

2.1 Introduction

A Josephson junction is made by sandwiching a thin layer of a nonsuperconducting material between two layers of superconducting material. The devices are named after Brian Josephson, who predicted in 1962 that pairs of superconducting electrons could "tunnel" right through the nonsuperconducting barrier from one superconductor to another. This is due to the quantum mechanical waves in the two superconductors of the Josephson junction overlapping with each other.

If we denote the difference in phases of the wave functions by ϕ, and the spatial and temporal variables along the junction by x and t, respectively, then the electron flow tunnelling across the barrier, i.e., the Josephson current, I is proportional to the sine of $\phi(x,t)$, i.e., $I \sim \sin\phi(x,t)$. In a ideal long Josephson junction, the phase difference ϕ satisfies a sine-Gordon equation.

The sine-Gordon equation occurs widely in the study of nonlinear systems, because of its multisoliton solutions, solitary wave solutions, periodic solutions and many more. The basic nonlinear localised excitations of sine-Gordon system are divided into two groups: the one-soliton (kink) and the two-soliton (breather) solution. Kinks have been used to describe crystal dislocations [102], domain walls representing structural phase transitions in incommensurate, ferroelectric, and ferromagnetic systems, polymerization mismatches in polyacetyline, spinwaves, charged density waves, and energy

transfer along hydrogen-bonded molecular chains. It has been noted that kinks are extremely stable under the influence of external forces, however, the influence of high frequency parametric force may change the dynamics of sine-Gordon system dramatically [86].

The sine-Gordon equation describes a variety of physical systems, for example, the propagation of magnetic flux in long Josephson junction [45], pattern formation, period-doubling, stochastic oscillations [65, 66, 67, 68], information transport in microtubules [71], nonlinear optics [72], the propagation of localised magnetohydrodynamic modes in plasma physics [73], *etc*.

In a standard long Josephson junction, the energetic ground state of the system is $\phi(x,t)$ constant (both in time and in space) satisfying $\sin\phi = \gamma$, where γ is an applied constant (dc) bias current, which is taken to be zero here. A novel type of Josephson junction was proposed by Bulaevskii, Kuzii, and Sabyanin [14, 15], in which a nontrivial ground state can be realized, characterized by the spontaneous generation of a fractional fluxon, i.e., a vortex carrying a fraction of a magnetic flux quantum. This remarkable property can be invoked by intrinsically building piecewise constant phase-shifts $\theta(x)$ into the junction. Due to the phase-shift, the supercurrent relation then becomes $I \sim \sin(\phi + \theta)$. Presently, one can impose a phase-shift in a long Josephson junction using several methods (see, e.g., [18, 19] and references therein).

Due to these properties, Josephson junctions with phase shifts may have promising applications in information storage and processing [16, 17]. Because of their potential applications, the next natural question is, "what is the eigenvalue of the ground state?" It is important because Josephson junction–based devices should not operate at frequencies close to the eigenfrequency of the system, as unwanted parasitic resonances can be induced.

The eigenfrequency of the ground state in the simplest case of Josephson junctions with one and two phase-shifts has been theoretically calculated in [32, 33, 34, 35, 36, 37]. More important, the eigenfrequency calculation in the former case has been recently confirmed experimentally in [38, 39]. The experimental measurements were performed by applying microwave radiation of fixed frequency and power to the Josephson junction. At some frequency, the junction, interestingly, switches to the resistive state, characterized by a nonzero junction voltage. In terms of the phase-difference ϕ, the averaged Josephson voltage $\langle V \rangle$ is proportional to

$$\langle V \rangle \sim \frac{1}{T} \int_0^T \int_{x \in \mathcal{D}} \phi_t(x,t)\, dx\, dt, \tag{2.1.1}$$

where $\mathcal{D}$ is the domain of the problem and $T \gg 1$. It was conjectured that the driving

frequency at which switching occurs is the same as the eigenfrequency of the ground state [38]. It is assumed that the jump to the resistive state is due to the resonant excitation of the breathing mode of the ground state and the applied microwaves, similar to the resonance phenomena observed in a periodically driven short (point-like) Josephson junction reported in [103, 104, 105].

It was also noted in [38] that the accuracy of the microwave spectroscopy depends on the magnitude of the eigenfrequency. To measure a large natural frequency, the method requires an applied microwave with high power, which influences the measurement due to the nonlinearity of the system. Here, we consider an infinitely long Josephson junction with phase-shifts and no applied constant (dc) bias current. We show that in such a system, the breathing mode cannot be excited to switch the junction into a resistive state provided that the microwave amplitude is small enough. This is the case even when the applied drive frequency is the same as the eigenfrequency, because of higher harmonic excitations from continuous wave emission. In other words, the breathing mode experiences radiative damping. Such damping is not present in short junctions, as the phase difference ϕ in that limit is effectively independent of x. This confirms the observed experimental results.

The governing equation we consider herein is

$$\phi_{xx}(x,t) - \phi_{tt}(x,t) = \sin(\phi + \theta(x)) + h\cos(\Omega t), \quad x \in \mathbb{R},\ t > 0, \tag{2.1.2}$$

describes an infinitely long Josephson junction with phase-shifts, $\theta(x)$, driven by a microwave field $h\cos(\Omega t)$. Equation (2.1.2) is dimensionless, and x and t are normalized by the Josephson penetration length λ_J and the inverse plasma frequency ω_p^{-1}, respectively. The applied time periodic ac-drive in the governing equation above has amplitude h, which is proportional to the applied microwave power, and frequency Ω. Here we study two cases of the internal phase-shift

$$\theta(x) = \begin{cases} 0, & |x| > a, \\ \pi, & |x| < a, \end{cases} \tag{2.1.3}$$

with $a < \pi/4$, as $\Phi_0(x,t) = 0(\mathrm{mod}2\pi)$ as the ground state for $0-\pi-0$ Josephson junction. Studying the stability of the constant solution, one finds there is a critical facet length $a_c = \pi/4$ above which the solution is unstable and the ground state is spatially nonuniform [32].

$$\theta(x) = \begin{cases} 0, & x < 0, \\ -\kappa, & x > 0, \end{cases} \tag{2.1.4}$$

with $0 < \kappa < 2\pi$, which is called $0-\kappa$ Josephson junction. The internal phase shift 2.1.3, 2.1.4 are the simplest configurations admitting a uniform and a nonuniform

ground state, respectively. The phase field ϕ is then naturally subject to the continuity conditions at the position of the jump in the Josephson phase (the discontinuity), i.e.,

$$\phi(\pm a^-) = \phi(\pm a^+), \quad \phi_x(\pm a^-) = \phi_x(\pm a^+), \tag{2.1.5}$$

for the $0-\pi-0$ junction and

$$\phi(0^-) = \phi(0^+), \quad \phi_x(0^-) = \phi_x(0^+), \tag{2.1.6}$$

for the $0-\kappa$ junction.

The unperturbed $0-\pi-0$ junction, i.e., (2.1.2) and (2.1.3) with $h=0$, has

$$\Phi_0 \;=\; 0(mod\, 2\pi), \tag{2.1.7}$$

as the ground state, and by linearizing around the uniform solution we find a localized breathing mode [32]

$$\Phi_1(x,t) \;=\; e^{i\omega t}\begin{cases} \cos(a\sqrt{1+\omega^2})e^{\sqrt{1-\omega^2}(a+x)}, & x<-a, \\ \cos(x\sqrt{1+\omega^2}), & |x|\le a, \\ \cos(a\sqrt{1+\omega^2})e^{\sqrt{1-\omega^2}(a-x)}, & x>a, \end{cases} \tag{2.1.8}$$

with the oscillation frequency ω given by the implicit relation

$$a \;=\; \frac{1}{\sqrt{1+\omega^2}}\tan^{-1}\sqrt{\frac{1-\omega^2}{1+\omega^2}}, \quad \omega^2<1. \tag{2.1.9}$$

As for the unperturbed $0-\kappa$ junction, i.e., (2.1.2) and (2.1.4) with $h=0$, the ground state of the system is (mod 2π)

$$\Phi_0(x,t) \;=\; \begin{cases} 4\tan^{-1}e^{x_0+x}, & x<0, \\ \kappa - 4\tan^{-1}e^{x_0-x}, & x>0, \end{cases} \tag{2.1.10}$$

where $x_0 = \ln\tan(\kappa/8)$. Physically, Φ_0 in (2.1.10) represents a fractional fluxon that is spontaneously generated at the discontinuity. A scanning microscopy image of fractional fluxons can be seen in, e.g., [23, 106]. Linearizing around the ground state Φ_0 in (2.1.10), we obtain the breathing mode [33, 35]

$$\Phi_1(x,t) \;=\; \widetilde{\Phi}_1(x)e^{i\omega t}, \tag{2.1.11}$$

with

$$\widetilde{\Phi}_1(x) \;=\; \begin{cases} e^{\Lambda(x_0+x)}\left[\tanh(x_0+x)-\Lambda\right], & x<0, \\ e^{\Lambda(x_0-x)}\left[\tanh(x_0-x)-\Lambda\right], & x>0, \end{cases} \tag{2.1.12}$$

$$\Lambda = \sqrt{1-\omega^2}, \tag{2.1.13}$$

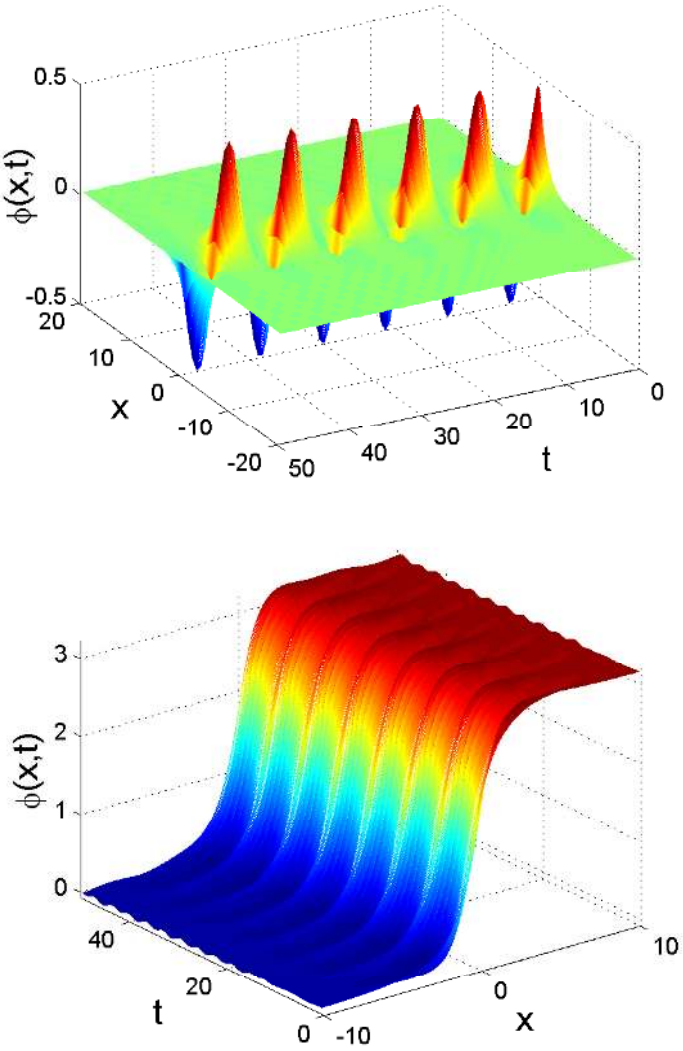

Figure 2.1: The typical dynamics of a breathing mode (top) and a wobbling kink (bottom) in an undriven $0-\pi-0$ and $0-\kappa$ junction, respectively.

and the oscillation frequency

$$\omega(\kappa) \quad = \quad \pm\sqrt{\frac{1}{2}\cos\frac{\kappa}{4}\left(\cos\frac{\kappa}{4}+\sqrt{4-3\cos^2\frac{\kappa}{4}}\right)}, \tag{2.1.14}$$

which satisfies $\omega(0) = \pm 1$, and $\omega(2\pi) = 0$. In addition to the eigenfrequency (2.1.9) or (2.1.14), a ground state in a Josephson junction also has a continuous spectrum in the range $\omega^2 > 1$.

If a ground state is perturbed by its corresponding localized mode, then the perturbation will oscillate periodically. The typical evolution of the initial condition

$$\phi \quad = \quad \Phi_0(x) + B_0\Phi_1(x,0), \quad \phi_t(x,0) = 0, \tag{2.1.15}$$

for some small initial amplitude $B_0 = 1/2\Phi(0,0)$, and $h = 0$ is shown in the top and bottom panels of Figure 2.1 for the two cases above (2.1.3)-(2.1.4). For a $0-\pi-0$ junction, one can see a clear mode oscillation on top of the uniform background state $\phi = 0$. The mode of oscillation do not grow. Later calculation determine that the mode decay for a long time (see Figure 2.2). In the case of a $0-\kappa$ junction, the periodic oscillation of the localized mode makes the fractional kink oscillate about the point of discontinuity, $x = 0$.

Using a multiple scale expansion, we show that in the absence of an ac-drive, such a breathing mode oscillation decays with a rate of at most $\mathcal{O}(t^{-1/4})$ and $\mathcal{O}(t^{-1/2})$ for a junction with a uniform and nonuniform ground state, respectively.

The coupling of a spatially localized breathing mode to radiation modes via a nonlinearity with the same decay rates has been discussed and obtained by others in several contexts (see [99] and references therein). Interactions of a breathing mode and a topological kink, creating the so-called "wobbling kink" or simply "wobbler" have also been considered before; see [99, 100] and the references therein to ϕ^4 wobblers and [107, 108, 109] for sine-Gordon wobblers. Nonetheless, the problem and results presented herein are novel and important from several points of view, which include the fact that our fractional wobbling kink is in principle different from the "normal" wobbler. Usually, a wobbler is a periodically expanding and contracting kink, due to the interaction of the kink and its *odd* eigenmode. Because our system is not translationally invariant, our wobbler will be composed of a fractional kink and an *even* eigenmode, representing a topological excitation oscillating about the discontinuity point (see also [110] for a similar situation in discrete systems, where a lattice kink interacts with its even mode). Such an oscillation can certainly be induced by a time-periodic direct driving, as considered herein. More important, our problem is relevant and can be readily confirmed experimentally (see also, e.g., [111, 112, 113] for experimental fabrications of $0-\pi-0$ Josephson junctions).

The presentation of the Chapter 2 is as follows. In Section 2.2, we construct a perturbation expansion for the breathing mode to obtain equations for the slow-time evolution of the oscillation amplitude in a $0-\pi-0$ junction by eliminating secular terms from our expansion. In Section 2.3, the method of multiple scales is applied to obtain the amplitude oscillation in the presence of driving, extending the preceding section. In Section 2.4 and 2.5, we apply the perturbation method to the wobbling kink in a $0-\kappa$ junction. We confirm our analytical results numerically in Section 2.6.

We also show in the same section that there is a threshold drive amplitude above which the junction switches to the resistive state. Yet, we observe that the switching to the

resistive state is due to the modulational instability of the background. We conclude the present work in Section 2.7.

2.2 Freely oscillating breathing mode in a $0 - \pi - 0$ junction

In this section we construct a breathing mode of the sine-Gordon Equation (2.1.2) with $h = 0$ and θ given by (2.1.3).

We apply a perturbation method to (2.1.2) by writing

$$\phi = \phi_0 + \epsilon\,\phi_1 + \epsilon^2\phi_2 + \epsilon^3\phi_3 + \cdots, \tag{2.2.1}$$

where ϵ is a small parameter, which is the initial amplitude in perturbation expansion for the undriven case. We will assume latter that $b = \epsilon B$, so that b is the natural amplitude oscillating mode, which is the small amplitude we will actually measure. We further use multiple scale expansions introducing the slow-time and space variables

$$X_n = \epsilon^n x, \quad T_n = \epsilon^n t, \quad n = 0, 1, 2, \ldots, \tag{2.2.2}$$

which describe long times and distances. In the small limit of ϵ, the scales become uncoupled and may be considered as independent variables.

In the following, we use the notation

$$\partial_n = \frac{\partial}{\partial X_n}, \quad D_n = \frac{\partial}{\partial T_n}, \tag{2.2.3}$$

such that the derivatives with respect to the original variables in terms of the scaled variables using the chain rule are given by

$$\frac{\partial}{\partial x} = \partial_0 + \epsilon\,\partial_1 + \epsilon^2\partial_2 + \epsilon^3\partial_3 + \cdots, \tag{2.2.4}$$

$$\frac{\partial}{\partial t} = D_0 + \epsilon\,D_1 + \epsilon^2 D_2 + \epsilon^3 D_3 + \cdots. \tag{2.2.5}$$

Substituting these expansions into the perturbed sine-Gordon Equation (2.1.2) along with the expansion of ϕ and equating like powers of ϵ, we obtain a hierarchy of partial differential equations (PDEs):

$$\mathcal{O}(1) \quad : \quad \partial_0^2\phi_0 - D_0^2\phi_0 = \sin(\theta + \phi_0), \tag{2.2.6}$$

$$\mathcal{O}(\epsilon) \quad : \quad \partial_0^2\phi_1 - D_0^2\phi_1 - \cos(\theta + \phi_0)\phi_1 = 2D_0D_1\phi_0 - 2\partial_0\partial_1\phi_0. \tag{2.2.7}$$

Solutions to the equations above for the $0 - \pi - 0$ junction are given by

$$\phi_0(X_0, T_0) = 0, \tag{2.2.8}$$

and

$$\phi_1(X_0, X_1, \dots, T_0, T_1, \dots) \quad = \quad B(X_1, \dots, T_1, \dots)\Phi_1(X_0, T_0) + c.c., \tag{2.2.9}$$

where Φ_1 is given by (2.1.8). $B(X_1, \dots, T_1, \dots)$ is the amplitude of the breathing mode, which is a function of the slow-time and space variables only. Throughout the chapter $c.c.$ stands for the complex conjugate of the immediately preceding term.

2.2.1 Equation at $\mathcal{O}(\epsilon^2)$

Next, we consider the $\mathcal{O}(\epsilon^2)$ equation

$$\partial_0^2\phi_2 - D_0^2\phi_2 - \cos(\theta + \phi_0)\phi_2 \quad = \quad 2D_0D_1\phi_1 - 2\partial_0\partial_1\phi_1. \tag{2.2.10}$$

Evaluating the right-hand side for the different regions, we obtain

$$\begin{aligned}
\partial_0^2\phi_2 - D_0^2\phi_2 - \phi_2 &= 2\cos(a\sqrt{1+\omega^2})\left[i\omega D_1 B - \sqrt{1-\omega^2}\partial_1 B\right] e^{\sqrt{1-\omega^2}(a+X_0)+i\omega T_0}, \\
\partial_0^2\phi_2 - D_0^2\phi_2 + \phi_2 &= 2\left[i\omega D_1 B\cos(X_0\sqrt{1+\omega^2}) + \sqrt{1+\omega^2}\partial_1 B\sin(X_0\sqrt{1+\omega^2})\right] e^{i\omega T_0}, \\
\partial_0^2\phi_2 - D_0^2\phi_2 - \phi_2 &= 2\cos(a\sqrt{1+\omega^2})\left[i\omega D_1 B + \sqrt{1-\omega^2}\partial_1 B\right] e^{\sqrt{1-\omega^2}(a-X_0)+i\omega T_0}.
\end{aligned}$$

for $X_0 < -a$, $|X_0| < a$, and $X_0 > a$, respectively. These are linear wave equations with forcing at frequency ω. Substituting the spectral ansatz

$$\phi_2(X_0, X_1, \dots, T_0, T_1, \dots) = \widetilde{\phi}_2(X_0, X_1, \dots, T_1, \dots)e^{i\omega T_0}, \tag{2.2.11}$$

we obtain the corresponding set of ordinary differential equations (ODEs) with forcing term, which has the frequency ω,

$$\begin{aligned}
\partial_0^2\widetilde{\phi}_2 - (1-\omega^2)\widetilde{\phi}_2 &= 2\cos(a\sqrt{1+\omega^2})\left[i\omega D_1 B - \sqrt{1-\omega^2}\partial_1 B\right] e^{\sqrt{1-\omega^2}(a+X_0)}, \\
\partial_0^2\widetilde{\phi}_2 + (1+\omega^2)\widetilde{\phi}_2 &= 2\left[i\omega D_1 B\cos(X_0\sqrt{1+\omega^2}) + \sqrt{1+\omega^2}\partial_1 B\sin(X_0\sqrt{1+\omega^2})\right], \\
\partial_0^2\widetilde{\phi}_2 - (1-\omega^2)\widetilde{\phi}_2 &= 2\cos(a\sqrt{1+\omega^2})\left[i\omega D_1 B + \sqrt{1-\omega^2}\partial_1 B\right] e^{\sqrt{1-\omega^2}(a-X_0)}.
\end{aligned}$$

We write the above equations in the form

$$\mathcal{L}\psi(x) = f(x), \tag{2.2.12}$$

where $\mathcal{L}$ is a linear self-adjoint operator ($\mathcal{L} = \mathcal{L}^\dagger$) given by the left hand side of the above system, and $\zeta : \mathbb{T} \to \mathbb{R}$ is a smooth periodic function. Let $L^2(\mathbb{R})$ be the Hilbert space with complex inner product

$$\langle g, h\rangle \quad = \quad \int_{-\infty}^{\infty} \overline{g}(\xi)h(\xi)d\xi. \tag{2.2.13}$$

Here $\overline{g}(\xi)$ is the complex conjugate of $g(\xi)$. The Fredholm theorem states that the necessary and sufficient condition for the inhomogeneous equation $\mathcal{L}\psi = f(x)$ to have a bounded solution is that $f(x)$ be orthogonal to the null-space of the operator $\mathcal{L}$. Hence, the solvability condition provided by the Fredholm theorem is

$$\int_{-\infty}^{\infty} \mathcal{L}f(x)\,dx \quad = \quad 0. \tag{2.2.14}$$

By applying the theorem, we find the solvability condition

$$D_1 B \quad = \quad 0. \tag{2.2.15}$$

The bounded solution of (2.2.10) is given by

$$\phi_2 = \partial_1 B e^{i\omega T_0} \begin{cases} C_{21} e^{\sqrt{1-\omega^2}X_0} - X_0 \cos\left(a\sqrt{1+\omega^2}\right) e^{\sqrt{1-\omega^2}(a+X_0)} + c.c., & X_0 < -a, \\ C_{22} \cos\left(X_0\sqrt{1+\omega^2}\right) - X_0 \cos\left(X_0\sqrt{1+\omega^2}\right) + c.c., & |X_0| \le a, \\ C_{23} e^{-\sqrt{1-\omega^2}X_0} - X_0 \cos\left(a\sqrt{1+\omega^2}\right) e^{\sqrt{1-\omega^2}(a-X_0)} + c.c., & X_0 > a, \end{cases}$$

where $C_{21} = C_{23} = \cos\left(a\sqrt{1-\omega^2}\right)$ and C_{22} are constants of integration that have to be found by applying the continuity conditions at the discontinuity points $X_0 = \pm a$.

It should be noted that $\partial_1 B$, as well as $\partial_n B$ in later calculations, does not appear in the solvability conditions. Therefore, we take the simplest choice by setting

$$\partial_1 B \quad = \quad 0. \tag{2.2.16}$$

This choice is also in accordance with the fact that if $\partial_1 B$ were nonzero, then $(\epsilon^2\phi_2)$ would become greater than $(\epsilon\phi_1)$, as $X_0 \to \pm\infty$ due to the term $(X_0 e^{\sqrt{1-\omega^2}(a\mp X_0)})$ in the expression of ϕ_2 above, leading to a nonuniformity in the perturbation expansion of ϕ. Hence we conclude that

$$\phi_2(X_0, \ldots, T_0, \ldots) \quad = \quad 0. \tag{2.2.17}$$

2.2.2 Equation at $\mathcal{O}(\epsilon^3)$

The equation at the third order in the perturbation expansion is

$$\partial_0^2\phi_3 - D_0^2\phi_3 - \cos(\theta)\phi_3 = 2(D_0 D_2 - \partial_0\partial_2)\phi_1 + (D_1^2 - \partial_1^2)\phi_1 - \frac{1}{6}\phi_1^3\cos(\theta). \tag{2.2.18}$$

Having evaluated the right-hand side using the functions ϕ_0 and ϕ_1, and splitting the solution into components proportional to simple harmonics, we obtain

$$\partial_0^2\phi_3 - D_0^2\phi_3 - \cos(\theta)\phi_3 \quad = \quad \begin{cases} F_1, & X_0 < -a, \\ F_2, & |X_0| \le a, \\ F_3, & X_0 > a, \end{cases} \tag{2.2.19}$$

where F_1, F_2, F_3 are given by

$$\begin{aligned} F_1 &= 2\left(i\omega D_2 B - \sqrt{1-\omega^2}\partial_2 B\right)\cos\left(a\sqrt{1+\omega^2}\right)e^{\sqrt{1-\omega^2}(a+X_0)+i\omega T_0} \\ &\quad -\frac{1}{2}B|B|^2\cos^3\left(a\sqrt{1+\omega^2}\right)e^{3\sqrt{1-\omega^2}(a+X_0)+i\omega T_0} \\ &\quad -\frac{1}{6}B^3\cos^3(a\sqrt{1+\omega^2})e^{3\sqrt{1-\omega^2}(a+X_0)+3i\omega T_0}, \end{aligned}$$

$$\begin{aligned} F_2 &= \left[2\,i\omega D_2 B\cos\left(\sqrt{1+\omega^2}X_0\right)+2\partial_2 B\sqrt{1+\omega^2}\sin\left(\sqrt{1+\omega^2}X_0\right)\right. \\ &\quad \left.+\frac{1}{2}B|B|^2\cos^3\left(\sqrt{1+\omega^2}X_0\right)\right]e^{i\omega T_0}+\frac{1}{6}B^3\cos^3\left(\sqrt{1+\omega^2}X_0\right)e^{3i\omega T_0}, \end{aligned}$$

$$\begin{aligned} F_3 &= 2\left(i\omega D_2 B + \sqrt{1-\omega^2}\partial_2 B\right)\cos\left(a\sqrt{1+\omega^2}\right)e^{\sqrt{1-\omega^2}(a-X_0)+i\omega T_0} \\ &\quad -\frac{1}{2}B|B|^2\cos^3\left(a\sqrt{1+\omega^2}\right)e^{3\sqrt{1-\omega^2}(a-X_0)+i\omega T_0} \\ &\quad -\frac{1}{6}B^3\cos^3(a\sqrt{1+\omega^2})e^{3\sqrt{1-\omega^2}(a-X_0)+3i\omega T_0}. \end{aligned}$$

These are linear wave equations with forcing at frequencies ω and 3ω. The former frequency is resonant with the discrete eigenmode, and the latter is assumed to lie in the continuous spectrum (phonon band),

$$9\omega^2 > 1. \tag{2.2.20}$$

This forcing is localised to the region near the origin and acts as a source of radiation. With this assumption $e^{3i\omega T_0}\phi_3^{(3)}$ will not decay in space and $e^{3i\omega T_0}\phi_3^{(3)} + c.c.$ will describe right and left moving radiation when $x \to \pm\infty$. Hence, the frequency-tripling effects of the nonlinearity have caused the breathing mode to become a source of radiation. It should be noted that $\omega = \omega(a)$ shown in (2.1.9).

As (2.2.18) is linear, the solution can be written as a combination of solutions each with frequencies as in the forcing terms, that is,

$$\phi_3 = \phi_3^{(0)} + \phi_3^{(1)}e^{i\omega T_0} + c.c. + \phi_3^{(2)}e^{2i\omega T_0} + c.c. + \phi_3^{(3)}e^{3i\omega T_0} + c.c. \tag{2.2.21}$$

This implies that $\phi_3^{(1)}$ satisfies the following inhomogeneous equations:

$$\partial_0^2\phi_3^{(1)} - \left(\cos(\theta)-\omega^2\right)\phi_3^{(1)} = \begin{cases} 2\,i\omega\,D_2 B\,\cos\left(a\sqrt{1+\omega^2}\right)e^{\sqrt{1-\omega^2}(a+X_0)} \\ -\frac{1}{2}\,B|B|^2\cos^3\left(a\sqrt{1+\omega^2}\right)e^{3\sqrt{1-\omega^2}(a+X_0)}, & X_0 < -a, \\ 2\,i\omega\,D_2 B\cos\left(\sqrt{1+\omega^2}X_0\right) \\ +\frac{1}{2}\,B|B|^2\cos^3\left(\sqrt{1+\omega^2}X_0\right), & |X_0| < a, \\ 2\,i\omega\,D_2 B\,\cos\left(a\sqrt{1+\omega^2}\right)e^{\sqrt{1-\omega^2}(a-X_0)} \\ -\frac{1}{2}\,B|B|^2\cos^3\left(a\sqrt{1+\omega^2}\right)e^{3\sqrt{1-\omega^2}(a-X_0)}, & X_0 > a. \end{cases}$$

In the above equation, it should be noted that we have imposed

$$\partial_2 B = 0, \tag{2.2.22}$$

as previously discussed.

The solvability condition for the first harmonic gives

$$D_2 B = k_1 B|B|^2 i, \tag{2.2.23}$$

where

$$k_1 = \frac{\left(3 - 7\,\omega^4 - 2\,\omega^6 - 2\,\omega^2 + 6\,\sqrt{1-\omega^4}\,\tan^{-1}\left(\sqrt{\frac{1-\omega^2}{1+\omega^2}}\right)\right)}{32\,\omega\,\left(1 + \omega^2 + \sqrt{1-\omega^4}\,\tan^{-1}\left(\sqrt{\frac{1-\omega^2}{1+\omega^2}}\right)\right)}. \tag{2.2.24}$$

We can write the solution of the Equation (2.2.23) is

$$B = e^{i(k_1 T_2 + C(T_3,\ldots,X_3,\ldots))}, \tag{2.2.25}$$

but this solution is purely oscillatory. In order to determine the stability, we need to go to higher orders. We do not solve further the solvability conditions individually, as solving the individual equations repeated at the different scales does not work because the equations cover more than one time scale. We will combine the slow time scale equations (solvability conditions) before solving them.

The solution for the first harmonic is then given by

$$\phi_3^{(1)}(X_0, T_0) = B|B|^2 \begin{cases} v_1(X_0), & X_0 < -a, \\ v_2(X_0), & |X_0| < a, \\ v_3(X_0), & X_0 > a, \end{cases} \tag{2.2.26}$$

where

$$\begin{aligned} v_1(X_0) &= C_{31} e^{\sqrt{1-\omega^2}X_0} - \frac{\sqrt{2\,(1+\omega^2)}\left(k_{31} e^{2\sqrt{1-\omega^2}X_0} - \widetilde{k}_{31}\right) e^{\sqrt{1-\omega^2}X_0}}{64\,\omega\,\sqrt{1-\omega^2}\,u_1}, \\ v_2(X_0) &= C_{32}\mathrm{Re}(e^{i\sqrt{1+\omega^2}X_0}) - \frac{\widetilde{k}_{32}\mathrm{Re}(e^{i\sqrt{1+\omega^2}X_0}) - k_{32}\mathrm{Im}(e^{i\sqrt{1+\omega^2}X_0})}{16\,\sqrt{1+\omega^2}u_2}, \\ v_3(X_0) &= C_{33} e^{-\sqrt{1-\omega^2}X_0} - \frac{\left(k_{33} e^{2\sqrt{1-\omega^2}X_0} - \widetilde{k}_{33}\right) e^{-\sqrt{1-\omega^2}X_0}}{32\,\sqrt{(2-\omega^2)(1-\omega^2)}\,u_1}, \end{aligned}$$

with

$$u_1 = 1 + \omega^2 + \sqrt{1-\omega^4}\,\tan^{-1}\left(\sqrt{\frac{1-\omega^2}{1+\omega^2}}\right), \tag{2.2.27}$$

$$u_2 = \omega^2 + \sqrt{1-\omega^4}\,\tan^{-1}\left(\sqrt{1-\omega^4}\right). \tag{2.2.28}$$

Expressions for the functions k_{3j} and $\widetilde{k}_{3j}$, $j = 1,2,3$, are given in (2.A.1)–(2.A.6). The coefficients $C_{31} = C_{32}$ and C_{33} are constants of integration that should be determined from the continuity conditions at $X_0 = \pm a$.

We do not consider the equation for the second harmonic $\phi_3^{(2)}$, as it does not appear in the leading order of the sought-after asymptotic equation describing the behavior of breathing mode amplitude.

The equation for the third harmonic $\phi_3^{(3)}$ is

$$\partial_0^2\phi_3^{(3)} - \left(\cos(\theta) - 9\omega^2\right)\phi_3^{(3)} = \begin{cases} -\frac{1}{6}\cos^3(\sqrt{1+\omega^2}a)e^{3\sqrt{1-\omega^2}(a+X_0)}, & X_0 < -a, \\ \frac{1}{6}\cos^3(\sqrt{1+\omega^2}X_0), & |X_0| < a, \\ -\frac{1}{6}\cos^3(\sqrt{1+\omega^2}a)e^{3\sqrt{1-\omega^2}(a-X_0)}, & X_0 > a, \end{cases}$$

whose solution, using the same procedure as above, is given by

$$\phi_3^{(3)}(X_0,T_0) = B^3 \begin{cases} P_{31}(X_0), & X_0 < -a, \\ P_{32}(X_0), & |X_0| < a, \\ P_{33}(X_0), & X_0 > a, \end{cases} \tag{2.2.29}$$

where

$$\begin{aligned} P_{31}(X_0) &= \widetilde{C}_{31}e^{\sqrt{1-9\,\omega^2}X_0} - \frac{1}{48}\cos^3\left(a\sqrt{1+\omega^2}\right)e^{3\sqrt{1-\omega^2}(a+X_0)}, \\ P_{32}(X_0) &= \widetilde{C}_{32}\cos(\sqrt{1+9\,\omega^2}X_0) - \frac{1}{192\,\omega^2}\left(\omega^2-3\right)\cos\left(X_0\sqrt{1+\omega^2}\right), \\ P_{33}(X_0) &= \widetilde{C}_{33}e^{-\sqrt{1-9\,\omega^2}X_0} - \frac{1}{48}\cos^3\left(a\sqrt{1+\omega^2}\right)e^{3\sqrt{1-\omega^2}(a-X_0)}, \end{aligned}$$

and $\widetilde{C}_{31}$, $\widetilde{C}_{32}$, and $\widetilde{C}_{33}$ are nonzero constants of integration that also are determined from the continuity conditions at the discontinuity points.

Note that due to the assumption (2.2.20), the second term in $P_{31}(X_0)$ and $P_{33}(X_0)$ will decay to zero. With the assumption (2.2.20), we see that $e^{3i\omega T_0}\phi_3^{(3)} + c.c.$ describes the left moving radiation for $X_0 < -a$ and right moving radiation for $X_0 > a$, which are responsible for energy loss in the final amplitude equation.

2.2.3 Equation at $\mathcal{O}(\epsilon^4)$

Solving equation at $\mathcal{O}(\epsilon^4)$,

$$\begin{aligned} \partial_0^2\phi_4 - D_0^2\phi_4 - \cos(\theta+\phi_0)\phi_4 &= 2\left(D_0D_1 - \partial_0\partial_1\right)\phi_3 + 2\left(D_1D_2 + D_0D_3\right)\phi_1 \\ &\quad -2\left(\partial_1\partial_2 + \partial_0\partial_3\right)\phi_1, \end{aligned} \tag{2.2.30}$$

from the solvability condition

$$D_3B = 0, \quad \partial_3B = 0, \tag{2.2.31}$$

and hence we impose

$$\phi_4 \;=\; 0, \tag{2.2.32}$$

which is similar to the case of ϕ_2.

2.2.4 Equation at $\mathcal{O}(\epsilon^5)$

Equating terms at $\mathcal{O}(\epsilon^5)$ gives the equation

$$\begin{aligned}\partial_0^2\phi_5 - D_0^2\phi_5 - \phi_5\cos\theta \;=\;& 2(D_0D_4 - \partial_0\partial_4)\phi_1 + 2(D_3D_1 - \partial_3\partial_1)\phi_1 \\ &+(D_2^2 - \partial_2^2)\phi_1 + \;(D_1^2 - \partial_1^2)\phi_3 + 2(D_2D_0 - \partial_2\partial_0)\phi_3 \\ &+\left(-\frac{1}{2}\,\phi_1^2\phi_3 + \frac{1}{120}\phi_1^5\right)\cos(\theta)\,.\end{aligned} \tag{2.2.33}$$

Having calculated the right-hand side using the known functions, we again split the solution into components proportional to simple harmonics, as we did before. The equation for the first harmonic is given by

$$\partial_0^2\phi_5^{(1)} - \left(\cos\theta - \omega^2\right)\phi_5^{(1)} \;=\; \begin{cases} G_1, & X_0 < -a, \\ G_2, & |X_0| < a, \\ G_3, & X_0 > a, \end{cases} \tag{2.2.34}$$

where

$$\begin{aligned} G_1 \;=\;& 2\,i\omega\,D_4B\cos\left(a\sqrt{1+\omega^2}\right)e^{\sqrt{1-\omega^2}(a+X_0)} \\ &-B|B|^4\Big[{k_1}^2\cos\left(a\sqrt{1+\omega^2}\right)e^{\sqrt{1-\omega^2}(a+X_0)} + 2\omega k_1 v_1(X_0) \\ &+\frac{1}{2}\,\cos^2\left(a\sqrt{1+\omega^2}\right)e^{2\sqrt{1-\omega^2}(a+X_0)}(3v_1(X_0) + P_{31}(X_0)) \\ &-\frac{1}{12}\,\cos^5\left(a\sqrt{1+\omega^2}\right)e^{5\sqrt{1-\omega^2}(a+X_0)}\Big], \\ G_2 \;=\;& 2\,i\omega\,D_4B\cos\left(X_0\sqrt{1+\omega^2}\right) - B|B|^4\Big[{k_1}^2\cos\left(X_0\sqrt{1+\omega^2}\right) + 2\omega k_1 v_2(X_0) \\ &-\frac{1}{2}\,\cos^2\left(X_0\sqrt{1+\omega^2}\right)(3\,v_2(X_0) + P_{32}(X_0)) + \frac{1}{12}\,\cos^5\left(X_0\sqrt{1+\omega^2}\right)\Big], \\ G_3 \;=\;& 2\,i\omega\,D_4B\cos\left(a\sqrt{1+\omega^2}\right)e^{\sqrt{1-\omega^2}(a-X_0)} \\ &-B|B|^4\Big[{k_1}^2\cos\left(a\sqrt{1+\omega^2}\right)e^{\sqrt{1-\omega^2}(a-X_0)} + 2\omega k_1 v_3(X_0) \\ &+\frac{1}{2}\,\cos^2\left(a\sqrt{1+\omega^2}\right)e^{2\sqrt{1-\omega^2}(a-X_0)}(3\,v_3(X_0) + P_{33}(X_0)) \\ &-\frac{1}{12}\,\cos^5\left(a\sqrt{1+\omega^2}\right)e^{5\sqrt{1-\omega^2}(a-X_0)}\Big]. \end{aligned}$$

Here, $v_1(X_0)$, $v_2(X_0)$, $v_3\,(X_0)$ are the bounded solutions of $\phi_3^{(1)}(X_0, T_0)$, and $P_{31}(X_0)$, $P_{32}(X_0)$, $P_{33}(X_0)$ are the bounded solutions of $\phi_3^{(3)}(X_0, T_0)$ as solved above.

The solvability condition of (2.2.34) is

$$D_4 B = k_2 B|B|^4, \tag{2.2.35}$$

where

$$k_2 = -\frac{\Upsilon_2\, i}{2\omega\Psi(\omega)}, \tag{2.2.36}$$

$$\begin{aligned}
\Upsilon_2 &= k_1^2\Psi(\omega) + 2\omega k_1\zeta + \alpha + \beta + \gamma, \\
\Psi(\omega) &= \frac{\left(\sqrt{1+\omega^2} + \sqrt{1-\omega^2}\tan^{-1}\left(\sqrt{\frac{1-\omega^2}{1+\omega^2}}\right)\right)}{\sqrt{1-\omega^4}},
\end{aligned}$$

$$\begin{aligned}
\zeta &= \int_{-\infty}^{-a} v_1(X_0)\cos\left(a\sqrt{1+\omega^2}\right) e^{\sqrt{1-\omega^2}(a+X_0)} dX_0 \\
&\quad + \int_{-a}^{a} v_2(X_0)\cos\left(X_0\sqrt{1+\omega^2}\right) dX_0 \\
&\quad + \int_{a}^{\infty} v_3(X_0)\cos\left(a\sqrt{1+\omega^2}\right) e^{\sqrt{1-\omega^2}(a-X_0)} dX_0, \\
\alpha &= \frac{1}{2}\int_{-\infty}^{-a} (3\,v_1(X_0) + P_{31}(X_0))\cos^3\left(a\sqrt{1+\omega^2}\right) e^{3\sqrt{1-\omega^2}(a+X_0)} dX_0 \\
&\quad - \frac{\cos^6(a\sqrt{1+\omega^2})}{72\sqrt{1-\omega^2}},
\end{aligned}$$

$$\begin{aligned}
\beta &= -\frac{1}{2}\int_{-a}^{a} (3\,v_2(X_0) + P_{32}(X_0))\cos^3\left(X_0\sqrt{1+\omega^2}\right) dX_0 \\
&\quad + \frac{1}{12}\int_{-a}^{a} \cos^6\left(X_0\sqrt{1+\omega^2}\right) dX_0, \\
\gamma &= \frac{1}{2}\int_{a}^{\infty} (3\,v_3\,(X_0) + P_{33}(X_0))\cos^3\left(a\sqrt{1+\omega^2}\right) e^{3\sqrt{1-\omega^2}(a-X_0)} dX_0 \\
&\quad - \frac{\cos^6(a\sqrt{1+\omega^2})}{72\sqrt{1-\omega^2}}.
\end{aligned}$$

We postpone the continuation of the perturbation expansion to higher orders, as we have obtained the decaying oscillatory behavior of the breathing amplitude (2.2.23) and (2.2.35), which is our main objective.

2.2.5 Amplitude equation

By noting that

$$\frac{dB}{dt} = \epsilon D_1 B + \epsilon^2 D_2 B + \epsilon^3 D_3 B + \epsilon^4 D_4 B + \ldots, \tag{2.2.37}$$

and defining $b = \epsilon B$, so that b is the natural amplitude of the breathing mode, i.e. the small amplitude one would actually measure. we combine (2.2.15), (2.2.23), (2.2.31), and (2.2.35) to obtain

$$\frac{db}{dt} = k_1 b|b|^2 i + k_2 b|b|^4 + \mathcal{O}(\epsilon^6). \tag{2.2.38}$$

It should be noted that k_1 is real number and b, k_2 are complex numbers. Since we know that

$$\frac{\partial|b|^2}{\partial t} = \frac{\partial(bb^*)}{\partial t} = b\frac{\partial b^*}{\partial t} + b^*\frac{\partial b}{\partial t}, \tag{2.2.39}$$

where b^* denotes the complex conjugate of b. We express the amplitude equation in terms of unscaled variables:

$$\frac{\partial|b|^2}{\partial t} = 2\mathrm{Re}(k_2)|b|^6. \tag{2.2.40}$$

One can calculate that the solution of (2.2.40) satisfies the relation

$$|b(t)| = \left(\frac{|b(0)|^4}{1 - 4\,\mathrm{Re}\,(k_2)\,|b(0)|^4 t}\right)^{1/4}, \tag{2.2.41}$$

where $b(0)$ is the initial amplitude of oscillation. The value of k_2 is given by Equation (2.2.36). Calculating the real part of k_2 numerically, one obtains that $\mathrm{Re}(k_2) < 0$ for all values of $a < \pi/4$. This equation describes the gradual decrease in the amplitude of the breathing mode with order $\mathcal{O}(t^{-1/4})$ as it emits energy in the form of radiation.

Remark 1. *The $\mathcal{O}\left(t^{-1/4}\right)$ decay of the oscillation amplitude is because of our assumption (2.2.20). If one has $(3\omega)^2 < 1$ instead, then the decay rate will be smaller than $\mathcal{O}\left(t^{-1/4}\right)$, as the coefficient k_2 in (2.2.35) would be purely imaginary.*

This leads us to the following conjecture

Conjecture 1. *If $n \geq 3$ is an odd integer such that*

$$1/(n-2)^2 > \omega^2 > 1/n^2,$$

then the decay rate of the breathing mode oscillation in $0 - \pi - 0$ Josephson junctions with $a < \pi/4$ is of order $\mathcal{O}(t^{-1/(n+1)})$.

This conjecture implies that the closer the eigenfrequency ω is to zero, i.e., $a \to \pi/4$, the longer the lifetime of the breathing mode oscillation.

2.3 Driven breathing mode in a $0-\pi-0$ junction

We now consider breathing mode oscillations in a $0-\pi-0$ junction in the presence of external driving with frequency near the natural breathing frequency of the mode, i.e., (2.1.2) and (2.1.3) with $h \neq 0$ and $\Omega = \omega(1+\rho)$.

By rescaling the time $\Omega t = \omega\tau$, (2.1.2) becomes

$$\phi_{xx}(x,\tau) - (1+\rho)^2\phi_{\tau\tau}(x,\tau) \quad = \quad \sin(\phi+\theta) + \frac{1}{2}h\left(e^{i\omega\tau} + c.c.\right). \tag{2.3.1}$$

Here, we use the driving amplitude and frequency are very small, namely,

$$h = \epsilon^3 H,\ \rho = \epsilon^3 R, \tag{2.3.2}$$

with $H, R \sim \mathcal{O}(1)$. Other scaling for h and ρ can also be consider (see section 2.5). Due to the time rescaling above, our slow temporal variables are now defined as

$$X_n = \epsilon^n x, \quad T_n = \epsilon^n \tau, \quad n = 0, 1, 2, \ldots. \tag{2.3.3}$$

In this case, we still use the shorthand notation (2.2.3), though the time is rescalled slightly $\tau/1+\rho$. Performing a perturbation expansion order by order as before, one obtains the same perturbation expansion up to and including $\mathcal{O}(\epsilon^2)$ as in the undriven case above.

2.3.1 Equation at $\mathcal{O}(\epsilon^3)$

At third order, we obtain

$$\begin{aligned}\partial_0^2\phi_3 - D_0^2\phi_3 - \cos(\theta)\phi_3 \quad = \quad & (D_1^2 - \partial_1^2)\phi_1 + 2(D_0D_2 - \partial_0\partial_2)\phi_1 + 2RD_0^2\phi_0 \\ & -\frac{1}{6}\phi_1^3\cos(\theta) + \frac{1}{2}H\left(e^{i\omega\tau} + c.c.\right).\end{aligned} \tag{2.3.4}$$

The only difference from the undriven case is the presence of a harmonic drive in the last term.

The first harmonic component of the above equation gives us the solvability condition

$$D_2B \quad = \quad k_1 B|B|^2\, i + l_1 H\, i, \tag{2.3.5}$$

where

$$l_1 \quad = \quad \frac{\sqrt{1+\omega^2}}{\sqrt{2}\,\omega\left(1+\omega^2+\sqrt{1-\omega^4}\tan^{-1}\left(\sqrt{\frac{1-\omega^2}{1+\omega^2}}\right)\right)}, \tag{2.3.6}$$

and k_1 is as given by (2.2.24). The solution for the first harmonic can be readily obtained as

$$\phi_3^{(1)} = \begin{cases} B|B|^2 v_1(X_0) + H\widetilde{v_1}(X_0), & X_0 < -a, \\ B|B|^2 v_2(X_0) + H\widetilde{v_2}(X_0), & |X_0| < a, \\ B|B|^2 v_3(X_0) + H\widetilde{v_3}(X_0), & X_0 > a, \end{cases}$$

where

$$\begin{aligned} \widetilde{v_1}(X_0) &= \widetilde{\aleph}_{31} e^{\sqrt{1-\omega^2}X_0} - \frac{\sqrt{1+\omega^2}\,(1-\omega^2)\tan^{-1}\left(\sqrt{\frac{1-\omega^2}{1+\omega^2}}\right)}{2\,(1-\omega^2)^{3/2}\,u_1} \\ &\quad + \frac{e^{u+X_0}\left((\omega^4-1)X_0 + \sqrt{1-\omega^2}(1+\omega^2)\right) - 2\sqrt{1-\omega^2}(1+\omega^2)}{4\,(1-\omega^2)^{3/2}\,u_1}, \\ \widetilde{v_2}(X_0) &= \widetilde{\aleph}_{32}\mathrm{Re}(e^{i\sqrt{1+\omega^2}X_0}) + \frac{1}{2\,(1+\omega^2)} \\ &\quad - \frac{\sqrt{1+\omega^2}X_0\mathrm{Im}\,(e^{i\sqrt{1+\omega^2}X_0}) + \mathrm{Re}(e^{i\sqrt{1+\omega^2}X_0})}{\sqrt{2}\,\sqrt{1+\omega^2}\,u_2}, \end{aligned}$$

$$\begin{aligned} \widetilde{v_3}(X_0) &= \widetilde{\aleph}_{33} e^{-\sqrt{1-\omega^2}X_0} - \frac{\tan^{-1}\left(\sqrt{\frac{1-\omega^2}{1+\omega^2}}\right)}{2\,u_1} \\ &\quad + \frac{e^{-\sqrt{1-\omega^2}X_0}((e^u - 2e^{\sqrt{1-\omega^2}X_0})\sqrt{1-\omega^2}(1+\omega^2) + 2\,e^u X_0(1-\omega^4))}{4\,(1-\omega^2)^{3/2}\,u_1}, \end{aligned}$$

with $u = \sqrt{1-\omega^2}\tan^{-1}(\frac{\sqrt{1-\omega^4}}{1+\omega^2})$. The values of u_1, u_2 are given in Equations (2.2.27)–(2.2.28). The constants of integration $\widetilde{\aleph}_{31} = \widetilde{\aleph}_{33}$ and $\widetilde{\aleph}_{32}$ are determined by applying the continuity conditions at the discontinuity points. The terms in ϕ_3^1 (see $\widetilde{v_1}(X_0) - -\widetilde{v_3}(X_0)$) proportional to driving amplitude (H) are independent of X_0. We therefore see that leading order driving term enters the equation. (the leading order driving also appears at $\mathcal{O}(\epsilon^5)$). We expect that, this leads the system to a non-zero constant amplitude, over the fast time scale as $t \to \infty$.

One can check that the solution for the third harmonic $\phi_3^{(3)}(X_0, T_0)$, as well as $\phi_3^{(2)}$, is the same as in the undriven case.

2.3.2 Equation at $\mathcal{O}(\epsilon^4)$

The equation at $\mathcal{O}(\epsilon^4)$ is

$$\begin{aligned} \partial_0^2\phi_4 - D_0^2\phi_4 - \cos(\theta+\phi_0)\,\phi_4 &= 2\,(D_0D_1 - \partial_0\partial_1)\,\phi_3 + 2\,(D_1D_2 + D_0D_3)\,\phi_1 \\ &\quad -2\,(\partial_1\partial_2 + \partial_0\partial_3)\,\phi_1 + 2\,RD_0^2\phi_1, \end{aligned} \tag{2.3.7}$$

with the solvability condition

$$D_3 B \;=\; -i\,\omega\, B\, R. \tag{2.3.8}$$

This implies that

$$\phi_4(X_0, T_0) \;=\; 0, \tag{2.3.9}$$

as for the case of ϕ_2.

2.3.3 Equation at $\mathcal{O}(\epsilon^5)$

At $\mathcal{O}(\epsilon^5)$, we obtain

$$\begin{aligned}\partial_0^2\phi_5 - D_0^2\phi_5 - \phi_5\cos(\theta) \;=\;& 2(D_0D_4 - \partial_0\partial_4)\phi_1 + 2(D_3D_1 - \partial_3\partial_1)\phi_1 + 4RD_0D_1\phi_1\\ &+(D_2^2 - \partial_2^2)\phi_1 + (D_1^2 - \partial_1^2)\phi_3 + 2(D_2D_0 - \partial_2\partial_0)\phi_3\\ &-\left(\frac{1}{2}\,\phi_1^2\phi_3 - \frac{1}{120}\phi_1^5\right)\cos(\theta) + 2R\,D_0^2\phi_2. \end{aligned}\tag{2.3.10}$$

Evaluating the right-hand side, we again split the solution into components proportional to simple harmonics as we did before. For the first harmonic, we obtain that

$$\partial_0^2\phi_5^{(1)} - \left(\cos\theta - \omega^2\right)\phi_5^{(1)} \;=\; \begin{cases} M_1, & X_0 < -a,\\ M_2, & |X_0| < a,\\ M_3, & X_0 > a, \end{cases} \tag{2.3.11}$$

where

$$\begin{aligned} M_1 \;=\;& \left(2\,i\omega\,D_4B - {k_1}^2B|B|^4 - k_1l_1|B|^2H\right)\cos\left(a\sqrt{1+\omega^2}\right)e^{\sqrt{1-\omega^2}(a+X_0)}\\ &-2\,\omega\,\left(k_1B|B|^4 + l_1|B|^2H\right)v_1(X_0) + \frac{1}{12}\,B|B|^4\cos^5\left(a\sqrt{1+\omega^2}\right)e^{5\sqrt{1-\omega^2}(a+X_0)}\\ &-\frac{1}{2}\,B|B|^4\left(3\,v_1\left(X_0\right) + P_{31}\left(X_0\right)\right)\cos^2\left(a\sqrt{1+\omega^2}\right)e^{2\sqrt{1-\omega^2}(a+X_0)}\\ &-\frac{1}{2}\,H\left(2\,|B|^2 + B^2\right)\widetilde{v}_1\left(X_0\right)\cos^2\left(a\sqrt{1+\omega^2}\right)e^{2\sqrt{1-\omega^2}(a+X_0)},\\ M_2 \;=\;& \left(2\,i\omega\,D_4B - {k_1}^2B|B|^4 - k_1l_1|B|^2H\right)\cos\left(X_0\sqrt{1+\omega^2}\right)\\ &-2\,\omega\,\left(k_1B|B|^4 + l_1|B|^2H\right)v_2\left(X_0\right) - \frac{1}{12}\,B|B|^4\cos^5\left(X_0\sqrt{1+\omega^2}\right)\\ &+\frac{1}{2}\,B|B|^4\left(3\,v_2\left(X_0\right) + P_{32}\left(X_0\right)\right)\cos^2\left(X_0\sqrt{1+\omega^2}\right)\\ &+\frac{1}{2}\,H\left(2\,|B|^2 + B^2\right)\widetilde{v_2}(X_0)\cos^2\left(X_0\sqrt{1+\omega^2}\right),\\ M_3 \;=\;& \left(2\,i\omega\,D_4B - {k_1}^2B|B|^4 - k_1l_1|B|^2H\right)\cos\left(a\sqrt{1+\omega^2}\right)e^{\sqrt{1-\omega^2}(a-X_0)}\\ &-2\,\omega\,\left(k_1B|B|^4 + l_1|B|^2H\right)v_3(X_0) + \frac{1}{12}\,B|B|^4\cos^5\left(a\sqrt{1+\omega^2}\right)e^{5\sqrt{1-\omega^2}(a-X_0)}\\ &-\frac{1}{2}\,B|B|^4\left(3\,v_3(X_0) + P_{33}(X_0)\right)\cos^2\left(a\sqrt{1+\omega^2}\right)e^{2\sqrt{1-\omega^2}(a-X_0)}\\ &-\frac{1}{2}\,H\left(2\,|B|^2 + B^2\right)\widetilde{v}_3(X_0)\cos^2\left(a\sqrt{1+\omega^2}\right)e^{2\sqrt{1-\omega^2}(a-X_0)}. \end{aligned}$$

The solvability condition for (2.3.11) is

$$D_4 B = k_2\, B|B|^4 + \left(l_2|B|^2 + l_3 B^2\right) Hi, \tag{2.3.12}$$

where l_1 is given by (2.3.6) and

$$\begin{aligned}
l_2 &= \frac{\Upsilon_{3,1}}{2\omega\Psi(\omega)},\ l_3 = \frac{\Upsilon_{3,2}}{2\omega\Psi(\omega)},\\
\Upsilon_{3,1} &= k_1 l_1 \Psi(\omega) + 2\omega l_1 \zeta + 2\left(\alpha_2 + \beta_2 + \gamma_2\right),\\
\Upsilon_{3,2} &= \alpha_2(X_0) + \beta_2(X_0) + \gamma_2(X_0),\\
\alpha_2 &= \frac{1}{2}\int_{-\infty}^{-a} \widetilde{v_1}(X_0)\cos^3\left(a\sqrt{1+\omega^2}\right) e^{3\sqrt{1-\omega^2}(a+X_0)} dX_0,\\
\beta_2 &= -\frac{1}{2}\int_{-a}^{a} \widetilde{v_2}(X_0)\cos^3\left(X_0\sqrt{1+\omega^2}\right) dX_0,\\
\gamma_2 &= \frac{1}{2}\int_{a}^{\infty} \widetilde{v_3}(X_0)\cos^3\left(a\sqrt{1+\omega^2}\right) e^{3\sqrt{1-\omega^2}(a-X_0)} dX_0.
\end{aligned}$$

So far we have obtained the sought-after leading order behavior of the breathing amplitude. Performing the same calculation as in (2.2.40), we obtain the governing dynamics of the oscillation amplitude in the presence of an external drive

$$\frac{\omega}{\Omega}\frac{db}{dt} = k_1 b|b|^2 i + k_2\, b|b|^4 + l_1 hi + \left(l_2|b|^2 + l_3 b^2\right) hi - i\,\omega\, b\,\rho + \mathcal{O}(\epsilon^6). \tag{2.3.13}$$

From Equation (2.3.13), one can deduce that a nonzero external driving can induce a breathing dynamic. It is expected that for large t, there will be a balance between the external drive and the radiation damping.

2.4 Freely oscillating breathing mode in a $0-\kappa$ junction

In this section, we consider (2.1.2) with θ given by (2.1.4), describing the dynamics of the Josephson phase in the $0-\kappa$ long Josephson junction.

By applying the method of multiple scales and the perturbation expansion as before to the governing equation, we obtain from the leading order $\mathcal{O}(1)$ and $\mathcal{O}(\epsilon)$ that

$$\phi_0 = \Phi_0(X_0), \quad \phi_1 = B(X_1\ldots, T_1\ldots)\Phi_1(X_0, T_0) + c.c., \tag{2.4.1}$$

where $B(X_1\ldots, T_1\ldots)$ is the amplitude of wobbling mode, depends on slow time and space variables. The value of Φ_0 and Φ_1 are given by (2.1.10) and (2.1.11), respectively.

2.4.1 Correction at $\mathcal{O}(\epsilon^2)$

Using the fact that ϕ_0 is a function of X_0 only, the equation at $\mathcal{O}(\epsilon^2)$ is

$$\partial_0^2\phi_2 - D_0^2\phi_2 - \cos(\theta+\phi_0)\phi_2 = 2D_0D_1\phi_1 - 2\partial_0\partial_1\phi_1 - \frac{1}{2}\phi_1^2\sin(\theta+\phi_0). \tag{2.4.2}$$

After a simple algebraic calculation, one can recognize the right-hand side consists of functions with frequencies 0, ω, and 2ω. Therefore, solutions to the above equation can be written as

$$\phi_2 = \phi_2^{(0)} + \phi_2^{(1)} e^{i\omega T_0} + c.c. + \phi_2^{(2)} e^{2i\omega T_0} + c.c., \tag{2.4.3}$$

which implies that $\phi_2^{(0)}$, $\phi_2^{(1)}$, and $\phi_2^{(2)}$ respectively satisfy the inhomogeneous equations in the regions $X_0 < 0$ and $X_0 > 0$

$$\begin{aligned}
&\Big(\partial_0^2 - \cos(\theta + \phi_0)\Big)\phi_2^{(0)} \\
&\quad = -|B|^2 \begin{cases} e^{2\sqrt{1-\omega^2}(x_0+X_0)}\Big[\tanh(x_0+X_0) - \sqrt{1-\omega^2}\Big]^2 \sin(\phi_0), & X_0 < 0, \\ e^{2\sqrt{1-\omega^2}(x_0-X_0)}\Big[\tanh(x_0-X_0) - \sqrt{1-\omega^2}\Big]^2 \sin(\phi_0 - \kappa), & X_0 > 0, \end{cases}
\end{aligned}$$

$$\begin{aligned}
&\Big(\partial_0^2 + \omega^2 - \cos(\theta + \phi_0)\Big)\phi_2^{(1)} \\
&\quad = \begin{cases} 2\Big[\Big(i\omega D_1 B - \partial_1 B\sqrt{1-\omega^2}\Big)\Big(\tanh(x_0+X_0) - \sqrt{1-\omega^2}\Big) \\ \quad -\partial_1 B \operatorname{sech}^2(x_0+X_0)\Big] e^{\sqrt{1-\omega^2}(x_0+X_0)}, & X_0 < 0, \\ 2\Big[\Big(i\omega D_1 B + \partial_1 B\sqrt{1-\omega^2}\Big)\Big(\tanh(x_0-X_0) - \sqrt{1-\omega^2}\Big) \\ \quad +\partial_1 B \operatorname{sech}^2(x_0-X_0)\Big] e^{\sqrt{1-\omega^2}(x_0-X_0)}, & X_0 > 0, \end{cases} \\
&\Big(\partial_0^2 + 4\omega^2 - \cos(\theta + \phi_0)\Big)\phi_2^{(2)} \\
&\quad = -\frac{B^2}{2} \begin{cases} e^{2\sqrt{1-\omega^2}(x_0+X_0)}\Big[\tanh(x_0+X_0) - \sqrt{1-\omega^2}\Big]^2 \sin(\phi_0), & X_0 < 0, \\ e^{2\sqrt{1-\omega^2}(x_0-X_0)}\Big[\tanh(x_0-X_0) - \sqrt{1-\omega^2}\Big]^2 \sin(\phi_0 - \kappa), & X_0 > 0. \end{cases}
\end{aligned}$$

By using arguments as in the preceding sections, we set

$$D_1 B = 0, \quad \partial_1 B = 0.$$

Hence, we find that $\phi_2^{(1)}(X_0, T_0) = 0$.

The solutions for the other harmonics are

$$\phi_2^{(0)} = |B|^2 \begin{cases} E_0(X_0), & X_0 < 0, \\ \widetilde{E}_0(X_0), & X_0 > 0, \end{cases} \tag{2.4.4}$$

$$\phi_2^{(2)} = B^2 \begin{cases} E_2(X_0), & X_0 < 0, \\ \widetilde{E}_2(X_0), & X_0 > 0, \end{cases} \tag{2.4.5}$$

where $E_0(X_0)$, $\widetilde{E}_0(X_0)$, $E_2(X_0)$, and $\widetilde{E}_2(X_0)$ are as given by (2.A.7)–(2.A.10). C_{01}, C_{02}, C_{21}, and C_{22} are constants of integration that should be found by applying a continuity condition at the point of discontinuity $X_0 = 0$.

In the following, we will assume that the harmonic 2ω is in the continuous spectrum, that is,

$$4\omega^2 > 1. \tag{2.4.6}$$

With this assumption, $\phi_2^{(2)}(X_0, T_0)$ will not decay in space, and $e^{2i\omega T_0}\phi_2^{(2)}(X_0, T_0) + c.c.$ describes right–moving radiation for positive X_0 and left moving radiation for negative X_0.

2.4.2 Correction at $\mathcal{O}(\epsilon^3)$

Equating the terms at $\mathcal{O}(\epsilon^3)$ gives the equation

$$\begin{aligned}\partial_0^2\phi_3 - D_0^2\phi_3 - \cos(\theta+\phi_0)\phi_3 &= (2D_0D_2 - 2\partial_0\partial_2)\phi_1 + (D_1^2 - \partial_1^2)\phi_1 \\ &\quad + (2D_0D_1 - 2\partial_0\partial_1)\phi_2 - \phi_1\phi_2\sin(\theta+\phi_0) \\ &\quad -\frac{1}{6}\phi_1^3\cos(\theta+\phi_0),\end{aligned} \tag{2.4.7}$$

where we have used the fact that ϕ_0 depends only on X_0. Having calculated the right-hand side using the known functions ϕ_0, ϕ_1, and ϕ_2, we again split the solution into components proportional to the harmonics of the right-hand side. Specifically for the first harmonic, we have

$$\left(\partial_0^2 + \omega^2 - \cos(\theta+\phi_0)\right)\phi_3^{(1)} = \begin{cases} L_1, & X_0 < 0, \\ L_2, & X_0 > 0, \end{cases} \tag{2.4.8}$$

where

$$\begin{aligned}L_1 &= 2i\omega\, D_2B\left[\tanh(x_0+X_0) - \sqrt{1-\omega^2}\right]e^{\sqrt{1-\omega^2}(x_0+X_0)} \\ &\quad -B|B|^2\left(E_0(X_0)+E_2(X_0)\right)\sin(\phi_0)\left[\tanh(x_0+X_0) - \sqrt{1-\omega^2}\right]e^{\sqrt{1-\omega^2}(x_0+X_0)} \\ &\quad -\frac{1}{2}B|B|^2\cos(\phi_0)\left[\tanh(x_0+X_0) - \sqrt{1-\omega^2}\right]^3 e^{3\sqrt{1-\omega^2}(x_0+X_0)},\end{aligned}$$

$$\begin{aligned}L_2 &= 2i\omega\, D_2B\left[\tanh(x_0-X_0) - \sqrt{1-\omega^2}\right]e^{\sqrt{1-\omega^2}(x_0-X_0)} \\ &\quad -B|B|^2\left(\widetilde{E}_0(X_0)+\widetilde{E}_2(X_0)\right)\sin(\phi_0-\kappa)\left[\tanh(x_0-X_0) - \sqrt{1-\omega^2}\right]e^{\sqrt{1-\omega^2}(x_0-X_0)} \\ &\quad -\frac{1}{2}B|B|^2\cos(\phi_0-\kappa)\left[\tanh(x_0-X_0) - \sqrt{1-\omega^2}\right]^3 e^{3\sqrt{1-\omega^2}(x_0-X_0)}.\end{aligned}$$

The solvability condition of the equation will give us

$$D_2B = m_1B|B|^2, \tag{2.4.9}$$

where

$$m_1 = -\frac{\Upsilon i}{\Psi_1(\omega)}, \tag{2.4.10}$$

and

$$
\begin{aligned}
\Upsilon &= \int_{-\infty}^{0} f_1(X_0)dX_0 + \int_{0}^{\infty} f_2(X_0)dX_0 + \frac{1}{2}\int_{-\infty}^{0} f_3(X_0)dX_0 + \frac{1}{2}\int_{0}^{\infty} f_4(X_0)dX_0,\\
\Psi_1(\omega) &= \frac{2\,\omega\, e^{2\sqrt{1-\omega^2}x_0}\left(2\sqrt{1-\omega^2}+2-\omega^2-e^{2x_0}\left(2\sqrt{1-\omega^2}+\omega^2-2\right)\right)}{\sqrt{1-\omega^2}(1+e^{2x_0})},\\
f_1(X_0) &= -2\left(E_0(X_0)+E_2(X_0)\right)\operatorname{sech}\left(x_0+X_0\right)\tanh(x_0+X_0)\\
&\quad\times\left[\tanh\left(x_0+X_0\right)-\sqrt{1-\omega^2}\right]^2 e^{2\sqrt{1-\omega^2}(x_0+X_0)},\\
f_2(X_0) &= 2\left(\widetilde{E}_0(X_0)+\widetilde{E}_2(X_0)\right)\operatorname{sech}\left(x_0-X_0\right)\tanh(x_0-X_0)\\
&\quad\times\left[\tanh(x_0-X_0)-\sqrt{1-\omega^2}\right]^2 e^{2\sqrt{1-\omega^2}(x_0-X_0)},\\
f_3(X_0) &= \left[\tanh\left(x_0+X_0\right)-\sqrt{1-\omega^2}\right]^4(1-2\operatorname{sech}^2(x_0+X_0))e^{4\sqrt{1-\omega^2}(x_0+X_0)},\\
f_4(X_0) &= \left[\tanh\left(x_0-X_0\right)-\sqrt{1-\omega^2}\right]^4(1-2\operatorname{sech}^2(x_0-X_0))e^{4\sqrt{1-\omega^2}(x_0-X_0)}.
\end{aligned}
$$

We will not continue the perturbation expansion to higher orders, as we have obtained the leading order behavior of the wobbling amplitude.

Using the chain-rule and writing $b = \epsilon B$, we obtain

$$\frac{\partial b}{\partial t} = m_1 b|b|^2. \tag{2.4.11}$$

It can be derived that

$$\frac{\partial |b|^2}{\partial t} = 2\,\mathrm{Re}(m_1)|b|^4, \tag{2.4.12}$$

with the solution given by

$$|b| = \sqrt{\frac{|b(0)|^2}{1-2\,\mathrm{Re}(m_1)|b(0)|^2 t}}, \tag{2.4.13}$$

and the initial amplitude $b(0)$. It can be clearly seen that the oscillation amplitude of the breathing mode decreases in time with order $\mathcal{O}(t^{-1/2})$. The value m_1 is given by Equation (2.4.10). Calculating the real part of m_1 numerically (the imaginary part can be calculated analytically), one obtains that $\mathrm{Re}(m_1) < 0$ for all values of $\omega(\kappa)$ with $0 < \kappa \leq \pi$.

Remark 2. *Similar to Remark 1, the $\mathcal{O}(t^{-1/2})$ amplitude decay is caused by the assumption (2.4.6).*

One therefore can introduce a similar conjecture as before.

Conjecture 2. *If $n \geq 2$ is an integer such that*

$$1/(n-1)^2 > \omega^2 > 1/n^2,$$

then the decay rate of the breathing mode oscillation in $0-\kappa$ Josephson junctions is $\mathcal{O}(t^{-1/n})$.

2.5 Driven breathing modes in a $0-\kappa$ junction

We now consider breathing mode oscillations in $0-\kappa$ junctions in the presence of external driving with frequency near the natural breathing frequency of the mode, i.e., (2.1.2) and (2.1.4) with $h \neq 0$ and $\Omega = \omega(1+\rho)$. Taking the same scaling as in the case of a driven $0-\pi-0$ junction, we obtain (2.3.1). Yet, here we assume that the driving amplitude and frequency are small, i.e.,

$$h = \epsilon^2 H, \quad \rho = \epsilon^2 R, \tag{2.5.1}$$

with $H, R \sim \mathcal{O}(1)$. Performing the same perturbation expansion as before, up to $\mathcal{O}(\epsilon)$ we obtain the same equations as in the undriven case, which we omit for brevity.

2.5.1 Correction at $\mathcal{O}(\epsilon^2)$

The equation at $\mathcal{O}(\epsilon^2)$ in the perturbation expansion is

$$\begin{aligned} \partial_0^2\phi_2 - D_0^2\phi_2 - \cos(\theta+\phi_0)\phi_2 &= 2\left(D_0D_1 - \partial_0\partial_1\right)\phi_1 - \frac{1}{2}\phi_1^2\sin(\theta+\phi_0) \\ &\quad + \frac{1}{2}H\left(e^{i\omega\tau} + c.c.\right). \end{aligned} \tag{2.5.2}$$

Again, one can write the solution ϕ_2 as a combination of solutions with harmonics present in the right-hand side. In this case, the first harmonic component is different from the undriven case due to the driving, yielding the solvability condition

$$D_1 B = mHi, \tag{2.5.3}$$

where

$$\begin{aligned} m &= \frac{\eta(x_0,\omega)}{2\Psi_1(\omega)}, \quad m \in \mathbb{R} \\ \eta(x_0,\omega) &= \int_{-\infty}^{0} e^{\sqrt{1-\omega^2}(x_0+X_0)}\left[\tanh(x_0+X_0) - \sqrt{1-\omega^2}\right]dX_0 \\ &\quad + \int_{0}^{\infty} e^{\sqrt{1-\omega^2}(x_0-X_0)}\left[\tanh\left(x_0-X_0\right) - \sqrt{1-\omega^2}\right]dX_0. \end{aligned}$$

The solution for the first harmonic is

$$\phi_2^{(1)}(X_0,T_0) = H\begin{cases} g(X_0)+n(X_0), & X_0<0, \\ \widetilde{g}(X_0)+\widetilde{n}(X_0), & X_0>0, \end{cases} \tag{2.5.4}$$

where

$$
\begin{aligned}
g(X_0) &= \frac{C_{g1}\left(2\sqrt{1-\omega^2}+2-\omega^2-\omega^2 e^{2(x_0+X_0)}\right)e^{\sqrt{1-\omega^2}(x_0+X_0)}}{1+e^{2(x_0+X_0)}} \\
&\quad + \frac{\eta(x_0,X_0)}{2\Psi_1(\omega)} g_1(X_0), \\
\widetilde{g}(X_0) &= \frac{C_{g2}\left(2\sqrt{1-\omega^2}-2+\omega^2+\omega^2 e^{-2(x_0-X_0)}\right)e^{\sqrt{1-\omega^2}(x_0-X_0)}}{1+e^{-2(x_0-X_0)}} \\
&\quad - \frac{\eta(x_0,X_0)}{2\Psi_1(\omega)} \widetilde{g}_1(X_0), \\
n(X_0) &= \frac{C_{h1}\left(2\sqrt{1-\omega^2}+2-\omega^2-\omega^2 e^{2(x_0+X_0)}\right)e^{\sqrt{1-\omega^2}(x_0+X_0)}}{1+e^{2(x_0+X_0)}} \\
&\quad + \frac{\left(\omega^2 e^{2(x_0+X_0)}-2\sqrt{1-\omega^2}-2+\omega^2\right)e^{\sqrt{1-\omega^2}(x_0+X_0)}A_1(X_0)}{4\omega^4\sqrt{1-\omega^2}(1+e^{2(x_0+X_0)})} \\
&\quad + \frac{\left(\omega^2 e^{2(x_0+X_0)}+2\sqrt{1-\omega^2}-2+\omega^2\right)e^{-\sqrt{1-\omega^2}(x_0+X_0)}A_2(X_0)}{4\omega^4\sqrt{1-\omega^2}(1+e^{2(x_0+X_0)})}, \\
\widetilde{n}(X_0) &= \frac{C_{h2}\left(\omega^2 e^{-2(x_0-X_0)}+2\sqrt{1-\omega^2}-2+\omega^2\right)e^{\sqrt{1-\omega^2}(x_0-X_0)}}{1+e^{-2(x_0-X_0)}} \\
&\quad + \frac{\left(\omega^2 e^{-2(x_0-X_0)}-2\sqrt{1-\omega^2}+2-\omega^2\right)e^{-\sqrt{1-\omega^2}(x_0-X_0)}A_3(X_0)}{4\omega^4\sqrt{1-\omega^2}(1+e^{-2(x_0-X_0)})} \\
&\quad + \frac{(e^{-2(x_0-X_0)}\omega^2+2\sqrt{1-\omega^2}-2+\omega^2)e^{\sqrt{1-\omega^2}(x_0-X_0)}A_4(X_0)}{4\omega^4\sqrt{1-\omega^2}(1+e^{-2(x_0-X_0)})}.
\end{aligned}
$$

Here, $g_1(X_0)$, $\widetilde{g}_1(X_0)$, and A_j, $j=1,\ldots,4$, are given by (2.A.11)–(2.A.16). C_{g1}, C_{g2}, C_{h1}, and C_{h2} are constants of integration chosen to satisfy continuity conditions. The other harmonics are the same as in the undamped, undriven case.

2.5.2 Correction at $\mathcal{O}(\epsilon^3)$

Equating the terms at $\mathcal{O}(\epsilon^3)$ gives the equation

$$
\begin{aligned}
\partial_0^2\phi_3 - D_0^2\phi_3 - \cos(\theta+\phi_0)\phi_3 &= 2(D_0D_2-\partial_0\partial_2)\phi_1 + (D_1^2-\partial_1^2)\phi_1 \\
&\quad + 2\left(D_0D_1-\partial_0\partial_1\right)\phi_2 - \phi_1\phi_2\sin(\theta+\phi_0) \\
&\quad - \frac{1}{6}\phi_1^3\cos(\theta+\phi_0) + 2RD_0^2\phi_1. \qquad (2.5.5)
\end{aligned}
$$

The solvability condition for the first harmonic of the above equation gives

$$
D_2B = m_1B|B|^2 - \omega BR\,i. \qquad (2.5.6)
$$

Equations (2.5.3) and (2.5.6) are the leading order equations governing the oscillation amplitude of the breathing mode. Combining equations (2.5.3) and (2.5.6) in terms of the original variable $b(t)$ gives

$$\frac{\omega}{\Omega}\frac{\partial b}{\partial t} = mhi + m_1 b|b|^2 - i\omega b\rho, \quad m \in \mathbb{R}, \quad m_1 \in \mathbb{C}. \tag{2.5.7}$$

As with (2.3.13), one expects that a nonzero external drive (m) induces a breathing mode oscillation.

2.6 Numerical calculations

To check our analytical results obtained in the above sections, we have numerically solved the governing Equation (2.1.2), with $\theta(x)$ given by (2.1.3) or (2.1.4). We discretize the Laplacian operator using a central difference and integrate the resulting system of differential equations using a fourth-order Runge–Kutta method, with a spatial and temporal discretization $\Delta x = 0.02$ and $\Delta t = 0.004$, respectively. The computational domain is $x \in (-L, L)$, with $L = 50$. At the boundaries, we use a periodic boundary condition. To model an infinitely long junction, we apply an increasing damping at the boundaries to reduce reflected continuous waves incoming from the boundaries. In all the results presented herein, we use the damping coefficient

$$\alpha = \begin{cases} (|x| - L + x_\alpha)/x_\alpha, & |x| > (L - x_\alpha), \\ 0, & |x| < (L - x_\alpha); \end{cases} \tag{2.6.1}$$

i.e., α increases linearly from $\alpha = 0$ at $x = \pm(L - x_\alpha)$ to $\alpha = 1$ at $x = \pm L$. We have taken $x_\alpha = 20$. To ensure that the numerical results are not influenced by the choice of the parameter values, we have taken different values as well as different boundary conditions and damping, where we obtained quantitatively similar results.

In this section, for the $0 - \pi - 0$ junction we fix the facet length $a = 0.4$, which implies that $\omega \approx 0.73825$, and for the $0 - \kappa$ junction we set $\kappa = \pi$, which implies that $x_0 \approx -0.8814$ and $\omega \approx 0.8995$. For the choice of parameters above, we obtain the coefficients in the analytically obtained approximations (2.2.40), (2.3.13), (2.4.11), and (2.5.7) as

k_1= 0.04330, k_2= -0.00324-0.0140 i, l_1= 0.6068,
l_2=-0.10027, m_1= -0.01820-0.0809 i, l_3= 0.05934,
m=- 0.6236.

First, we consider the undriven case, $h = 0$. With the initial condition (2.1.15) and

$$B(0) = \frac{1}{2\Phi_1(0,0)}, \tag{2.6.2}$$

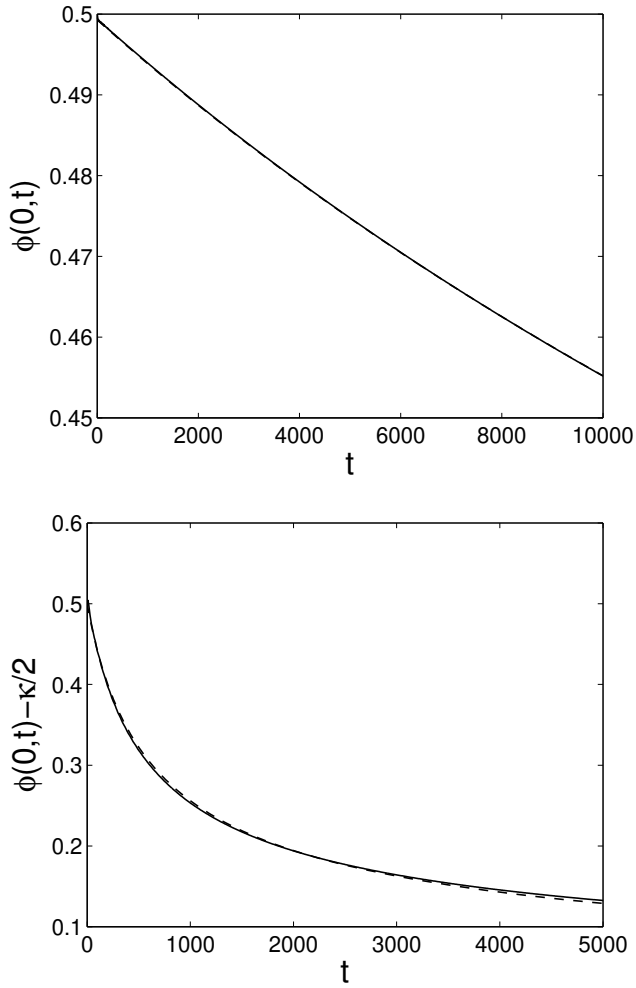

Figure 2.2: The *envelope* of the oscillation amplitude of the breathing mode in a $0-\pi-0$ (top panel) and $0-\kappa$ (bottom panel) junction. The solid curves are from the original governing Equation (2.1.2), clearly indicating the decay of the oscillation. Analytical approximations (2.2.41) for the top panel and (2.4.13) for the bottom panel are shown as dashed lines.

where $\Phi_1(x,t)$ is given by (2.1.8) for $0-\pi-0$ junctions and by (2.1.11) for $0-\kappa$ junctions, we record the *envelope* of the oscillation amplitude $\phi(0,t)$ from the governing Equation (2.1.2). In Figure 2.2, we plot $\phi(0,t)$ as solid lines for the $0-\pi-0$ and $0-\kappa$ junctions in the top and bottom panels, respectively. From Figure 2.2, one can see that the oscillation amplitude decreases in time. The mode experiences damping. The damping is intrinsically present because the breathing mode emits radiation due to higher harmonics excitations with frequency in the dispersion relation.

It is instructive to compare the numerical results with our analytical calculations. With

the initial condition

$$\phi(x,t) \quad = \quad \Phi_0(x) + B(t)\widetilde{\Phi}_1(x), \tag{2.6.3}$$

where

$$B(t) \quad = \quad b(t)e^{i\omega t} + \overline{b}(t)e^{-i\omega t}, \tag{2.6.4}$$

and $\widetilde{\Phi}_1(x)$ is given by (2.1.12). From (2.6.4) and by assuming $\mathrm{Im}(b(0)) = 0$, we have

$$b(0) \quad = \quad B(0)/2, \tag{2.6.5}$$

where $B(0)$ is given by (2.6.2). Since our asymptotics are only expected to be valid for long times, while there could be a short initial transient, it may be necessary to allow a fitting parameter F. therefore, we take

$$b(0) \quad = \quad B(0)/2F, \tag{2.6.6}$$

where F is a fitting parameter. The analytical approximation is then given by $2F|b(t)|$, where $|b(t)|$ is given by (2.2.41) and (2.4.13) for the $0-\pi-0$ and $0-\kappa$ Josephson junctions, respectively. In general, the factor F is simply $F = 1$. Yet, by treating F as a fitting parameter we observed that the best fit is not given by the aforementioned value. For the initial condition (2.6.2), we found that optimum fits are, respectively, provided by $F = 1.03$ and $F = 0.9$, which are both close to the expected value of $F = 1$.

Our approximation is shown as a dashed line in Figure 2.2, where one can see a good agreement with the numerically obtained oscillation. In the top panel, the approximation coincides with the numerical result.

Next, we consider the case of driven Josephson junctions, (2.1.2) with $h \neq 0$. In this case, the initial condition to the governing Equation (2.1.2) is (2.1.15), with

$$B_0 \quad = \quad 0. \tag{2.6.7}$$

Taking $\Omega = \omega$ (hence $\rho = 0$), we present the amplitude of the oscillatory mode $\phi(0,t)$ of $0-\pi-0$ junctions with $h = 0.002$ and $h = 0.003$ in the top and middle panels, respectively, of Figure 2.3. These are typical dynamics of the oscillation amplitude of the breathing mode, where for the first case the envelope oscillates periodically over a long time scale, and for the second case the amplitude tends to a constant.

To assess the accuracy of the asymptotic analysis, we have solved the amplitude Equations (2.3.13) and (2.5.7) numerically using a fourth-order Runge–Kutta method with a relatively fine time discretization parameter, as exact analytical solutions are not available. The analytical approximation is again given by $2F|b(t)|$, where F in this case is

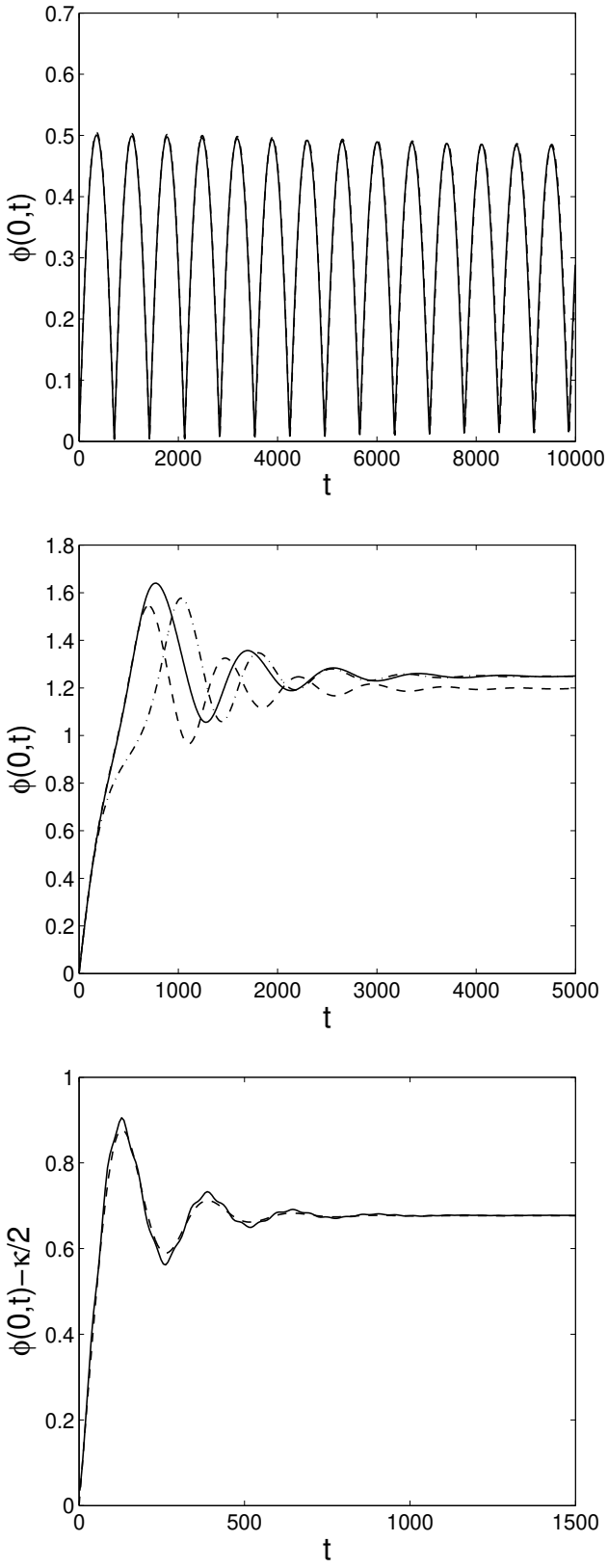

Figure 2.3: The same as in Figure 2.2, but for nonzero driving amplitude. Top and middle panels correspond to driven $0-\pi-0$ junctions with $h = 0.002$ and $h = 0.003$, respectively. Bottom panel corresponds to driven $0-\kappa$ junctions with $h = 0.01$.

taken to be exactly $F = 1$. It is important to note that ideally $\rho = 0$, as the driving frequency was taken to be the same as the internal frequency of the infinitely–long continuous Josephson junctions. Yet, one needs to note that to simulate the governing equation numerically, it is discretized and solved on a finite interval, which implies that the system's internal frequency is likely to be different from the original equation. Therefore, ρ may not be necessarily zero.

Treating ρ as a fitting parameter, we are able to find a good agreement between the numerics and the approximations for $\rho \approx 0$. Shown in the top panel of Figure 2.3 as a dashed line is the approximation (2.3.13) using $\rho = 0.00607$, where one can see that our approximation is in good agreement, as it is indistinguishable from the numerical result. In the middle panel, as dashed and dash-dotted lines, are the approximations for the driving amplitude $h = 0.003$ with $\rho = 0.006$ and $\rho = 0.00665$, respectively. The two values of ρ give a good approximations in different time intervals. It is surprising to see that the amplitude equation is still able to quantitatively capture the numerical result, considering the large amplitude produced by the forcing, which is beyond the smallness assumption of the oscillation amplitude.

In the bottom panel of Figure 2.3, we plot the amplitude of the breathing mode in the $0 - \kappa$ junction case with $h = 0.01$. One can see that the envelope of the oscillation amplitude tends to a constant. The dashed curve depicts our approximation (2.5.7) with $\rho = -0.0015$, and good agreement is obtained.

Considering the panels in Figure 2.3, we observe that the mode in the two junction types does not oscillate with an unbounded or growing amplitude. After a while, there is a balance of energy input into the breathing mode due to the external drive and the radiative damping. The regular oscillation of the mode in the top panel indicates that the junction voltage vanishes, even when the driving frequency is the same as the system's eigenfrequency. This raises the question of whether the breathing mode of a junction with a phase-shift can be excited further by increasing the driving amplitude to switch the junction to a nonzero voltage. To answer this question, we have solely used numerical simulations of (2.1.2), as it is beyond our perturbation analysis.

In the top left and right panels of Figure 2.4, we present the average voltage (2.1.1) with $T = 100$ as a function of the external driving amplitude h for the case of $0 - \pi - 0$ and $0 - \kappa$ junctions, respectively. We have taken different values of T, where we obtained similar results. One can clearly see that in both cases, there is a minimum amplitude above which the junction has a large nonzero voltage. For the first and second junctions, the critical amplitude is, respectively, $h \approx 0.34$ and $h \approx 0.1$. The time dynamics of the transition from the superconducting state $\langle V \rangle \approx 0$ to a resistive state

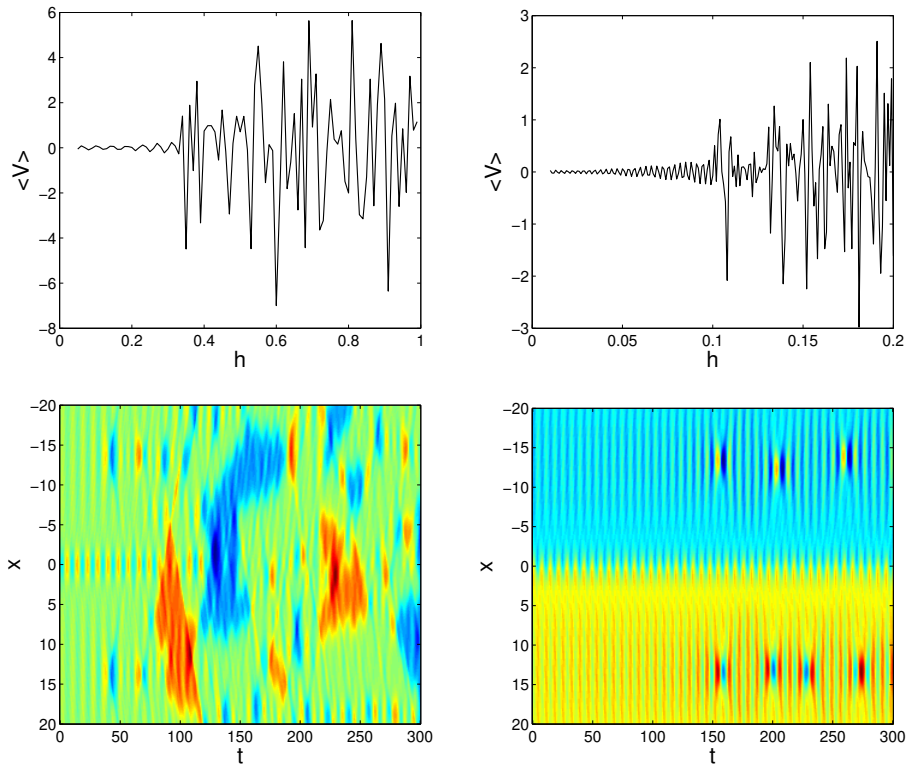

Figure 2.4: The average voltage $\langle V \rangle$ as a function of the driving amplitude h in a $0-\pi-0$ (top left) and a $0-\kappa$ (top right) junction, respectively. Bottom panels show the dynamics at the switching point, where the voltage becomes nonzero.

$|\langle V \rangle| \gg 0$ is shown in the bottom panels of the same figure.

From the panels, it is important to note that apparently the switch from a superconducting to a resistive state is not caused by the breathing mode, but rather because of the continuous wave background emitted by the breathing mode. It shows that the continuous wave becomes modulationally unstable. As the typical dynamics, the instability causes breathers to be created, which then interact and destroy the breathing mode. Hence, we conclude that a breathing mode in these cases cannot be excited to make the junction resistive by applying an external drive, even with a relatively large driving amplitude.

2.7 Conclusions

We have considered a spatially inhomogeneous sine-Gordon equation with a time-periodic drive, modelling a microwave–driven long Josephson junctions with phase-shifts. Due to the inhomogeneity, the system has a breathing mode corresponding to a

periodic in time and localised in space solution. We constructed a perturbation expansion for the breathing mode with a small amplitude excitations to obtain equations for the slow time evolution of the oscillation amplitude for the $0-\pi-0$ and $0-\kappa$ Josephson junctions respectively. We used multiple scales method which deals with situations in which parameters introduced in the perturbative construction have a slow dependence on the space and time variables, and allows one to determine this dependence. We showed that this slow dependence is a result of the energy carried away from the internal mode by the radiation waves. A similar approach has been used by Oxtoby and Barashenkov [99, 100] for the ϕ^4 equation.

We derived differential equations for the slowly varying oscillation amplitude for the $0-\pi-0$ and $0-\kappa$ Josephson junctions respectively. We avoided arithmetic unboundedness in radiation functions by using multiscale expansion. The obtained amplitude equations do not predict unbounded or growing amplitude, which is arrested by the terms $k_2 b|b|^4$ (see(2.2.38)) for $0-\pi-0$ junction and $m_1 b|b|^2$ (see(2.4.11)) for $0-\kappa$ junction. This shows that the emission of radiation has the effect of damping the breathing. The damping is present because the breathing mode emits radiation due to frequency tripling effect of the nonlinearity, which causes the breathing mode to become a source of radiation. We showed that in the absence of an ac-drive, a breathing mode oscillation which decays with rates of at most $\mathcal{O}(t^{-1/4})$ and $\mathcal{O}(t^{-1/2})$ for junctions with uniform and nonuniform ground states, respectively.

Next, we applied the method of multiple scales to obtain the oscillation amplitude in the presence of external driving with frequency near the natural frequency of the wobbler in the $0-\pi-0$ and $0-\kappa$ junctions. The presence of nonzero external drive settles the breathing mode oscillation to a stable fixed point as $t \to \infty$. We show that there is a balance of energy input into the breathing mode due to the external drive and the radiative damping.

In the context of Josephson junctions, the study is mentioned by recent experiments as the measurement of the eigenfrequency of Josephson junctions with phase shifts. It was conjectured that the driving frequency at which switching to a resistive state occurs is the same as the eigenfrequency of the ground state [38].

From an analytical results, we have shown that in an infinitely long Josephson junction, an external drive cannot excite the defect mode of a junction, i.e., a breathing mode, to switch the junction into a resistive state. We used numerical computations to compare our theoretical analysis, and obtained a good agreement.

From the numerical simulations, for a small drive amplitude, there is an energy balance between the energy input from the external drive and the energy output due to

so-called radiative damping experienced by the mode. When the external drive amplitude is large enough, the junction can switch to a resistive state. This is caused by a modulational instability of the continuous wave emitted by the oscillating mode.

Despite the agreement with the experiments obtained herein, our analysis is based on a simplified model. It is of interest to extend the study to the case of *dc, driven long but finite* Josephson junctions with phase-shifts, as experimentally used in [38, 39].

In microwave driven finite junctions, the boundaries can be a major external drive (see, e.g., [114, 115]), which is not present in our study. A constant *dc*-bias current, which plays an important role in the measurements reported by Buckenmaier and collaborators in [38], is not included in our work, even though the results presented herein should still hold for small constant drive. Another open problem is the interaction of multiple defect modes in Josephson junctions with phase-shifts as fabricated by [116], which will be addressed in Chapter 4. This is experimentally relevant, as the so-called zigzag junctions have been successfully fabricated by Hilgenkamp *et al.* [23].

2.A Appendix: Explicit expressions

The functions k_{3j} and $\widetilde{k}_{3j}$ in the expression of v_j (2.2.26), $j = 1,2,3$, are given by

$$k_{31} = 2\omega \tan^{-1}\left(\sqrt{\frac{1-\omega^2}{1+\omega^2}}\right)\left(e^{3u+2X_0\sqrt{1-\omega^2}}(1+\omega^2)^{\frac{3}{2}} + 3e^u X_0\sqrt{1-\omega^4}\right) \tag{2.A.1}$$
$$+\frac{2e^{3u+2X_0\sqrt{1-\omega^2}}\omega\,(1+\omega^2)^2}{\sqrt{1-\omega^2}} - e^u\omega X_0\left(2\omega^6-3+2\omega^2+7\omega^4\right),$$

$$\widetilde{k}_{31} = \frac{e^{u+2X_0\sqrt{1-\omega^2}}\omega\sqrt{1-\omega^4}\tan^{-1}\left(\sqrt{\frac{1-\omega^2}{1+\omega^2}}\right)\left(e^{2u+2X_0\sqrt{1-\omega^2}}(1+\omega^2)+3\right)}{\sqrt{1-\omega^2}} \tag{2.A.2}$$
$$+\frac{e^{3u+4X_0\sqrt{1-\omega^2}}\omega\,(1+\omega^2)^2}{\sqrt{1-\omega^2}} - \frac{e^{u+2X_0\sqrt{1-\omega^2}}\omega\,(2\omega^6-3+2\omega^2+7\omega^4)}{2\sqrt{1-\omega^2}},$$

$$k_{32} = \frac{\sin\left(2\sqrt{1+\omega^2}X_0\right)(2\omega^2+3)(\omega^2+1)^2}{4\sqrt{1+\omega^2}} + \frac{X_0}{2}(2\omega^2+3)(\omega^2+1)^2 \tag{2.A.3}$$
$$+\frac{2\cos^3\left(\sqrt{1+\omega^2}X_0\right)\sin\left(\sqrt{1+\omega^2}X_0\right)\left(\sqrt{1-\omega^4}\tan^{-1}\left(\sqrt{\frac{1-\omega^2}{1+\omega^2}}\right)+1+\omega^2\right)}{\sqrt{1+\omega^2}},$$

$$\widetilde{k}_{32} = \frac{\cos^2\left(\sqrt{1+\omega^2}X_0\right)\left(6\sqrt{1-\omega^4}\tan^{-1}\left(\sqrt{\frac{1-\omega^2}{1+\omega^2}}\right)-7\omega^4-2\omega^2+3-2\omega^6\right)}{2\sqrt{1+\omega^2}} \tag{2.A.4}$$
$$-\frac{2\cos^4\left(\sqrt{1+\omega^2}X_0\right)\left(\sqrt{1-\omega^4}\tan^{-1}\left(\sqrt{\frac{1-\omega^2}{1+\omega^2}}\right)+1+\omega^2\right)}{\sqrt{1+\omega^2}},$$

$$k_{33} = \frac{e^{u-2X_0\sqrt{1-\omega^2}}\left(2\omega^6-3+2\omega^2+7\omega^4\right)}{2\sqrt{1-\omega^2}} - \frac{(1+\omega^2)^2 e^{3u-4X_0\sqrt{1-\omega^2}}}{\sqrt{1-\omega^2}} \tag{2.A.5}$$
$$-\frac{\left(e^{2u}+e^{2u}\omega^2+3e^{2X_0\sqrt{1-\omega^2}}\right)e^{u-4X_0\sqrt{1-\omega^2}}\sqrt{1-\omega^4}\tan^{-1}\left(\sqrt{\frac{1-\omega^2}{1+\omega^2}}\right)}{\sqrt{1-\omega^2}},$$

$$\widetilde{k}_{33} = -(2e^{3u-2X_0\sqrt{1-\omega^2}})(1+\omega^2)\left(\sqrt{1+\omega^2}\tan^{-1}\left(\sqrt{\frac{1-\omega^2}{1+\omega^2}}\right)-\frac{(1+\omega^2)}{\sqrt{1-\omega^2}}\right) \tag{2.A.6}$$
$$+e^u X_0\left(6\sqrt{1-\omega^4}\tan^{-1}\left(\sqrt{\frac{1-\omega^2}{1+\omega^2}}\right)-7\omega^4-2\omega^2+3-2\omega^6\right).$$

The functions $E_j(X_0)$ and $\widetilde{E}_j(X_0)$ in $\phi_2^{(j)}$ (2.4.4)–(2.4.5) ($j=0,2$) are given by

$$
\begin{aligned}
E_0(X_0) &= \frac{e^{(X_0+x_0)}C_{01}}{1+e^{2(X_0+x_0)}} - \frac{2\,(2+\sqrt{1-\omega^2})e^{(X_0+x_0)(2\sqrt{1-\omega^2}+3)}}{\sqrt{1-\omega^2}(1+e^{2(X_0+x_0)})^5} \\
&\quad - \frac{(1+\sqrt{1-\omega^2})e^{(2\sqrt{1-\omega^2}+1)(X_0+x_0)}}{\sqrt{1-\omega^2}(1+e^{2(X_0+x_0)})^5} \\
&\quad - \frac{2\,(2-\sqrt{1-\omega^2})e^{(X_0+x_0)\left(2\sqrt{1-\omega^2}+7\right)} + 6\,e^{(X_0+x_0)\left(5+2\sqrt{1-\omega^2}\right)}}{\sqrt{1-\omega^2}(1+e^{2(X_0+x_0)})^5} \\
&\quad + \frac{2\,(1+2\sqrt{1-\omega^2}-\omega^2)e^{(X_0+x_0)(2\sqrt{1-\omega^2}+3)}}{(1+e^{2(X_0+x_0)})^5},
\end{aligned}
\tag{2.A.7}
$$

$$
\begin{aligned}
\widetilde{E_0}(X_0) &= \frac{e^{(X_0-x_0)}C_{02}}{1+e^{2(X_0-x_0)}} + \frac{2\,e^{(-X_0+x_0)(2\sqrt{1-\omega^2}-7)}(2+\sqrt{1-\omega^2})}{\sqrt{1-\omega^2}(1+e^{2(X_0-x_0)})^5} \\
&\quad - \frac{2\,e^{(-X_0+x_0)\left(2\sqrt{1-\omega^2}-3\right)}(2-\sqrt{1-\omega^2}) - 6\,e^{(-X_0+x_0)\left(2\sqrt{1-\omega^2}-5\right)}}{\sqrt{1-\omega^2}(1+e^{2(X_0-x_0)})^5} \\
&\quad + \frac{e^{(x_0-X_0)\left(2\sqrt{1-\omega^2}-1\right)}(1-\sqrt{1-\omega^2}) + e^{(x_0-X_0)\left(2\sqrt{1-\omega^2}-9\right)}(1+\sqrt{1-\omega^2})}{\sqrt{1-\omega^2}(1+e^{2(X_0-x_0)})^5},
\end{aligned}
\tag{2.A.8}
$$

$$
\begin{aligned}
E_2(X_0) &= \frac{\left(2\omega^2 e^{2(X_0+x_0)} - (1+\sqrt{1-4\omega^2}-2\omega^2)\right)e^{\sqrt{1-4\omega^2}(X_0+x_0)}C_{21}}{1+e^{2(X_0+x_0)}} \\
&\quad - \frac{\left(\left(2\sqrt{1-\omega^2}+1\right)e^{3(X_0+x_0)} + (2\sqrt{1-\omega^2}-1)e^{7(X_0+x_0)}\right)e^{2\sqrt{1-\omega^2}(X_0+x_0)}}{(1+e^{2(X_0+x_0)})^5} \\
&\quad + \frac{-6\sqrt{1-\omega^2}e^{(X_0+x_0)(5+2\sqrt{1-\omega^2})} - e^{2\sqrt{1-\omega^2}(X_0+x_0)+X_0+x_0}(1+\sqrt{1-\omega^2})}{2(1+e^{2(X_0+x_0)})^5} \\
&\quad + \frac{(1-\sqrt{1-\omega^2})e^{(X_0+x_0)(9+2\sqrt{1-\omega^2})}}{2(1+e^{2(X_0+x_0)})^5},
\end{aligned}
\tag{2.A.9}
$$

$$
\begin{aligned}
\widetilde{E_2}(X_0) &= \frac{\left(2\,\omega^2 e^{2\,(X_0-x_0)} + 2\,\omega^2 + \sqrt{1-4\,\omega^2} - 1\right)e^{-\sqrt{1-4\,\omega^2}(X_0-x_0)}C_{22}}{1+e^{2(X_0-x_0)}} \\
&\quad + \frac{\left(e^{9\,(X_0-x_0)} - 2\,e^{3\,(X_0-x_0)} - e^{(X_0-x_0)}\right)e^{-2\sqrt{1-\omega^2}(X_0-x_0)}}{2(1+e^{2(X_0-x_0)})^5} \\
&\quad + \frac{2e^{-(X_0-x_0)(2\sqrt{1-\omega^2}-7)} + 4e^{-(X_0+x_0)(2\sqrt{1-\omega^2}-3)}\sqrt{1-\omega^2}}{2(1+e^{2(X_0-x_0)})^5} \\
&\quad + \frac{\sqrt{1-\omega^2}(6\,e^{-(X_0-x_0)(2\sqrt{1-\omega^2}-5)} + e^{-(X_0-x_0)(2\sqrt{1-\omega^2}-1)})}{2(1+e^{2(X_0-x_0)})^5} \\
&\quad + \frac{\sqrt{1-\omega^2}(e^{-(X_0-x_0)(2\sqrt{1-\omega^2}-9)} + 4\,e^{-(X_0-x_0)(2\sqrt{1-\omega^2}-7)})}{2(1+e^{2(X_0-x_0)})^5}.
\end{aligned}
\tag{2.A.10}
$$

The functions $g_1(X_0)$, $\widetilde{g}_1(X_0)$, and A_j, $j = 1, \ldots, 4$, in (2.5.5)–(2.5.5) are

$$
\begin{aligned}
g_1(X_0) &= \frac{((x_0+X_0)\omega^2+1)\sqrt{1-\omega^2}-\frac{1}{2}\omega^2+1)e^{(x_0+X_0)(\sqrt{1-\omega^2}+2)}}{\omega\sqrt{1-\omega^2}(\frac{1}{2}+e^{2(x_0+X_0)}+\frac{1}{2}\,e^{4(x_0+X_0)})} \qquad (2.A.11)\\
&+\frac{\left((x_0+X_0)\omega^4-(x_0+X_0-\frac{5}{2})\omega^2-2\right)\sqrt{1-\omega^2}e^{\sqrt{1-\omega^2}(x_0+X_0)}}{2\omega\sqrt{1-\omega^2}(\omega+1)(\omega-1)(\frac{1}{2}+e^{2(x_0+X_0)}+\frac{1}{2}\,e^{4(x_0+X_0)})}\\
&+\frac{(2+(-\frac{1}{2}+x_0+X_0)\omega^2)(\omega^2-1))e^{\sqrt{1-\omega^2}(x_0+X_0)}}{2\omega\sqrt{1-\omega^2}(\omega+1)(\omega-1)(\frac{1}{2}+e^{2(x_0+X_0)}+\frac{1}{2}\,e^{4(x_0+X_0)}}\\
&+\frac{\omega^2((x_0+X_0)\omega^2-x_0-X_0-\frac{1}{2})\sqrt{1-\omega^2}e^{(x_0+X_0)(4+\sqrt{1-\omega^2})}}{2\omega\sqrt{1-\omega^2}(\omega+1)(\omega-1)(\frac{1}{2}+e^{2(x_0+X_0)}+\frac{1}{2}\,e^{4(x_0+X_0)})}\\
&+\frac{((-x_0-X_0-\frac{1}{2})\omega^2+x_0+X_0+\frac{1}{2})e^{(x_0+X_0)(4+\sqrt{1-\omega^2})}}{2\omega\sqrt{1-\omega^2}(\omega+1)(\omega-1)(\frac{1}{2}+e^{2(x_0+X_0)}+\frac{1}{2}\,e^{4(x_0+X_0)})},\\
\widetilde{g}_1(X_0) &= \frac{((1-(x_0-X_0)\omega^2)\sqrt{1-\omega^2}+\frac{1}{2}\,\omega^2-1)e^{(\sqrt{1-\omega^2}-2)(x_0-X_0)}}{\omega\sqrt{1-\omega^2}(\frac{1}{2}+e^{-2(x_0-X_0)}+\frac{1}{2}\,e^{-4(x_0-X_0)})} \qquad (2.A.12)\\
&+\frac{((2+(-\frac{1}{2}-x_0+X_0)\omega^2)(\omega^2-1)+2\omega^4)e^{-\sqrt{1-\omega^2}(-x_0+X_0)}}{2\omega\sqrt{1-\omega^2}(\omega+1)(\omega-1)(\frac{1}{2}+e^{-2(x_0-X_0)}+\frac{1}{2}\,e^{-4(x_0-X_0)})}\\
&+\frac{(((X_0-x_0)\omega^4+(x_0-X_0+\frac{5}{2})\omega^2)\sqrt{1-\omega^2})e^{-\sqrt{1-\omega^2}(-x_0+X_0)}}{2\omega\sqrt{1-\omega^2}(\omega+1)(\omega-1)(\frac{1}{2}+e^{-2(x_0-X_0)}+\frac{1}{2}\,e^{-4(x_0-X_0)})}\\
&+\frac{\omega^2((-x_0+X_0)\omega^2+x_0-X_0-\frac{1}{2})\sqrt{1-\omega^2}e^{-(-x_0+X_0)(\sqrt{1-\omega^2}-4)}}{2\omega\sqrt{1-\omega^2}(\omega+1)(\omega-1)(\frac{1}{2}+e^{-2(x_0-X_0)}+\frac{1}{2}\,e^{-4(x_0-X_0)})}\\
&+\frac{(\omega+1)(-x_0+X_0+\frac{1}{2})(-1+\omega)e^{-(-x_0+X_0)(\sqrt{1-\omega^2}-4)}}{2\omega\sqrt{1-\omega^2}(\omega+1)(\omega-1)(\frac{1}{2}+e^{-2(x_0-X_0)}+\frac{1}{2}\,e^{-4(x_0-X_0)})},\\
A_1(X_0) &= \int \frac{\left(2\sqrt{1-\omega^2}-2+\omega^2+\omega^2 e^{2(x_0+X_0)}\right)e^{-\sqrt{1-\omega^2}(x_0+X_0)}}{1+e^{2(x_0+X_0)}}\,dX_0, \qquad (2.A.13)\\
A_2(X_0) &= \int \frac{\left(2\sqrt{1-\omega^2}+2-\omega^2-\omega^2 e^{2(x_0+X_0)}\right)e^{\sqrt{1-\omega^2}(x_0+X_0)}}{1+e^{2(x_0+X_0)}}\,dX_0, \qquad (2.A.14)\\
A_3(X_0) &= \int \frac{\left(2\sqrt{1-\omega^2}-2+\omega^2+\omega^2 e^{-2(x_0-X_0)}\right)e^{\sqrt{1-\omega^2}(x_0-X_0)}}{1+e^{-2(x_0-X_0)}}\,dX_0, \qquad (2.A.15)\\
A_4(X_0) &= \int \frac{\left(2\sqrt{1-\omega^2}+2-\omega^2-\omega^2 e^{-2(x_0-X_0)}\right)e^{-\sqrt{1-\omega^2}(x_0-X_0)}}{1+e^{-2(x_0-X_0)}}\,dX_0. \qquad (2.A.16)
\end{aligned}
$$

CHAPTER 3

Rapidly oscillating ac-driven long Josephson junctions with phase-shifts

The contents of this chapter have been submitted to Physica D (Nonlinear Phenomena).

3.1 Introduction

A Josephson junction is an electronic circuit consisting of two superconductors connected by a thin non-superconducting layer, and is the basis of a large number of developments both in fundamental research and in application to electronic devices [45]. Even though there is no applied voltage difference, a flow of electrons can tunnel from one superconductor to the other due to the overlapping quantum mechanical waves in the two superconductors of the Josephson junction. If we denote the difference in phases of the wave functions by ϕ and the spatial and temporal variable along the junction by x and t, respectively, the electron flow tunnelling across the barrier, i.e. the Josephson current, I is proportional to the sine of $\phi(x,t)$. In an ideal long Josephson junction, the phase difference ϕ satisfies the sine-Gordon equation.

A particular solution of the sine-Gordon equation is a kink solution, which is a topological soliton. The solution represents a twist in the variable ϕ which takes the system from one solution $\phi = 0$ to an adjacent one with $\phi = 2\pi$. In the context of long Josephson junctions, this kink corresponds to a vortex of supercurrent, which can be formed inside the Josephson barrier. The supercurrents circulate around the vortex's center and carry a magnetic field with the total flux equal to a single flux quantum $\Phi_0 \approx 2.07 \times 10^{-15} Wb$. Therefore, such a vortex is also referred to as a (Josephson)

fluxon. The study of fluxons in Josephson junctions has been the subject of interest over the last few decades due to their nonlinear nature and applications [45, 46, 64, 89].

One of the important properties of Josephson junctions is their behaviour when irradiated with external radio-frequency (rf) microwave fields [9, 117]. This can be modelled by a sine-Gordon equation driven with a periodic (ac) force. In particular, interactions of fluxons in long Josephson junctions and ac-drives may yield rich dynamics, including oscillatory and effectively progressive motions of fluxons (see, e.g., [118, 119, 120] and references therein). Microwave driven Josephson junctions have also been used to study this ratchet effect, that is, the unidirectional motion under the influence of a force with zero mean [46, 121]. When the driving frequency and amplitude of the applied microwave are larger than the Josephson plasma frequency ω_p, one may also obtain unstable, but long-lived half-fluxons (π-kinks), which are not present in the undriven system [122, 123].

Recently, the study of the effects of microwave field radiation has been extended to the so-called Josephson junctions with phase-shifts both experimentally and theoretically [38, 39, 124, 125]. Such junctions were first proposed by Bulaevskii *et al*. [14, 15]. A nontrivial ground-state can be realized in the junctions, characterised by the spontaneous generation of a fractional fluxon, i.e. a vortex carrying a fraction of magnetic flux quantum. This remarkable property can be invoked by intrinsically building piecewise constant phase-shifts $\theta(x)$ into the junction. Due to the phase-shift, the supercurrent relation becomes $I \sim \sin(\phi + \theta)$. Presently, one can impose phase-shifts in long Josephson junctions using several methods, such as by installing magnetic impurities [126] or Abrikosov vortices [127], using multilayer junctions with controlled thicknesses over the insulating barrier [128, 129], pairs of current injectors [29] and junctions with unconventional order parameter symmetry [20, 23, 130]. When irradiated with magnetic fields, such novel types of junctions exhibit interesting dynamics, such as half-integer Shapiro steps [124] and different characteristics of self-resonance modes known as Fiske modes [131]. As the aforementioned works were concentrated on the *dynamics* of the junctions, in this chapter we consider for the first time the influence of high-frequency radiation fields to the existence of *static* ground states of the junctions.

The dynamics of the phase difference ϕ of a Josephson junction with phase-shifts is modelled by the perturbed sine-Gordon equation

$$\phi_{tt}(x,t) - \phi_{xx}(x,t) + \sin(\phi + \theta) = \gamma - \alpha\phi_t + f\cos(\Omega t). \tag{3.1.1}$$

Equation (3.1.1) is dimensionless, x and t are normalized to the Josephson penetration length λ_J and the inverse plasma frequency ω_p^{-1}, respectively, and α is the damping

coefficient due to electron tunnelling across the junction. The parameter γ represents an applied (dc) bias current. The applied time periodic (ac) drive is represented by the final term of the governing equation above. Because of the nondimensionalisation of the temporal variable t, the Josephson plasma frequency ω_p corresponds to $\Omega = 1$. Here, we consider the experimentally relevant case $\Omega \gg 1$. The case $\Omega < 1$ has been considered theoretically in Chapter 2 (see also [38, 39] for the experiments).

In this chapter, we consider two particular configurations of phase shift, namely

$$\theta(x) = \begin{cases} 0, & |x| > a, \\ \pi, & |x| < a, \end{cases} \tag{3.1.2}$$

and

$$\theta(x) = \begin{cases} 0, & x < 0, \\ -\kappa, & x > 0, \end{cases} \tag{3.1.3}$$

which are referred to as the $0-\pi-0$ and $0-\kappa$ Josephson junctions, respectively. The phase field ϕ is then naturally subject to the continuity conditions at the position of the jump in the Josephson phase (the discontinuity), i.e.

$$\phi(\pm a^-) = \phi(\pm a^+), \quad \phi_x(\pm a^-) = \phi_x(\pm a^+), \tag{3.1.4}$$

for the $0-\pi-0$ junction and

$$\phi(0^-) = \phi(0^+), \quad \phi_x(0^-) = \phi_x(0^+), \tag{3.1.5}$$

for the $0-\kappa$ junction. The quantity ϕ_{xx} may be discontinuous at the points where θ is discontinuous.

The unperturbed $0-\pi-0$ junction, i.e. (3.1.1) and (3.1.2) with $\gamma = f = 0$, has

$$\Phi_0(x,t) = 0, \tag{3.1.6}$$

(mod 2π) as the ground state. Studying the stability of the constant solution, one finds there is a critical facet length $a_c = \pi/4$ above which the solution is unstable and the ground state is spatially nonuniform [32]. The ground state represents a pair of fractional fluxons of opposite polarities. A scanning microscopy image of fractional fluxons can be seen in, e.g., [23, 106].

As for the unperturbed $0-\kappa$ junction, i.e. (3.1.1) and (3.1.3) with $\gamma = f = 0$, the ground state of the system is (mod 2π)

$$\Phi_0(x,t) = \begin{cases} 4\tan^{-1} e^{x_0+x}, & x < 0, \\ \kappa - 4\tan^{-1} e^{x_0-x}, & x > 0, \end{cases} \tag{3.1.7}$$

where $x_0 = \ln \tan(\kappa/8)$. Physically, $\Phi_0(x,t)$ (3.1.7) represents a fractional fluxon that is spontaneously generated at the discontinuity. In the presence of an applied dc bias current ($\gamma \neq 0$), the fractional fluxon will be deformed. When the current is large enough, the static ground state will cease to exist and the junction switches to a resistive state by alternately releasing travelling fluxons and antifluxons. The minimum current at which the junction switches to such a state is called the critical current $\gamma_c = 2\sin(\kappa/2)/\kappa$ [132, 133].

When $f \neq 0$, the threshold distance in $0-\pi-0$ junctions and the critical current γ_c in $0-\kappa$ junctions can be expected to be different. Here, we show that rapidly oscillating ac drives will increase the threshold distance in $0-\pi-0$ junctions and decrease the critical current in $0-\kappa$ junctions. This is the main result of the present chapter. We derive and study an 'average' equation describing the average dynamics of the system. The average equation has the form of a double sine-Gordon equation, and is obtained through the method of averaging. The idea of the method is to determine conditions under which solutions of an autonomous dynamical system can be used to approximate solutions of a more complicated (i.e. non-autonomous) time-varying dynamical system. Here, the method is based on multiple time scales analysis.

A double sine-Gordon equation describing the slow-time dynamics of a rapidly driven sine-Gordon equation was obtained previously through restricting the phase ϕ to Fourier series expansion [134, 135] and normal form technique [122]. In the normal form technique, several canonical transformations are applied to the Hamiltonian system to move mean-zero terms to higher order [136, 137]. In [134, 135], Kivshar et al. decompose the phase ϕ into the sum of slowly- and rapidly- varying parts. The method solely uses asymptotic expansions rather than averaging over the fast oscillation. In both methods, the coefficients of the double sine-Gordon equation are given in terms of the Bessel functions. With the method proposed herein, one has more control on the scales of the driving parameters and the coefficients of the 'average' equation are given by simple explicit functions, which will be shown later to be a series expansion of the coefficients obtained in [122, 134, 135].

This chapter is organised as follows; in Sections 3.2 and 3.3, we derive the average equation that represents the slowly-varying dynamics of the phase due to direct ac driving force. In Section 3.4, we discuss the threshold facet length of $0-\pi-0$ junctions, and the critical bias currents in $0-\kappa$ junctions in the presence of ac drives, based on our analytical results obtained in Section 3.2. Numerical results accompanying our analysis are presented in Section 3.5. Interestingly for the critical current in $0-\kappa$ junctions we show numerically that there is a critical driving amplitude, which is a function of the

driving frequency, at which the critical dc current is zero. Finally, Section 3.6 is devoted to conclusions.

3.2 Multiscale averaging with large driving amplitude

In this section, we derive an average nonlinear equation to describe the slowly-varying dynamics of the sine-Gordon model (3.1.1). Even though in the following we derive an average equation for a general configuration $\theta(x)$, we will see that the phase shift does not play any role in the derivation. We consider a particularly experimentally-relevant case where the ac force is rapidly oscillating, i.e. $\Omega \gg 1$, and define a small parameter $0 < \epsilon = 1/\Omega \ll 1$. In experiments the drive amplitude f can be small or large. Nevertheless, as we will see later and as noted in [134, 135] when $f \sim \Omega^2$ or larger the modulation due to the fast oscillating drive will no longer be small. Because of that, we consider a drive amplitude scaled as

$$f = F/\epsilon^{3/2}, \tag{3.2.1}$$

with $F \sim \mathcal{O}(1)$. For a reason that it is close to the threshold scaling, but the calculation is relatively simple and tractable. Other scaling, including the experimentally relevant case of small f, can be considered similarly.

Clearly the system (3.1.1) not only depends on the $t = \mathcal{O}(1)-$time scale, but also on the fast time scale $t = \mathcal{O}(\epsilon)$, hence we define a series of timescales

$$T_n = \epsilon^{n/2} t, \quad n = -2, -1, 0, \dots. \tag{3.2.2}$$

We seek a solution in terms of the asymptotic expansion

$$\phi(x,t) \;=\; \phi_0 + \epsilon^{1/2}\phi_1 + \epsilon\,\phi_2 + \epsilon^{3/2}\phi_3 + \epsilon^2\phi_4 + \dots, \tag{3.2.3}$$

where $\phi_j = \phi_j(x, T_{-2}, T_{-1}, T_0, \dots)$.

It should be noted that $T_{-2} = t/\epsilon$ is the fast variable and it will be shown later that ϕ_0 is independent of T_{-2}. For $0 < \epsilon \ll 1$ the variable T_{-2} changes more rapidly than T_j for $j > -2$, and we can think of $T_j (j > -2)$ as being constant. When considering the problem over the slow timescales, we will assume that the average

$$\langle \phi_i \rangle = \frac{1}{2\pi} \int_0^{2\pi} \phi_i(x, T_{-2}, \dots)\, dT_{-2} = 0, \tag{3.2.4}$$

that is, $\phi_i(x, T_{-2}, T_{-1}, \dots)$, $i = 1, 2, \dots$, has zero mean and is periodic in T_{-2} with period 2π. The assumption (3.2.4) is possible because any arbitrary function in ϕ_i that is

independent of T_{-2} can be absorbed into ϕ_0. In this way, $\phi_0(x, T_{-2}, T_{-1}, T_0, \dots)$ represents the average of $\phi(x,t)$ and for that reason the governing equation for ϕ_0 is referred to as the 'average' equation.

Denoting $D_n = \partial/\partial T_n$, the multiscale expansion for the time variable implies that partial derivative becomes

$$\frac{\partial}{\partial t} = \epsilon^{-1}D_{-2} + \epsilon^{-1/2}D_{-1} + D_0 + \epsilon^{1/2}D_1 + \epsilon\, D_2 + \epsilon^{3/2}D_3 + \epsilon^2 D_4 + \dots . \quad (3.2.5)$$

Substituting (3.2.3) and (3.2.5) into (3.1.1), expanding and collecting powers of ϵ, one obtains a hierarchy of equations.

Terms of order $\mathcal{O}(\epsilon^{-2})$ give

$$D_{-2}^2\phi_0 = 0, \quad (3.2.6)$$

which implies

$$\phi_0(x, T_{-2}, \dots) = C(x, T_{-1}, T_0, \dots)T_{-2} + C_0(x, T_{-1}, T_0, \dots), \quad (3.2.7)$$

where C and C_0 are arbitrary at this stage. We set $C(x, T_{-1}, T_0, \dots) = 0$, so that ϕ_0 is periodic in T_{-2}. This shows that the first term in the multiscale expansion is independent of T_{-2}. In other words

$$\phi_0 = \phi_0(x, T_{-1}, T_0, \dots). \quad (3.2.8)$$

Terms of order $\mathcal{O}(\epsilon^{-3/2})$ give

$$D_{-2}^2\phi_1 + 2\, D_{-2}D_{-1}\phi_0 = F\cos(T_{-2}). \quad (3.2.9)$$

By using the solution (3.2.8), we obtain the solution at $\mathcal{O}(\epsilon^{-3/2})$ as

$$\phi_1(x, T_{-2}, T_{-1}, \dots) = -F\cos(T_{-2}) + C_1(x, T_{-1}, T_0, ...). \quad (3.2.10)$$

Here and in the following calculations, we set the unknown function $C_1(x, T_{-1}, T_0, ...) = 0$ since such a term would make ϕ_1 violate the assumption (3.2.4). Hence

$$\phi_1(x, T_{-2}, T_{-1}, \dots) = -F\cos(T_{-2}). \quad (3.2.11)$$

The terms of order $\mathcal{O}(1/\epsilon)$ give

$$D_{-2}^2\phi_2 + 2D_{-2}D_{-1}\phi_1 + \left(2D_{-2}D_0 + D_{-1}^2 + \alpha D_{-2}\right)\phi_0 = 0. \quad (3.2.12)$$

Since ϕ_1 is independent of T_{-1} and ϕ_0 is independent of T_{-2}, the above equation can be simplified to

$$D_{-2}^2\phi_2 + D_{-1}^2\phi_0 = 0. \quad (3.2.13)$$

To obtain a bounded ϕ_2, we average (3.2.13) over T_{-2} using (3.2.4)

$$D_{-1}^2\phi_0 \quad = \quad 0, \tag{3.2.14}$$

which implies that ϕ_0 is independent of T_{-1}. Thus, we conclude from (3.2.8) and (3.2.14) that

$$\phi_0 \quad = \quad \phi_0(x, T_0, T_1, \dots). \tag{3.2.15}$$

Subtracting (3.2.14) form (3.2.13), we obtain

$$D_{-2}^2\phi_2 = 0, \tag{3.2.16}$$

which can be integrated to obtain

$$\phi_2(x, T_{-2}, T_{-1}, \dots) \quad = \quad 0. \tag{3.2.17}$$

Note that condition (3.2.14) can also be obtained from the Fredholm alternative. At any order expansion, the equation we obtain is always of the form $\mathcal{L}\psi\,(T_{-2}) = g\,(T_{-2})$ where $\mathcal{L} = D_{-2}^2$ is clearly a self-adjoint operator and $g : \mathbb{T} \to \mathbb{R}$ is a smooth 2π-periodic function, with $\mathbb{T}$ being the circle of length 2π. Let $L^2(\mathbb{T})$ be the Hilbert space of 2π-periodic with inner product

$$< y(T_{-2}), z(T_{-2}) > \quad = \quad \int_{\mathbb{T}} \overline{y}(T_{-2}) z(T_{-2})\, dT_{-2}, \tag{3.2.18}$$

where $\overline{y}$ is the complex conjugate of y. The Fredholm theorem states that the necessary and sufficient condition for the inhomogeneous equation $\mathcal{L}\psi = g$ to have a bounded solution is that $g(T_{-2})$ be orthogonal to the null-space of the operator $\mathcal{L}$. In $L^2(\mathbb{T})$ the null-space is clearly spanned by a (normalized) constant solution $\psi = 1$. Hence, the solvability condition provided by the Fredholm theorem is

$$\int_0^{2\pi} g(T_{-2})\, dT_{-2} \quad = \quad 0. \tag{3.2.19}$$

This condition is what we refer to as the solvability condition in the following calculations.

From the terms of order $\mathcal{O}(\epsilon^{-1/2})$, we obtain

$$D_{-2}^2\phi_3 + \alpha\, D_{-2}\phi_1 \quad = \quad 0, \tag{3.2.20}$$

which can be integrated to

$$\phi_3(x, T_{-2}, T_{-1}, \dots) \quad = \quad \alpha\, F \sin(T_{-2}). \tag{3.2.21}$$

The terms of order $\mathcal{O}(1)$ give

$$D_{-2}^2\phi_4 - \phi_{0,xx} + D_0^2\phi_0 + \alpha\, D_0\phi_0 + \sin\left(\phi_0+\theta\right) - \gamma \;=\; 0. \tag{3.2.22}$$

Averaging over the fast-time scale, we obtain the solvability condition

$$-\phi_{0,xx} + D_0^2\phi_0 + \alpha D_0\phi_0 + \sin(\phi_0+\theta) - \gamma \;=\; 0, \tag{3.2.23}$$

which subtracting (3.2.23) from (3.2.22) yields $D_{-2}^2\phi_4 = 0$, hence

$$\phi_4(x, T_{-2}, T_{-1}, \dots) \;=\; 0. \tag{3.2.24}$$

Equation (3.2.23) will be used later in the construction of our averaged equation.

The terms of the order of $\mathcal{O}(\epsilon^{1/2})$ give

$$D_{-2}^2\phi_5 + \alpha\left(D_{-2}\phi_3 + D_1\phi_0\right) + 2D_0D_1\phi_0 + \cos\left(\phi_0+\theta\right)\phi_1 \;=\; 0, \tag{3.2.25}$$

with the solvability condition

$$2\,D_0D_1\phi_0 + \alpha\, D_1\phi_0 \;=\; 0. \tag{3.2.26}$$

Subtracting (3.2.26) from (3.2.25), we obtain

$$D_{-2}^2\phi_5 + \alpha\, D_{-2}\phi_3 + \cos\left(\phi_0+\theta\right)\phi_1 \;=\; 0, \tag{3.2.27}$$

whose solution is

$$\phi_5(x, T_{-2}, \dots) \;=\; -F\cos\left(\phi_0+\theta\right)\cos(T_{-2}) + \alpha^2\, F\cos(T_{-2}). \tag{3.2.28}$$

The terms of order $\mathcal{O}(\epsilon)$ give

$$D_{-2}^2\phi_6 + 2D_{-2}D_{-1}\phi_5 + 2\,D_0D_2\phi_0 + D_1^2\phi_0 + \alpha D_2\phi_0 - \frac{1}{2}\phi_1^2\sin\left(\phi_0+\theta\right) = 0, \tag{3.2.29}$$

which gives the solvability condition

$$\left(2D_0D_2 + D_1^2\right)\phi_0 + \alpha D_2\phi_0 - \frac{1}{2}\langle\phi_1^2\rangle\sin\left(\phi_0+\theta\right) \;=\; 0. \tag{3.2.30}$$

Subtracting (3.2.30) from (3.2.29), we obtain

$$D_{-2}^2\phi_6 + 2\,D_{-2}D_{-1}\phi_5 - \frac{1}{2}\left(\phi_1^2 - \langle\phi_1^2\rangle\right)\sin\left(\phi_0+\theta\right) \;=\; 0. \tag{3.2.31}$$

In [122, 134, 135], a double sine-Gordon equation is obtained as the governing equation for the dynamics on the slow timescale. To obtain a similar equation for ϕ_0, we need to proceed with the further calculations. Nevertheless, from hereon we are not going to

calculate the explicit solutions of $\phi_j (j \geq 6)$ that contribute to higher-order corrections, we focus on finding the solvability conditions.

From the terms of order $\mathcal{O}(\epsilon^{3/2})$, we obtain

$$D_{-2}^2\phi_7 + 2D_{-2}D_{-1}\phi_6 + \left(2D_{-2}D_0 + D_{-1}^2\right)\phi_5 + 2\left(D_0D_3 + D_1D_2\right)\phi_0 \\ +\alpha\left(D_{-2}\phi_5 + D_3\phi_0\right) + \cos\left(\phi_0 + \theta\right)\left(\phi_3 - \frac{1}{6}\phi_1^3\right) = 0, \qquad (3.2.32)$$

from which one obtains the solvability condition

$$2\left(D_0D_3 + D_1D_2\right)\phi_0 + \alpha D_3\phi_0 \quad = \quad 0. \qquad (3.2.33)$$

The terms of the order of $\mathcal{O}(\epsilon^2)$ give

$$D_{-2}^2\phi_8 + 2D_{-2}D_{-1}\phi_7 + 2D_{-2}D_0\phi_6 + D_{-1}^2\phi_6 + 2\left(D_{-2}D_1 + D_{-1}D_0\right)\phi_5 \\ +2(D_0D_4 + D_1D_3)\phi_0 + D_2^2\phi_0 + \alpha\left(D_{-2}\phi_6 + D_{-1}\phi_5 + D_4\phi_0\right) \\ + \left(\frac{1}{24}\phi_1^4 - \phi_3\phi_1\right)\sin\left(\phi_0 + \theta\right) = 0. \qquad (3.2.34)$$

Using the Fredholm alternative, the solvability condition for the above equation is

$$D_2^2\phi_0 + \left(2\,D_0D_4 + 2\,D_1D_3\right)\phi_0 + \alpha\,D_4\phi_0 + \frac{1}{24}\langle\phi_1^4\rangle\,\sin\left(\phi_0 + \theta\right) = 0. \qquad (3.2.35)$$

Terms of order $\mathcal{O}(\epsilon^{5/2})$ give

$$D_{-2}^2\phi_9 + 2\,D_{-2}D_{-1}\phi_8 + 2\,D_{-2}D_0\phi_7 + D_{-1}^2\phi_7 + 2\left(D_{-2}D_1 + D_{-1}D_0\right)\phi_6 \\ +2\left(D_{-2}D_2 + D_{-1}D_1\right)\phi_5 + D_0^2\phi_5 + 2\,\left(D_0D_5 + D_1D_4 + D_2D_3\right)\phi_0 \\ +\alpha\Big(D_{-1}\phi_6 + D_0\phi_5 + D_{-2}\phi_7 + D_5\phi_0\Big) + \cos\left(\phi_0 + \theta\right)\phi_5 \\ -\left(\frac{1}{2}\phi_3\phi_1^2 - \frac{1}{120}\phi_1^5\right)\cos\left(\phi_0 + \theta\right) = 0, \qquad (3.2.36)$$

which yields the solvability condition

$$2(D_0D_5 + D_1D_4 + D_2D_3)\phi_0 + \alpha D_5\phi_0 \quad = \quad 0. \qquad (3.2.37)$$

Terms of order $\mathcal{O}(\epsilon^3)$ give

$$D_{-2}^2\phi_{10} + 2\,D_{-2}D_{-1}\phi_9 + 2\,D_{-2}D_0\phi_8 + D_{-1}^2\phi_8 + 2\left(D_{-2}D_1 + D_{-1}D_0\right)\phi_7 \\ +D_0^2\phi_6 + 2\left(D_{-2}D_2 + D_{-1}D_1\right)\phi_6 + 2\left(D_{-2}D_3 + D_{-1}D_2 + D_0D_1\right)\phi_5 + D_3^2\phi_0 \\ +2\left(D_1D_5 + D_2D_4 + D_0D_6\right)\phi_0 + \alpha\Big(D_6\phi_0 + D_{-2}\phi_8 + D_{-1}\phi_7 + D_0\phi_6 + D_1\phi_5\Big) \\ +\Big(\frac{1}{6}\phi_3\phi_1^3 - \frac{1}{720}\phi_1^6 - \frac{1}{2}\phi_3^2 - \phi_5\phi_1\Big)\sin\left(\phi_0 + \theta\right) + \cos\left(\phi_0 + \theta\right)\phi_6 = 0, \qquad (3.2.38)$$

from which we obtain the solvability condition

$$D_3^2\phi_0 + 2\left(D_1D_5 + D_2D_4 + D_0D_6\right)\phi_0 + \alpha D_6\phi_0 - \left[\langle\phi_5\phi_1\rangle + \frac{1}{720}\langle\phi_1^6\rangle + \frac{1}{2}\langle\phi_3^2\rangle\right]\sin\left(\phi_0+\theta\right) = 0. \tag{3.2.39}$$

We will not proceed further, as we have obtained a double-angle term in the average equation, through the terms $\langle\phi_5\phi_1\rangle$ (see, (3.2.11) and (3.2.28)).

To obtain an average equation, we add Equations (3.2.14), (3.2.23), (3.2.26), (3.2.30), (3.2.33), (3.2.37), (3.2.35), (3.2.39), to obtain the averaged equation up to $\mathcal{O}(\epsilon^3)$ as

$$\frac{\partial^2\phi_0}{\partial t^2} - \frac{\partial^2\phi_0}{\partial x^2} + \alpha\frac{\partial\phi_0}{\partial t} + \sin\left(\phi_0+\theta\right) - \gamma = \left[\frac{1}{2}\epsilon\langle\phi_1^2\rangle - \frac{1}{24}\epsilon^2\langle\phi_1^4\rangle + \epsilon^3\left(\langle\phi_5\phi_1\rangle + \frac{1}{720}\langle\phi_1^6\rangle + \frac{1}{2}\langle\phi_3^2\rangle\right)\right]\sin\left(\phi_0+\theta\right), \tag{3.2.40}$$

calculating the right hand side, thus

$$\frac{\partial^2\phi_0}{\partial t^2} - \frac{\partial^2\phi_0}{\partial x^2} + \alpha\frac{\partial\phi_0}{\partial t} - \gamma = \left(\frac{\epsilon F^2}{4} - \frac{\epsilon^2F^4}{64} + \frac{\epsilon^3F^6}{2304} - \frac{\epsilon^3\alpha^2F^2}{4} - 1\right)\sin(\phi_0+\theta) + \frac{\epsilon^3F^2}{4}\sin\left(2\phi_0+2\theta\right), \tag{3.2.41}$$

reintroducing the original scaling (3.2.1) , we obtain the 'average' equation the double sine-Gordon equation

$$\frac{\partial^2\phi_0}{\partial x^2} - \frac{\partial^2\phi_0}{\partial t^2} - \alpha\frac{\partial\phi_0}{\partial t} + \gamma = j_1\sin(\phi_0+\theta) - j_2\sin\left(2\,\phi_0+2\,\theta\right), \tag{3.2.42}$$

with

$$j_1 = 1 - \frac{f^2}{4\,\Omega^4} + \frac{f^4}{64\,\Omega^8} + \frac{\alpha^2f^2}{4\,\Omega^6} - \frac{f^6}{2304\,\Omega^{12}} + \ldots, \tag{3.2.43}$$

$$j_2 = \frac{f^2}{4\,\Omega^6} + \ldots. \tag{3.2.44}$$

In [122, 134, 135], using different methods and for $\theta \equiv 0$, the coefficients j_i of the average equation above were given by

$$j_1 = J_0\left(a_1\right) + \frac{a_1^2\alpha^2\left(J_2(a_1) - J_0(a_1)\right)}{4\Omega^2} + \frac{a_1\alpha^2J_1(a_1)}{\Omega^2}, \tag{3.2.45}$$

$$j_2 = \frac{J_1^2(a_1)}{\Omega^2} + \frac{a_1^2\alpha^2J_0(a_1)J_2(a_1)}{32\Omega^4} + \frac{a_1\alpha^2J_1(a_1)J_2(a_1)}{16\Omega^4}, \tag{3.2.46}$$

with $a_1 = -f/\Omega^2$ and J_i for $i = 0, 1, 2$ are Bessel functions of the first kind. Via simple inspection, one can confirm that (3.2.43) and (3.2.44) are the leading order series expansions of (3.2.45) and (3.2.46). With the method proposed herein, one has more control on the scales of the driving parameters and the coefficients of the 'average' equation are given by simple explicit functions.

3.3 Multiscale averaging with small driving amplitude

Next, we consider the case of slowly oscillating direct driving force in the sine-Gordon Equation (3.1.1) with, $\Omega = 1/\epsilon$, $f = \epsilon H$. In experiments the drive amplitude f can be small or large. Nevertheless, as we noted in [134, 135] when $f \sim \Omega^2$. Therefore other scaling, including the experimentally relevant case of f, can be considered similarly.

In order to derive an average equation, we use multiscale expansion

$$T_n = \epsilon^n t, \quad n = -1, 0, 1, 2, \ldots, \tag{3.3.1}$$

$$\phi \;=\; \phi_0 + \epsilon\,\phi_1 + \epsilon^2\phi_2 + ..., \tag{3.3.2}$$

where $\phi_i(x, T_{-1}, T_0, T_1, ..)$ are periodic in T_{-1} with period 2π. For the problem above, it should be noted that we choose $T_{-1} = t/\epsilon$ as the fast variable. For further details see Section 3.2.

To derive an effective equation for the function ϕ_0, we substitute (3.3.2) into (3.1.1), expanding order by order to obtain a hierarchy of equations.

The terms at order $\mathcal{O}(\epsilon^{-2})$, give

$$D_{-1}^2\phi_0 \;=\; 0, \tag{3.3.3}$$

which implies

$$\phi_0 \;=\; \phi_0(T_0, T_1, ..). \tag{3.3.4}$$

This shows that $\phi_0(T_0, T_1, ..)$ is independent of T_{-1}.

The terms at order $\mathcal{O}(1/\epsilon)$, give

$$D_{-1}{}^2\phi_1 + 2\,D_{-1}D_0\phi_0 + \alpha\,D_{-1}\phi_0 \;=\; 0, \tag{3.3.5}$$

by integrating over $0 \le T_{-1} \le 2\pi$ we obtain

$$\phi_1(x, T_{-1}, T_0, T_1...) \;=\; 0. \tag{3.3.6}$$

The terms at order $\mathcal{O}(1)$, give

$$D_{-1}{}^2\phi_2 - \phi_{0,xx} + D_0{}^2\phi_0 + \alpha\,D_0\phi_0 + \sin\left(\phi_0 + \theta(x)\right) - \gamma \;=\; 0. \tag{3.3.7}$$

The solvability condition for this equation is

$$-\phi_{0,xx} + D_0{}^2\phi_0 + \alpha\,D_0\phi_0 + \sin\left(\phi_0 + \theta(x)\right) - \gamma \;=\; 0, \tag{3.3.8}$$

from (3.3.7) and (3.3.8) we obtain

$$D_{-1}{}^2\phi_2 \quad = \quad 0, \tag{3.3.9}$$

which implies

$$\phi_2(x, T_0, T_1, ..) \quad = \quad 0. \tag{3.3.10}$$

The terms at order $\mathcal{O}(\epsilon)$ give

$$\begin{aligned} D_{-1}{}^2\phi_3 + 2D_0D_1\phi_0 + \alpha D_1\phi_0 + (D_0^2 + \alpha D_0 + \cos(\phi_0 + \theta))\phi_1 \\ = H\cos(T_{-1}), \end{aligned} \tag{3.3.11}$$

the solvability condition for the above equation is

$$2\,D_0D_1\phi_0 + \alpha\,D_1\phi_0 \quad = \quad 0. \tag{3.3.12}$$

Subtracting (3.3.12) from (3.3.11) and integrating twice, we obtain

$$\phi_3(x, T_{-1}, T_0, T_1, ..) \quad = \quad -H\cos(T_{-1}). \tag{3.3.13}$$

Terms at order $\mathcal{O}(\epsilon^2)$ give

$$D_{-1}^2\phi_4 + \left(2\,D_0D_2 + D_1^2\right)\phi_0 + \alpha\,\left(D_{-1}\phi_3 + D_2\phi_0\right) \quad = \quad 0, \tag{3.3.14}$$

for which the solvability condition is

$$\left(2\,D_0D_2 + D_1^2\right)\phi_0 + \alpha\,D_2\phi_0 \quad = \quad 0. \tag{3.3.15}$$

Subtracting (3.3.15) from (3.3.14) we obtain

$$\phi_4(x, T_{-1}, T_0, T_1, ..) \quad = \quad \alpha\,H\sin(T_{-1}). \tag{3.3.16}$$

The terms at order $\mathcal{O}(\epsilon^3)$, give

$$D_{-1}^2\phi_5 + 2\left(D_2D_1 + D_3D_0\right)\phi_0 + \alpha\left(D_{-1}\phi_4 + D_3\phi_0\right) + \cos\left(\phi_0 + \theta\right)\phi_3 = 0, \tag{3.3.17}$$

the solvability condition for which is

$$2\,\left(D_2D_1 + D_3D_0\right)\phi_0 + \alpha\,D_3\phi_0 \quad = \quad 0. \tag{3.3.18}$$

Subtracting (3.3.18) from (3.3.17) we have

$$D_{-1}^2\phi_5 + \alpha\,D_{-1}\phi_4 + \cos\left(\phi_0 + \theta(x)\right)\phi_3 = 0, \tag{3.3.19}$$

by integrating the above equation, we obtain

$$\phi_5(x, T_{-1}, T_0, T_1, ..) \quad = \quad \alpha^2\,H\cos(T_{-1}) - H\cos\left(\phi_0 + \theta(x)\right)\cos(T_{-1}). \tag{3.3.20}$$

From hereon, we do not calculate the explicit solutions as they do not appear in the final averaged equation. However, we will calculate the solvability conditions to obtain an averaged equation for ϕ_0.
The terms at order $\mathcal{O}(\epsilon^4)$, give

$$D_{-1}^2\phi_6 + 2\,D_{-1}D_0\phi_5 + \left(D_2^2 + 2\,D_4D_0 + 2\,D_1D_3\right)\phi_0 + \alpha\,\left(D_{-1}\phi_5 + D_4\phi_0\right) + \cos\left(\phi_0 + \theta(x)\right)\phi_4 = 0, \quad (3.3.21)$$

the solvability condition for the above equation is

$$\left(D_2{}^2 + 2\,D_4D_0 + 2\,D_1D_3\right)\phi_0 + \alpha\,D_4\phi_0 \;=\; 0. \quad (3.3.22)$$

The terms at order $\mathcal{O}(\epsilon^5)$ give

$$D_{-1}^2\phi_7 + 2D_{-1}D_0\phi_6 + \left(2D_{-1}D_1 + D_0^2\right)\phi_5 + 2\left(D_2D_3 + D_0D_5\right)\phi_0 + 2\,D_4D_1\phi_0 + \alpha\,\left(D_{-1}\phi_6 + D_0\phi_5 + D_5\phi_0\right) + \cos\left(\phi_0 + \theta(x)\right)\phi_5 = 0, \quad (3.3.23)$$

the solvability condition for which is

$$2\,\left(D_2D_3 + D_0D_5 + D_4D_1\right)\phi_0 + \alpha\,D_5\phi_0 \;=\; 0. \quad (3.3.24)$$

The terms at order $\mathcal{O}(\epsilon^6)$ give

$$D_{-1}^2\phi_8 + 2\,D_{-1}D_0\phi_7 + \left(2\,D_{-1}D_1 + D_0^2\right)\phi_6 + 2\,\left(D_{-1}D_2 + D_0D_1\right)\phi_5 + D_3^2\phi_0 + 2\left(D_2D_4 + D_0D_6 + D_1D_5\right)\phi_0 + \alpha\left(D_{-1}\phi_7 + D_0\phi_6 + D_1\phi_5\right) + \alpha D_6\phi_0 - \frac{1}{2}\,\sin\left(\phi_0 + \theta(x)\right)\phi_3^2 + \cos\left(\phi_0 + \theta(x)\right)\phi_6 = 0, \quad (3.3.25)$$

the solvability condition for which is

$$D_3{}^2\phi_0 + 2\left(D_2D_4 + D_0D_6 + D_1D_5\right)\phi_0 + \alpha D_6\phi_0 - \frac{1}{2}\langle\phi_3^2\rangle\sin\left(\phi_0 + \theta\right) = 0. \quad (3.3.26)$$

The terms at order $\mathcal{O}(\epsilon^7)$ give

$$D_{-1}^2\phi_9 + 2\,D_{-1}D_0\phi_8 + \left(2\,D_{-1}D_1 + D_0^2\right)\phi_7 + 2\left(D_2D_{-1} + D_1D_0\right)\phi_6 + D_1^2\phi_5 + 2\,\left(D_{-1}D_3 + D_2D_0\right)\phi_5 + 2\left(D_1D_6 + D_5D_2 + D_4D_3 + D_7D_0\right)\phi_0 + \alpha D_0\phi_7 + \alpha\left(D_{-1}\phi_8 + D_7\phi_0 + D_2\phi_5 + D_1\phi_6\right) - \sin\left(\phi_0 + \theta(x)\right)\phi_4\phi_3 + \cos\left(\phi_0 + \theta(x)\right)\phi_7 = 0, \quad (3.3.27)$$

the solvability condition for which is

$$2\,\left(D_1D_6 + D_5D_2 + D_4D_3 + D_7D_0\right)\phi_0 + \alpha\,D_7\phi_0 \;=\; 0. \quad (3.3.28)$$

The terms at order $\mathcal{O}(\epsilon^8)$ give

$$\begin{aligned}
&D_{-1}^2\phi_{10} + 2\,D_{-1}D_0\phi_9 + \left(2\,D_{-1}D_1 + D_0^2\right)\phi_8 + 2\,\left(D_2D_{-1} + D_1D_0\right)\phi_7 + D_1^2\phi_6 \\
&+2\left(D_{-1}D_3 + D_2D_0\right)\phi_6 + 2\left(D_{-1}D_4 + D_3D_0 + D_2D_1\right)\phi_5 + \left(D_4^2 + 2D_1D_7\right)\phi_0 \\
&+2\left(D_8D_0 + D_3D_5 + D_6D_2\right)\phi_0 + \alpha\left(D_{-1}\phi_9 + D_0\phi_8 + D_3\phi_5 + D_8\phi_0 + D_1\phi_7\right) \\
&+\alpha\,D_2\phi_6 - \left(\phi_5\phi_3 + \frac{1}{2}\,{\phi_4}^2\right)\sin\left(\phi_0 + \theta(x)\right) + \cos\left(\phi_0 + \theta(x)\right)\phi_8 = 0, \qquad (3.3.29)
\end{aligned}$$

the solvability condition for which is

$$\begin{aligned}
&D_4^2\phi_0 + 2\left(\,D_1D_7 + D_8D_0 + D_3D_5 + D_6D_2\right)\phi_0 \\
&\quad - \left(\langle\phi_5\phi_3\rangle + \frac{1}{2}\langle\phi_4^2\rangle\right)\sin\left(\phi_0 + \theta(x)\right) = 0. \qquad (3.3.30)
\end{aligned}$$

Adding (3.3.8), (3.3.12), (3.3.15), (3.3.18), (3.3.22), (3.3.24), (3.3.26), (3.3.28), (3.3.30), with appropriate scalings, we obtain the averaged equation up to $\mathcal{O}(\epsilon^8)$ as

$$\begin{aligned}
&\frac{\partial^2\phi_0}{\partial t^2} - \frac{\partial^2\phi_0}{\partial x^2} + \alpha\frac{\partial\phi_0}{\partial t} + \sin\left(\phi_0 + \theta(x)\right) - \gamma \\
&= \left[\epsilon^6\langle\phi_3^2\rangle + \epsilon^8\left(\langle\phi_3\phi_5\rangle + \frac{1}{2}\langle\phi_4^2\rangle\right)\right]\sin\left(\phi_0 + \theta(x)\right). \qquad (3.3.31)
\end{aligned}$$

The right hand side can be calculated further

$$\frac{\partial^2\phi_0}{\partial x^2} - \frac{\partial^2\phi_0}{\partial t^2} - \alpha\frac{\partial\phi_0}{\partial t} + \gamma \;=\; J_1\sin\left(\phi_0 + \theta(x)\right) - J_2\sin\left(2\phi_0 + 2\theta(x)\right), \qquad (3.3.32)$$

with

$$J_1 \;=\; 1 - \frac{f^2}{2\,\Omega^4} + \frac{\alpha^2 f^2}{4\,\Omega^6} + \ldots, \qquad (3.3.33)$$

$$J_2 \;=\; \frac{f^2}{4\,\Omega^6}. \qquad (3.3.34)$$

Noting the similarity between (3.2.43) and (3.3.33), we may expect that the average Equation (3.2.42) will also provide a good approximation on the case $|f| \ll 1$. Because of that, in the following we will only consider (3.2.42).

3.4 Critical facet length and critical current in long Josephson junctions with phase-shifts

In this section, we discuss the effect of the oscillating drive to the ground state of Josephson junctions with phase-shifts $\theta\,(x)$ defined by (3.1.2) or (3.1.3).

3.4.1 $0-\pi-0$ junctions without dc-current

We consider first the case of $0-\pi-0$ junctions, i.e. $\theta(x)$ given by (3.1.2) in the absence of a constant bias current ($\gamma = 0$). Note that the length of the π region is also referred to as the facet length. The ground state of such a junction crucially depends on the parameter a. As mentioned above, there is a critical facet length a_c above which the ground state is nonuniform. Such a ground state represents an antiferromagnetically ordered semivortex-antisemivortex state [32].

One may calculate the critical facet length of the average Equation (3.2.42) through calculating the value of a at which the zero solution changes its stability. Using a simple calculation, one can obtain the linearized equation about $\phi_0 = 0$ of (3.2.42)

$$\varphi_{1,xx} - \varphi_{1,tt} = j_1 \cos(\theta)\varphi_1 - 2\, j_2 \cos(2\theta)\, \varphi_1, \tag{3.4.1}$$

whose solution can be easily calculated as

$$\varphi_1(x,t) = B\, e^{i\omega t} \begin{cases} \cos(a\sqrt{j_1 - 2\,j_2 + \omega^2}) e^{\sqrt{j_1 - 2\,j_2 - \omega^2}(a+x)}, & x < -a, \\ \cos(x\sqrt{j_1 - 2\,j_2 + \omega^2}), & |x| < a, \\ \cos(a\sqrt{j_1 - 2\,j_2 + \omega^2}) e^{\sqrt{j_1 - 2\,j_2 - \omega^2}(a-x)}, & x > a. \end{cases} \tag{3.4.2}$$

The relation $a = a(\omega)$ is then given by

$$a = \frac{\tan^{-1}\left(\sqrt{\frac{j_1 - 2j_2 - \omega^2}{j_1 - 2j_2 + \omega^2}}\right)}{\sqrt{j_1 - 2j_2 + \omega^2}}. \tag{3.4.3}$$

Half the critical facet length a_c is defined as the point where $\omega = 0$, that is,

$$a_c = \frac{\pi}{4\sqrt{j_1 - 2\,j_2}}. \tag{3.4.4}$$

3.4.2 $0-\kappa$ junctions with constant bias current

For the phase-shift configuration $\theta(x)$ given by (3.1.3), there is a critical bias current γ_c above which the junction has no static ground states. Here, we follow the calculation of, e.g., [27] to derive an analytical approximation to the critical bias current in the presence of ac-drive. First, we rescale

$$x = \frac{\widetilde{x}}{\sqrt{j_1}}, \quad \widetilde{d} = -\frac{j_2}{j_1}, \quad \widetilde{\gamma} = \frac{\gamma}{j_1}, \quad \widetilde{\gamma_c} = \frac{\gamma_c}{j_1}. \tag{3.4.5}$$

With the above scalings, Equation (3.2.42) becomes

$$\frac{\partial^2 \phi_0}{\partial \widetilde{x}^2} = \sin(\phi_0 + \theta) + \widetilde{d}\, \sin(2\,(\phi_0 + \theta)) - \widetilde{\gamma}. \tag{3.4.6}$$

The boundary conditions at the discontinuity point $\widetilde{x}$ are given by [32, 138, 139]

$$\phi_0(0^+) = \phi_0(0^-), \quad \frac{\partial}{\partial\widetilde{x}}\phi_0(0^+) = \frac{\partial}{\partial\widetilde{x}}\phi_0(0^-). \tag{3.4.7}$$

Next, we need to determine the equation for $\phi_{0_{\widetilde{x}}}$. The first integral of Equation (3.4.6) is

$$\frac{1}{2}\left(\frac{\partial\phi_0}{\partial\widetilde{x}}\right)^2 = -\cos(\phi_0+\theta) - \frac{\widetilde{d}}{2}\cos\left(2\,(\phi_0+\theta)\right) - \widetilde{\gamma}\phi_0 + C_\pm, \tag{3.4.8}$$

where $C_\pm$ are constants of integration, i.e. C_+ for the region $x > 0$ and C_- for $x < 0$. The constants are obtained from the boundary conditions

$$\lim_{\widetilde{x}\to\pm\infty}\phi_0(\widetilde{x}) = \phi_{0_\pm},$$

a consequence of this

$$\lim_{\widetilde{x}\to\pm\infty}\phi_{0_{\widetilde{x}}}(\widetilde{x}) = 0,$$

which correspond to kink solutions with nonzero constant drive. The integral constants $C_\pm$ can then be calculated as

$$C_- = \cos(\phi_{0_-}) + \frac{\widetilde{d}}{2}\cos\left(2\,\phi_{0_-}\right) + \widetilde{\gamma}\phi_{0_-}, \tag{3.4.9}$$

$$C_+ = \cos(\phi_{0_+} - \kappa) + \frac{\widetilde{d}}{2}\cos\left(2\,\phi_{0_+} - \kappa\right) + \widetilde{\gamma}\phi_{0_+}. \tag{3.4.10}$$

Equations (3.4.6) and (3.4.8) and the conditions in (3.4.7) determine γ_c as a function of κ and $\widetilde{d}$.

Rather than obtaining an explicit expression of γ for any $\widetilde{d}$, here we calculate it perturbatively for small $\widetilde{d}$, which is relevant for the scaling (3.2.1). Hence, we expand all quantities as follows

$$\phi_0 \approx \phi^{(0)} + \widetilde{d}\,\phi^{(1)}, \quad \widetilde{\gamma} \approx \widetilde{\gamma}^{(0)} + \widetilde{d}\,\widetilde{\gamma}^{(1)}, \quad \widetilde{\gamma}_c \approx \widetilde{\gamma}_c^{(0)} + \widetilde{d}\,\widetilde{\gamma}_c^{(1)}.$$

Substituting these expansions into (3.4.6) and (3.4.8), equating the $\mathcal{O}(\widetilde{d})$ terms we obtain the equations

$$\phi^{(1)}_{\widetilde{x}\widetilde{x}} = \begin{cases} \phi^{(1)}\cos(\phi^{(0)}) + \sin 2\,(\phi^{(0)}) - \widetilde{\gamma}^{(1)}, & (\widetilde{x} < 0), \\ \phi^{(1)}\cos(\phi^{(0)} - \kappa) + \sin 2\,(\phi^{(0)} - \kappa) - \widetilde{\gamma}^{(1)}, & (\widetilde{x} > 0), \end{cases} \tag{3.4.11}$$

$$\phi^{(0)}_{\widetilde{x}}\phi^{(1)}_{\widetilde{x}} = \begin{cases} \phi^{(1)}_-\sin(\phi^{(0)}_-) - \phi^{(1)}\sin(\phi^{(0)}) - \widetilde{\gamma}^{(0)}(\phi^{(1)} - \phi^{(1)}_-) \\ -\widetilde{\gamma}^{(1)}(\phi^{(0)} - \phi^{(0)}_-) + \frac{1}{2}(\cos 2\,(\phi^{(0)}_-) - \cos 2\,(\phi^{(0)})), & (\widetilde{x} < 0), \\ \phi^{(1)}_+\sin(\phi^{(0)}_+ - \kappa) - \phi^{(1)}\sin(\phi^{(0)} - \kappa) - \widetilde{\gamma}^{(0)}(\phi^{(1)} - \phi^{(1)}_+) \\ -\widetilde{\gamma}^{(1)}(\phi^{(0)} - \phi^{(0)}_+) + \frac{1}{2}(\cos 2\,(\phi^{(0)}_+ - \kappa) - \cos 2\,(\phi^{(0)} - \kappa)), & (\widetilde{x} > 0), \end{cases} \tag{3.4.12}$$

where

$$\phi_{\pm}^{(i)} = \lim_{\tilde{x}\to\pm\infty} \phi^{(i)}, \quad i = 0, 1.$$

We also conclude that

$$\phi_{-}^{(0)} = \arcsin \widetilde{\gamma}^{(0)} = \phi_{+}^{(0)} - \kappa, \tag{3.4.13}$$

$$\phi_{-}^{(1)} = \phi_{+}^{(1)} = \frac{\widetilde{\gamma}^{(1)}}{\sqrt{1-\widetilde{\gamma}^{(0)2}}}. \tag{3.4.14}$$

From the condition (cf. (3.4.7))

$$\lim_{\tilde{x}\to 0^{+}} \phi_{\tilde{x}\tilde{x}}^{(i)} = \lim_{\tilde{x}\to 0^{-}} \phi_{\tilde{x}\tilde{x}}^{(i)}, \quad i = 0, 1,$$

we obtain

$$\phi^{(0)}(0) = \frac{\kappa}{2} + \frac{\pi}{2}, \quad \phi^{(1)}(0) = -2\cos(\kappa/2).$$

The critical bias current of $\mathcal{O}(1)$ and $\mathcal{O}(\widetilde{d})$ are then given respectively by

$$\widetilde{\gamma}_c^{(0)} = -\frac{2\sin(\kappa/2)}{\kappa}, \qquad \widetilde{\gamma}_c^{(1)} = 0, \tag{3.4.15}$$

i.e. the second harmonic does not influence the critical current. Hence, reverting to scaling (3.4.5) at leading order the critical current is

$$\gamma_c = -\frac{2j_1\sin(\kappa/2)}{\kappa}, \tag{3.4.16}$$

from which we obtain that the ac-drive term of amplitude f has the effect of reducing the critical bias current by an amount of $\mathcal{O}(f^2/\Omega^4)$.

3.5 Numerical results

Here, we compare the analytical results obtained in the preceding section with the numerics of the original governing Equation (3.1.1). In all the results presented herein, we set $\alpha = 0.2$. We use periodic boundary conditions in a relatively long domain, i.e. $|x| < L$, $L \gg 1$ (particularly for $L = 100$), to simulate the infinite regime. The derivative with respect to x is approximated with either finite difference or spectral discretization with the spatial discretization $\delta x = 0.05$. The derivative with respect to t is integrated using a Runge-Kutta solver of fourth order using the temporal discretization $\delta t = 0.005$.

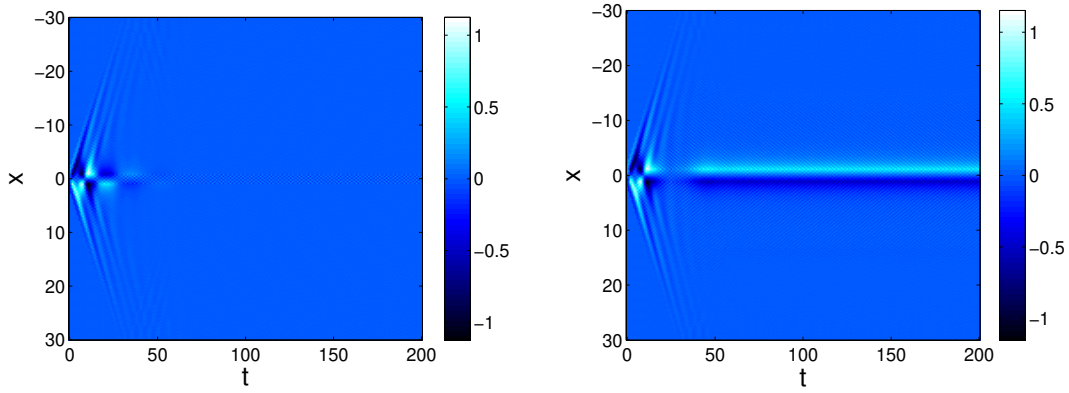

(a) $a = 1.0$ **(b)** $a = 1.1$

Figure 3.1: We plot ϕ_x against (x,t) to illustrate the time dynamics of the phase-difference ϕ of (3.1.1) with θ given in (3.1.2), $f = 140$ and $\Omega = 10$. Half the facet length is depicted in the caption of each panel.

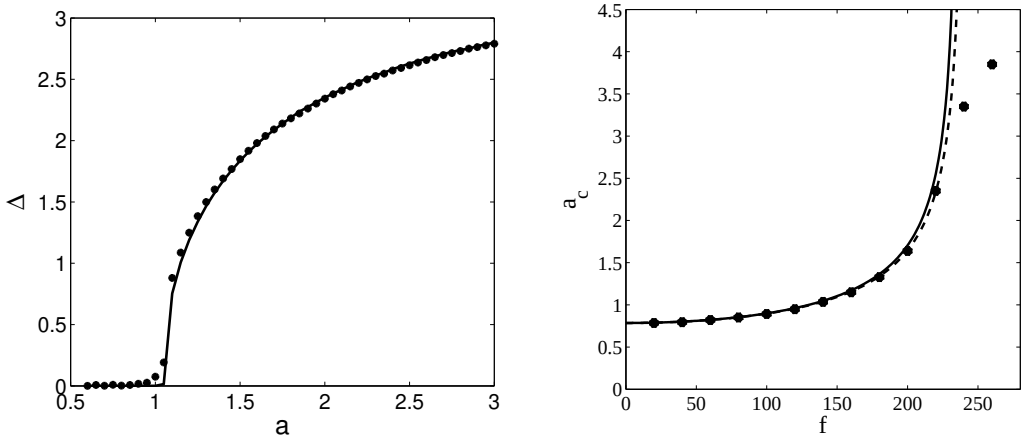

Figure 3.2: The left panel shows the amplitude of the ground state Δ of the junction as a function of a. Filled circles are data from (3.1.1) and solid line is from (3.2.42). The right panel depicts half the critical facet length a_c as a function of the oscillation amplitude f with $\Omega = 10$. Filled-circles are data obtained from a numerical simulation of the governing Equation (3.1.1) and the solid line is the analytical result (3.4.4) with j_i obtained using our method (3.2.43)-(3.2.44). The dashed line is the analytical result (3.4.4) with j_i from [134, 135], i.e. (3.2.45)-(3.2.46).

3.5.1 $0-\pi-0$ junctions without a constant bias current

First, we consider the ground state of $0-\pi-0$ junctions with $\gamma = 0$. In the absence of ac drives ($f = 0$), when half the facet length a is larger than $\pi/4$, the uniform zero solution is unstable [32].

Figure 3.1(a) shows the dynamics of the phase-difference $\phi(x,t)$ for $a = 1$. At $t = 0$, we use a zero initial displacement and velocity. With $f = 140$ and $\Omega = 10$, one notices that the zero solution is stable, even though $a > \pi/4$. Yet, when $a = 1.1$ it can be easily seen in Fig. 3.1(b) that the ground state is nonuniform. In the left panel of Fig. 3.2, we show the amplitude of the ground state Δ as a function of half the facet length a (filled circles). Because the background is rapidly oscillating due to the presence of the ac drive, here we calculate Δ as the temporal average of the quantity $\delta\phi = \phi(L,t) - \phi(0,t)$ after the transient state disappears. Half the critical facet length is the point where a solution with nonzero Δ bifurcates from the trivial solution ($\Delta = 0$, corresponds to uniform solution). From the figure 3.1(a), one can deduce that the critical facet length is larger than $\pi/4$ for nonzero f. The solid line in the figure is the amplitude of the ground state Δ obtained from the average Equation (3.2.42) with j_i given by (3.2.43)-(3.2.44). We see that (3.2.42) indeed approximates the slow time dynamics of (3.1.1).

Performing the same calculations at several values of f, one will obtain $a_c(f)$. The right panel of Figure 3.2 shows the numerical results obtained from solving the governing Equation (3.1.1). We also plot in the same figure (solid curve) the analytical approximation given by (3.4.4) with j_i given by (3.2.43)-(3.2.44), where good agreement is obtained. For completeness, we also plot the analytical approximation (3.4.4) with j_i given by (3.2.45)-(3.2.46). For $\Omega = 10$, one can note that the numerics deviates from the approximations at $f \approx 220$. Using our method, we may need a different scaling to capture this range of f. One possibility is to choose $\Omega = 1/\epsilon$ and $f = F/\epsilon^p$, where $p \geq 2$. Nevertheless, it can be seen that, e.g., for $p = 2$, the leading order terms (cf. (3.2.6)) will contain the drive $F\sin(T_{-2})$. In other words, the leading order term in the expansion of ϕ will be due to the ac force, unlike the case considered herein. Such a scaling can still be analysed using the method presented in this work and this case is suggested as future work.

3.5.2 $0-\kappa$ junctions with constant bias current

Next, we study the effect of ac-drive to the critical bias current of a $0-\kappa$ junction. Here, we only consider the case of $\kappa = \pi$, which is representative for this type of junctions as the other values of κ can be calculated similarly.

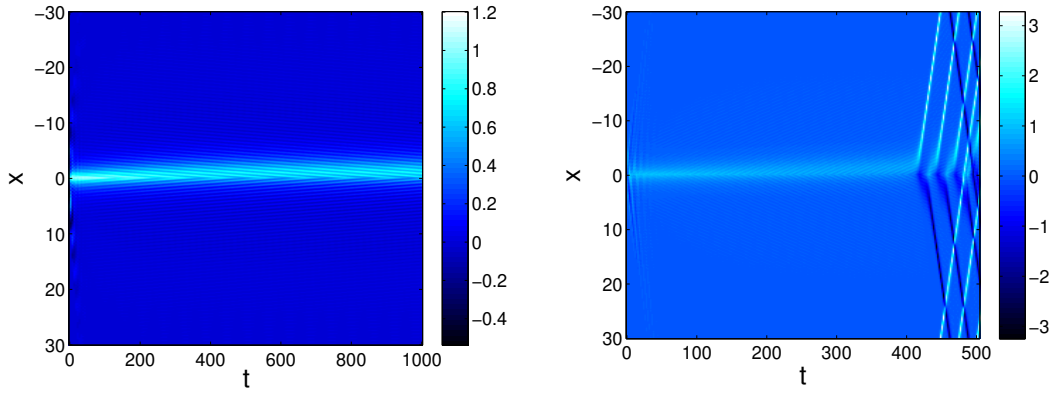

(a) $\gamma_\infty = 0.36$ **(b)** $\gamma_\infty = 0.37$

Figure 3.3: we plot ϕ_x against (x,t) to illustrate the time dynamics of the phase-difference ϕ of (3.1.1) with θ given in (3.1.3), $f = 140$ and $\Omega = 10$. The constant bias current is depicted in the caption of each panel.

In the absence of an ac-drive, it is known that when $\gamma > 2/\pi$, $0 - \pi$ junctions switch into a resistive state where at the point of the phase-shift, i.e. the discontinuity point, fluxons and antifluxons are periodically released.

Using numerical simulation to determine the critical bias current γ_c of Eq. (3.1.1) with $\theta(x)$ given in (3.1.3), one cannot immediately apply a fixed constant γ, as this will create shock and will switch the junction into nonzero voltage states. Because of that, in the simulation we slowly increase the bias current

$$\gamma = \gamma_\infty \left(1 - e^{-t/\tau}\right), \tag{3.5.1}$$

with $\tau = 100$. This choice of function allows the ground state to gradually adjust itself to the presence of the ac-drive. Larger values of τ have been tested as well and we did not see any prominent quantitative difference. At $t = 0$, the initial profile is an exact solution of the system with $f = 0$ and a zero initial velocity.

In Fig. 3.3(a) we show a typical evolution of ϕ_x in the presence of an ac-drive with $f = 140$ and $\Omega = 10$ and an external bias current that is slowly increased to the value of $\gamma_\infty = 0.36$. One can notice that the nonuniform state is deformed due to the dc bias current and tends to a steady state in the limit $t \to \infty$.

In Fig. 3.3(b), we depict the dynamics of the variable ϕ_x when $\gamma_\infty = 0.37$. Here, we see a periodic release of fluxons and antifluxon indicating that the value of the bias current is above the threshold value γ_c. It is important to note that $0.37 < 2/\pi$, i.e. the presence of $f \neq 0$ can indeed decrease the value of the critical bias current γ_c.

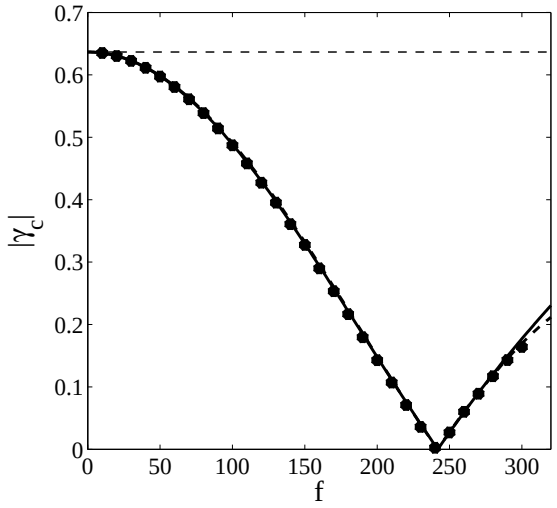

Figure 3.4: Plot of the critical bias current density γ_c as a function of the forcing amplitude f, with $\Omega = 10$. Filled-circles are data obtained from the governing Equation (3.1.1) and solid line is the analytical result (3.4.4) with j_i obtained using our method (3.2.43)-(3.2.44). The dashed line is the analytical result (3.4.16) with j_i from [134, 135], i.e. (3.2.45)-(3.2.46).

The critical bias current γ_c for different values of the driving amplitude f with $\Omega = 10$ is shown in Fig. 3.4, where the filled circles are data obtained numerically from (3.1.1) and the solid line is the analytical result (3.4.16) with j_i given by (3.2.43)-(3.2.44). We observe good agreement between the approximation and the numerics. Note that there is a threshold value of f at which the critical bias current vanishes, i.e. at $f \approx 240$. As the ac-driving amplitude is increased further, we obtain a situation where the numerical data deviates slightly from the approximation.

As a comparison, we also plot the analytical approximation (3.4.16) with j_i given by (3.2.45)-(3.2.46), where we still obtain good agreement between numerics and the approximation. Hence, we argue that the deviation is due to the truncation error in (3.2.43)-(3.2.44), unlike the case in $0 - \pi - 0$ junctions in the previous section.

3.6 Conclusions

We have studied the dynamics of long Josephson junctions with phase-shifts in the presence of a rapidly varying driving force modelled by a periodically driven sine-Gordon equation. We considered the experimentally relevant case of large driving frequency compared to the system's plasma frequency. The case $\Omega < 1$ has been con-

sidered theoretically in [38, 39, 101]. We derived analytically an average equation for the slowly-varying dynamics using multiple scales analysis. The obtained equation takes the form of a damped, forced double sine-Gordon equation.

A double sine-Gordon equation describing the slow-time dynamics of a rapidly driven sine-Gordon equation without phase shift was obtained previously through restricting the phase $\phi(x,t)$ to a Fourier series expansion [134, 135] and a normal form technique [122]. In the normal form technique, several canonical transformations are applied to the Hamiltonian system to move mean-zero terms to higher order [136, 137]. In [134, 135], Kivshar et al. decompose the phase $\phi(x,t)$ into the sum of slowly- and rapidly-varying parts. The method solely uses asymptotic expansions rather than averaging over the fast oscillation. In both methods, the coefficients of the double sine-Gordon equation are given in terms of Bessel functions.

With the method proposed herein, one has more control on the scales of the driving parameters and the coefficients of the 'average' equation are given by simple explicit functions. We obtained analytically the critical value of the applied constant bias current γ_c for the $0-\kappa$ junctions and the the critical facet length in the absence of an external constant bias current for the $0-\pi-0$ junctions from the averaged double sine-Gordon equation.

In the absence of an ac drive, studying the stability of the constant solution in $0-\pi-0$ junction, one finds that there is a critical facet length $a_c = \pi/4$ above which the solution is unstable and the ground state is spatially nonuniform [32], which represents a pair of fractional fluxons of opposite polarities. Here we showed analytically and numerically that in the presence of an ac drive the threshold distance a_c in $0-\pi-0$ junction increases. To compare our approximation as well as that obtained in [134, 135] with numerics, we observed that the numerics slightly deviates at a particular driving amplitude. Using our method, it seems that we require a different scaling of an external drive amplitude mentioned in this work. The applicability of the method presented in this work in that case is suggested as future work.

Next, we studied the effect of ac-drive to the critical bias current of a $0-\kappa$ junction. Here, we only considered the case of $\kappa = \pi$, which is representative for this type of junctions as the other values of κ can be calculated similarly.

It is known that in the presence of an applied dc bias current ($\gamma \neq 0$), the fractional fluxon will be deformed. When the current is large enough, the static ground state will cease to exist and the junction switches to a resistive state by alternately releasing travelling fluxons and antifluxons. In the absence of an external ac-drive the minimum current at which the junction switches to such a state is called the critical current $\gamma_c =$

$2\sin(\kappa/2)/\kappa$ [132, 133]. Hence, $0-\pi$ junctions are in a resistive state when $\gamma > 2/\pi$ with fluxons and antifluxons being periodically released from the discontinuity point.

Using numerical simulations, we determined the critical bias current in the presence of an external ac-drive in $0-\kappa$ junctions. We showed numerically that in the presence of an ac-drive the value of the critical bias current γ_c decreased which confirmed the approximation.

CHAPTER 4

Localised defect modes of sine-Gordon equation with a double well potential with phase-shift

4.1 Introduction

A Josephson junction is a system where two superconducting electrodes are coupled via an insulator whose properties were first predicted by Josephson [140] and observed experimentally by Anderson et al. [141]. The Josephson tunnelling that describes the flow of supercurrent through a tunnel barrier is a subject of considerable research. The flow of electrons along the superconductors, in the absence of an applied voltage, is called the Josephson current and the movement of electrons across the barrier is called Josephson tunnelling. Josephson junctions have many applications in electronics, including sensitive superconducting magnetometers [45], superconducting ratchets, amplifiers [46, 47, 48], superconducting terahertz emitters [142], and quantum information [50].

Josephson phase discontinuities may appear in specially designed long Josephson junctions. A junction containing a region with a phase jump of π is called a $0-\pi$ Josephson junction and is described by $0-\pi$ sine-Gordon equation. The Josephson phase has a π discontinuity at the point where 0 and π parts join. The idea of π phase shift in Josephson junctions was first proposed by Bulaevskii [14, 15]. It was suggested that π phase-shifts may occur in the sine-Gordon equation due to magnetic impurities. There are many technologies available for manufacturing $0-\pi$ Josephson junctions [18, 19]. They were fabricated by using d-wave superconductors [20, 21, 22, 23, 24] or were obtained using a ferromagnetic barrier [25, 26].

Present technological advances can also impose a π phase-shift in a long Josephson junction as they promise important advantages for Josephson junction based electronics. A $0-\pi$ Josephson junctions also admits a half magnetic flux (semifluxon), sometimes called π-fluxon, at the discontinuity point [23]. A semifluxon is represented by a π-kink solution of the $0-\pi$ sine-Gordon equation [27].

The supercurrent, I, in Josephson junctions is proportional to the sine of the phase-difference of the electrons across the insulator, which is denoted by ϕ, i.e. $I \sim \sin\phi$. Due to the phase-shift, which is denoted by $\theta(x)$, the supercurrent relation is $I \sim \sin(\phi+\theta)$. Presently, one can impose a phase-shift in a long Josephson junction using several methods [18, 19, 128, 129, 130]. There are many promising technologies available for fabricating $0-\pi$ Josephson junctions, including using d-wave superconductors [20, 21, 22, 23, 24] or using a ferromagnetic barrier [25, 26]. A Josephson junction with phase shift shows a variety of interesting physical phenomena and reveals promising applications in superconducting electronics.

The dynamics of a Josephson junction with a double well potential are of particular interest. The dynamics of localised modes in a double-well potential in Josephson junctions can be described by two dynamical variables using a two mode approximation. The validity of the two-mode approximation for Bose Einstien condensates in a double well potential has been considered [143, 144, 145]. It has also been used in localized mode interactions in $0-\pi$ long Josephson junctions [146], in annular Josephson junctions for manipulation of a trapped vortex [147], and Josephson tunnelling of dark solitons [148].

Here, we consider the dynamics of long Josephson junction governed by perturbed sine-Gordon equation

$$\phi_{xx}(x,t) - \phi_{tt}(x,t) = \sin(\phi+\theta) + h\cos(\Omega t), \quad x \in \mathbb{R},\ t > 0, \tag{4.1.1}$$

for the one dimensional phase difference $\phi(x,t)$ between the two superconductors of the junction. In Equation (4.1.1), x denotes the coordinate along the junction normalized to the Josephson penetration depth λ_J, and time t is normalized to the inverse plasma frequency ω_p^{-1}. The applied time periodic drive in the governing equation has an amplitude h and frequency Ω. Here we study the internal phase shift formation as a double well potential

$$\theta(x) = \begin{cases} 0, & |x| > L+a, \\ \pi, & L < |x| < L+a, \\ 0, & 0 < |x| < L, \end{cases} \tag{4.1.2}$$

called a $0-\pi-0-\pi-0$ Josephson junction. The phase difference, ϕ, is naturally

subject to the continuity conditions at the position of the jump in the Josephson phase (the discontinuity), i.e.

$$\lim_{x\to\pm\{L,L+a\}^+}\phi(x,t) = \lim_{x\to\pm\{L,L+a\}^-}\phi(x,t), \tag{4.1.3}$$

$$\lim_{x\to\pm\{L,L+a\}^+}\phi_x(x,t) = \lim_{x\to\pm\{L,L+a\}^-}\phi_x(x,t). \tag{4.1.4}$$

We consider the ground state for $0-\pi-0-\pi-0$ junction $\phi_0 = 0 \pmod{2\pi}$. To find a coupled-mode oscillation for Josephson junctions, we consider the interactions of two modes of different symmetries, i.e. symmetric and antisymmetric, or even and odd. We are interested in time periodic states with frequencies λ_1, λ_2, such that $\lambda_1 < \lambda_2$ corresponding in the physical space to solutions of the sine-Gordon equation in the form

$$\phi_1(X_0,T_0) = B_1\Phi_1(X_0)e^{i\lambda_1 T_0} + c.c. + B_2\Phi_2(X_0)e^{i\lambda_2 T_0} + c.c., \tag{4.1.5}$$

where $B_1 = B_1(T_1,T_2,...)$, $B_2 = B_2(T_1,T_2,...)$ are unknown time-dependent complex amplitude of oscillations. c.c. stands for the complex conjugate throughout the proceeding work. By linearizing Equation (4.1.1) around the uniform solution, we find the bounded solutions satisfying the boundary conditions (4.1.3) and (4.1.4) are

$$\Phi_1(X_0) = \begin{cases} e^{-\sqrt{1-\lambda_1^2}(X_0-L-a)}, & X_0 > L+a, \\ \cos\left(\sqrt{1+\lambda_1^2}(X_0-L-a)\right) & \\ +C_1\sin\left(\sqrt{1+\lambda_1^2}(X_0-L-a)\right), & L < X_0 < L+a, \\ K_1\cosh\left(\sqrt{1-\lambda_1^2}\,X_0\right), & 0 < X_0 < L, \end{cases} \tag{4.1.6}$$

$$\Phi_2(X_0) = \begin{cases} e^{-\sqrt{1-\lambda_2^2}(X_0-L-a)}, & X_0 > L+a, \\ \cos\left(\sqrt{1+\lambda_2^2}(X_0-L-a)\right) & \\ +C_2\sin\left(\sqrt{1+\lambda_2^2}(X_0-L-a)\right), & L < X_0 < L+a, \\ K_2\sinh\left(\sqrt{1-\lambda_2^2}\,X_0\right), & 0 < X_0 < L, \end{cases} \tag{4.1.7}$$

as given by Susanto et al. [146], with the oscillation frequencies λ_1 and λ_2, satisfying

$$\frac{\sqrt{1-\lambda_1^4}}{\tan(\sqrt{1+\lambda_1^2}\,a)} - \lambda_1^2 - e^{-2\sqrt{1-\lambda_1^2}L} = 0, \tag{4.1.8}$$

$$\frac{\sqrt{1-\lambda_2^4}}{\tan(\sqrt{1+\lambda_2^2}\,a)} - \lambda_2^2 \mp e^{-2\sqrt{1-\lambda_2^2}L} = 0, \tag{4.1.9}$$

and

$$C_i = -\sqrt{\frac{1-\lambda_i^2}{1+\lambda_i^2}}, \quad K_i = \frac{2\,e^{-\sqrt{1-\lambda_i^2}L}\sin(\sqrt{1+\lambda_i^2}\,a)}{\sqrt{1-\lambda_i^4}}. \tag{4.1.10}$$

The two eigenvalues λ_i are functions of a and L.

Due to the nonlinear coupling, energy transfers from the discrete mode to the continuous spectrum has been addressed before by Soffer et al. [149, 150]. This phenomenon is responsible for the time decay [151, 152, 153, 154]. The same decay rates for the single mode oscillation have been discussed and obtained in [99, 100, 101]. We show that the two modes also decay in time. In particular exciting two modes at the same time will increase the decay rate. We also consider the case when one of the wells confines the excited state.

In Section 4.2, we construct a perturbation expansion to solve the unperturbed sine-Gordon equation for the coupled mode to obtain equations for the slow time evolution of oscillation amplitude in $0-\pi-0-\pi-0$ junction. In Section 4.3, the method of multiple scales is applied to obtain the amplitude of oscillation in the presence of driving. Section 4.4 is devoted to the discussions for the obtained results in the previous sections and numerical calculations, which confirm our asymptotic calculations.

4.2 Freely oscillating breathing mode in $0-\pi-0-\pi-0$ junctions

In this section we construct the dynamics of long Josephson junctions governed by sine-Gordon Equation (4.1.1), with $h = 0$, and $\theta(x)$ given by (4.4.1), which represents a double well potential comprising two $\pi-$junctions of length a separated by a $0-$junction of length $2L$. We apply a perturbation expansion to equation (4.1.1) by writing

$$\phi \quad = \quad \phi_0 + \epsilon\,\phi_1 + \epsilon^2\phi_2 + \epsilon^3\phi_3 + \ldots, \tag{4.2.1}$$

where ϵ is a small parameter, which is the initial amplitude of the breathing mode oscillation in the perturbation expansion for the undriven case. We further use multiple scales expansions by introducing the slow space and time variables

$$X_n = \epsilon^n x, \quad T_n = \epsilon^n t, \quad n = 0, 1, 2, \ldots. \tag{4.2.2}$$

The multiscale expansions is asymptotic,i.e.only valid for small amplitudes of the breathing mode. However, in the small amplitude limit the expansion provides a faithful description of the breather, independent of any assumptions and mode pre-selections. We also use the notation

$$\partial_n = \frac{\partial}{\partial X_n}, \quad D_n = \frac{\partial}{\partial T_n}, \tag{4.2.3}$$

so that the derivatives with respect to the original variables in terms of the scaled variables using the chain rule are given by

$$\frac{\partial}{\partial x} = \partial_0 + \epsilon\,\partial_1 + \epsilon^2\partial_2 + \epsilon^3\partial_3 + \cdots, \tag{4.2.4}$$

$$\frac{\partial}{\partial t} = D_0 + \epsilon\,D_1 + \epsilon^2 D_2 + \epsilon^3 D_3 + \cdots. \tag{4.2.5}$$

Inserting (4.2.2) into Equation (4.1.1) and equating like powers of ϵ we find a system of partial differential equations for the functions of the slow time and space variables X_0, T_0.

4.2.1 Leading order and first correction equations

At leading and next order, we obtain

$$\mathcal{O}(1) \;:\; \partial_0^2\phi_0 - D_0^2\phi_0 = \sin(\theta+\phi_0). \tag{4.2.6}$$

$$\mathcal{O}(\epsilon) \;:\; \partial_0^2\phi_1 - D_0^2\phi_1 = \cos(\theta+\phi_0)\phi_1 + 2D_0D_1\phi_0 - 2\partial_0\partial_1\phi_0. \tag{4.2.7}$$

A stable solution representing a uniform background for Equation (4.2.6) is

$$\phi_0(X_0,T_0) = 0, \tag{4.2.8}$$

while the solution for Equation (4.2.7) for $0-\pi-0-\pi-0$ junction is given by

$$\phi_1(X_0,T_0) = B_1\Phi_1(X_0)e^{i\,\lambda_1\,T_0} + c.c. + B_2\Phi_2(X_0)e^{i\,\lambda_2\,T_0} + c.c., \tag{4.2.9}$$

with $\Phi_{1,2}$ given by (4.1.6)–(4.1.7), satisfying the conditions, $\Phi_1(-X_0) = \Phi_1(X_0)$ and $\Phi_2(-X_0) = -\Phi_2(X_0)$. To derive an effective equation for the complex mode amplitudes B_1, B_2, we continue the perturbation expansion order by order and proceed to find the solvability conditions for the coupled equations.

4.2.2 Equation at $\mathcal{O}(\epsilon^2)$

The terms at the order $\mathcal{O}(\epsilon^2)$ give

$$\partial_0^2\phi_2 - D_0^2\phi_2 - \cos(\theta)\phi_2 = 2D_0D_1\phi_1 - 2\partial_0\partial_1\phi_1. \tag{4.2.10}$$

Substituting the spectral ansatz

$$\phi_2(X_0,T_0) = \widetilde{\phi}_{21}(X_0)e^{i\lambda_1T_0} + c.c. + \widetilde{\phi}_{22}(X_0)e^{i\lambda_2T_0} + c.c., \tag{4.2.11}$$

we obtain the corresponding set of ordinary differential equations

$$\partial_0^2\widetilde{\phi}_{21} - (\cos(\theta) - \lambda_1^2)\widetilde{\phi}_{21} = 2\,i\lambda_1D_1B_1\Phi_1, \tag{4.2.12}$$

$$\partial_0^2\widetilde{\phi}_{22} - (\cos(\theta) - \lambda_2^2)\widetilde{\phi}_{22} = 2\,i\lambda_2D_1B_2\Phi_2. \tag{4.2.13}$$

To find a bounded solution for $\widetilde{\phi}_{21}$, $\widetilde{\phi}_{22}$, Equations (4.2.12), (4.2.13) generate constraints on the right hand sides that are solvability conditions which lead to an important equation for the amplitudes B_1, B_2 as well as to equations at higher order when the expansion is continued further [155, 156].

We write equations (4.2.12)–(4.2.13) in the form

$$\mathcal{L}\psi(x) = f(x), \tag{4.2.14}$$

where $\mathcal{L}$ is a linear self-adjoint operator ($\mathcal{L} = \mathcal{L}^\dagger$) given by the left hand side of the above system, and $\zeta : \mathbb{T} \to \mathbb{R}$ is a smooth periodic function. Let $L^2(\mathbb{R})$ be the Hilbert space with complex inner product

$$\langle g, h\rangle \quad = \quad \int_{-\infty}^{\infty} \overline{g}(\xi)h(\xi)d\xi. \tag{4.2.15}$$

Here $\overline{g}(\xi)$ is the complex conjugate of $g(\xi)$. The Fredholm theorem states that the necessary and sufficient condition for the inhomogeneous equation $\mathcal{L}\psi = f(x)$ to have a bounded solution is that $f(x)$ be orthogonal to the null-space of the operator $\mathcal{L}$. Hence, the solvability condition provided by the Fredholm theorem is

$$\int_{-\infty}^{\infty} \mathcal{L}f(x)\,dx \quad = \quad 0. \tag{4.2.16}$$

By applying the theorem, we find the solvability conditions for the above system are

$$D_1B_1 = 0, \quad D_1B_2 = 0. \tag{4.2.17}$$

Hence B_j are independent of T_1.

By putting the solvability conditions (4.2.17) in Equations (4.2.12)–(4.2.13), we obtain the result which is similar to that at $\mathcal{O}(\epsilon)$, that is, Equation (4.2.7). Due to uniformity in the perturbation expansion we conclude that $\phi_2(X_0, T_0) = 0$.

4.2.3 Equation at $\mathcal{O}(\epsilon^3)$

Equating terms at $\mathcal{O}(\epsilon^3)$, we obtain an equation of the form

$$\begin{aligned}\partial_0^2\phi_3 - D_0^2\phi_3 - \cos(\theta+\phi_0)\phi_3 \quad &= \quad 2(D_0D_2 - \partial_0\partial_2)\phi_1 + (D_1^2 - \partial_1^2)\phi_1 \\ &\quad -\frac{1}{6}\phi_1^3\cos(\theta).\end{aligned} \tag{4.2.18}$$

Calculating the right hand side of Equation (4.2.18), we obtain

$$\partial_0^2\phi_3 - D_0^2\phi_3 - \cos(\theta+\phi_0)\phi_3 \tag{4.2.19}$$

$$\begin{aligned}&= 2\,i\lambda_1 D_2B_1\Phi_1e^{i\lambda_1T_0} + 2\,i\lambda_2D_2B_2\Phi_2e^{i\lambda_2T_0} - \frac{1}{6}\Big[B_1^3\Phi_1^3e^{3\,i\lambda_1T_0} + B_2^3\Phi_2^3e^{3\,i\lambda_2T_0} \\ &+3\,B_1|B_1|^2\Phi_1^3e^{i\lambda_1T_0} + 3\,B_2|B_2|^2\Phi_2^3e^{i\lambda_2T_0} + 3\,B_1^2\overline{B}_2\,\Phi_1^2\,\Phi_2e^{(2\,\lambda_1-\lambda_2)T_0\,i} \\ &+3\,\overline{B}_1B_2^2\Phi_1\Phi_2^2e^{(2\,\lambda_2-\lambda_1)T_0\,i} + 6\,|B_1|^2B_2\Phi_1^2\Phi_2e^{\lambda_2T_0\,i} + 6\,B_1|B_2|^2\Phi_1\Phi_2^2e^{\lambda_1T_0\,i} \\ &+3\,B_1^2B_2\Phi_1^2\Phi_2e^{(2\,\lambda_1+\lambda_2)T_0\,i} + 3\,B_1B_2^2\Phi_1\Phi_2^2e^{(2\,\lambda_2+\lambda_1)T_0\,i}\Big]\cos(\theta) + c.c..\end{aligned} \tag{4.2.20}$$

This equation has solutions in which there is a nonlinear resonant interaction between the bound state and continuous radiation, which leads to energy transfer from the "discrete" to "continuous" mode. The solutions in continuous spectrum are referred to as "phonon modes".

Equation (4.2.20) is linear, so its solution can be written as the linear combination of solutions with frequencies present in the forcing terms, therefore the solution will consist of the harmonics present in Equation (4.2.20), that is

$$\begin{aligned}\phi_3 &= \phi_{311}e^{i\lambda_1 T_0} + c.c. + \phi_{312}e^{i\lambda_2 T_0} + c.c. + \phi_{321}e^{(2\lambda_1+\lambda_2)T_0\, i} + c.c. \\ &\quad + \phi_{322}e^{(2\lambda_1-\lambda_2)T_0\, i} + c.c. + \phi_{331}e^{3i\,\lambda_1 T_0} + c.c. + \phi_{332}e^{3i\,\lambda_2 T_0} + c.c. \\ &\quad + \phi_{341}e^{(2\,\lambda_2+\lambda_1)T_0\, i} + c.c. + \phi_{342}e^{(2\,\lambda_2-\lambda_1)T_0\, i} + c.c..\end{aligned} \tag{4.2.21}$$

The functions ϕ_{311}, ϕ_{312} are functions of the space variable X_0 which satisfy the following linear inhomogeneous equations

$$\partial_0^2\phi_{311} - \Big(\cos(\theta+\phi_0) - \lambda_1^2\Big)\phi_{311} = \begin{cases} E_1, & X_0 > L+a, \\ E_2, & L < X_0 < L+a, \\ E_3, & 0 < X_0 < L, \end{cases} \tag{4.2.22}$$

$$\partial_0^2\phi_{312} - \Big(\cos(\theta+\phi_0) - \lambda_2^2\Big)\phi_{312} = \begin{cases} F_1, & X_0 > L+a, \\ F_2, & L < X_0 < L+a, \\ F_3, & 0 < X_0 < L, \end{cases} \tag{4.2.23}$$

with

$$E_1 = 2\,i\lambda_1 D_2 B_1\,\Phi_1 - \frac{1}{2}B_1|B_1|^2\,\Phi_1^3 - B_1|B_2|^2\,\Phi_1\Phi_2^2, \tag{4.2.24}$$

$$E_2 = 2\,i\lambda_1 D_2 B_1\,\Phi_1 + \frac{1}{2}B_1|B_1|^2\,\Phi_1^3 + B_1|B_2|^2\,\Phi_1\Phi_2^2, \tag{4.2.25}$$

$$E_3 = 2\,i\lambda_1 D_2 B_1\,\Phi_1 - \frac{1}{2}B_1|B_1|^2\,\Phi_1^3 - B_1|B_2|^2\,\Phi_1\Phi_2^2, \tag{4.2.26}$$

$$F_1 = 2\,i\lambda_2 D_2 B_2\,\Phi_2 - \frac{1}{2}B_2|B_2|^2\,\Phi_2^3 - B_2|B_1|^2\,\Phi_2\Phi_2^1, \tag{4.2.27}$$

$$F_2 = 2\,i\lambda_2 D_2 B_2\,\Phi_2 + \frac{1}{2}B_2|B_2|^2\,\Phi_2^3 + B_2|B_1|^2\,\Phi_2\Phi_2^1, \tag{4.2.28}$$

$$F_3 = 2\,i\lambda_2 D_2 B_2\,\Phi_2 - \frac{1}{2}B_2|B_2|^2\,\Phi_2^3 - B_2|B_1|^2\,\Phi_2\Phi_2^1. \tag{4.2.29}$$

The homogenous solutions of these equations are given by the eigenfunctions (4.1.6) and (4.1.7). Using the Fredholm alternative, the solvability conditions for Equations (4.2.22)–(4.2.23) are

$$D_2 B_1 = \alpha_1\, B_1|B_1|^2\, i + \alpha_2\, B_1|B_2|^2\, i, \tag{4.2.30}$$

$$D_2 B_2 = \alpha_3\, B_2|B_2|^2\, i + \alpha_4\, B_2|B_1|^2\, i, \tag{4.2.31}$$

with

$$\alpha_1 = -\frac{p_2}{p_1}, \quad \alpha_2 = -\frac{p_3}{p_1}, \quad \alpha_3 = -\frac{p_5}{p_4}, \quad \alpha_4 = -\frac{p_6}{p_4},$$

given in Section (4.A.1) with explicit expressions. Putting the conditions (4.2.30)–(4.2.31) into (4.2.22)–(4.2.23) respectively and solving, then we obtain a bounded solution of the form

$$\phi_{311} = B_1 \begin{cases} \psi_1, & X_0 > L + a, \\ \psi_2, & L < X_0 < L + a, \\ \psi_3, & 0 < X_0 < L, \end{cases} \tag{4.2.32}$$

$$\phi_{312} = B_2 \begin{cases} \psi_4, & X_0 > L + a, \\ \psi_5, & L < X_0 < L + a, \\ \psi_6, & 0 < X_0 < L, \end{cases} \tag{4.2.33}$$

where ψ_i, for $i = 1, 2, .., 6$, can be seen in Section (4.A.1). To obtain the final amplitude equations, we have to find bounded solutions for other harmonics present in (4.2.20), as these will appear in next stage. To do this we assume that

$$(3\lambda_1)^2 > 1, \tag{4.2.34}$$

i.e. the third harmonics lie in continuous (phonon) spectrum. For $\lambda_2 > \lambda_1$ and with assumption (4.2.34), so we have

$$(2\lambda_1 + \lambda_2)^2 > 1, \qquad (2\lambda_2 + \lambda_1)^2 > 1, \tag{4.2.35}$$

also lies in the continuous spectrum. The equations for the harmonics $(2\lambda_1 + \lambda_2)$, $(2\lambda_1 - \lambda_2)$ are

$$\begin{aligned} \partial_0^2 \phi_{321} + (2\lambda_1 + \lambda_2)^2 \phi_{321} - \cos(\theta + \phi_0)\phi_{321} &= -\frac{1}{2} B_1^2 B_2 \Phi_1^2 \Phi_2 \cos(\theta), \\ \partial_0^2 \phi_{322} + (2\lambda_1 - \lambda_2)^2 \phi_{322} - \cos(\theta + \phi_0)\phi_{322} &= -\frac{1}{2} B_1^2 \overline{B}_2 \Phi_1^2 \Phi_2 \cos(\theta), \end{aligned}$$

with bounded solutions

$$\phi_{321} = B_1^2 B_2 \begin{cases} \psi_7, & X_0 > L + a, \\ \psi_8, & L < X_0 < L + a, \\ \psi_9, & 0 < X_0 < L, \end{cases} \tag{4.2.36}$$

$$\phi_{322} = B_1^2 \overline{B_2} \begin{cases} \psi_{10}, & X_0 > L + a, \\ \psi_{11}, & L < X_0 < L + a, \\ \psi_{12}, & 0 < X_0 < L, \end{cases} \tag{4.2.37}$$

where $\psi_7, \ldots, \psi_{12}$ are given in 4.A.1. The equations for the third harmonics are

$$\begin{aligned}
\partial_0^2\phi_{331} + 9\,\lambda_1^2\phi_{331} - \cos(\theta+\phi_0)\phi_{331} &= -\frac{1}{6}\,B_1^3\Phi_1^3\,\cos(\theta),\\
\partial_0^2\phi_{332} + 9\,\lambda_2^2\phi_{332} - \cos(\theta+\phi_0)\phi_{332} &= -\frac{1}{6}\,B_2^3\Phi_2^3\,\cos(\theta),
\end{aligned}$$

with solutions

$$\phi_{331} = B_1^3\begin{cases}\psi_{13}, & X_0 > L+a,\\ \psi_{14}, & L < X_0 < L+a,\\ \psi_{15}, & 0 < X_0 < L,\end{cases} \tag{4.2.38}$$

$$\phi_{332} = B_2^3\begin{cases}\psi_{16}, & X_0 > L+a,\\ \psi_{17}, & L < X_0 < L+a,\\ \psi_{18}, & 0 < X_0 < L,\end{cases} \tag{4.2.39}$$

where $\psi_{13}, \ldots, \psi_{18}$ are given by in Section 4.A.1. The equations for the harmonics $(\lambda_1 + 2\,\lambda_2)$, $(\lambda_1 - 2\,\lambda_2)$ are

$$\begin{aligned}
\partial_0^2\phi_{341} + (\lambda_1+2\,\lambda_2)^2\,\phi_{341} - \cos(\theta+\phi_0)\phi_{341} &= -\frac{1}{2}\,B_1B_2^2\Phi_1\Phi_2^2\,\cos(\theta),\\
\partial_0^2\phi_{342} + (\lambda_1-2\,\lambda_2)^2\,\phi_{342} - \cos(\theta+\phi_0)\phi_{342} &= -\frac{1}{2}\,\overline{B}_1B_2^2\Phi_1\Phi_2^2\,\cos(\theta),
\end{aligned}$$

with solutions

$$\phi_{341} = B_1\,B_2^2\begin{cases}\psi_{19}, & X_0 > L+a,\\ \psi_{20}, & L < X_0 < L+a,\\ \psi_{21}, & 0 < X_0 < L,\end{cases} \tag{4.2.40}$$

$$\phi_{342} = B_2^2\,\overline{B_1}\begin{cases}\psi_{22}, & X_0 > L+a,\\ \psi_{23}, & L < X_0 < L+a,\\ \psi_{24}, & 0 < X_0 < L.\end{cases} \tag{4.2.41}$$

The functions $\psi_{19}, \ldots, \psi_{24}$ are given in Section 4.A.1. With the assumption (4.2.34) i.e. $\lambda_1 > 1/3$, we see that solutions ϕ_{321}, ϕ_{311}, ϕ_{332}, ϕ_{341} describe the right moving radiation in $X_0 > L+a$ and left moving radiation in $X_0 < L$, which are responsible for the energy loss in the final amplitude equations.

4.2.4 Equation at $\mathcal{O}(\epsilon^4)$

The terms at the order $\mathcal{O}(\epsilon^4)$ give

$$\begin{aligned}
{D_0}^2\phi_4 - {\partial_0}^2\phi_4 - \cos\left(\Phi_0+\theta\right)\phi_4 &= 2\,\left(D_1D_2 + D_0D_3 - \partial_1\partial_2 - \partial_0\partial_3\right)\phi_1\\
&\quad +2\,\left(D_0D_1 - \partial_0\partial_1\right)\phi_3\\
&\quad +\left(\frac{1}{24}\phi_1^4 - \phi_3\phi_1\right)\sin\left(\phi_0+\theta\right).
\end{aligned} \tag{4.2.42}$$

Using the same procedure as we did before the solvability conditions for the above equations are

$$D_3 B_1 = 0, \quad D_3 B_2 = 0, \tag{4.2.43}$$

and hence we impose that $\phi_4 = 0$, as we did for ϕ_2. This implies that $B_j = B_j(T_2, T_4, \dots)$ are independent of T_3.

4.2.5 Equation at $\mathcal{O}(\epsilon^5)$

Equating terms at $\mathcal{O}(\epsilon^5)$ gives the equation

$$\begin{aligned} {\partial_0}^2\phi_5 - {D_0}^2\phi_5 - \cos(\theta)\phi_5 &= 2(D_0D_4 - \partial_0\partial_4)\phi_1 + 2(D_3D_1 - \partial_3\partial_1)\phi_1 + (D_2^2 - \partial_2^2)\phi_1 \\ &\quad + (D_1^2 - \partial_1^2)\phi_3 + 2(D_2D_0 - \partial_2\partial_0)\phi_3 \\ &\quad + \left(-\frac{1}{2}{\phi_1}^2\phi_3 + \frac{1}{120}{\phi_1}^5\right)\cos(\theta). \end{aligned} \tag{4.2.44}$$

It should be noted that we have ignored all the terms involving ϕ_i, $i = 0, 2, 4$, in (4.2.44) for simplification as these have no role in the expansion. Having calculated the right hand side using the known functions ϕ_1, ϕ_3, we again split the solution into components proportional to simple harmonics as we did before, and calculate the first harmonic, as we expect to obtain the leading order amplitude equation. The equations for the first harmonics are given by

$$\partial_0^2\phi_{511} - \left(\cos(\theta) - \lambda_1^2\right)\phi_{511} = \begin{cases} G_1, & X_0 > L + a, \\ G_2, & L < X_0 < L + a, \\ G_3, & 0 < X_0 < L, \end{cases} \tag{4.2.45}$$

$$\partial_0^2\phi_{512} - \left(\cos(\theta) - \lambda_2^2\right)\phi_{512} = \begin{cases} H_1, & X_0 > L + a, \\ H_2, & L < X_0 < L + a, \\ H_3, & 0 < X_0 < L, \end{cases} \tag{4.2.46}$$

where G_i, H_i are given in Section 4.A.1.

We do not calculate the other harmonics as we expect to obtain oscillatory behaviour over the long time scale of the localised mode here. Using the Fredholm theorem the solvability conditions for the first harmonics are

$$D_4 B_1 = \beta_1 B_1 |B_1|^4 + \beta_2 B_1 |B_2|^4 + \beta_3 B_1 |B_1|^2 |B_2|^2, \tag{4.2.47}$$

$$D_4 B_2 = \gamma_1 B_2 |B_2|^4 + \gamma_2 B_2 |B_1|^4 + \gamma_3 B_2 |B_1|^2 |B_2|^2. \tag{4.2.48}$$

where β_i, γ_i are given in Section 4.4.

We do not proceed further to perturbation expansion of high orders, as we have obtained the equations governing the decaying oscillatory behaviour of the localized modes for a system with two regions of phase shift, which has the effect in a double–well potential.

4.2.6 Amplitude equations

By noting that

$$\frac{d}{dt}B_1 = \epsilon D_1 B_1 + \epsilon^2 D_2 B_1 + \epsilon^3 D_3 B_1 + \epsilon^4 D_4 B_1 + \ldots, \tag{4.2.49}$$

$$\frac{d}{dt}B_2 = \epsilon D_1 B_2 + \epsilon^2 D_2 B_2 + \epsilon^3 D_3 B_2 + \epsilon^4 D_4 B_2 + \ldots, \tag{4.2.50}$$

writing $b_i = \epsilon B_i$, $i = 1, 2$, so that b_i is the natural amplitude of oscillating modes, which is the small amplitude we actually measure. The parameter ϵ is the initial amplitude in perturbation expansion for the undriven case. Combining the solvability conditions (4.2.17), (4.2.30), (4.2.31), (4.2.43), (4.2.47), (4.2.48), we obtain the system of two coupled equations,

$$\frac{d}{dt}|b_1|^2 = 2\left(\mathrm{Re}(\beta_1)|b_1|^6 + \mathrm{Re}(\beta_2)|b_1|^2|b_2|^4 + \mathrm{Re}(\beta_3)|b_1|^4|b_2|^2\right) + \mathcal{O}(\epsilon^6), \tag{4.2.51}$$

$$\frac{d}{dt}|b_2|^2 = 2\left(\mathrm{Re}(\gamma_1)|b_2|^6 + \mathrm{Re}(\gamma_2)|b_2|^2|b_1|^4 + \mathrm{Re}(\gamma_3)|b_2|^4|b_1|^2\right) + \mathcal{O}(\epsilon^6). \tag{4.2.52}$$

By assuming that $Re(\beta_i), Re(\gamma_i) < 0$, for $i = 1, 2, 3$ as will be shown later in Section 4.4, Equations (4.2.51)–(4.2.52) describe the gradual decrease in the amplitude of coupled oscillations due to energy emission in the form of radiation. Here we discuss two types of solutions.

When $b_2 = 0$, and $b_1 \neq 0$, Equations (4.2.51)–(4.2.52), satisfy the relation

$$|b_1(t)| = \left(\frac{|b_1(0)|^4}{1 - 4\,\mathrm{Re}\,(\gamma_1)\,|b_1(0)|^4 t}\right)^{1/4}, \tag{4.2.53}$$

since $Re(\gamma_1) < 0$, this describes algebraic decay of b_1 with increasing time. Similarly when $b_1 = 0$, and $b_2 \neq 0$, we obtain

$$|b_2(t)| = \left(\frac{|b_2(0)|^4}{1 - 4\,\mathrm{Re}\,(\beta_1)\,|b_2(0)|^4 t}\right)^{1/4}, \tag{4.2.54}$$

similarly since $Re(\beta_1) < 0$, this describes algebraic decay of b_2 with increasing time.

4.2.7 Resonance condition: $(3\lambda_1)^2 < 1 < (3\lambda_2)^2$

In the previous subsection we considered the case when $(3\lambda_2)^2 > (3\lambda_1)^2 > 1$. Here we choose values of L and a such that

$$(3\lambda_1)^2 < 1 < (3\lambda_2)^2. \tag{4.2.55}$$

By using the same perturbation expansion as at the start of this section, the solvability conditions at $\mathcal{O}(\epsilon^2)$ are

$$D_1 B_1 = 0, \quad D_1 B_2 = 0, \tag{4.2.56}$$

hence $B_i = B_i(T_2, T_3, \dots)$. Solving the Equation (4.2.18) we obtain the solvability condition

$$D_2 B_1 = d_{11} B_1 |B_1|^2 i + d_{12} B_1 |B_2|^2 i, \tag{4.2.57}$$

$$D_2 B_2 = d_{21} B_2 |B_2|^2 i + d_{22} B_2 |B_1|^2 i. \tag{4.2.58}$$

With the assumption (4.2.55) we observe that the solution ϕ_{332}, ϕ_{321}, ϕ_{341} describe the right moving radiation for $X_0 > L + a$ and left moving radiation for $X_0 < L$. Similarly from equation (4.2.42) at $\mathcal{O}(\epsilon^4)$ we obtain

$$D_3 B_1 = 0, \quad D_3 B_2 = 0. \tag{4.2.59}$$

Hence $B_j = B_j(T_2, T_4, \dots)$. Solving Equation (4.2.44) and using (4.A.1)–(4.A.6), the solvability conditions at $\mathcal{O}(\epsilon^5)$ are

$$D_4 B_1 = e_{11} B_1 |B_1|^4 i + e_{12} B_1 |B_2|^4 + e_{13} B_1 |B_1|^2 |B_2|^2, \tag{4.2.60}$$

$$D_4 B_2 = e_{21} B_2 |B_2|^4 + e_{22} B_2 |B_1|^4 + e_{23} B_2 |B_1|^2 |B_2|^2. \tag{4.2.61}$$

Combining Equations (4.2.57), (4.2.58), (4.2.60) and (4.2.61), we obtain

$$\frac{d|b_1|^2}{dt} = 2\left(\mathrm{Re}(e_{12})|b_1|^2|b_2|^4 + \mathrm{Re}(e_{13})|b_1|^4|b_2|^2\right) + \mathcal{O}(\epsilon^6), \tag{4.2.62}$$

$$\frac{d|b_2|^2}{dt} = 2\left(\mathrm{Re}(e_{21})|b_2|^6 + \mathrm{Re}(e_{22})|b_2|^2|b_1|^4 + \mathrm{Re}(e_{23})|b_2|^4|b_1|^2\right) + \mathcal{O}(\epsilon^6). \tag{4.2.63}$$

It is interesting to note that even though $(3\lambda_1)^2 < 1$. The coupled Equations (4.2.62)–(4.2.63) still show that ϕ_1 decay in time. For (4.2.62)–(4.2.63), if $b_2 = 0$, then $b_1 = 0$. When $b_1 = 0$, and $b_2 \neq 0$, we obtain

$$|b_2(t)| = \left(\frac{|b_2(0)|^4}{1 - 4\,\mathrm{Re}\,(e_{21})\,|b_2(0)|^4 t}\right)^{1/4}, \tag{4.2.64}$$

clearly shows the decay in the long time.

4.3 Driven breathing mode in $0-\pi-0-\pi-0$ junctions

We now consider the dynamics of a perturbed sine-Gordon equation, that is, Equation (4.1.1) perturbed by a time-dependent external force modelling a driven $0-\pi-0-\pi-0$ junction with $h \neq 0$ and $\Omega = \lambda_1(1+\rho)$. For notational compactness, we make transformation

$$\Omega t = \lambda_1 \tau. \tag{4.3.1}$$

The Equation (4.1.1) then becomes

$$\phi_{xx}(x,\tau) - (1+\rho)^2 \phi_{\tau\tau}(x,\tau) = \sin(\phi+\theta) + \frac{1}{2}h\left(e^{i\lambda_1\tau} + c.c.\right). \tag{4.3.2}$$

Here, we assume that the driving amplitude h is small and the driving frequency is close to resonance with the fundamental mode of the homogenous system. In this case we consider

$$h = \epsilon^3 H, \quad \rho = \epsilon^3 R, \tag{4.3.3}$$

with $H, R \sim \mathcal{O}(1)$. Due to the time rescaling above, our slow temporal variables are now defined as

$$X_n = \epsilon^n x, \quad T_n = \epsilon^n \tau, \quad n = 0, 1, 2, \ldots, \tag{4.3.4}$$

with the short hand notation (4.2.3). Performing the perturbation expansion order by order as in Section 4.2, we obtain the same perturbation expansion up to $\mathcal{O}(\epsilon^2)$.

4.3.1 Equation at $\mathcal{O}(\epsilon^3)$

The terms at order of $\mathcal{O}(\epsilon^3)$ give

$$\begin{aligned} \partial_0^2\phi_3 - D_0^2\phi_3 - \cos(\theta+\phi_0)\phi_3 \;&=\; 2(D_0D_2 - \partial_0\partial_2)\phi_1 + (D_1^2 - \partial_1^2)\phi_1 \\ &\quad -\frac{1}{6}\phi_1^3\cos(\theta) + \frac{1}{2}H(e^{i\lambda_1\tau} + c.c.). \end{aligned} \tag{4.3.5}$$

Calculating the right hand side, we obtain various harmonics, namely

$$\begin{aligned} &\partial_0^2\phi_3 - D_0^2\phi_3 - \cos(\theta+\phi_0)\phi_3 \\ &= 2\,i\lambda_1 D_2 B_1\Phi_1 e^{i\lambda_1 T_0} + 2\,i\lambda_2 D_2 B_2\Phi_2 e^{i\lambda_2 T_0} - \frac{1}{6}\Big[B_1^3\Phi_1^3 e^{3\,i\lambda_1 T_0} + B_2^3\Phi_2^3 e^{3\,i\lambda_2 T_0} \\ &+3\,B_1|B_1|^2\Phi_1^3 e^{i\lambda_1 T_0} + 3\,B_2|B_2|^2\Phi_2^3 e^{i\lambda_2 T_0} + 3\,B_1^2 B_2\Phi_1^2\Phi_2 e^{(2\lambda_1+\lambda_2)T_0\,i} \\ &+3\,B_1 B_2^2\Phi_1\Phi_2^2 e^{(2\lambda_2+\lambda_1)T_0\,i} + 3\,B_1^2\overline{B}_2\,\Phi_1^2\,\Phi_2 e^{(2\lambda_1-\lambda_2)T_0\,i} + 6\,B_1|B_2|^2\Phi_1\Phi_2^2 e^{\lambda_1 T_0\,i} \\ &+3\,\overline{B}_1 B_2^2\Phi_1\Phi_2^2 e^{(2\lambda_2-\lambda_1)T_0\,i} + 6\,|B_1|^2 B_2\Phi_1^2\Phi_2 e^{\lambda_2 T_0\,i}\Big]\cos\theta + \frac{1}{2}H e^{i\lambda_1\tau} + c.c.. \end{aligned} \tag{4.3.6}$$

Using (4.2.21), we split the harmonics as in Section 4.2. Using the Fredholm alternative, the solvability condition for the first harmonic is

$$D_2 B_1 \;=\; \alpha_1 B_1 |B_1|^2\, i + \alpha_2 B_1 |B_2|^2\, i + \mu_1 H\, i, \tag{4.3.7}$$

where α_i, μ_1 are given in Section (4.4). The solvability condition $D_2 B_2$ is the same as (4.2.31). With (4.3.7), the solution for the first harmonic is obtained in the form

$$\widetilde{\phi}_{311} \;=\; \begin{cases} Z_1 \mathrm{e}^{-\sqrt{1-{\lambda_1}^2}(X_0-L-a)} + B_1\Psi_1 + H\,\Psi_2 & X_0 > L+a, \\ Z_2 \cos\left(\sqrt{1+{\lambda_1}^2}\,(X_0-L-a)\right) + B_1\Psi_3 + & \\ Z_3 \sin\left(\sqrt{1+{\lambda_1}^2}\,(X_0-L-a)\right) + H\,\Psi_4, & L < X_0 < L+a, \\ Z_4 \cosh\left(\sqrt{1-\lambda_1^2}X_0\right) + B_1\Psi_5 + H\,\Psi_6, & 0 < X_0 < L, \end{cases} \tag{4.3.8}$$

where $\Psi_i = \Psi_i\left(|B_1|^2, |B_2|^2, \lambda_1, \lambda_2\right)$ for $i = 1,2,3,4$ that appears in $\widetilde{\phi}_{311}$ can be seen in Section 4.A.1. The constant of integration $Z_i = Z_i\left(B_1, H, |B_1|^2, |B_2|^2, \lambda_1, \lambda_2\right)$ for $i = 1,2,3,4$ that appears in $\widetilde{\phi}_{311}$, can be found by applying the continuity conditions at the discontinuity points. We do not calculate the other harmonics appearing in (4.3.6) as these are similar to the undriven case considered in Section 4.2.

4.3.2 Equation at $\mathcal{O}(\epsilon^4)$

Equating terms at $\mathcal{O}(\epsilon^4)$ we obtain

$$\begin{aligned} {D_0}^2\phi_4 - {\partial_0}^2\phi_4 - \cos\left(\Phi_0+\theta\right)\phi_4 \;=\;& 2\left(D_1D_2 + 2\,D_0D_3 - \partial_1\partial_2 - \partial_0\partial_3\right)\phi_1 \\ & + 2\left(D_0D_1 - \partial_0\partial_1\right)\phi_3 + 2\,R{D_0}^2\phi_1 \\ & + \left(\frac{1}{24}\phi_1^4 - \phi_3\phi_1\right)\sin\left(\phi_0+\theta\right). \end{aligned} \tag{4.3.9}$$

Calculating the right hand side and applying the Fredholm alternative, the solvability conditions for the first harmonics are

$$D_3 B_1 = -\lambda_1\, B_1\, R\, i, \quad D_3 B_2 \;=\; -\lambda_2\, B_2\, R\, i. \tag{4.3.10}$$

At this stage we impose that $\phi_4 = 0$.

Since $\lambda_1, \lambda_2, R \in \mathbb{R}$ these are purely oscillating being given by

$$B_1 \;=\; B_1(T_2, T_4, \dots)\mathrm{e}^{-\lambda_1 R T_3 i}, \tag{4.3.11}$$

$$B_2 \;=\; B_2(T_2, T_4, \dots)\mathrm{e}^{-\lambda_2 R T_3 i}. \tag{4.3.12}$$

4.3.3 Equation at $\mathcal{O}(\epsilon^5)$

The terms at the order of $\mathcal{O}(\epsilon^5)$ give

$$\begin{aligned}\partial_0^2\phi_5 - D_0^2\phi_5 - \phi_5\cos(\theta) &= 2(D_0D_4 - \partial_0\partial_4)\phi_1 + 2(D_3D_1 - \partial_3\partial_1)\phi_1 + 4\,R\,D_0D_1\phi_1 \\ &\quad +(D_2^2 - \partial_2^2)\phi_1 + (D_1^2 - \partial_1^2)\phi_3 + 2(D_2D_0 - \partial_2\partial_0)\phi_3 \\ &\quad - \left(\frac{1}{2}\phi_1^2\phi_3 - \frac{1}{120}\phi_1^5\right)\cos(\theta). \end{aligned} \tag{4.3.13}$$

In calculating the right hand side, we consider only the first harmonics as our main aim is to obtain the amplitude equation at this stage, i.e.

$$\partial_0^2\phi_{511} - \left(\cos(\theta) - \lambda_1^2\right)\phi_{511} = \begin{cases} L_1, & X_0 > L + a, \\ L_2, & L < X_0 < L + a, \\ L_3, & 0 < X_0 < L, \end{cases} \tag{4.3.14}$$

$$\partial_0^2\phi_{512} - \left(\cos(\theta) - \lambda_1^2\right)\phi_{512} = \begin{cases} M_1, & X_0 > L + a, \\ M_2, & L < X_0 < L + a, \\ M_3, & 0 < X_0 < L, \end{cases} \tag{4.3.15}$$

where L_i, M_i are given in Section 4.A.2.

Using the Fredholm alternative, the solvability conditions for Equations (4.3.14)-(4.3.15) are

$$\begin{aligned} D_4B_1 &= a_1B_1|B_1|^4 + a_2B_1|B_2|^4 + a_3B_1|B_1|^2|B_2|^2 \\ &\quad + \left(a_4|B_1|^2 + a_5|B_2|^2 + a_6B_1^2\right)Hi, \end{aligned} \tag{4.3.16}$$

$$\begin{aligned} D_4B_2 &= c_1B_2|B_2|^4 + c_2B_2|B_1|^4 + c_3B_1|B_2|^2|B_2|^2 \\ &\quad + c_4B_2\left(B_1 + \overline{B_1}\right)Hi. \end{aligned} \tag{4.3.17}$$

where a_j, c_j are given in Section 4.A.1.

4.3.4 Amplitude equations

Equations (4.3.16), (4.3.17) are the leading order equations for the coupled mode oscillations. Combining all the solvability conditions (4.2.30), (4.3.7), (4.3.10), (4.3.16), (4.3.17), and considering $b_i = \epsilon B_i$ for $i = 1, 2$ we obtain

$$\begin{aligned} \frac{\Omega}{\lambda_1}\frac{\partial b_1}{\partial t} &= \alpha_1 b_1|b_1|^2 i + \alpha_2 b_1|b_2|^2 i + \mu_1 h i - \lambda_1 b_1 \rho i + a_1 b_1|b_1|^4 + a_2 b_1|b_2|^4 \\ &\quad + a_3 b_1|b_1|^2|b_2|^2 + \left(a_4|b_1|^2 + a_5|b_2|^2 + a_6 b_1^2\right)h i + \mathcal{O}(\epsilon^6), \end{aligned} \tag{4.3.18}$$

$$\begin{aligned} \frac{\Omega}{\lambda_1}\frac{\partial b_2}{\partial t} &= \alpha_3 b_2|b_2|^2 i + \alpha_4 b_2|b_1|^2 i - \lambda_2 b_2 \rho i + c_1 b_2|b_2|^4 + c_2 b_2|b_1|^4 \\ &\quad + c_3 b_2|b_1|^2|b_2|^2 + c_4\, b_2\left(b_1 + \overline{b_1}\right)h i + \mathcal{O}(\epsilon^6), \end{aligned} \tag{4.3.19}$$

where α_i are given in Section 4.A.1.

From the above equations, we expect that the presence of a non-zero external drive will induce the mode oscillations. Note in Equations (4.3.18)–(4.3.19), there is a solution with $b_2 = 0$ and $b_1 \neq 0$ as well as $b_1 \neq 0$ and $b_2 \neq 0$, but with $b_1 = 0$ and $b_2 \neq 0$, is in general impossible (it requires $|b_2|^2 = \mu_1/a_5$).

4.3.5 Resonance condition: $(3\lambda_1)^2 < 1 < (3\lambda_2)^2$ in the driven case

Now we consider the case in section 4.2.7, but in the driven case. Repeating the same procedure as above, the solvability conditions at $\mathcal{O}(\epsilon^2)$ and $\mathcal{O}(\epsilon^4)$ are the same as Equations (4.2.56) and (4.3.10).

The solvability condition at $\mathcal{O}(\epsilon^3)$ from Equation (4.3.5) gives

$$D_2 B_1 = d_{11} B_1 |B_1|^2 i + d_{12} B_1 |B_2|^2 i + d_{13} H i, \tag{4.3.20}$$

$$D_2 B_2 = d_{21} B_2 |B_2|^2 i + d_{22} B_2 |B_1|^2 i. \tag{4.3.21}$$

Similarly from Equation (4.3.13) the solvability conditions at $\mathcal{O}(\epsilon^5)$ yield

$$\begin{aligned} D_4 B_1 = {} & \zeta_{11} B_1 |B_1|^4 i + \zeta_{12} B_1 |B_2|^4 + \zeta_{13} B_1 |B_1|^2 |B_2|^2 \\ & + \left(\zeta_{14} |B_1|^2 + \zeta_{15} |B_2|^2 + \zeta_{16} B_1^2\right) H i, \end{aligned} \tag{4.3.22}$$

$$\begin{aligned} D_4 B_2 = {} & \zeta_{21} B_2 |B_2|^4 + \zeta_{22} B_2 |B_1|^4 + \zeta_{23} B_2 |B_1|^2 |B_2|^2 \\ & + \zeta_{24} (B_1 + \bar{B_1}) B_2 H i. \end{aligned} \tag{4.3.23}$$

Combining (4.2.30), (4.3.10), (4.3.20)–(4.3.21) and (4.3.22)–(4.3.23) and considering $b_i = \epsilon B_i$ for $i = 1, 2$, we obtain amplitude equations of the form

$$\begin{aligned} \frac{\Omega}{\lambda_1} \frac{\partial b_1}{\partial t} = {} & d_{11} b_1 |b_1|^2 i + d_{12} b_1 |b_2|^2 i + d_{13} h i - \lambda_1 b_1 \rho i + \zeta_{11} b_1 |b_1|^4 i + \zeta_{12} b_1 |b_2|^4 \\ & + \zeta_{13} b_1 |b_1|^2 |b_2|^2 + \left(\zeta_{14} |b_1|^2 + \zeta_{15} |b_2|^2 + \zeta_{16} b_1^2\right) h i + \mathcal{O}(\epsilon^6), \end{aligned} \tag{4.3.24}$$

$$\begin{aligned} \frac{\Omega}{\lambda_1} \frac{\partial b_2}{\partial t} = {} & d_{21} b_2 |b_2|^2 i + d_{22} b_2 |b_1|^2 i - \lambda_2 b_2 \rho i + \zeta_{21} b_2 |b_2|^4 + \zeta_{22} b_2 |b_1|^4 \\ & + \zeta_{23} b_2 |b_1|^2 |b_2|^2 + \zeta_{24} \left(b_1 + \overline{b_1}\right) b_2 h i + \mathcal{O}(\epsilon^6). \end{aligned} \tag{4.3.25}$$

Similar to (4.3.18)-(4.3.19), from the above equations we also expect that the non-zero external drive amplitude induces coupled mode oscillations.

Note in Equations (4.3.24)–(4.3.25), there is a solution with $b_2 = 0$ and $b_1 \neq 0$ as well as $b_1 \neq 0$ and $b_2 \neq 0$, but with $b_1 = 0$ and $b_2 \neq 0$, is in general impossible (it requires $|b_2|^2 = d_{13}/\zeta_{15}$).

4.4 Numerical calculations

To check the analytical results obtained in the above sections, we have numerically solved the governing Equation (4.1.1), with $\theta(x)$ given by (4.4.1). We discretise the Laplacian operator using central differences and integrate the resulting system of differential equations using a fourth-order Runge–Kutta method, with a spatial and temporal discretizations of $\Delta x = 0.01$ and $\Delta t = 0.002$, respectively. The computational domain is $x \in (-L_1, L_1)$, with $L_1 = 50$. At the boundaries, we use a periodic boundary condition. To model an infinitely long junction, we apply an increasing damping at the boundaries to reduce reflected continuous waves incoming from the boundaries. In all the results presented herein, we use the damping coefficient

$$\alpha = \begin{cases} (|x| - L_1 + x_\alpha)/x_\alpha, & |x| > (L_1 - x_\alpha), \\ 0, & |x| < (L_1 - x_\alpha); \end{cases} \tag{4.4.1}$$

that is, α increases linearly from $\alpha = 0$ at $x = \pm(L_1 - x_\alpha)$ to $\alpha = 1$ at $x = \pm L_1$. We have taken $x_\alpha = 20$. To ensure that the numerical results are not influenced by the choice of the parameter values, we have taken different values (Δx, Δt, L_1) as well as different boundary conditions and damping, and we obtained quantitatively similar results.

In this Section, for the $0 - \pi - 0 - \pi - 0$ junction we fix the facet length $a = 1$ and $L = 2$, which implies that we are in the case $\lambda_2 > \lambda_1 > 1/3$, since

$$\begin{aligned} &\lambda_1 \approx 0.59941, \quad && K_1 \approx 0.39734, \quad && C_1 \approx -0.68655, \\ &\lambda_2 \approx 0.64247, \quad && K_2 \approx 0.44002, \quad && C_2 \approx -0.64471. \end{aligned}$$

For the choice of parameters above, we obtain the coefficients in the analytic approximations (4.2.51)–(4.2.52) and (4.3.18)–(4.3.19) as

$$\begin{aligned} &\alpha_1 = 0.15864, && \alpha_2 = 0.32326, && \alpha_3 = 0.16753, \\ &\alpha_4 = 0.34044, && \mu_1 = 0.55168, && a_4 = 0.29191, \\ &a_5 = -0.21275, && a_6 = 1.55308, && c_4 = 0.02164, \\ &\beta_1 = -0.00832 - 0.14102\,i, && \beta_2 = -0.01272 - 0.08509\,i, \\ &\beta_3 = -0.16295 + 7.78699\,i, && \gamma_1 = -0.02967 - 0.10655\,i, \\ &\gamma_2 = -0.06474 - 1.77612\,i, && \gamma_3 = -0.02680 - 1.52120\,i, \\ &a_1 = -0.00832 + 0.45010\,i, && a_2 = -0.01272 - 0.08511\,i, \\ &a_3 = -0.12295 - 3.23490\,i, && c_1 = -0.02957 - 0.20650\,i, \\ &c_2 = -0.07974 - 1.82500\,i, && c_3 = -0.04680 + 2.14572\,i. \end{aligned}$$

To illustrate the case $\lambda_1 < 1/3 < \lambda_2$, we choose $L = 0.5$, $a = 1.1$, that is,

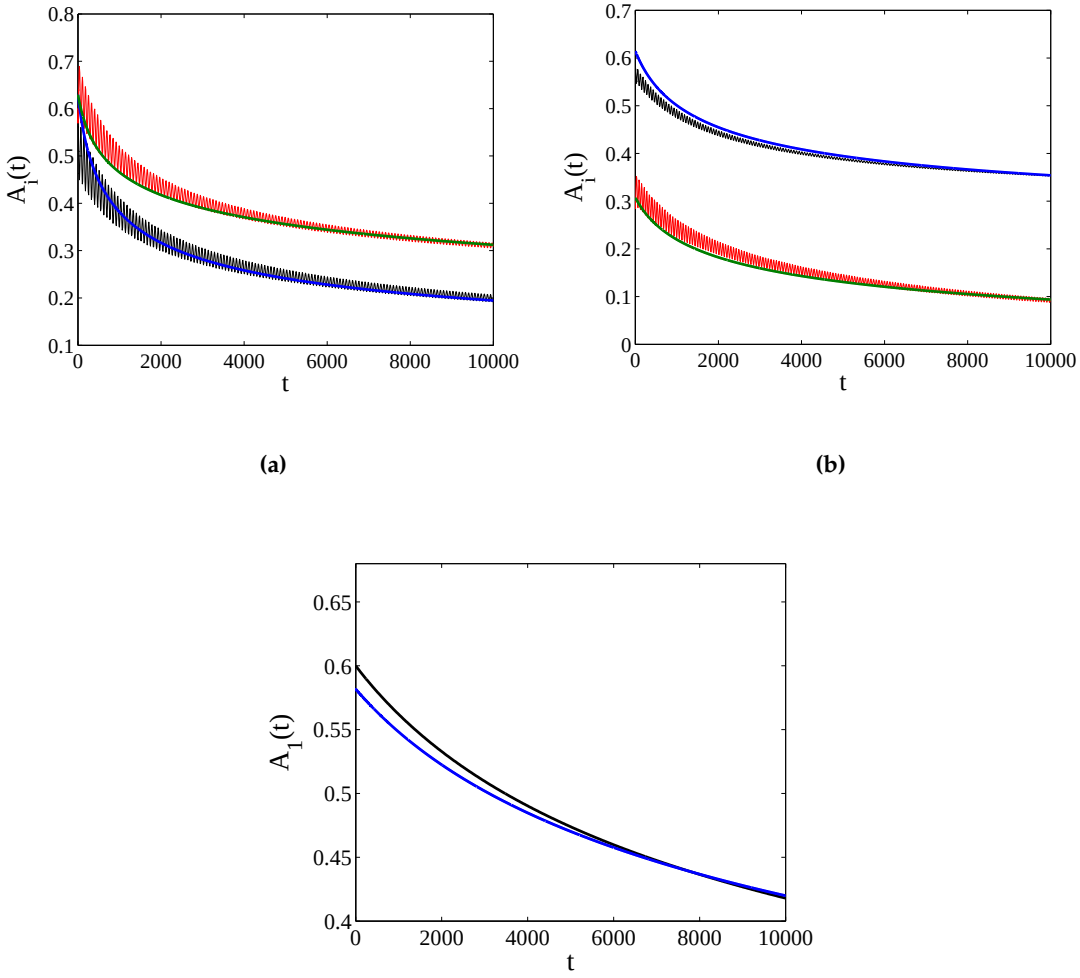

Figure 4.1: Oscillation amplitude of the breathing coupled mode in a $0-\pi-0-\pi-0$ junction. The case $\lambda_2 > \lambda_1 > 1/3$, with no driving ($h = 0$). (a): $A_2(0) = 0.6$, (b): $A_2(0) = 0.3$, (c): $A_2(0) = 0$, while in all cases $A_1(0) = 0.6$. The black oscillation curves are from the oscillation amplitude $A_1(t)$ and red for $A_2(t)$ obtained from the original governing Equation (4.1.1), clearly indicating the decay of the coupled mode oscillation. Analytical approximations (4.2.51) and (4.2.52) are shown as $A_1(t)$ for blue curves and $A_2(t)$ as green solid curves.

$$\begin{aligned} \lambda_1 &\approx 0.27431, \quad & K_1 &\approx 1.12709, \quad & C_1 &\approx -0.92738, \\ \lambda_2 &\approx 0.82148, \quad & K_2 &\approx 2.01578, \quad & C_2 &\approx -0.44062. \end{aligned}$$

In this case, we obtain the coefficients in the analytically obtained approximations (4.2.62)-(4.2.63) and (4.3.24)-(4.3.25) as

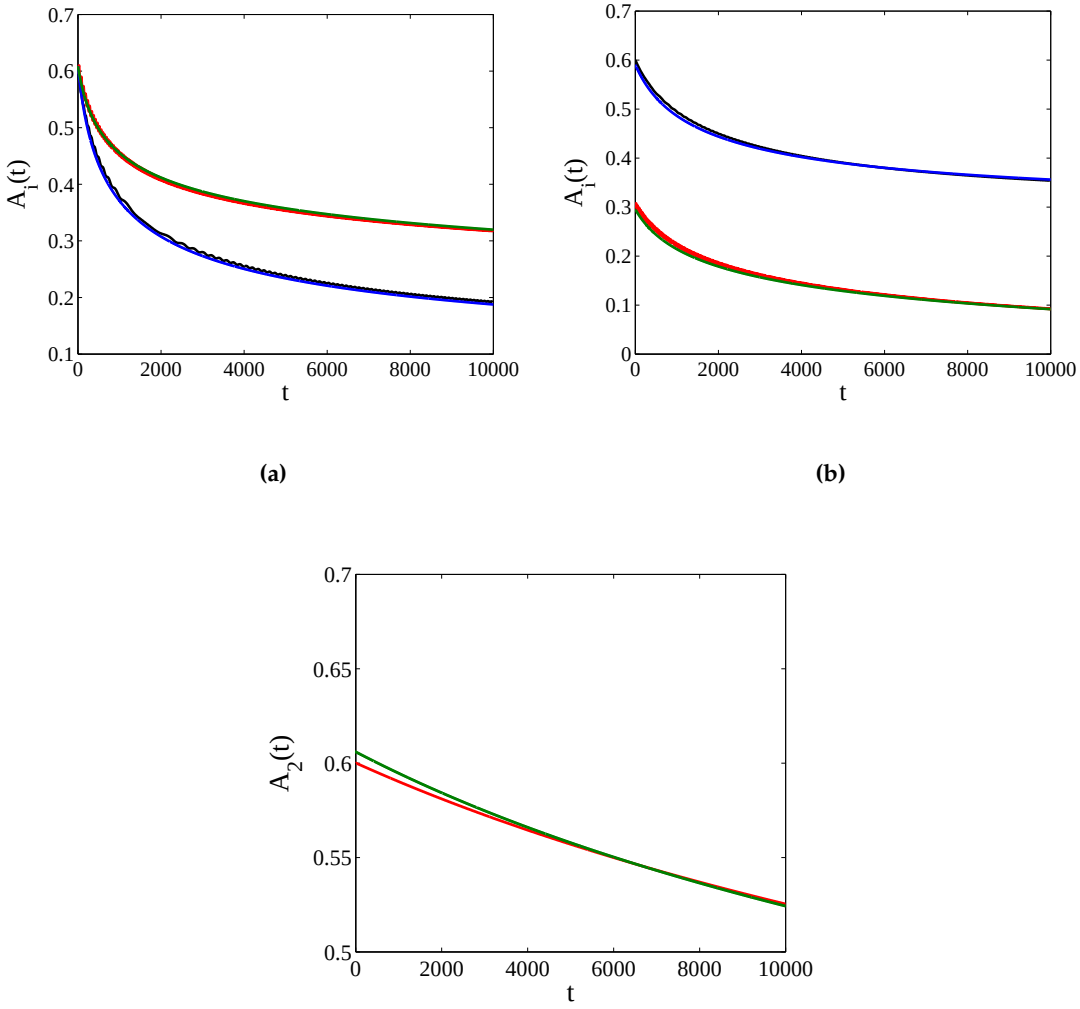

Figure 4.2: The case $\lambda_2 > 1/3 > \lambda_1$ with no driving i.e. $h = 0$. The other details are the same as in Figure 4.1. Analytical approximations (4.2.62) and (4.2.63) for the three panels are shown as green and blue lines.

$$
\begin{aligned}
&d_{11} = 0.53642, && d_{12} = 0.76104, && d_{13} = 0.92035,\\
&d_{21} = 0.09243, && d_{22} = 0.38662, && e_{11} = -1.79763,\\
&\zeta_{11} = 0.10120, && \zeta_{14} = -1.2231, && \zeta_{15} = -2.02615,\\
&\zeta_{16} = 2.27324, && \zeta_{24} = -1.21283,
\end{aligned}
$$

$$
\begin{aligned}
e_{12} &= -0.00162 + 0.33406\,i, & e_{13} &= -0.15674 + 0.50224\,i,\\
e_{21} &= -0.00252 + 0.01212\,i, & e_{22} &= -0.04699 - 0.92783\,i,\\
e_{23} &= -0.04619 - 0.05882\,i, & \zeta_{12} &= -0.035621 + 0.34056\,i,\\
\zeta_{13} &= -0.36524 + 1.47270\,i, & \zeta_{21} &= -0.002519 - 0.0558\,i,\\
\zeta_{22} &= -0.06229 + 0.43752\,i, & \zeta_{23} &= -0.03619 + 0.60335\,i.
\end{aligned}
$$

First, we consider the undriven case, $h = 0$. To calculate the oscillation amplitude of the two modes from the full Equation (4.1.1), we assume the initial condition similar to the expansion (4.2.1), (3.2.8)–(4.1.5) namely

$$\phi(x,t) \quad = \quad A_1(t)\Phi_1(x) + A_2(t)\Phi_2(x), \tag{4.4.2}$$

hence

$$A_j(t) \quad = \quad b_j e^{i\lambda_i t} + \overline{b_j} e^{-i\lambda_i t}. \tag{4.4.3}$$

Mathematically, $A_j(t)$ is approximated by

$$A_j(t) \quad = \quad \frac{\int_{-L}^{L} \phi(x,t)\Phi_j(x)dx}{\int_{-L}^{L} \Phi_j^2(x)dx}. \tag{4.4.4}$$

With the initial condition

$$A_1(0) = 0.6, \quad A_2(0) = 0.6, 0.3, 0, \tag{4.4.5}$$

we record the *envelope* for the coupled mode of the oscillation amplitudes $A_j(t)$ from the governing Equation (4.1.1). In Figures 4.1, and 4.2, we plot $A_1(t)$, $A_2(t)$ as red and black curves respectively. From Figures 4.1 and 4.2, one can see that the coupled mode oscillation amplitude decreases in time. The mode experiences damping. The damping is intrinsically present because the breathing mode emits radiation due to higher harmonic excited due to the nonlinearity which have frequency in the dispersion relation.

It is instructive to compare the numerical results with our analytical calculations. With the initial condition

$$|b_j(0)|^2 \quad = \quad \frac{A_j^2(0)}{4F^2}, \tag{4.4.6}$$

for the coupled Equations (4.2.51)-(4.2.52) and (4.2.62)-(4.2.63), that are solved numerically using a fourth-order Runge–Kutta method with a relatively fine time discretisation parameter, as general analytical solutions are not available. The analytical approximations are then given by $2F|b_1(t)|$ and $2F|b_2(t)|$. In general, the factor is simply $F = 1$. Yet, by treating F as a fitting parameter we observed that the best fit is not given by the aforementioned values. For the initial conditions (4.4.5), we found that optimum fits

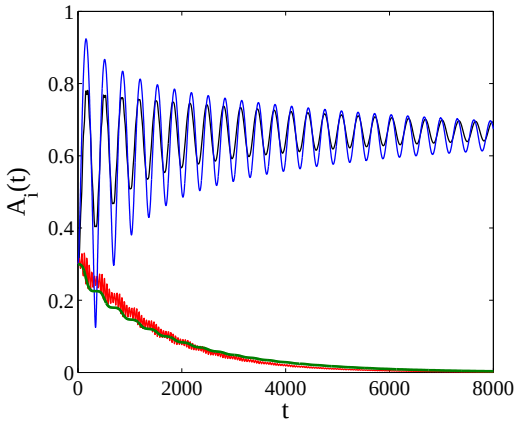

(a)

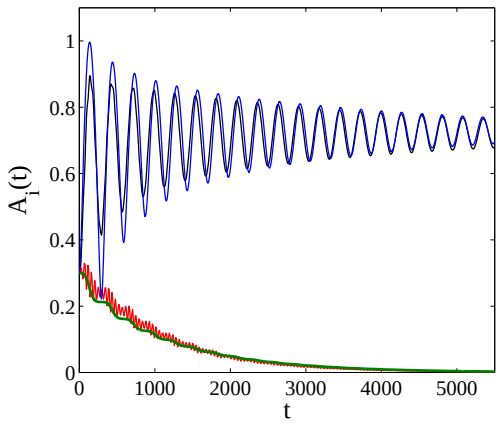

(b)

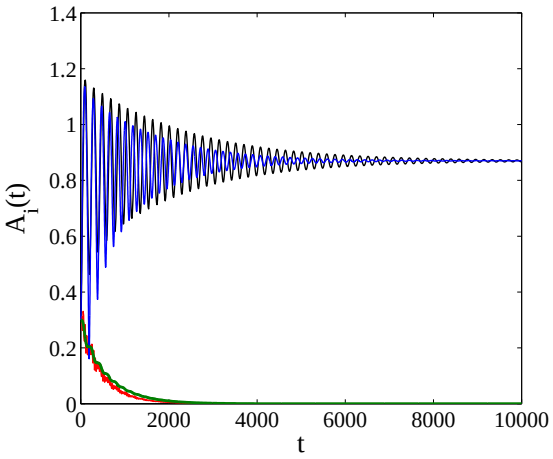

(c)

Figure 4.3: The same as in Figure 4.1, but for nonzero driving amplitude with $\lambda_1 \approx 0.59941$ and $\lambda_2 \approx 0.64247$. The three panels corresponds to $h = 0.006$, $h = 0.008$, $h = 0.015$. Analytical approximations (4.3.18)-(4.3.19) for the three panels are shown as green and blue lines.

are, respectively, provided by $F = 1.1, 1.05, 0.94$ for Figure 4.1 and $F = 1.03, 0.97, 1.02$ for Figures 4.2 respectively. The differences can be explained by the fact that our asymptotic approximations are only valid for long times, thus there is a short initial transient, which can be accented by allowing $F \neq 1$. In panels (a) and (b) of Fig. 4.1 and Fig. 4.2, we observe that exciting the two modes at the same time increases the decay rate. This is due to higher harmonic excitation and coupling of the oscillation amplitudes $b_j(t)$, that can be seen in the analytically obtained approximation. Simil-

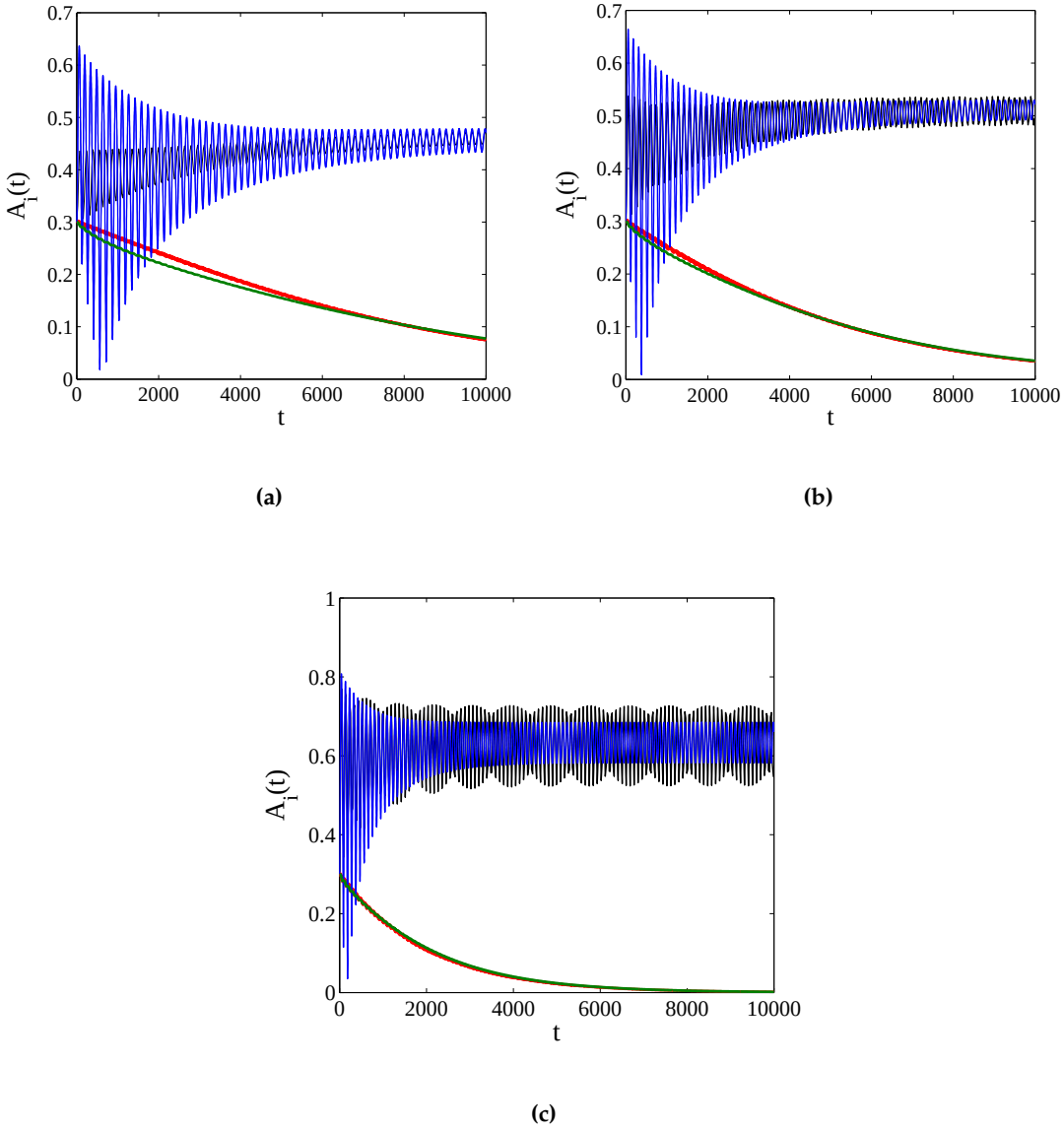

Figure 4.4: The same as in the figure 4.3 with $\lambda_1 \approx 0.27431$, $\lambda_2 \approx 0.82148$ and $3\lambda_1 < 1 < 3\lambda_2$. The three panels corresponds to driven $0-\pi-0-\pi-0$ junction with $h = 0.006$, $h = 0.008$, $h = 0.015$. Analytical approximations (4.3.24)-(4.3.25) for the three panels are shown as green and blue lines.

arly in the panels (c) of Fig. 4.1, and Fig. 4.2, by exciting one mode, we see that the decay rate is very slow for a long time compared to top panels (Note different range on the vertical axes). Our approximations are shown as green and blue solid lines in Figure 4.1 and Figure 4.2 where one can see good agreement with the numerically obtained oscillation.

Next, we consider the case of driven Josephson junctions, i.e. (4.1.1) with $h \neq 0$. In

this case, the initial condition to the governing Equation (4.1.1) is the same as before. Taking $\Omega = \lambda_1$, we present the amplitude of the oscillatory coupled mode $A_j(t)$ for $0-\pi-0-\pi-0$ junctions with $h = 0.006$, $h = 0.008$, $h = 0.015$, in the three panels, respectively, of Figures 4.3 and 4.4. The initial amplitudes are $A_j(0) = 0.3$, where for all the cases the envelope of $A_1(t)$ oscillates and slowly tends to a constant amplitude while the envelope of $A_2(t)$ vanishes. Hence, it is important to note that the drive acts to damp the antisymmetric mode. In other words, we have a synchronized oscillation between a localised mode in the two wells.

Considering the panels in Figures 4.3 and 4.4, we observe that the modes do not oscillate with an unbounded or growing amplitude. After a while, there is a balance between the energy input into the breathing mode due to the external drive and the radiative damping. The regular oscillation of the modes indicates that the junction voltage vanishes, even when the driving frequency is the same as the system's eigenfrequency.

To assess the accuracy of the asymptotic analysis, we have solved the amplitude Equations (4.3.18)-(4.3.19) and (4.3.24)-(4.3.25) numerically. The analytical approximations is again given by $2F|b(t)|$, where F in this case is taken as $F = 1.15$, $F = 1.15$, $F = 1.14$ for Figure 4.3, while $F = 1.05$, $F = 1.035$, $F = 1.05$ for Figure 4.4 respectively.

In the three panels of Figures 4.3 and 4.4, green and blue lines shown the approximation (4.3.18)-(4.3.19) and (4.3.24)-(4.3.25) respectively using $\rho = 0$, where one can see that our approximation is in good agreement, as it is indistinguishable from the numerical result.

4.5 Conclusions

We have considered a spatially inhomogeneous sine-Gordon equation with a time-periodic drive and two regions of π phase shift, modelling $0-\pi-0-\pi-0$ long Josephson junctions. We discussed the internal phase shift formation acting as a double well potential. Due to the type of the inhomogeneities, there is a pair of eigenmodes of different symmetries, *i.e.* symmetric and antisymmetric. We constructed a perturbation expansion for the coupled modes and obtained differential equations for the slow time evolution of the oscillation amplitudes in the $0-\pi-0-\pi-0$ long Josephson junctions.

In the absence of an ac-drive, the coupled amplitude equations describe the gradual decrease in the amplitude of the coupled mode oscillation which is due to the energy emission in the form of radiation. Similar investigation of the effects of radiations, the

resonance of breathing modes at its natural oscillating frequency and the same decay rates for the single mode oscillation for sine-Gordon equation in the context of long Josephson junctions and for ϕ^4 models have been discussed and obtained in [99, 100, 101].

Using multiple scale expansions, we have shown that due to the energy transfer from the discrete to continuous modes, two mode oscillation decays algebraically in time. The flow of energy from resonant discrete modes to continuum modes due to the nonlinear coupling has been addressed in [149, 150]. The phenomenon obtained in this study which is responsible for the time decay due to the energy transfer from the discrete to continuous modes is analyzed by Soffer, Weinstien, Sigal, and others for nonlinear Klein-Gordon equations and nonlinear Schrödinger equations in [151, 152, 153, 154].

We also discussed the resonance condition when the antisymmetric mode is excited, while the symmetric mode lies in the discrete spectrum. Interestingly the solutions of obtained coupled amplitude equations still decay in time. This shows that the two modes influence each other, when oscillating in the long time regime. We also showed that, by exciting one mode, the decay rate is significantly reduced over the long time compared to the two modes.

Next, we discussed the coupled mode oscillation in the presence of an ac-drive. We observed that the modes do not oscillate with an unbounded or growing amplitude but for a small drive amplitude, there is a balance between the energy input given by the external drive and the energy output due to the radiative damping experienced by the coupled modes.

Comparing the amplitudes of the two modes, we observed that the amplitude of the symmetric mode oscillates and slowly tends to constant, while the envelope of the antisymmetric mode vanishes. This shows that an ac-drive acts as a damping to antisymmetric mode. In other words, we have a synchronized oscillations of localised modes in the two wells. The regular oscillation of the modes indicates that the junction voltage vanishes, even when the driving frequency is the same as one of the system's eigenfrequency.

4.A Appendix: Explicit expressions

4.A.1 Functions in Section 4.2

$$
\begin{aligned}
G_1 &= 2i\lambda_1 D_4 B_1 \Phi_1 + B_1 \left(2i\lambda_1 \left(\alpha_1 |B_1|^2 i + \alpha_2 |B_2|^2 i\right) - \frac{3}{2}|B_1|^2\Phi_1^2 - |B_2|^2 {\Phi_2}^2\right)\psi_1 \\
&\quad + B_1 \left(\alpha_1 |B_1|^2 i + \alpha_2 |B_2|^2 i\right)^2 \Phi_1 + \frac{1}{12} B_1 |B_1|^4 {\Phi_1}^5 + \frac{1}{2} B_1 |B_1|^2 |B_2|^2 \Phi_1^3 \Phi_2^2 \\
&\quad + \frac{1}{4} B_1 |B_2|^4 \Phi_1 \Phi_2^4 - 2\, B_1 |B_2|^2 \Phi_1 \Phi_2 \psi_4 - B_1 |B_1|^2 |B_2|^2 \Phi_1 \Phi_2 \psi_7 - \frac{1}{2} B_1 |B_1|^4 \Phi_1^2 \psi_{13} \\
&\quad - B_1 |B_1|^2 |B_2|^2 \Phi_1 \Phi_2 \psi_{10} - \frac{1}{2} B_1 |B_2|^4 {\Phi_2}^2 \psi_{19} - \frac{1}{2} B_1 |B_2|^4 {\Phi_2}^2 \psi_{22}, \qquad (4.A.1)
\end{aligned}
$$

$$
\begin{aligned}
G_2 &= 2i\lambda_1 D_4 B_1 \Phi_1 + B_1 \left(2i\lambda_1 \left(\alpha_1 |B_1|^2 i + \alpha_2 |B_2|^2 i\right) + \frac{3}{2}|B_1|^2\Phi_1^2 + |B_2|^2 {\Phi_2}^2\right)\psi_2 \\
&\quad + B_1 \left(\alpha_1 |B_1|^2 i + \alpha_2 |B_2|^2 i\right)^2 \Phi_1 - \frac{1}{12} B_1 |B_1|^4 {\Phi_1}^5 - \frac{1}{2} B_1 |B_1|^2 |B_2|^2 \Phi_1^3 \Phi_2^2 \\
&\quad - \frac{1}{4} B_1 |B_2|^4 \Phi_1 \Phi_2^4 + 2\, B_1 |B_2|^2 \Phi_1 \Phi_2 \psi_5 + B_1 |B_1|^2 |B_2|^2 \Phi_1 \Phi_2 \psi_8 + \frac{1}{2} B_1 |B_1|^4 \Phi_1^2 \psi_{14} \\
&\quad + B_1 |B_1|^2 |B_2|^2 \Phi_1 \Phi_2 \psi_{11} + \frac{1}{2} B_1 |B_2|^4 {\Phi_2}^2 \psi_{20} + \frac{1}{2} B_1 |B_2|^4 {\Phi_2}^2 \psi_{23}, \qquad (4.A.2)
\end{aligned}
$$

$$
\begin{aligned}
G_3 &= 2i\lambda_1 D_4 B_1 \Phi_1 + B_1 \left(2i\lambda_1 \left(\alpha_1 |B_1|^2 i + \alpha_2 |B_2|^2 i\right) - \frac{3}{2}|B_1|^2\Phi_1^2 - |B_2|^2 {\Phi_2}^2\right)\psi_3 \\
&\quad + B_1 \left(\alpha_1 |B_1|^2 i + \alpha_2 |B_2|^2 i\right)^2 \Phi_1 + \frac{1}{12} B_1 |B_1|^4 {\Phi_1}^5 + \frac{1}{2} B_1 |B_1|^2 |B_2|^2 \Phi_1^3 \Phi_2^2 \\
&\quad + \frac{1}{4} B_1 |B_2|^4 \Phi_1 \Phi_2^4 - 2\, B_1 |B_2|^2 \Phi_1 \Phi_2 \psi_6 - B_1 |B_1|^2 |B_2|^2 \Phi_1 \Phi_2 \psi_9 - \frac{1}{2} B_1 |B_1|^4 \Phi_1^2 \psi_{15} \\
&\quad - B_1 |B_1|^2 |B_2|^2 \Phi_1 \Phi_2 \psi_{12} - \frac{1}{2} B_1 |B_2|^4 {\Phi_2}^2 \psi_{21} - \frac{1}{2} B_1 |B_2|^4 {\Phi_2}^2 \psi_{24}, \qquad (4.A.3)
\end{aligned}
$$

$$
\begin{aligned}
H_1 &= 2i\lambda_2 D_4 B_2 \Phi_2 + B_2 \left(2i\lambda_2 \left(\alpha_3 |B_2|^2 i + \alpha_4 |B_1|^2 i\right) - \frac{3}{2}|B_2|^2 {\Phi_2}^2 - |B_1|^2 {\Phi_1}^2\right)\psi_4 \\
&\quad + B_2 \left(\alpha_3 |B_2|^2 i + \alpha_4 |B_1|^2 i\right)^2 \Phi_2 + \frac{1}{12} B_2 |B_2|^4 \Phi_2^5 + \frac{1}{2} B_2 |B_1|^2 |B_2|^2 \Phi_1^2 \Phi_2^3 \\
&\quad + \frac{1}{4} B_2 |B_1|^4 {\Phi_1}^4 \Phi_2 - 2\, B_2 |B_1|^2 \Phi_1 \Phi_2 \psi_1 - \frac{1}{2} B_2 |B_1|^4 {\Phi_1}^2 \psi_7 - \frac{1}{2} B_2 |B_1|^4 {\Phi_1}^2 \psi_{10} \\
&\quad - \frac{1}{2} B_2 |B_2|^4 {\Phi_2}^2 \psi_{16} - B_2 |B_1|^2 |B_2|^2 \Phi_1 \Phi_2 \psi_{19} - B_2 |B_1|^2 |B_2|^2 \Phi_1 \Phi_2 \psi_{22}, \qquad (4.A.4)
\end{aligned}
$$

$$
\begin{aligned}
H_2 &= 2i\lambda_2 D_4 B_2 \Phi_2 + B_2 \left(2i\lambda_2 \left(\alpha_3 |B_2|^2 i + \alpha_4 |B_1|^2 i\right) + \frac{3}{2}|B_2|^2 {\Phi_2}^2 + |B_1|^2 {\Phi_1}^2\right)\psi_5 \\
&\quad + B_2 \left(|B_2|^2 \alpha_3 i + |B_1|^2 \alpha_4 i\right)^2 \Phi_2 - \frac{1}{12} B_2 |B_2|^4 \Phi_2^5 - \frac{1}{2} B_2 |B_1|^2 |B_2|^2 \Phi_1^2 \Phi_2^3 \\
&\quad - \frac{1}{4} B_2 |B_1|^4 {\Phi_1}^4 \Phi_2 + 2\, B_2 |B_1|^2 \Phi_1 \Phi_2 \psi_2 + \frac{1}{2} B_2 |B_1|^4 {\Phi_1}^2 \psi_8 + \frac{1}{2} B_2 |B_1|^4 {\Phi_1}^2 \psi_{11} \\
&\quad + \frac{1}{2} B_2 |B_2|^4 {\Phi_2}^2 \psi_{17} + B_2 |B_1|^2 |B_2|^2 \Phi_1 \Phi_2 \psi_{20} + B_2 |B_1|^2 |B_2|^2 \Phi_1 \Phi_2 \psi_{23}, \qquad (4.A.5)
\end{aligned}
$$

$$
\begin{aligned}
H_3 &= 2\,i\lambda_2 D_4 B_2 \Phi_2 + B_2\left(2\,i\lambda_2\left(\alpha_3|B_2|^2\,i+\alpha_4|B_1|^2\,i\right)-\frac{3}{2}|B_2|^2{\Phi_2}^2-|B_1|^2{\Phi_1}^2\right)\psi_6\\
&\quad +B_2\left(\alpha_3|B_2|^2\,i+\alpha_4|B_1|^2\,i\right)^2\Phi_2+\frac{1}{12}B_2|B_2|^4\Phi_2^5+\frac{1}{2}B_2|B_1|^2|B_2|^2\Phi_1^2{\Phi_2}^3\\
&\quad +\frac{1}{4}B_2|B_1|^4{\Phi_1}^4\Phi_2-2\,B_2|B_1|^2\Phi_1\Phi_2\psi_3-\frac{1}{2}B_2|B_1|^4{\Phi_1}^2\psi_9-\frac{1}{2}B_2|B_1|^4{\Phi_1}^2\psi_{12}\\
&\quad -\frac{1}{2}B_2|B_2|^4{\Phi_2}^2\psi_{18}-B_2|B_1|^2|B_2|^2\Phi_1\Phi_2\psi_{21}-B_2|B_1|^2|B_2|^2\Phi_1\Phi_2\psi_{24}, \qquad (4.A.6)
\end{aligned}
$$

$$
\begin{aligned}
p_1 &= \frac{\lambda_1\left[\left(1-C_1^2\right)\sin(2\sqrt{1+{\lambda_1}^2}a)+2(1+{C_1}^2)\sqrt{1+{\lambda_1}^2}a-4C_1\sin^2(\sqrt{1+{\lambda_1}^2}a)\right]}{2\sqrt{1+\lambda_1^2}}\\
&\quad +\frac{\lambda_1\left(2+K_1^2\left(\sinh\left(2\sqrt{1-{\lambda_1}^2}L\right)+2\sqrt{1-{\lambda_1}^2}L\right)\right)}{2\sqrt{1-\lambda_1^2}}, \qquad (4.A.7)\\
p_2 &= \frac{3\,L{K_1}^4-6\,{C_1}^2a-3\left({C_1}^4+1\right)a}{16}+\frac{8\,C_1\left(1+{C_1}^2-2\,{C_1}^2\cos^2\left(\sqrt{1+{\lambda_1}^2}a\right)\right)}{16\sqrt{1+\lambda_1^2}}\\
&\quad +\frac{8\,C_1\left(C_1^2-1\right)\cos^4\left(\sqrt{1+{\lambda_1}^2}a\right)}{16\sqrt{1+{\lambda_1}^2}}+\frac{\left(5\,{C_1}^4-6\,C_1^2-3\right)\sin\left(2\sqrt{1+{\lambda_1}^2}a\right)}{32\sqrt{1+{\lambda_1}^2}}\\
&\quad -\frac{2\left({C_1}^4-6\,{C_1}^2+1\right)\cos^3\left(\sqrt{1+{\lambda_1}^2}a\right)\sin\left(\sqrt{1+{\lambda_1}^2}a\right)}{16\sqrt{1+\lambda_1^2}}+\frac{1}{8\sqrt{1-\lambda_1^2}}\\
&\quad +\frac{{K_1}^4\sinh\left(2\sqrt{1-{\lambda_1}^2}L\right)\left(2\cosh^2\left(\sqrt{1-{\lambda_1}^2}L\right)+3\right)}{32\sqrt{1-{\lambda_1}^2}}, \qquad (4.A.8)\\
p_3 &= -\frac{\sqrt{1-{\lambda_1}^2}-\sqrt{1-{\lambda_2}^2}}{2\left({\lambda_1}^2-{\lambda_2}^2\right)}-\frac{\left(\int_L^{L+a}A_1(X_0)\,dX_0\lambda_1^2-\int_L^{L+a}A_1(X_0)\,dX_0\lambda_2^2\right)}{\lambda_1^2-\lambda_2^2}\\
&\quad +\frac{K_1^2K_2^2\left(\int_0^L A_2(X_0)\,dX_0\lambda_1^2-\int_0^L A_2(X_0)\,dX_0\lambda_2^2\right)}{\lambda_1^2-\lambda_2^2}, \qquad (4.A.9)\\
p_4 &= \frac{\lambda_2\left(2\left(C_2^2+1\right)\sqrt{1+\lambda_2^2}a-\left(C_2^2-1\right)\sin(2\sqrt{1+{\lambda_2}^2}a)-4C_2\sin^2(\sqrt{1+\lambda_2^2}a)\right)}{2\sqrt{1+{\lambda_2}^2}}\\
&\quad +\frac{\lambda_2\left(2+{K_2}^2\sinh\left(2\sqrt{1-{\lambda_2}^2}L\right)-2\,{K_2}^2\sqrt{1-{\lambda_2}^2}L\right)}{2\sqrt{1-{\lambda_2}^2}}, \qquad (4.A.10)\\
p_6 &= -\frac{\sqrt{1-{\lambda_1}^2}-\sqrt{1-{\lambda_2}^2}}{2\left({\lambda_1}^2-{\lambda_2}^2\right)}-\frac{\left(\int_L^{L+a}A_1(X_0)\,dX_0\lambda_1^2-\int_L^{L+a}A_1(X_0)\,dX_0\lambda_2^2\right)}{\lambda_1^2-\lambda_2^2}\\
&\quad +\frac{K_1^2K_2^2\left(\int_0^L A_2(X_0)\,dX_0\lambda_1^2-\int_0^L A_2(X_0)\,dX_0\lambda_2^2\right)}{\lambda_1^2-\lambda_2^2}, \qquad (4.A.11)
\end{aligned}
$$

$$
\begin{aligned}
p_5 \;=\; & \frac{\sin\left(2\sqrt{1+{\lambda_2}^2}a\right)\left(5{C_2}^4-6{C_2}^2-3\right)-6a\sqrt{1+{\lambda_2}^2}\left({C_2}^4+2{C_2}^2+1\right)}{32\sqrt{1+{\lambda_2}^2}} \\
& -\frac{{C_2}^3\cos^2\left(\sqrt{1+{\lambda_2}^2}a\right)\left(16+C_2\sin\left(2\sqrt{1+{\lambda_2}^2}a\right)\right)}{16\sqrt{1+{\lambda_2}^2}}+\frac{C_2\left({C_2}^2+1\right)}{2\sqrt{1+{\lambda_2}^2}} \\
& +\frac{\cos^3(\sqrt{1+\lambda_2^2}a)\left[(6C_2^2-1)\sin(\sqrt{1+\lambda_2^2}a)+4C_2(C_2^2-1)\cos(\sqrt{1+{\lambda_2}^2}a)\right]}{8\sqrt{1+{\lambda_2}^2}} \\
& +\frac{{K_2}^4\sinh\left(2\sqrt{1-{\lambda_2}^2}L\right)\left(2\cosh^2\left(\sqrt{1-{\lambda_2}^2}L\right)-5\right)}{32\sqrt{1-\lambda_2^2}} \\
& +\frac{2+3\,{K_2}^4\sqrt{1-{\lambda_2}^2}L}{16\sqrt{1-{\lambda_2}^2}}, \qquad (4.A.12)
\end{aligned}
$$

$$
\begin{aligned}
\psi_1 \;=\; & z_1 e^{-\sqrt{1-{\lambda_1}^2}(X_0-L-a)}-\frac{|B_1|^2e^{-3\sqrt{1-\lambda_1^2}(X_0-L-a)}}{16\left(1-{\lambda_1}^2\right)} \\
& +\frac{\lambda_1(\alpha_1|B_1|^2+\alpha_2|B_2|^2)\left(1+2\sqrt{1-{\lambda_2}^2}X_0\right)e^{-\sqrt{1-{\lambda_1}^2}(X_0-L-a)}}{2\sqrt{1-{\lambda_1}^2}\left(\sqrt{1-{\lambda_1}^2}+\sqrt{1-{\lambda_2}^2}\right)} \\
& +\frac{\lambda_1(\alpha_1|B_1|^2+\alpha_2|B_2|^2)\left(\sqrt{1-{\lambda_2}^2}+2\,X_0\left(1-{\lambda_1}^2\right)\right)e^{-\sqrt{1-{\lambda_1}^2}(X_0-L-a)}}{2\left(1-{\lambda_1}^2\right)\left(\sqrt{1-{\lambda_1}^2}+\sqrt{1-{\lambda_2}^2}\right)} \\
& -\frac{|B_2|^2e^{-\left(\sqrt{1-\lambda_1^2}+2\sqrt{1-\lambda_2^2}\right)(X_0-L-a)}}{4\sqrt{1-\lambda_2^2}\left(\sqrt{1-\lambda_1^2}+\sqrt{1-\lambda_2^2}\right)}, \qquad (4.A.13) \\
\psi_2 \;=\; & z_2\cos\left(\sqrt{1+{\lambda_1}^2}\,(X_0-L-a)\right)+z_3\sin\left(\sqrt{1+{\lambda_1}^2}\,(X_0-L-a)\right) \\
& +\frac{1}{2\sqrt{1+\lambda_1^2}}\Big[\int F_1(X_0)\,dX_0\sin(\sqrt{1+{\lambda_1}^2}X_0) \\
& +\int G_1(X_0)\,dX_0\cos(\sqrt{1+{\lambda_1}^2}X_0)\Big], \qquad (4.A.14) \\
\psi_4 \;=\; & z_1 e^{-\sqrt{1-\lambda_2^2}(X_0-L-a)}-\frac{|B_1|^2e^{-\left(2\sqrt{1-{\lambda_1}^2}+\sqrt{1-{\lambda_2}^2}\right)(X_0-L-a)}}{4\sqrt{1-{\lambda_1}^2}\left(\sqrt{1-{\lambda_2}^2}+\sqrt{1-{\lambda_1}^2}\right)} \\
& -\frac{|B_2|^2e^{-3\sqrt{1-{\lambda_2}^2}(X_0-L-a)}}{16(1-{\lambda_2}^2)} \\
& +\frac{\lambda_2\left(\alpha_3|B_2|^2+\alpha_4|B_1|^2\right)\left(1+2\sqrt{1-{\lambda_2}^2}X_0\right)e^{-\sqrt{1-{\lambda_2}^2}(X_0-L-a)}}{2\left(1-{\lambda_2}^2\right)}, \qquad (4.A.15)
\end{aligned}
$$

$$
\begin{aligned}
\psi_3 &= z_4 \cosh\left(\sqrt{1-{\lambda_1}^2}X_0\right) + \frac{|B_1|^2 K_1^3}{64\,(1-\lambda_1^2)} \times \\
&\Big[\Big(8\sinh(2\sqrt{1-\lambda_1^2}X_0) + \sinh(4\sqrt{1-\lambda_1^2}X_0) + 12\sqrt{1-\lambda_1^2}X_0)\sinh(\sqrt{1-\lambda_1^2}X_0\Big) \\
&+4\cosh(2\sqrt{1-{\lambda_1}^2}X_0) + \cosh(4\sqrt{1-{\lambda_1}^2}X_0)\cosh(\sqrt{1-{\lambda_1}^2}X_0)\Big] \\
&-\frac{1}{2}|B_2|^2 K_1 K_2^2\Big[\frac{\cosh\left(2\sqrt{1-{\lambda_1}^2}X_0\right)\cosh\left(\sqrt{1-{\lambda_1}^2}X_0\right)}{8\,(1-{\lambda_1}^2)} + \frac{X_0\sinh\left(\sqrt{1-{\lambda_1}^2}X_0\right)}{4\sqrt{1-\lambda_1^2}} \\
&+\frac{\cosh\left(\sqrt{1-{\lambda_1}^2}X_0\right)\left(\sqrt{1-{\lambda_1}^2}+\sqrt{1-{\lambda_2}^2}\right)\cosh\left(2\left(\sqrt{1-{\lambda_1}^2}-\sqrt{1-{\lambda_2}^2}\right)X_0\right)}{16\sqrt{1-{\lambda_1}^2}\left({\lambda_1}^2-{\lambda_2}^2\right)} \\
&+\frac{\cosh\left(\sqrt{1-{\lambda_1}^2}X_0\right)\left(\sqrt{1-{\lambda_1}^2}-\sqrt{1-{\lambda_2}^2}\right)\cosh\left(2\left(\sqrt{1-{\lambda_1}^2}+\sqrt{1-{\lambda_2}^2}\right)X_0\right)}{16\sqrt{1-{\lambda_1}^2}\left({\lambda_1}^2-{\lambda_2}^2\right)} \\
&-\frac{\sinh\left(\sqrt{1-{\lambda_1}^2}X_0\right)\left(\sqrt{1-{\lambda_1}^2}+\sqrt{1-{\lambda_2}^2}\right)\sinh\left(2\left(\sqrt{1-{\lambda_1}^2}-\sqrt{1-{\lambda_2}^2}\right)X_0\right)}{16\sqrt{1-{\lambda_1}^2}\left({\lambda_1}^2-{\lambda_2}^2\right)} \\
&-\frac{\sinh\left(\sqrt{1-{\lambda_1}^2}X_0\right)\left(\sqrt{1-{\lambda_1}^2}-\sqrt{1-{\lambda_2}^2}\right)\sinh\left(2\left(\sqrt{1-{\lambda_1}^2}+\sqrt{1-{\lambda_2}^2}\right)X_0\right)}{16\sqrt{1-{\lambda_1}^2}\left({\lambda_1}^2-{\lambda_2}^2\right)} \\
&+\frac{\left(\sqrt{1-\lambda_2^2}\sinh(2\sqrt{1-\lambda_1^2}X_0) - \sqrt{1-\lambda_1^2}\sinh(2\sqrt{1-\lambda_2^2}X_0)\right)\sinh\left(\sqrt{1-\lambda_1^2}X_0\right)}{8\sqrt{1-\lambda_2^2}(1-\lambda_1^2)}\Big] \\
&+\left(\alpha_1|B_1|^2+\alpha_2|B_2|^2\right)\Big[\frac{\lambda_1\cosh\left(2\sqrt{1-{\lambda_1}^2}X_0\right)\cosh\left(\sqrt{1-{\lambda_1}^2}X_0\right)}{2\,(1-{\lambda_1}^2)} \\
&+\frac{\lambda_1\left(\sinh\left(2\sqrt{1-{\lambda_1}^2}X_0\right)+2\sqrt{1-{\lambda_1}^2}X_0\right)\sinh\left(\sqrt{1-{\lambda_1}^2}X_0\right)}{2\,(1-\lambda_1^2)}\Big], \qquad \text{(4.A.16)} \\
\psi_5 &= z_2\cos\left(\sqrt{1+\lambda_2^2}\,(X_0-L-a)\right) + z_3\sin\left(\sqrt{1+\lambda_2^2}\,(X_0-L-a)\right) \\
&-\frac{1}{2\sqrt{1+\lambda_2^2}}\Big[\int F_0(X_0)dX_0\sin(\sqrt{1+{\lambda_2}^2}X_0) \\
&-\int G_0(X_0)dX_0\cos(\sqrt{1+{\lambda_2}^2}X_0)\Big], \qquad \text{(4.A.17)} \\
\psi_7 &= z_1 \mathrm{e}^{-\sqrt{1-(2\lambda_1+\lambda_2)^2}(X_0-L-a)} \\
&-\frac{\left(1+\lambda_1\lambda_2-\sqrt{1-\lambda_1^2}\sqrt{1-\lambda_2^2}\right)\mathrm{e}^{-\left(2\sqrt{1-{\lambda_1}^2}+\sqrt{1-{\lambda_2}^2}\right)(X_0-L-a)}}{8\,\left(\lambda_1+\lambda_2\right)^2}, \qquad \text{(4.A.18)}
\end{aligned}
$$

$$
\begin{aligned}
\psi_6 &= z_4 \sinh\left(\sqrt{1-{\lambda_2}^2}X_0\right) - \frac{1}{2}K_1^2 K_2 |B_1|^2 \times \\
&\Big[\frac{\cosh\left(\sqrt{1-\lambda_2^2}X_0\right)\left(\sqrt{1-\lambda_1^2}+\sqrt{1-\lambda_2^2}\right)\sinh\left(2(\sqrt{1-\lambda_1^2}-\sqrt{1-\lambda_2^2})X_0\right)}{8\sqrt{1-{\lambda_2}^2}\left({\lambda_1}^2-{\lambda_2}^2\right)} \\
&+\frac{\cosh\left(\sqrt{1-{\lambda_2}^2}X_0\right)\left(\sqrt{1-{\lambda_1}^2}-\sqrt{1-{\lambda_2}^2}\right)\sinh\left(2(\sqrt{1-{\lambda_1}^2}+\sqrt{1-{\lambda_2}^2})X_0\right)}{8\sqrt{1-{\lambda_2}^2}\left({\lambda_1}^2-{\lambda_2}^2\right)} \\
&+\frac{\sinh\left(\sqrt{1-{\lambda_2}^2}X_0\right)\left(\sqrt{1-{\lambda_1}^2}+\sqrt{1-{\lambda_2}^2}\right)\cosh\left(2(\sqrt{1-{\lambda_1}^2}-\sqrt{1-{\lambda_2}^2})X_0\right)}{8\sqrt{1-{\lambda_2}^2}\left({\lambda_1}^2-{\lambda_2}^2\right)} \\
&-\frac{\sinh\left(\sqrt{1-{\lambda_2}^2}X_0\right)\left(\sqrt{1-{\lambda_1}^2}-\sqrt{1-{\lambda_2}^2}\right)\cosh\left(2(\sqrt{1-{\lambda_1}^2}+\sqrt{1-{\lambda_2}^2})X_0\right)}{8\sqrt{1-{\lambda_2}^2}\left({\lambda_1}^2-{\lambda_2}^2\right)} \\
&-\frac{\left(\sqrt{1-\lambda_1^2}\sinh(2\sqrt{1-\lambda_2^2}X_0)-\sqrt{1-\lambda_2^2}\sinh(2\sqrt{1-\lambda_1^2}X_0)\right)\cosh\left(\sqrt{1-\lambda_2^2}X_0\right)}{16\sqrt{1-\lambda_1^2}\left(1-\lambda_2^2\right)} \\
&+\frac{\cosh\left(2\sqrt{1-{\lambda_2}^2}X_0\right)\sinh\left(\sqrt{1-{\lambda_2}^2}X_0\right)}{4\left(1-{\lambda_2}^2\right)}+\frac{\cosh\left(\sqrt{1-{\lambda_2}^2}X_0\right)X_0}{8\sqrt{1-{\lambda_2}^2}}\Big] \\
&-\frac{|B_2|^2K_2^3}{64(1-\lambda_2^2)}\Big[\left(4\cosh(2\sqrt{1-\lambda_2^2}X_0)-\cosh(4\sqrt{1-\lambda_2^2}X_0)\right)\sinh\left(2\sqrt{1-\lambda_2^2}X_0\right) \\
&-\left(\sinh\left(4\sqrt{1-{\lambda_2}^2}X_0\right)-8\sqrt{1-{\lambda_1}^2}\sinh\left(2\sqrt{1-{\lambda_2}^2}X_0\right)+12\sqrt{1-{\lambda_2}^2}X_0\right) \\
&\times\cosh\left(\sqrt{1-{\lambda_2}^2}X_0\right)\Big] \\
&-\frac{K_2(\alpha_3|B_2|^2+\alpha_4|B_1|^2)}{2(1-\lambda_2^2)}\Big[\lambda_2\cosh\left(2\sqrt{1-{\lambda_2}^2}X_0\right)\sinh\left(\sqrt{1-{\lambda_2}^2}X_0\right) \\
&+\cosh\left(2\sqrt{1-{\lambda_2}^2}X_0\right)\lambda_2\left(2\sqrt{1-{\lambda_2}^2}X_0-\sinh\left(2\sqrt{1-{\lambda_2}^2}X_0\right)\right)\Big], \qquad (4.A.19)
\end{aligned}
$$

$$
\begin{aligned}
\psi_8 &= z_2\cos(\sqrt{1+(2\lambda_1+\lambda_2)^2}(X_0-L-a))+z_3\sin(\sqrt{1+(2\lambda_1+\lambda_2)^2}\,(X_0-L-a)) \\
&+\frac{\int\cos\left(\sqrt{1+(2\,\lambda_1+\lambda_2)^2}X_0\right)G_2(X_0)\,dX_0\sin\left(\sqrt{1+(2\,\lambda_1+\lambda_2)^2}X_0\right)}{2\sqrt{1+(2\,\lambda_1+\lambda_2)^2}} \\
&-\frac{\int\sin\left(\sqrt{1+(2\,\lambda_1+\lambda_2)^2}X_0\right)G_2(X_0)\,dX_0\cos\left(\sqrt{1+(2\,\lambda_1+\lambda_2)^2}X_0\right)}{2\sqrt{1+(2\,\lambda_1+\lambda_2)^2}}, \qquad (4.A.20)
\end{aligned}
$$

$$
\begin{aligned}
\psi_{10} &= z_1 e^{-\sqrt{1-(2\,\lambda_1-\lambda_2)^2}(X_0-L-a)} \\
&+\frac{\left(\lambda_1\lambda_2+\sqrt{1-\lambda_1^2}\sqrt{1-\lambda_2^2}-1\right)e^{-\left(2\sqrt{1-\lambda_1^2}+\sqrt{1-\lambda_2^2}\right)(X_0-L-a)}}{8\,(\lambda_1-\lambda_2)^2}, \qquad (4.A.21)
\end{aligned}
$$

$$\begin{aligned}
\psi_9 &= z_4 \cosh\left(\sqrt{1-(2\lambda_1+\lambda_2)^2}X_0\right) - \frac{K_1^2 K_2}{2\sqrt{(2\lambda_1+\lambda_2)^2-1}} \times \\
&\Big[\int F_4(X_0)\,dX_0 \sin(\sqrt{(2\lambda_1+\lambda_2)^2-1}X_0) \\
&- \int G_4(X_0)\,dX_0 \cos(\sqrt{(2\lambda_1+\lambda_2)^2-1}X_0)\Big], \qquad (4.A.22)\\
\psi_{11} &= z_2 \cos(\sqrt{1+(2\lambda_1-\lambda_2)^2}\,(X_0-L-a)) + z_3 \sin(\sqrt{1+(2\lambda_1-\lambda_2)^2}\,(X_0-L-a)) \\
&+ \frac{\int \cos\left(\sqrt{1+(2\lambda_1-\lambda_2)^2}X_0\right) G_2(X_0)\,dX_0 \sin\left(\sqrt{1+(2\lambda_1-\lambda_2)^2}X_0\right)}{2\sqrt{1+(2\lambda_1-\lambda_2)^2}} \\
&- \frac{\int \sin\left(\sqrt{1+(2\lambda_1-\lambda_2)^2}X_0\right) G_2(X_0)\,dX_0 \cos\left(\sqrt{1+(2\lambda_1-\lambda_2)^2}X_0\right)}{2\sqrt{1+(2\lambda_1-\lambda_2)^2}} \qquad (4.A.23)\\
\psi_{12} &= z_4 \cosh\left(\sqrt{1-(2\lambda_1-\lambda_2)^2}X_0\right) - \frac{K_1^2 K_2}{4\sqrt{1-(2\lambda_1-\lambda_2)^2}} \times \\
&\Big[\int F_5(X_0)\,dX_0 e^{\sqrt{1-(2\lambda_1-\lambda_2)^2}X_0} - \int G_5(X_0)\,dX_0 e^{-\sqrt{1-(2\lambda_1+\lambda_2)^2}X_0}\Big], \qquad (4.A.24)\\
\psi_{13} &= z_1 e^{-\sqrt{1-9\lambda_1^2}(X_0-L-a)} - \frac{1}{48} e^{-3\sqrt{1-\lambda_1^2}(X_0-L-a)}, \qquad (4.A.25)\\
\psi_{14} &= z_2 \sin\left(\sqrt{1+9\lambda_1^2}\,(X_0-L-a)\right) + z_3 \cos\left(\sqrt{1+9{\lambda_1}^2}\,(X_0-L-a)\right) \\
&+ \frac{3\left(C_1^2+1\right)\left(C_1 \sin\left(\sqrt{1+\lambda_1^2}\,(X_0-L-a)\right) - \cos\left(\sqrt{1+\lambda_1^2}\,(X_0-L-a)\right)\right)}{192\,\lambda_1^2} \\
&+ \frac{\left(3C_1^2-1\right)\cos(3\sqrt{1+\lambda_1^2}\,(X_0-L-a))}{192} \\
&+ \frac{C_1\left(C_1^2-3\right)\sin(3\sqrt{1+\lambda_1^2}\,(X_0-L-a))}{192}, \qquad (4.A.26)\\
\psi_{16} &= z_1 e^{-\sqrt{1-9\lambda_2^2}(X_0-L-a)} - \frac{1}{48} e^{-3\sqrt{1-\lambda_2^2}(X_0-L-a)}, \qquad (4.A.27)\\
\psi_{17} &= z_2 \cos\left(\sqrt{1+9{\lambda_2}^2}\,(X_0-L-a)\right) + z_3 \sin\left(\sqrt{1+9{\lambda_2}^2}\,(X_0-L-a)\right) \\
&+ \frac{3\left(C_2^2+1\right)\left(C_2 \sin\left(\sqrt{1+\lambda_2^2}\,(X_0-L-a)\right) - \cos\left(\sqrt{1+\lambda_2^2}\,(X_0-L-a)\right)\right)}{192\,\lambda_2^2} \\
&+ \frac{\left(3\,{C_2}^2-1\right)\cos\left(3\sqrt{1+{\lambda_2}^2}\,(X_0-L-a)\right)}{192} \\
&+ \frac{C_2\left({C_2}^2-3\right)\sin\left(3\sqrt{1+{\lambda_2}^2}\,(X_0-L-a)\right)}{192}, \qquad (4.A.28)
\end{aligned}$$

$$
\begin{aligned}
\psi_{15} &= z_4 \cosh\left(\sqrt{1-9\,{\lambda_1}^2}X_0\right) - \frac{K_1^3 \cosh\left(\sqrt{1-9\,\lambda_1^2}X_0\right)}{384\,\lambda_1^2\sqrt{1-9\,\lambda_1^2}} \times \\
&\Big[3\left(\sqrt{1-9\,{\lambda_1}^2}+\sqrt{1-{\lambda_1}^2}\right)\cosh\left((\sqrt{1-9\,{\lambda_1}^2}-\sqrt{1-{\lambda_1}^2})X_0\right) \\
&+{\lambda_1}^2\left(\sqrt{1-9\,{\lambda_1}^2}+3\sqrt{1-{\lambda_1}^2}\right)\cosh\left((\sqrt{1-9\,{\lambda_1}^2}-3\sqrt{1-{\lambda_1}^2})X_0\right) \\
&+{\lambda_1}^2\left(\sqrt{1-9\,{\lambda_1}^2}-3\sqrt{1-{\lambda_1}^2}\right)\cosh\left((\sqrt{1-9\,{\lambda_1}^2}+3\sqrt{1-{\lambda_1}^2})X_0\right) \\
&+3\left(\sqrt{1-9\,{\lambda_1}^2}-\sqrt{1-{\lambda_1}^2}\right)\cosh\left(\left(\sqrt{1-9\,{\lambda_1}^2}+\sqrt{1-{\lambda_1}^2}\right)X_0\right)\Big] \\
&-\frac{K_1^3 \sinh\left(\sqrt{1-9\,\lambda_1^2}X_0\right)}{384\,\lambda_1^2\sqrt{1-9\,\lambda_1^2}} \times \\
&\Big[3\left(\sqrt{1-9\,{\lambda_1}^2}+\sqrt{1-{\lambda_1}^2}\right)\sinh\left(\left(\sqrt{1-9\,{\lambda_1}^2}-\sqrt{1-{\lambda_1}^2}\right)X_0\right) \\
&-{\lambda_1}^2\left(\sqrt{1-9\,{\lambda_1}^2}-3\sqrt{1-{\lambda_1}^2}\right)\sinh\left(\left(\sqrt{1-9\,{\lambda_1}^2}+3\sqrt{1-{\lambda_1}^2}\right)X_0\right) \\
&-3\left(\sqrt{1-9\,{\lambda_1}^2}-\sqrt{1-{\lambda_1}^2}\right)\sinh\left(\left(\sqrt{1-9\,{\lambda_1}^2}+\sqrt{1-{\lambda_1}^2}\right)X_0\right) \\
&-\lambda_1^2\left(\sqrt{1-9\lambda_1^2}+3\sqrt{1-\lambda_1^2}\right)\sinh\left((\sqrt{1-9\lambda_1^2}-3\sqrt{1-\lambda_1^2})X_0\right)\Big], \qquad (4.A.29)
\end{aligned}
$$

$$
\begin{aligned}
\psi_{18} &= z_4 \sinh\left(\sqrt{1-9\,{\lambda_2}^2}X_0\right) + \frac{K_2^3 \sinh\left(2\sqrt{1-9\,\lambda_2^2}X_0\right)}{384\,{\lambda_2}^2\sqrt{1-9\,\lambda_2^2}} \times \\
&\Big[3\left(\sqrt{1-9\,{\lambda_2}^2}+\sqrt{1-{\lambda_2}^2}\right)\cosh\left(\left(\sqrt{1-9\,{\lambda_2}^2}-\sqrt{1-\lambda_2^2}\right)X_0\right) \\
&-{\lambda_2}^2\left(\sqrt{1-9\,{\lambda_2}^2}+3\sqrt{1-{\lambda_2}^2}\right)\cosh\left(\left(\sqrt{1-9\,{\lambda_2}^2}-3\sqrt{1-{\lambda_2}^2}\right)X_0\right) \\
&+{\lambda_2}^2\left(\sqrt{1-9\,{\lambda_2}^2}-3\sqrt{1-{\lambda_2}^2}\right)\cosh\left(\left(\sqrt{1-9\,{\lambda_2}^2}+3\sqrt{1-{\lambda_2}^2}\right)X_0\right) \\
&-3\left(\sqrt{1-9\,{\lambda_2}^2}-\sqrt{1-{\lambda_2}^2}\right)\cosh\left(\left(\sqrt{1-9\,{\lambda_2}^2}+\sqrt{1-{\lambda_2}^2}\right)X_0\right)\Big] \\
&-\frac{K_2^3 \cosh\left(2\sqrt{1-9\,{\lambda_2}^2}X_0\right)}{384\,{\lambda_2}^2\sqrt{1-9\,\lambda_2^2}} \times \\
&\Big[3\left(\sqrt{1-9\,{\lambda_2}^2}+\sqrt{1-{\lambda_2}^2}\right)\sinh\left(\left(\sqrt{1-9\,{\lambda_2}^2}-\sqrt{1-{\lambda_2}^2}\right)X_0\right) \\
&+{\lambda_2}^2\left(\sqrt{1-9\,{\lambda_2}^2}-3\sqrt{1-{\lambda_2}^2}\right)\sinh\left(\left(\sqrt{1-9\,{\lambda_2}^2}+3\sqrt{1-{\lambda_2}^2}\right)X_0\right) \\
&-3\left(\sqrt{1-9\,{\lambda_2}^2}-\sqrt{1-{\lambda_2}^2}\right)\sinh\left(\left(\sqrt{1-9\,{\lambda_2}^2}+\sqrt{1-{\lambda_2}^2}\right)X_0\right) \\
&-\lambda_2^2\left(\sqrt{1-9\lambda_2^2}+3\sqrt{1-\lambda_2^2}\right)\sinh\left((\sqrt{1-9\lambda_2^2}-3\sqrt{1-\lambda_2^2})X_0\right)\Big], \qquad (4.A.30)
\end{aligned}
$$

$$\psi_{19} = z_1 \mathrm{e}^{-\sqrt{1-(\lambda_1+2\lambda_2)^2}(X_0-L-a)} - \frac{\left(1+\lambda_1\lambda_2-\sqrt{(1-\lambda_2^2)(1-\lambda_1^2)}\right)\mathrm{e}^{-\left(2\sqrt{1-\lambda_2^2}+\sqrt{1-\lambda_1^2}\right)(X_0-L-a)}}{8\ (\lambda_1+\lambda_2)^2}, \quad (4.A.31)$$

$$\psi_{20} = z_2 \cos\left(\sqrt{1+(\lambda_1+2\lambda_2)^2}\,(X_0-L-a)\right) + z_3 \sin\left(\sqrt{1+(\lambda_1+2\lambda_2)^2}\,(X_0-L-a)\right) + \frac{\int \cos\left(\sqrt{1+(\lambda_1+2\lambda_2)^2}X_0\right) F_2(X_0)\,dX_0 \sin\left(\sqrt{1+(\lambda_1+2\lambda_2)^2}X_0\right)}{2\sqrt{1+(\lambda_1+2\lambda_2)^2}} - \frac{\int \sin\left(\sqrt{1+(\lambda_1+2\lambda_2)^2}X_0\right) F_2 dX_0 \cos\left(\sqrt{1+(\lambda_1+2\lambda_2)^2}X_0\right)}{2\sqrt{1+(\lambda_1+2\lambda_2)^2}}, \quad (4.A.32)$$

$$\psi_{21} = z_4 \cosh\left(\sqrt{1-(\lambda_1+2\lambda_2)^2}X_0\right) - \frac{K_1K_2^2}{4\ (\lambda_1+2\lambda_2)^2} \times \left[\int F_3(X_0)\,dX_0 \mathrm{e}^{\sqrt{1-(\lambda_1+2\lambda_2)^2}X_0} - \int G_3(X_0)\,dX_0 \mathrm{e}^{-\sqrt{1-(\lambda_1+2\lambda_2)^2}X_0}\right], \quad (4.A.33)$$

$$\psi_{22} = z_1 \mathrm{e}^{-\sqrt{1-(\lambda_1-2\lambda_2)^2}(X_0-L-a)} + \frac{\left(\sqrt{1-\lambda_1^2}\sqrt{1-\lambda_2^2}-1+\lambda_1\lambda_2\right)\mathrm{e}^{-\left(\sqrt{1-\lambda_1^2}+2\sqrt{1-\lambda_2^2}\right)(X_0-L-a)}}{8\ (\lambda_1-\lambda_2)^2}, \quad (4.A.34)$$

$$\psi_{23} = z_2 \cos\left(\sqrt{1+(\lambda_1-2\lambda_2)^2}\,(X_0-L-a)\right) + z_3 \sin\left(\sqrt{1+(\lambda_1-2\lambda_2)^2}\,(X_0-L-a)\right) + \frac{\int \cos\left(\sqrt{1+(\lambda_1-2\lambda_2)^2}X_0\right) F_2(X_0)\,dX_0 \sin\left(\sqrt{1+(\lambda_1-2\lambda_2)^2}X_0\right)}{2\sqrt{1+(\lambda_1-2\lambda_2)^2}} - \frac{\int \sin\left(\sqrt{1+(\lambda_1-2\lambda_2)^2}X_0\right) F_2(X_0) dX_0 \cos\left(\sqrt{1+(\lambda_1-2\lambda_2)^2}X_0\right)}{2\sqrt{1+(\lambda_1-2\lambda_2)^2}}, \quad (4.A.35)$$

$$\psi_{24} = z_4 \cosh\left(\sqrt{1-(\lambda_1-2\lambda_2)^2}X_0\right) - \frac{K_1K_2^2}{4\ (\lambda_1-2\lambda_2)^2} \times \left[\int F_{41}(X_0)\,dX_0\,\mathrm{e}^{\sqrt{1-(\lambda_1-2\lambda_2)^2}X_0} - \int G_{41}(X_0)\,dX_0\,\mathrm{e}^{-\sqrt{1-(\lambda_1-2\lambda_2)^2}X_0}\right], \quad (4.A.36)$$

with

$$
\begin{aligned}
F_0(X_0) &= 2|B_1|^2\left(\cos(\sqrt{1+{\lambda_2}^2}\,(X_0-L-a))+C_2\sin(\sqrt{1+{\lambda_2}^2}\,(X_0-L-a))\right)\\
&\times\Big[(C_1^2-1)\cos^2(\sqrt{1+\lambda_1^2}\,(X_0-L-a))-C_1\sin(2\sqrt{1+\lambda_1^2}\,(X_0-L-a))-C_1^2\Big]\\
&\times\cos\left(\sqrt{1+{\lambda_2}^2}X_0\right)+|B_2|^2\Big(\left(3\,C_2^2-1\right)\cos^3\left(\sqrt{1+\lambda_2^2}\,(X_0-L-a)\right)\\
&+C_2\left(C_2^2-3\right)\sin\left(\sqrt{1+\lambda_2^2}\,(X_0-L-a)\right)\cos^2\left(\sqrt{1+{\lambda_2}^2}\,(X_0-L-a)\right)\\
&-3C_2^2\cos\left(\sqrt{1+\lambda_2^2}\,(X_0-L-a)\right)-C_2^3\sin\left(\sqrt{1+\lambda_2^2}+(X_0-L-a)\right)\Big)\\
&\times\cos\left(\sqrt{1+\lambda_2^2}X_0\right)+4\lambda_2\left(\alpha_3|B_2|^2+\alpha_4|B_1|^2\right)\Big(\cos(\sqrt{1+\lambda_2^2}\,(X_0-L-a))\\
&+C_2\sin(\sqrt{1+\lambda_2^2}\,(X_0-L-a))\Big)\cos\left(\sqrt{1+{\lambda_2}^2}X_0\right),\\
G_0(X_0) &= 2|B_1|^2\left(\cos(\sqrt{1+{\lambda_2}^2}\,(X_0-L-a))+C_2\sin(\sqrt{1+{\lambda_2}^2}\,(X_0-L-a))\right)\\
&\times\Big[(C_1^2-1)\cos^2(\sqrt{1+\lambda_1^2}\,(X_0-L-a))-C_1\sin(2\sqrt{1+\lambda_1^2}\,(X_0-L-a))-C_1^2\Big]\\
&\times\sin\left(\sqrt{1+{\lambda_2}^2}X_0\right)+|B_2|^2\Big(\left(3C_2^2-1\right)\cos^3\left(\sqrt{1+\lambda_2^2}\,(X_0-L-a)\right)\\
&+C_2\left(C_2^2-3\right)\sin\left(\sqrt{1+\lambda_2^2}\,(X_0-L-a)\right)\cos^2\left(\sqrt{1+{\lambda_2}^2}\,(X_0-L-a)\right)\\
&-3\,C_2^2\cos\left(\sqrt{1+\lambda_2^2}\,(X_0-L-a)\right)-C_2^3\sin\left(\sqrt{1+\lambda_2^2}+(X_0-L-a)\right)\Big)\\
&\times\sin\left(\sqrt{1+\lambda_2^2}X_0\right)+4\lambda_2\left(\alpha_3|B_2|^2+\alpha_4|B_1|^2\right)\Big(\cos\left(\sqrt{1+\lambda_2^2}\,(X_0-L-a)\right)\\
&+C_2\sin\left(\sqrt{1+\lambda_2^2}\,(X_0-L-a)\right)\Big)\sin\left(\sqrt{1+{\lambda_2}^2}X_0\right),\\
F_1(X_0) &= |B_1|^2\cos\left(\sqrt{1+\lambda_1^2}X_0\right)\Big[(3{C_1}^2-1)\cos^3\left(\sqrt{1+{\lambda_1}^2}\,(X_0-L-a)\right)\\
&+C_1(C_1^2-3)\sin\left(\sqrt{1+{\lambda_1}^2}\,(X_0-L-a)\right)\cos^2\left(\sqrt{1+{\lambda_1}^2}\,(X_0-L-a)\right)\\
&-3C_1^2\cos\left(\sqrt{1+{\lambda_1}^2}\,(X_0-L-a)\right)-C_1^3\sin\left(\sqrt{1+{\lambda_1}^2}\,(X_0-L-a)\right)\Big]\\
&-2|B_2|^2\cos\left(\sqrt{1+\lambda_1^2}X_0\right)\Big[\cos\left(\sqrt{1+{\lambda_1}^2}\,(X_0-L-a)\right)\\
&+C_1\sin\left(\sqrt{1+\lambda_1^2}(X_0-L-a)\right)\Big]\Big[(C_2^2-1)\cos^2\left(\sqrt{1+\lambda_2^2}(X_0-L-a)\right)\\
&-C_2\sin(2\sqrt{1+{\lambda_2}^2}\,(X_0-L-a))-C_2^2\Big]\\
&-4\lambda_1\left(\alpha_1|B_1|^2+\alpha_2B_2|^2\right)\cos\left(\sqrt{1+{\lambda_1}^2}X_0\right)\Big[\cos\left(\sqrt{1+{\lambda_1}^2}\,(X_0-L-a)\right)\\
&+C_1\sin\left(\sqrt{1+{\lambda_1}^2}\,(X_0-L-a)\right)\Big],
\end{aligned}
$$

$$
\begin{aligned}
G_1(X_0) &= -|B_1|^2 \sin\left(\sqrt{1+{\lambda_1}^2}X_0\right)\Big[\left(3{C_1}^2-1\right)\cos^3\left(\sqrt{1+{\lambda_1}^2}\,(X_0-L-a)\right)\\
&\quad +C_1({C_1}^2-3)\sin\left(\sqrt{1+{\lambda_1}^2}(X_0-L-a)\right)\cos^2\left(\sqrt{1+{\lambda_1}^2}(X_0-L-a)\right)\\
&\quad -\left(3\,{C_1}^2-4\,\lambda_1\alpha_1\right)\cos\left(\sqrt{1+{\lambda_1}^2}\,(X_0-L-a)\right)-C_1\left({C_1}^2-4\,\lambda_1\alpha_1\right)\\
&\quad \times\sin\left(\sqrt{1+{\lambda_1}^2}\,(X_0-L-a)\right)\Big]-2|B_2|^2\sin\left(\sqrt{1+{\lambda_1}^2}X_0\right)\\
&\quad \left(\cos(\sqrt{1+{\lambda_1}^2}\,(X_0-L-a))+C_1\sin(\sqrt{1+{\lambda_1}^2}\,(X_0-L-a))\right)\times\Big[\\
&\quad ({C_2}^2-1)\cos^2\left(\sqrt{1+\lambda_2^2}(X_0-L-a)\right)-2C_2\sin\left(\sqrt{1+\lambda_2^2}(X_0-L-a)\right)\\
&\quad \times\cos\left(\sqrt{1+{\lambda_2}^2}\,(X_0-L-a)\right)-{C_2}^2+2\,\lambda_1\alpha_2\Big],\\
A_1(X_0) &= \Big[\cos(\sqrt{1+{\lambda_1}^2}(X_0-L-a))+C_1\sin(\sqrt{1+{\lambda_1}^2}\,(X_0-L-a))\Big]^2\\
&\quad \times\Big[\cos(\sqrt{1+{\lambda_2}^2}\,(X_0-L-a))+C_2\sin(\sqrt{1+{\lambda_2}^2}\,(X_0-L-a))\Big]^2,\\
A_2(X_0) &= \cosh^2\left(\sqrt{1-\lambda_1^2}X_0\right)\sinh^2\left(\sqrt{1-\lambda_2^2}X_0\right),\\
F_2(X_0) &= \left[\cos\left(\sqrt{1+\lambda_1^2}\,(X_0-L-a)\right)+C_1\sin\left(\sqrt{1+\lambda_1^2}\,(X_0-L-a)\right)\right]\\
&\quad \times\left[\cos\left(\sqrt{1+\lambda_2^2}\,(X_0-L-a)\right)+C_2\sin\left(\sqrt{1+{\lambda_2}^2}\,(X_0-L-a)\right)\right]^2,\\
G_2(X_0) &= \left[\cos\left(\sqrt{1+\lambda_1^2}\,(X_0-L-a)\right)+C_1\sin\left(\sqrt{1+\lambda_1^2}\,(X_0-L-a)\right)\right]^2\\
&\quad \times\left[\cos\left(\sqrt{1+\lambda_2^2}\,(X_0-L-a)\right)+C_2\sin\left(\sqrt{1+\lambda_2^2}\,(X_0-L-a)\right)\right],\\
F_3(X_0) &= \mathrm{e}^{-\sqrt{1-(\lambda_1+2\lambda_2)^2}X_0}\cosh(\sqrt{1-\lambda_1^2}\,X_0)\sinh^2(\sqrt{1-\lambda_2^2}\,X_0),\\
G_3(X_0) &= \mathrm{e}^{\sqrt{1-(\lambda_1+2\lambda_2)^2}X_0}\cosh(\sqrt{1-\lambda_1^2}\,X_0)\sinh^2(\sqrt{1-\lambda_2^2}\,X_0),\\
F_4(X_0) &= \mathrm{e}^{-\sqrt{1-(\lambda_1-2\lambda_2)^2}X_0}\cosh(\sqrt{1-\lambda_1^2}\,X_0)\sinh^2(\sqrt{1-\lambda_2^2}\,X_0),\\
G_4(X_0) &= \mathrm{e}^{\sqrt{1-(\lambda_1-2\lambda_2)^2}X_0}\cosh(\sqrt{1-\lambda_1^2}\,X_0)\sinh^2(\sqrt{1-\lambda_2^2}\,X_0).\\
F_{41}(X_0) &= \cos\left(\sqrt{(2\,\lambda_1+\lambda_2)^2-1}\,X_0\right)\cosh^2(\sqrt{1-\lambda_1^2}\,X_0)\sinh(\sqrt{1-\lambda_2^2}\,X_0),\\
G_{41}(X_0) &= \sin\left(\sqrt{(2\,\lambda_1+\lambda_2)^2-1}\,X_0\right)\cosh^2(\sqrt{1-\lambda_1^2}\,X_0)\sinh(\sqrt{1-\lambda_2^2}\,X_0),\\
F_5(X_0) &= \mathrm{e}^{-\sqrt{1-(2\,\lambda_1-\lambda_2)^2}\,X_0}\cosh^2(\sqrt{1-\lambda_1^2}\,X_0)\sinh(\sqrt{1-\lambda_2^2}\,X_0),\\
G_5(X_0) &= \mathrm{e}^{\sqrt{1-(2\,\lambda_1-\lambda_2)^2}\,X_0}\cosh^2(\sqrt{1-\lambda_1^2}\,X_0)\sinh(\sqrt{1-\lambda_2^2}\,X_0).
\end{aligned}
$$

4.A.2 Functions in Section 4.3

$$
\begin{aligned}
L_1 \;=\;& 2i\lambda_1 D_4 B_1 \Phi_1 - \left(\alpha_1 |B_1|^2 + \alpha_2 |B_2|^2\right)\left(\alpha_1 B_1 |B_1|^2 + \alpha_2 B_1 |B_2|^2 + \mu_1 H\right)\Phi_1 \\
& -2\lambda_1\left(\alpha_1 B_1 |B_1|^2 + \alpha_2 B_1 |B_2|^2 + \mu_1 H\right)\Psi_1 + \frac{1}{12} B_1 |B_1|^4 \Phi_1^5 + \frac{1}{2} B_1 |B_1|^2 |B_2|^2 \Phi_1^3 \Phi_2^2 \\
& + \frac{1}{4} B_1 |B_2|^4 \Phi_1 \Phi_2^4 - \frac{3}{2} B_1 |B_1|^2 \Phi_1^2 \Psi_1 - |B_2|^2 B_1 \Phi_2^2 \Psi_1 - |B_1|^2 H \Phi_1^2 \Psi_2 - |B_2|^2 H \Phi_2^2 \Psi_2 \\
& - \frac{1}{2} B_1{}^2 H \Phi_1{}^2 \Psi_2 - 2\, B_1 \left|B_2\right|^2 \Phi_1 \Phi_2 \psi_4 - \frac{1}{2} B_1 \left|B_1\right|^4 \Phi_1{}^2 \psi_{13} - \frac{1}{2} B_1 \left|B_2\right|^4 \Phi_2^2 \psi_{22} \\
& - \frac{1}{2} B_1 \left|B_2\right|^4 \Phi_2{}^2 \psi_{19} - B_1 \left|B_1\right|^2 \left|B_2\right|^2 \Phi_1 \Phi_2 \psi_7 - B_1 \left|B_1\right|^2 \left|B_2\right|^2 \Phi_1 \Phi_2 \psi_{10}, \qquad \text{(4.A.37)}
\end{aligned}
$$

$$
\begin{aligned}
L_2 \;=\;& 2i\lambda_1 D_4 B_1 \Phi_1 - \left(\alpha_1 |B_1|^2 + \alpha_2 |B_2|^2\right)\left(\alpha_1 B_1 |B_1|^2 + \alpha_2 B_1 |B_2|^2 + \mu_1 H\right)\Phi_1 \\
& -2\lambda_1\left(\alpha_1 B_1 |B_1|^2 + \alpha_2 B_1 |B_2|^2 + \mu_1 H\right)\Psi_3 - \frac{1}{12} B_1 |B_1|^4 \Phi_1^5 - \frac{1}{2} B_1 |B_1|^2 |B_2|^2 \Phi_1^3 \Phi_2^2 \\
& - \frac{1}{4} B_1 |B_2|^4 \Phi_1 \Phi_2^4 + \frac{3}{2} B_1 |B_1|^2 \Phi_1^2 \Psi_3 + |B_2|^2 B_1 \Phi_2^2 \Psi_3 + |B_1|^2 H \Phi_1^2 \Psi_4 + |B_2|^2 H \Phi_2^2 \Psi_4 \\
& + \frac{1}{2} B_1{}^2 H \Phi_1{}^2 \Psi_4 + 2\, B_1 \left|B_2\right|^2 \Phi_1 \Phi_2 \psi_5 + \frac{1}{2} B_1 \left|B_1\right|^4 \Phi_1{}^2 \psi_{14} + \frac{1}{2} B_1 \left|B_2\right|^4 \Phi_2{}^2 \psi_{23} \\
& + \frac{1}{2} B_1 \left|B_2\right|^4 \Phi_2{}^2 \psi_{20} + B_1 \left|B_1\right|^2 \left|B_2\right|^2 \Phi_1 \Phi_2 \psi_8 + B_1 \left|B_1\right|^2 \left|B_2\right|^2 \Phi_1 \Phi_2 \psi_{11}, \qquad \text{(4.A.38)}
\end{aligned}
$$

$$
\begin{aligned}
L_3 \;=\;& 2i\lambda_1 D_4 B_1 \Phi_1 - \left(\alpha_1 |B_1|^2 + \alpha_2 |B_2|^2\right)\left(\alpha_1 B_1 |B_1|^2 + \alpha_2 B_1 |B_2|^2 + \mu_1 H\right)\Phi_1 \\
& -2\lambda_1\left(\alpha_1 B_1 |B_1|^2 + \alpha_2 B_1 |B_2|^2 + \mu_1 H\right)\Psi_5 + \frac{1}{12} B_1 |B_1|^4 \Phi_1^5 + \frac{1}{2} B_1 |B_1|^2 |B_2|^2 \Phi_1^3 \Phi_2^2 \\
& + \frac{1}{4} B_1 |B_2|^4 \Phi_1 \Phi_2^4 - \frac{3}{2} B_1 |B_1|^2 \Phi_1^2 \Psi_5 - |B_2|^2 B_1 \Phi_2^2 \Psi_5 - |B_1|^2 H \Phi_1^2 \Psi_6 - |B_2|^2 H \Phi_2^2 \Psi_6 \\
& - \frac{1}{2} B_1{}^2 H \Phi_1{}^2 \Psi_6 - 2\, B_1 \left|B_2\right|^2 \Phi_1 \Phi_2 \psi_6 - \frac{1}{2} B_1 \left|B_1\right|^4 \Phi_1{}^2 \psi_{15} - \frac{1}{2} B_1 \left|B_2\right|^4 \Phi_2{}^2 \psi_{24} \\
& - \frac{1}{2} B_1 \left|B_2\right|^4 \Phi_2{}^2 \psi_{21} - B_1 \left|B_1\right|^2 \left|B_2\right|^2 \Phi_1 \Phi_2 \psi_9 - B_1 \left|B_1\right|^2 \left|B_2\right|^2 \Phi_1 \Phi_2 \psi_{12}, \qquad \text{(4.A.39)}
\end{aligned}
$$

$$
\begin{aligned}
M_1 \;=\;& 2i\lambda_2 D_4 B_2 \Phi_2 - B_2 \left(\alpha_3 \left|B_2\right|^2 + \alpha_4 \left|B_1\right|^2\right)^2 \Phi_2 - 2\lambda_2 B_2 \left(\alpha_3 \left|B_2\right|^2 + \alpha_4 \left|B_1\right|^2\right)\psi_4 \\
& + \frac{1}{12} B_2 |B_2|^4 \Phi_2^5 + \frac{1}{2} B_2 |B_1|^2 |B_2|^2 \Phi_1^2 \Phi_2^3 + \frac{1}{4} B_2 |B_1|^4 \Phi_1^4 \Phi_2 \\
& - 2\, B_2 \left|B_1\right|^2 \Phi_1 \Phi_2 \Psi_1 - B_1 B_2 H \Phi_1 \Phi_2 \Psi_2 - B_2 \overline{B_1} \Phi_1 \Phi_2 H \Psi_2 - \frac{3}{2} B_2 \left|B_2\right|^2 \Phi_2{}^2 \psi_4 \\
& - \frac{1}{2} B_2 \left|B_2\right|^4 \Phi_2{}^2 \psi_{16} - \frac{1}{2} B_2 \left|B_1\right|^4 \Phi_1{}^2 \psi_{10} - \frac{1}{2} B_2 \left|B_1\right|^4 \Phi_1{}^2 \psi_7 - B_2 \left|B_1\right|^2 \Phi_1{}^2 \psi_4 \\
& - B_2 \left|B_1\right|^2 \left|B_2\right|^2 \Phi_1 \Phi_2 \psi_{19} - B_2 \left|B_1\right|^2 \left|B_2\right|^2 \Phi_1 \Phi_2 \psi_{22}, \qquad \text{(4.A.40)}
\end{aligned}
$$

$$
\begin{aligned}
M_2 &= 2\,i\lambda_2 D_4 B_2\Phi_2 - B_2\left(\alpha_3\left|B_2\right|^2+\alpha_4\left|B_1\right|^2\right)^2\Phi_2 - 2\lambda_2 B_2\left(\alpha_3\left|B_2\right|^2+\alpha_4\left|B_1\right|^2\right)\psi_5 \\
&\quad -\frac{1}{12}B_2|B_2|^4\Phi_2^5 - \frac{1}{2}B_2|B_1|^2|B_2|^2\Phi_1^2\Phi_2^3 - \frac{1}{4}B_2|B_1|^4\Phi_1^4\Phi_2 \\
&\quad +2\,B_2\left|B_1\right|^2\Phi_1\Phi_2\Psi_3 + B_1B_2H\Phi_1\Phi_2\Psi_4 + B_2\overline{B_1}\Phi_1\Phi_2H\Psi_4 + \frac{3}{2}B_2\left|B_2\right|^2{\Phi_2}^2\psi_5 \\
&\quad +\frac{1}{2}B_2\left|B_2\right|^4{\Phi_2}^2\psi_{17} + \frac{1}{2}B_2\left|B_1\right|^4{\Phi_1}^2\psi_{11} + \frac{1}{2}B_2\left|B_1\right|^4{\Phi_1}^2\psi_8 + B_2\left|B_1\right|^2{\Phi_1}^2\psi_5 \\
&\quad +B_2\left|B_1\right|^2\left|B_2\right|^2\Phi_1\Phi_2\psi_{20} + B_2\left|B_1\right|^2\left|B_2\right|^2\Phi_1\Phi_2\psi_{23}, \qquad (4.A.41)
\end{aligned}
$$

$$
\begin{aligned}
M_3 &= 2\,i\lambda_2 D_4 B_2\Phi_2 - B_2\left(\alpha_3\left|B_2\right|^2+\alpha_4\left|B_1\right|^2\right)^2\Phi_2 - 2\lambda_2 B_2\left(\alpha_3\left|B_2\right|^2+\alpha_4\left|B_1\right|^2\right)\psi_6 \\
&\quad +\frac{1}{12}B_2|B_2|^4\Phi_2^5 + \frac{1}{2}B_2|B_1|^2|B_2|^2\Phi_1^2\Phi_2^3 + \frac{1}{4}B_2|B_1|^4\Phi_1^4\Phi_2 \\
&\quad -2\,B_2\left|B_1\right|^2\Phi_1\Phi_2\Psi_5 - B_1B_2H\Phi_1\Phi_2\Psi_6 - B_2\overline{B_1}\Phi_1\Phi_2H\Psi_6 - \frac{3}{2}B_2\left|B_2\right|^2{\Phi_2}^2\psi_6 \\
&\quad -\frac{1}{2}B_2\left|B_2\right|^4{\Phi_2}^2\psi_{18} - \frac{1}{2}B_2\left|B_1\right|^4{\Phi_1}^2\psi_{12} - \frac{1}{2}B_2\left|B_1\right|^4{\Phi_1}^2\psi_9 - B_2\left|B_1\right|^2{\Phi_1}^2\psi_6 \\
&\quad -B_2\left|B_1\right|^2\left|B_2\right|^2\Phi_1\Phi_2\psi_{21} - B_2\left|B_1\right|^2\left|B_2\right|^2\Phi_1\Phi_2\psi_{24}. \qquad (4.A.42)
\end{aligned}
$$

$$
\begin{aligned}
\Psi_1 &= |B_1|^2\Big[\frac{\lambda_1\alpha_1\left(-2\,X_0{\lambda_2}^2+\sqrt{1-{\lambda_2}^2}+2\,X_0\right)\mathrm{e}^{\sqrt{1-{\lambda_1}^2}(L+a-X_0)}}{2\sqrt{1-{\lambda_1}^2}\sqrt{1-{\lambda_2}^2}\left(\sqrt{1-{\lambda_1}^2}+\sqrt{1-{\lambda_2}^2}\right)} \\
&\quad -\frac{\mathrm{e}^{3\sqrt{1-{\lambda_1}^2}(L+a-X_0)}}{16(1-{\lambda_1}^2)} - \frac{\lambda_1\alpha_1\left(2\,X_0{\lambda_1}^2-2\,X_0-\sqrt{1-{\lambda_2}^2}\right)\mathrm{e}^{\sqrt{1-{\lambda_1}^2}(L+a-X_0)}}{2\left(1-{\lambda_1}^2\right)\left(\sqrt{1-{\lambda_1}^2}+\sqrt{1-{\lambda_2}^2}\right)}\Big] \\
&\quad +|B_2|^2\Big[\frac{\lambda_1\alpha_2\left(-2\,X_0{\lambda_2}^2+\sqrt{1-{\lambda_2}^2}+2\,X_0\right)\mathrm{e}^{\sqrt{1-{\lambda_1}^2}(L+a-X_0)}}{2\sqrt{1-{\lambda_1}^2}\sqrt{1-{\lambda_2}^2}\left(\sqrt{1-{\lambda_1}^2}+\sqrt{1-{\lambda_2}^2}\right)} \\
&\quad -\frac{\lambda_1\alpha_2\left(2\,X_0{\lambda_1}^2-2\,X_0-\sqrt{1-{\lambda_2}^2}\right)\mathrm{e}^{\sqrt{1-{\lambda_1}^2}(L+a-X_0)}}{2\left(1-{\lambda_1}^2\right)\left(\sqrt{1-{\lambda_1}^2}+\sqrt{1-{\lambda_2}^2}\right)} \\
&\quad -\frac{\mathrm{e}^{\left(\sqrt{1-{\lambda_1}^2}+2\sqrt{1-{\lambda_2}^2}\right)(L-X_0+a)}}{4(\sqrt{1-{\lambda_2}^2}\sqrt{1-{\lambda_1}^2}+1-{\lambda_2}^2)}\Big], \qquad (4.A.43)
\end{aligned}
$$

$$
\begin{aligned}
\Psi_2 &= \frac{\lambda_1\mu_1\left(\left(x{\lambda_1}^2-x\right)\sqrt{1-{\lambda_2}^2}-\frac{1}{2}+\frac{1}{2}{\lambda_2}^2\right)\mathrm{e}^{\sqrt{1-{\lambda_1}^2}(-x+a+L)}}{\left(1-{\lambda_1}^2\right)\left(-\sqrt{1-{\lambda_2}^2}\sqrt{1-{\lambda_1}^2}-1+{\lambda_2}^2\right)} \\
&\quad +\frac{\mu_1\lambda_1\left(x{\lambda_2}^2-1/2\sqrt{1-{\lambda_2}^2}-x\right)\mathrm{e}^{\sqrt{1-{\lambda_1}^2}(-x+a+L)}}{\sqrt{1-{\lambda_1}^2}\left(-\sqrt{1-{\lambda_2}^2}\sqrt{1-{\lambda_1}^2}-1+{\lambda_2}^2\right)} - \frac{1}{2(1-\lambda_1^2)}, \qquad (4.A.44)
\end{aligned}
$$

$$
\begin{aligned}
\Psi_3 &= \frac{\int F_6(X_0)\cos\left(\sqrt{1+\lambda_1^2}X_0\right)dX_0\sin\left(\sqrt{1+\lambda_1^2}X_0\right)}{\sqrt{1+\lambda_1^2}} \\
&\quad -\frac{\int F_6(X_0)\sin\left(\sqrt{1+\lambda_1^2}X_0\right)dX_0\cos\left(\sqrt{1+\lambda_1^2}X_0\right)}{\sqrt{1+\lambda_1^2}}, \qquad (4.A.45)
\end{aligned}
$$

$$\Psi_4 = \frac{\int G_6(X_0)\cos\left(\sqrt{1+\lambda_1^2}X_0\right)dX_0 \sin\left(\sqrt{1+\lambda_1^2}X_0\right)}{\sqrt{1+\lambda_1^2}} - \frac{\int G_6(X_0)\sin\left(\sqrt{1+\lambda_1^2}X_0\right)dX_0 \cos\left(\sqrt{1+\lambda_1^2}X_0\right)}{\sqrt{1+\lambda_1^2}}, \quad (4.A.46)$$

$$\Psi_5 = \frac{\int \mathrm{e}^{-\sqrt{1-\lambda_1^2}X_0}F_7(X_0)d\,X_0\mathrm{e}^{\sqrt{1-\lambda_1^2}X_0}}{4\sqrt{1-\lambda_1^2}} \frac{\int \mathrm{e}^{\sqrt{1-\lambda_1^2}X_0}F_7(X_0)dX_0\mathrm{e}^{-\sqrt{1-\lambda_1^2}X_0}}{4\sqrt{1-\lambda_1^2}}, \quad (4.A.47)$$

$$\Psi_6 = \frac{\int \mathrm{e}^{-\sqrt{1-\lambda_1^2}X_0}G_7(X_0)dX_0\mathrm{e}^{\sqrt{1-\lambda_1^2}X_0}}{4\sqrt{1-\lambda_1^2}} - \frac{\int \mathrm{e}^{\sqrt{1-\lambda_1^2}X_0}G_7(X_0)dX_0\mathrm{e}^{-\sqrt{1-\lambda_1^2}X_0}}{4\sqrt{1-\lambda_1^2}}, \quad (4.A.48)$$

$$\begin{aligned}
F_6(X_0) &= 8|B_1|^2\left(1-3C_1^2\right)\cos^3\left(\sqrt{1+{\lambda_1}^2}\left(X_0-L-a\right)\right) \\
&\quad -\frac{1}{2}|B_1|^2C_1\left(C_1^2-3\right)\sin\left(\sqrt{1+\lambda_1^2}\left(X_0-L-a\right)\right)\cos^2\left(\sqrt{1+\lambda_1^2}\left(X_0-L-a\right)\right) \\
&\quad +\frac{1}{2}|B_1|^2C_1^2\left(3\cos\left(\sqrt{1+\lambda_1^2}\left(X_0-L-a\right)\right)+C_1\sin\left(\sqrt{1+\lambda_1^2}\left(X_0-L-a\right)\right)\right) \\
&\quad -\Big[|B_2|^2\left(C_2^2-1\right)\cos^2\left(\sqrt{1+\lambda_2^2}\left(X_0-L-a\right)\right) \\
&\quad -C_2|B_2|^2\sin\left(2\sqrt{1+\lambda_2^2}\left(X_0-L-a\right)\right)-|B_2|^2C_2^2+2\lambda_1\left(\alpha_1|B_1|^2+\alpha_2|B_2|^2\right)\Big] \\
&\quad \times\left[\cos\left(\sqrt{1+\lambda_1^2}\left(X_0-L-a\right)\right)+C_1\sin\left(\sqrt{1+\lambda_1^2}\left(X_0-L-a\right)\right)\right], \\
G_6(X_0) &= \frac{1}{2}-\lambda_1\mu_1\left[2\cos\left(\sqrt{1+\lambda_1^2}\left(X_0-L-a\right)\right)+C_1\sin\left(\sqrt{1+\lambda_1^2}\left(X_0-L-a\right)\right)\right], \\
F_7(X_0) &= 2K_1\left(|B_2|^2K_2^2-2\lambda_1\left(\alpha_1|B_1|^2+\alpha_2|B_2|^2\right)\right)\cosh\left(\sqrt{1-{\lambda_1}^2}X_0\right) \\
&\quad -2|B_2|^2K_1\cosh\left(\sqrt{1-{\lambda_1}^2}X_0\right)K_2^2\cosh^2\left(\sqrt{1-\lambda_2^2}X_0\right) \\
&\quad -|B_1|^2K_1^3\cosh^3\left(\sqrt{1-\lambda_1^2}X_0\right), \\
G_7(X_0) &= 1-4\,\lambda_1\mu_3K_1\cosh\left(\sqrt{1-{\lambda_1}^2}X_0\right).
\end{aligned}$$

CHAPTER 5

Wave radiation in stacked long Josephson junctions with phase-shifts

5.1 Introduction

Over recent decades of systematic investigation into static and dynamic properties of single Josephson junctions, there have been many theoretical, numerical and experimental studies on the dynamics of stacked long Josephson junctions [157, 158, 159, 160]. Stacked Josephson junctions can provide larger power output from a smaller width than a single Josephson junction [161]. In a stacked system, one junction is placed directly above another with a separating layer that is thin compared to the London penetration depth.

The coupled Josephson junctions lead to nontrivial dynamic effects like current locking and Cherenkov radiation by Josephson fluxons in low-T_c (e.g. $Nb/AlO_x/Nb$) as well as in high-T_c (e.g. $Bi_2Sr_2CaCu_2O_8$) stacked junctions [142, 162]. Multi-stack Josephson junctions are being seriously considered to multiply the physical effect of one layer. The Josephson voltage standard, the Josephson computer, and the microwave generators based on many junctions are a few examples of coupled Josephson junctions. The coupling of two junctions is symmetric in the sense that each junction has one outermost electrode and one electrode shared with the second junction, however this symmetry is broken in larger stack [163].

The fluxon dynamics in coupled long Josephson junctions have been studied over the last few decades. Fluxons are nonlinear electromagnetic excitations, which can be perturbed by many external factors [155]. One possible application for the long Josephson

junction stack is generation of radiation in the hundreds of GHz range. The single flux flow oscillators are known as radiation sources [164, 165], which are based on the unidirectional viscous flow of Josephson vortices along the junction [166, 167]. The fluxons can be made to shuttle back and forth in the stack and radiate when near the edges of the stack [168]. The fluxon dynamics in the inductively stacked long Josephson junction were first considered theoretically by Mineev et al. [169].

Recently, great attention has been given to coupled long Josephson junction systems described by coupled sine-Gordon equations [89, 158, 170]. The coupled sine-Gordon equation describes complex behaviour of interchanging systems, such as atoms in periodic potential [171] magnetic multilayers [172] and stacked Josephson junctions [170, 173, 174].

The coupling of the junctions is the basis for many applications, such as voltage standards and high frequency oscillators. The coupled sine-Gordon equation has been used to model the phase locking of fluxons in systems of two parallel long Josephson junctions. The stack Josephson junctions when interact with each other displaying many characteristics, such as voltage locking [175, 176] and current locking [177, 178, 179]. When the junctions are closely spaced under the appropriate bias conditions the critical currents of the junctions are pulled together. This effect is called current locking, which was proposed by Jillie et al. [177]. The study of voltage locked junctions can help us understand the internal dynamics of the junction. Other explanation such as inductive interaction between two junctions [178] and modulation of critical current of one junction by radiation from the other junction [179] have been given for current locking [180].

Sakai *et* al. [170] derived a coupled sine-Gordon equation for arbitrary strong coupling between junctions. The perturbation approach for small coupling has been investigated in [181, 182].

Here we introduce the dynamics of two stacked long Josephson junctions with phase-shifts, governed by the coupled sine-Gordon equation

$$\phi^1_{xx} - \phi^1_{tt} = \sin\left(\phi^1 + \theta(x)\right) + S\,\phi^2_{xx} + h\cos(\Omega t), \tag{5.1.1}$$

$$\phi^2_{xx} - \phi^2_{tt} = \sin\left(\phi^2 + \theta(x)\right) + S\,\phi^1_{xx} + h\cos(\Omega t), \tag{5.1.2}$$

for the one-dimensional phase difference $\phi(x,t)$ between the order parameters of superconductors layers of the junctions, driven by a microwave field $h\cos(\Omega t)$, $x \in \mathbb{R}$ and $t > 0$. The strength of magnetic induction coupling between two long Josephson

junctions is denoted by S. The phase-shift considered is

$$\theta(x) = \begin{cases} 0, & x < -a, \\ \pi, & |x| \leq a, \\ 0, & x > a, \end{cases} \tag{5.1.3}$$

with the boundary conditions

$$\phi(\pm a^-) = \phi(\pm a^+), \qquad \phi_x(\pm a^-) = \phi_x(\pm a^+). \tag{5.1.4}$$

Using a multiple scales expansion we show that in the absence of the external drive and with different magnetic inductance the system in the stacked Josephson junction has a bounded time periodic solution. We also show that the periodic solutions of coupled sine-Gordon equations, decay in time with the same rate.

The organization of this chapter is as follows. In Sections 5.2 and 5.3, we construct the analytical approximation of two stacked long Josephson junction as coupled sine-Gordon equations with different magnetic inductances. In Section 5.4, the method of multiple scales is applied to obtain the amplitude of oscillations in the presence of driving.

5.2 Coupled long Josephson junctions for $S \sim \mathcal{O}(\epsilon^2)$

In this section, we construct the dynamics of two stacked long Josephson junction governed by coupled sine-Gordon Equations (5.1.1)–(5.1.2) with no driving, that is, $h = 0$, $\theta(x)$ given by (5.1.3), which represents the phase shift for coupled $0 - \pi - 0$ sine-Gordon equations. To describe the dynamics of the breathing modes of stacked long Josephson junctions, we first consider the case of weak coupling where, $S = \epsilon^2$, and derive an asymptotic expansion by writing

$$\phi^1 = \phi_0^1 + \epsilon\,\phi_1^1 + \epsilon^2\phi_2^1 + \epsilon^3\phi_3^1 + \ldots, \tag{5.2.1}$$

$$\phi^2 = \phi_0^2 + \epsilon\,\phi_1^2 + \epsilon^2\phi_2^2 + \epsilon^3\phi_3^3 + \ldots. \tag{5.2.2}$$

We use multiple scale expansions by introducing the slow time and space variables [101]

$$X_n = \epsilon^n x, \quad T_n = \epsilon^n t, \quad n = 0, 1, 2, \ldots, \tag{5.2.3}$$

for simplicity we also use the notation

$$\partial_n = \frac{\partial}{\partial X_n}, \quad D_n = \frac{\partial}{\partial T_n}. \tag{5.2.4}$$

Putting relations (5.2.1)–(5.2.2) in (5.1.1)–(5.1.2) and using multiscale expansions as noted above, we obtain a hierarchy of equations.

5.2.1 Equations at $\mathcal{O}(1)$

At leading order the $\mathcal{O}(1)$-equations give

$$\partial_0^2\phi_0^1 - D_0^2\phi_0^1 = \sin\left(\phi_0^1+\theta\right), \tag{5.2.5}$$
$$\partial_0^2\phi_0^2 - D_0^2\phi_0^2 = \sin\left(\phi_0^2+\theta\right). \tag{5.2.6}$$

We consider a stable solution representing a uniform background solution

$$\phi_0^1 = \phi_0^2 = 0. \tag{5.2.7}$$

5.2.2 Equations at $\mathcal{O}(\epsilon)$

The terms at $\mathcal{O}(\epsilon)$ give

$$\partial_0^2\phi_1^1 - D_0^2\phi_1^1 = \cos(\theta+\phi_0^1)\phi_1^1, \tag{5.2.8}$$
$$\partial_0^2\phi_1^2 - D_0^2\phi_1^2 = \cos(\theta+\phi_0^2)\phi_1^2. \tag{5.2.9}$$

By using the spectral ansatz

$$\phi_1^{(1,2)}(X_0,T_0) = \mu(X_0)\mathrm{e}^{i\omega T_0} + c.c., \tag{5.2.10}$$

together with the boundary conditions (5.1.4), we obtain the ground state for a breathing mode for stacked long Josephson junctions

$$\phi_1^1(X_0,T_0) = B_1 e^{i\omega T_0}\begin{cases}\cos(a\sqrt{1+\omega^2})e^{\sqrt{1-\omega^2}(a+X_0)}+c.c., & X_0<-a,\\ \cos(X_0\sqrt{1+\omega^2})+c.c., & |X_0|<a,\\ \cos(a\sqrt{1+\omega^2})e^{\sqrt{1-\omega^2}(a-X_0)}+c.c., & X_0>a,\end{cases} \tag{5.2.11}$$

$$\phi_1^2(X_0,T_0) = B_2 e^{i\omega T_0}\begin{cases}\cos(a\sqrt{1+\omega^2})e^{\sqrt{1-\omega^2}(a+X_0)}+c.c., & X_0<-a,\\ \cos(X_0\sqrt{1+\omega^2})+c.c., & |X_0|<a,\\ \cos(a\sqrt{1+\omega^2})e^{\sqrt{1-\omega^2}(a-X_0)}+c.c., & X_0>a,\end{cases} \tag{5.2.12}$$

where $B_i = B_i\,(T_1,T_2,..)$ for $i=1,2$, are the amplitudes of oscillation, and depend on the slow time scales. Throughout the chapter *c.c.* stands for the complex conjugate of the immediately preceding terms. The oscillation frequency of the system, ω, is given by the implicit relation

$$a = \sqrt{\frac{1}{1+\omega^2}}\tan^{-1}\left(\sqrt{\frac{1-\omega^2}{1+\omega^2}}\right), \quad \omega^2<1, \tag{5.2.13}$$

where a is the facet length of the junction, which has a unique solution for each $0\leqslant a\leqslant \pi/4$. As $a\to 0^+$, $\omega\to 1^{-1}$, and as $a\to\pi/4$, $\omega\to 0$.

5.2.3 Equations at $\mathcal{O}(\epsilon^2)$

Equating terms in (5.1.1)–(5.1.2) at $\mathcal{O}(\epsilon^2)$ we obtain

$$\partial_0^2\phi_2^1 - D_0^2\phi_2^1 - \cos(\theta + \phi_0^1)\phi_2^1 = 2D_0D_1\phi_1^1 - 2\partial_0\partial_1\phi_1^1 + \partial_0^2\phi_0^2, \tag{5.2.14}$$

$$\partial_0^2\phi_2^2 - D_0^2\phi_2^2 - \cos(\theta + \phi_0^2)\phi_2^2 = 2D_0D_1\phi_1^2 - 2\partial_0\partial_1\phi_1^2 + \partial_0^2\phi_0^1. \tag{5.2.15}$$

To find a bounded solution for ϕ_2^1, ϕ_2^2, Equations (5.2.14)–(5.2.15) generate constraints on the right hand sides that are solvability conditions which lead to an important equation for the amplitudes B_1, B_2 as well as to equations at higher order when the expansion is continued further [155, 156].

We write Equations (5.2.14)–(5.2.15) in the form

$$\mathcal{L}\psi(x) = f(x), \tag{5.2.16}$$

where $\mathcal{L}$ is a linear self-adjoint operator ($\mathcal{L} = \mathcal{L}^\dagger$) given by the left hand side of the above system, and $\zeta : \mathbb{T} \to \mathbb{R}$ is a smooth periodic function. Let $L^2(\mathbb{R})$ be the Hilbert space with complex inner product

$$\langle g, h\rangle = \int_{-\infty}^{\infty} \overline{g}(\xi)h(\xi)d\xi. \tag{5.2.17}$$

Here $\overline{g}(\xi)$ is the complex conjugate of $g(\xi)$. The Fredholm theorem states that the necessary and sufficient condition for the inhomogeneous equation $\mathcal{L}\psi = f(x)$ to have a bounded solution is that $f(x)$ be orthogonal to the null-space of the operator $\mathcal{L}$. Hence, the solvability condition provided by the Fredholm theorem is

$$\int_{-\infty}^{\infty} \mathcal{L}f(x)\,dx = 0. \tag{5.2.18}$$

Calculating the right hand sides of (5.2.14)-(5.2.15) by using the known functions ϕ_0^1, ϕ_0^2, ϕ_1^1, ϕ_1^2 and using the Fredholm theorem, the solvability conditions for Equations (5.2.14)–(5.2.15) are

$$D_1B_1 = 0, \quad D_1B_2 = 0. \tag{5.2.19}$$

The B_j are independent of T_1 and are only functions of $T_2, T_3, \ldots$. By using the solvability conditions (5.2.19), we see that the Equations (5.2.14)–(5.2.15) becomes the same as $\mathcal{O}(\epsilon)$. For the uniformity in the perturbation expansion, we conclude that

$$\phi_2^1 = \phi_2^2 = 0. \tag{5.2.20}$$

5.2.4 Equations at $\mathcal{O}(\epsilon^3)$

The terms at $\mathcal{O}(\epsilon^3)$ give

$$\begin{aligned}\partial_0^2\phi_3^1 - D_0^2\phi_3^1 - \cos(\theta+\phi_0^1)\phi_3^1 &= 2(D_0D_2 - \partial_0\partial_2)\phi_1^1 + (D_1^2 - \partial_1^2)\phi_1^1 \\ &\quad -\frac{1}{6}{\phi_1^1}^3\cos(\theta) + \partial_0^2\phi_1^2, \qquad (5.2.21)\\ \partial_0^2\phi_3^2 - D_0^2\phi_3^2 - \cos(\theta+\phi_0^2)\phi_3^2 &= 2(D_0D_2 - \partial_0\partial_2)\phi_1^2 + (D_1^2 - \partial_1^2)\phi_1^2 \\ &\quad -\frac{1}{6}{\phi_1^2}^3\cos(\theta) + \partial_0^2\phi_1^1. \qquad (5.2.22)\end{aligned}$$

Having evaluated the right hand side using the functions ϕ_1^1 and ϕ_1^2 and splitting the solutions into components proportional to simple harmonics, we obtain

$$\partial_0^2\phi_3^1 - D_0^2\phi_3^1 - \cos(\theta)\phi_3^1 = \begin{cases} F_1, & X_0 < -a, \\ F_2, & |X_0| < a, \\ F_3, & X_0 > a, \end{cases} \qquad (5.2.23)$$

$$\partial_0^2\phi_3^2 - D_0^2\phi_3^2 - \cos(\theta)\phi_3^2 = \begin{cases} G_1, & X_0 < -a, \\ G_2, & |X_0| < a, \\ G_3, & X_0 > a, \end{cases} \qquad (5.2.24)$$

with F_i, G_i given in Appendix 5.A.1.

The terms in Equations (5.A.1)–(5.A.6) contain forcing at frequencies ω and 3ω. The former frequency is resonant with the discrete eigenmode and the latter is assumed to lie in the continuous spectrum (phonon band), that is,

$$(3\omega)^2 > 1. \qquad (5.2.25)$$

As the Equations (5.2.23)–(5.2.24) are linear in ϕ_3^1, ϕ_3^2 the solution can be written as a combination of solutions with frequencies present in the forcing, that is,

$$\begin{aligned}\phi_3^1 &= \phi_{3\,(0)}^1 + \phi_{3\,(1)}^1 e^{i\omega T_0} + c.c. + \phi_{3\,(2)}^1 e^{2i\omega T_0} + c.c. + \phi_{3\,(3)}^1 e^{3i\omega T_0} + c.c., \qquad (5.2.26)\\ \phi_3^2 &= \phi_{3\,(0)}^2 + \phi_{3\,(1)}^2 e^{i\omega T_0} + c.c. + \phi_{3\,(2)}^2 e^{2i\omega T_0} + c.c. + \phi_{3\,(3)}^2 e^{3i\omega T_0} + c.c.. \qquad (5.2.27)\end{aligned}$$

This implies that $\phi_{3\,(1)}^1$, $\phi_{3\,(1)}^2$ satisfy the following inhomogeneous equations in the three regions below

$$\partial_0^2\phi_{3\,(1)}^1 - \left(\cos(\theta) - \omega^2\right)\phi_{3\,(1)}^1 = \begin{cases} L_1, & X_0 < -a, \\ L_2, & |X_0| < a, \\ L_3, & X_0 > a. \end{cases} \qquad (5.2.28)$$

$$\partial_0^2\phi_{3\,(1)}^2 - \left(\cos(\theta) - \omega^2\right)\phi_{3\,(1)}^2 = \begin{cases} M_1, & X_0 < -a, \\ M_2, & |X_0| < a, \\ M_3, & X_0 > a, \end{cases} \qquad (5.2.29)$$

with L_i, M_i being subsets of the terms in F_i, G_i given by

$$\begin{aligned} L_1 &= \left(2\,i\omega\,D_2B_1 + B_2\left(1-\omega^2\right)\right)\cos\left(a\sqrt{1+\omega^2}\right)\mathrm{e}^{\sqrt{1-\omega^2}(a+X_0)} \\ &\quad -\frac{1}{2}\,B_1|B_1|^2\cos^3\left(a\sqrt{1+\omega^2}\right)\mathrm{e}^{3\sqrt{1-\omega^2}(a+X_0)}, \qquad (5.2.30) \\ L_2 &= \left(2i\omega\,D_2B_1 - B_2\left(1+\omega^2\right)\right)\cos(\sqrt{1+\omega^2}X_0) \\ &\quad +\frac{1}{2}B_1|B_1|^2\cos^3(\sqrt{1+\omega^2}X_0), \qquad (5.2.31) \\ L_3 &= \left(2\,i\omega D_2B_1 + B_2\left(1-\omega^2\right)\right)\cos\left(a\sqrt{1+\omega^2}\right)\mathrm{e}^{\sqrt{1-\omega^2}(a-X_0)} \\ &\quad -\frac{1}{2}\,B_1|B_1|^2\cos^3\left(a\sqrt{1+\omega^2}\right)\mathrm{e}^{3\sqrt{1-\omega^2}(a-X_0)}, \qquad (5.2.32) \end{aligned}$$

$$\begin{aligned} M_1 &= \left(2\,i\omega\,D_2B_2 + B_1\left(1-\omega^2\right)\right)\cos\left(a\sqrt{1+\omega^2}\right)\mathrm{e}^{\sqrt{1-\omega^2}(a+X_0)} \\ &\quad -\frac{1}{2}\,B_2|B_2|^2\cos^3\left(a\sqrt{1+\omega^2}\right)\mathrm{e}^{3\sqrt{1-\omega^2}(a+X_0)}, \qquad (5.2.33) \\ M_2 &= \left(2i\omega\,D_2B_2 - B_1\left(1+\omega^2\right)\right)\cos(\sqrt{1+\omega^2}X_0) \\ &\quad +\frac{1}{2}B_2|B_2|^2\cos^3(\sqrt{1+\omega^2}X_0), \qquad (5.2.34) \\ M_3 &= \left(2\,i\omega D_2B_2 + B_1\left(1-\omega^2\right)\right)\cos\left(a\sqrt{1+\omega^2}\right)\mathrm{e}^{\sqrt{1-\omega^2}(a-X_0)} \\ &\quad -\frac{1}{2}\,B_2|B_2|^2\cos^3\left(a\sqrt{1+\omega^2}\right)\mathrm{e}^{3\sqrt{1-\omega^2}(a-X_0)}. \qquad (5.2.35) \end{aligned}$$

Using the Fredholm theorem, the solvability conditions for Equations (5.2.28)–(5.2.29) are

$$\begin{aligned} D_2B_1 &= \zeta_1B_1|B_1|^2\,i - \zeta_2B_2\,i, \qquad (5.2.36) \\ D_2B_2 &= \zeta_1B_2|B_2|^2\,i - \zeta_2B_1\,i. \qquad (5.2.37) \end{aligned}$$

The quantities ζ_1, ζ_2 are given in Appendix in 5.A.1 as well as in Section 5.5, are real and independent of X_0, so solutions of (5.2.36)-(5.2.37) are oscillating in time. We have not determined the stability of the oscillations, so we will have to go to higher order in ϵ.

Substituting (5.2.36) and (5.2.37) back to Equations (5.2.28) and (5.2.29) respectively, and using the boundary conditions (5.1.4) to prevent incoming radiation from $X_0 \to \pm\infty$, we obtain bounded solutions of the form

$$\phi^1_{3\,(1)} = \begin{cases} B_1|B_1|^2\,\Psi_1\left(X_0\right) + B_2\,\Psi_2\left(X_0\right), & X_0 < -a, \\ B_1|B_1|^2\,\Psi_3\left(X_0\right) + B_2\,\Psi_4\left(X_0\right), & |X_0| < a, \\ B_1|B_1|^2\,\Psi_5\left(X_0\right) + B_2\,\Psi_6\left(X_0\right), & X_0 > a, \end{cases} \qquad (5.2.38)$$

$$\phi^2_{3\,(1)} = \begin{cases} B_2|B_2|^2\,\Psi_7\left(X_0\right) + B_1\,\Psi_8\left(X_0\right), & X_0 < -a, \\ B_2|B_2|^2\,\Psi_9\left(X_0\right) + B_1\,\Psi_{10}\left(X_0\right), & |X_0| < a, \\ B_2|B_2|^2\,\Psi_{11}\left(X_0\right) + B_1\,\Psi_{12}\left(X_0\right), & X_0 > a. \end{cases} \qquad (5.2.39)$$

$\Psi_1, .., \Psi_{12}$, are given at the end of the chapter in 5.A.1. Similarly, the solutions for the third harmonics are

$$\phi^1_{3\,(3)}\,(X_0, T_0) \;=\; B^3_1 \begin{cases} \Psi_{13}(X_0), & X_0 < -a, \\ \Psi_{14}(X_0), & |X_0| < a, \\ \Psi_{15}(X_0), & X_0 > a, \end{cases} \tag{5.2.40}$$

$$\phi^2_{3\,(3)}\,(X_0, T_0) \;=\; B^3_2 \begin{cases} \Psi_{13}(X_0), & X_0 < -a, \\ \Psi_{14}(X_0), & |X_0| < a, \\ \Psi_{15}(X_0), & X_0 > a. \end{cases} \tag{5.2.41}$$

With the assumption (5.2.25), we see that Equations (5.2.40)–(5.2.41) show the left and right moving radiation *(oscillations)* for $X_0 < a$ and $X_0 > a$, respectively. The quantities $\Psi_{13}, .., \Psi_{14}$, are given in Appendix 5.A.1.

5.2.5 Equations at $\mathcal{O}(\epsilon^4)$

The terms from (5.1.1)-(5.1.2) at $\mathcal{O}(\epsilon^4)$ give

$$\begin{aligned} \partial_0{}^2\phi^1_4 - D_0{}^2\phi^1_4 - \cos\left(\phi^1_0 + \theta\right)\phi^1_4 \;&=\; 2\left(D_1D_2 + D_0D_3 - \partial_1\partial_2 - \partial_0\partial_3\right)\phi^1_1 \\ &\quad +2\left(D_0D_1 - \partial_0\partial_1\right)\phi^1_3 + \partial_0^2\phi^2_2 \\ &\quad + \left(\frac{1}{24}\phi_1^{1^4} - \phi^1_3\phi^1_1\right)\sin\left(\phi^1_0 + \theta\right), \end{aligned} \tag{5.2.42}$$

$$\begin{aligned} \partial_0{}^2\phi^2_4 - D_0{}^2\phi^2_4 - \cos\left(\phi^2_0 + \theta\right)\phi^2_4 \;&=\; 2\left(D_1D_2 + D_0D_3 - \partial_1\partial_2 - \partial_0\partial_3\right)\phi^2_1 \\ &\quad +2\left(D_0D_1 - \partial_0\partial_1\right)\phi^2_3 + \partial_0^2\phi^1_2 \\ &\quad + \left(\frac{1}{24}\phi_1^{2^4} - \phi^2_3\phi^2_1\right)\sin\left(\phi^2_0 + \theta\right). \end{aligned} \tag{5.2.43}$$

By the Fredholm theorem, the solvability conditions for Equations (5.2.42)–(5.2.43) are

$$D_3B_1 = 0, \quad D_3B_2 = 0, \tag{5.2.44}$$

that is, B_j are independent of T_3, and $B_j = B_j(T_2, T_4, \dots,)$. Hence we conclude that $\phi^{(1,2)}_4 = 0$, as in case of $\phi^{(1,2)}_2$.

5.2.6 Equations at $\mathcal{O}(\epsilon^5)$

Equating terms at $\mathcal{O}(\epsilon^5)$ gives the equations

$$\begin{aligned} \partial_0{}^2\phi^1_5 - D_0{}^2\phi^1_5 - \cos\left(\theta\right)\phi^1_5 \;&=\; 2\left(D_0D_4 - \partial_0\partial_4\right)\phi^1_1 + 2(D_3D_1 - \partial_3\partial_1)\phi^1_1 \\ &\quad + \left(D_2^2 - \partial_2^2\right)\phi^1_1 + \left(D_1^2 - \partial_1^2\right)\phi^1_3 + 2\left(D_2D_0 - \partial_2\partial_0\right)\phi^1_3 \\ &\quad + \left(-\frac{1}{2}\,\phi_1^{1^2}\phi^1_3 + \frac{1}{120}\phi_1^{1^5}\right)\cos\left(\theta\right) + \partial_0^2\,\phi^2_3, \end{aligned} \tag{5.2.45}$$

$$\begin{aligned}\partial_0{}^2\phi_5^2 - D_0{}^2\phi_5^2 - \cos(\theta)\,\phi_5^2 &= 2\,(D_0D_4 - \partial_0\partial_4)\phi_1^2 + 2(D_3D_1 - \partial_3\partial_1)\phi_1^2 \\ &\quad + \left(D_2^2 - \partial_2^2\right)\phi_1^2 + \left(D_1^2 - \partial_1^2\right)\phi_3^2 + 2\,(D_2D_0 - \partial_2\partial_0)\,\phi_3^2 \\ &\quad + \left(-\frac{1}{2}\,\phi_1^{2^2}\phi_3^2 + \frac{1}{120}\phi_1^{2^5}\right)\cos(\theta) + \partial_0^2\,\phi_3^1. \qquad (5.2.46)\end{aligned}$$

Again calculating the right hand sides using the known functions ϕ_1^1, ϕ_1^2, ϕ_3^1 and ϕ_3^2 we again split the solutions into components proportional to simple harmonics as in (5.2.26)–(5.2.27) at $\mathcal{O}(\epsilon^3)$. The equations for the first harmonics are given by

$$\partial_0^2\phi_{5\,(1)}^1 - \left(\cos(\theta) - \omega^2\right)\phi_{5\,(1)}^1 = \begin{cases} P_1, & X_0 < -a, \\ P_2, & |X_0| < a, \\ P_3, & X_0 > a, \end{cases} \qquad (5.2.47)$$

$$\partial_0^2\phi_{5\,(1)}^2 - \left(\cos(\theta) - \omega^2\right)\phi_{5\,(1)}^2 = \begin{cases} Q_1, & X_0 < -a, \\ Q_2, & |X_0| < a, \\ Q_3, & X_0 > a, \end{cases} \qquad (5.2.48)$$

where $P_1, .., P_3$, $Q_1, .., Q_3$, can be seen in Appendix 5.A.1.

By using the Fredholm theorem, we obtain the solvability conditions for Equations (5.2.47)–(5.2.48) by using the relation (5.A.24)–(5.A.29)

$$D_4B_1 = \zeta_3B_1|B_1|^4 + \zeta_4B_2|B_2|^2\,i + \zeta_5\,B_1^2\overline{B_2}\,i + \zeta_6B_2|B_1|^2\,i + \zeta_7B_1\,i, \qquad (5.2.49)$$

$$D_4B_2 = \zeta_3B_2|B_2|^4 + \zeta_4B_1|B_1|^2\,i + \zeta_5\,B_2^2\overline{B_1}\,i + \zeta_6B_1|B_2|^2\,i + \zeta_7B_2\,i, \qquad (5.2.50)$$

where $\zeta_3, .., \zeta_7$, are given in Section 5.5.

We do not calculate other harmonics at $\mathcal{O}(\epsilon^5)$, as we expect to have the desired amplitude equations at this stage. The fact that $\zeta_3 \in \mathbb{C}$ and is not purely imaginary implies that oscillation will decay in amplitude. So there is no need to go to higher order in ϵ.

5.2.7 Amplitude equations

Combining the solvability conditions (5.2.19), (5.2.36)–(5.2.37), (5.2.44), (5.2.49)–(5.2.50) and writing $b_i = \epsilon B_i$ for $i = 1, 2$, we obtain

$$\begin{aligned}\frac{db_1(t)}{dt} &= \zeta_3b_1|b_1|^4 + \zeta_1b_1|b_1|^2i - \zeta_7S^4b_1i \\ &\quad + S^2\left(\zeta_4b_2|b_2|^2 + \zeta_6b_2|b_1|^2 + \zeta_5b_1^2\overline{b_2} - \zeta_2b_2\right)\,i, \qquad (5.2.51) \\ \frac{db_2(t)}{dt} &= \zeta_3b_2|b_2|^4 + \zeta_1b_2|b_2|^2i - \zeta_7S^4b_2i \\ &\quad + S^2\left(\zeta_4b_1|b_1|^2 + \zeta_6b_1|b_2|^2 + \zeta_5b_2^2\overline{b_1} - \zeta_2b_1\right)\,i, \qquad (5.2.52)\end{aligned}$$

by using the relation

$$\frac{\partial|b|^2}{\partial t} = \frac{\partial(bb^*)}{\partial t} = b\frac{\partial b^*}{\partial t} + b^*\frac{\partial b}{\partial t}, \tag{5.2.53}$$

we obtain

$$\begin{aligned}\frac{d}{dt}|b_1|^2 &= 2\mathrm{Re}(\zeta_3)|b_1|^6 + S^2\left(\zeta_2 - \zeta_4|b_2|^2 + \zeta_5|b_1|^2 - \zeta_6|b_1|^2\right)\left(b_1\overline{b_2} - b_2\overline{b_1}\right)i \\ &\quad +\mathcal{O}(\epsilon^6), \end{aligned} \tag{5.2.54}$$

$$\begin{aligned}\frac{d}{dt}|b_2|^2 &= 2\mathrm{Re}(\zeta_3)|b_2|^6 + S^2\left(\zeta_2 - \zeta_4|b_1|^2 + \zeta_5|b_2|^2 - \zeta_6|b_2|^2\right)\left(b_2\overline{b_1} - b_1\overline{b_2}\right)i \\ &\quad +\mathcal{O}(\epsilon^6). \end{aligned} \tag{5.2.55}$$

From Equations (5.2.54)–(5.2.55), we expect that it describes the gradual decrease with the same amplitude of oscillation, as it emits energy in the form of radiation. It should be noted that solutions of Equations (5.2.54)–(5.2.55) decay at the same rate. With the above equation we observe especially that when $b_1 \sim \mathcal{O}(1)$, $b_2 \sim \mathcal{O}(1)$ they decay as $\mathcal{O}(t^{-1/4})$.

5.3 Coupled long Josephson junctions with $S \sim \mathcal{O}(1)$

In this section we construct the dynamics of coupled sine-Gordon Equation (5.1.1)–(5.1.2) without any driving, that is with $h = 0$, and when the magnetic induction coupling between long Josephson junctions is strong, i.e. $S \sim \mathcal{O}(1)$ with $|S| < 1$. By using the boundary conditions (5.1.4) together with multiple scales expansion (5.2.3), we obtain the following orders of equations.

5.3.1 Leading order corrections

The leading order terms are $\mathcal{O}(1)$ and give

$$\partial_0^2\phi_0^1 - D_0^2\phi_0^1 = \sin\left(\phi_0^1 + \theta\right) + S\,\partial_0^2\phi_0^2, \tag{5.3.1}$$

$$\partial_0^2\phi_0^2 - D_0^2\phi_0^2 = \sin\left(\phi_0^2 + \theta\right) + S\,\partial_0^2\phi_0^1. \tag{5.3.2}$$

A solution representing a uniform background is

$$\phi_0^1 = \phi_0^2 = 0. \tag{5.3.3}$$

5.3.2 First order corrections

The terms in (5.1.1)-(5.1.2) at order $\mathcal{O}(\epsilon)$ give

$$\partial_0^2\phi_1^1 - D_0^2\phi_1^1 = \cos\left(\theta\right)\phi_1^1 + S\,\partial_0^2\phi_1^2, \tag{5.3.4}$$

$$\partial_0^2\phi_1^2 - D_0^2\phi_1^2 = \cos\left(\theta\right)\phi_1^2 + S\,\partial_0^2\phi_1^1. \tag{5.3.5}$$

Note that the equations are coupled. Here we assume that the solutions are either even or odd namely

$$\phi_1^2 = \phi_1^1, \quad \text{or} \quad \phi_1^2 = -\phi_1^1. \tag{5.3.6}$$

With the above assumption Equations (5.3.4)–(5.3.5) then become

$$(1-S)\,\partial_0^2\phi_1^{(1,2)} - D_0^2\phi_1^{(1,2)} = \cos(\theta+\phi_0^1)\phi_1^{(1,2)}, \tag{5.3.7}$$

or

$$(1+S)\,\partial_0^2\phi_1^{(1,2)} - D_0^2\phi_1^{(1,2)} = \cos(\theta+\phi_0^1)\phi_1^{(1,2)}. \tag{5.3.8}$$

By linearisation, we obtain the solution for the above equations in the form

$$\phi_1^1 = B_1\,\Phi_1(X_0,T_0)e^{i\omega_1 T_0} + c.c. + B_2\,\Phi_2(X_0,T_0)e^{i\omega_2 T_0} + c.c., \tag{5.3.9}$$

$$\phi_1^2 = B_1\,\Phi_1(X_0,T_0)e^{i\omega_1 T_0} + c.c. - B_2\,\Phi_2(X_0,T_0)e^{i\omega_2 T_0} + c.c., \tag{5.3.10}$$

where $B_i = B_i\,(T_0, T_1, ..)$ for $i = 1, 2$ are the amplitudes of oscillation. The oscillation frequencies ω_1 and ω_2 are given by the implicit relations

$$a = \sqrt{\frac{1\mp S}{1+\omega_i^2}}\,\tan^{-1}\left(\sqrt{\frac{1-\omega_i{}^2}{1+\omega_i{}^2}}\right), \quad |S|<1, \quad i=1,2, \tag{5.3.11}$$

where a is the facet length of the junctions. There are two critical facet lengths, corresponding to each of $\omega_i \to 0$, namely

$$a_{ci} = \frac{\pi}{4}\sqrt{1\mp S}. \tag{5.3.12}$$

The quantities Φ_j are given by

$$\Phi_1(X_0,T_0) = \begin{cases} \cos\left(\sqrt{\frac{1+\omega_1{}^2}{1-S}}\,a\right)\mathrm{e}^{(a+X_0)\sqrt{(1-\omega_1{}^2)/(1-S)}}, & X_0 < -a, \\ \cos\left(\sqrt{\frac{1+\omega_1{}^2}{1-S}}\,X_0\right), & |X_0| < a, \\ \cos\left(\sqrt{\frac{1+\omega_1{}^2}{1-S}}\,a\right)\mathrm{e}^{(a-X_0)\sqrt{(1-\omega_1{}^2)/(1-S)}}, & X_0 > a, \end{cases} \tag{5.3.13}$$

$$\Phi_2(X_0,T_0) = \begin{cases} \cos\left(\sqrt{\frac{1+\omega_2{}^2}{1+S}}\,a\right)\mathrm{e}^{(a+X_0)\sqrt{(1-\omega_2{}^2)/(1+S)}}, & X_0 < -a, \\ \cos\left(\sqrt{\frac{1+\omega_2{}^2}{1+S}}\,X_0\right), & |X_0| < a, \\ \cos\left(\sqrt{\frac{1+\omega_2{}^2}{1+S}}\,a\right)\mathrm{e}^{(a-X_0)\sqrt{(1-\omega_2{}^2)/(1+S)}}, & X_0 > a. \end{cases} \tag{5.3.14}$$

5.3.3 Second order corrections

From the terms in (5.1.1)–(5.1.2) at order $\mathcal{O}(\epsilon^2)$, we obtain a pair of equations

$$(1-S)\,\partial_0^2\phi_2^j - D_0^2\phi_2^j - \cos(\theta + \phi_0^1)\phi_2^j = 2D_0D_1\phi_1^j - 2\partial_0\partial_1\phi_1^j, \tag{5.3.15}$$

$$(1+S)\,\partial_0^2\phi_2^j - D_0^2\phi_2^j - \cos(\theta + \phi_0^1)\phi_2^j = 2D_0D_1\phi_1^j - 2\partial_0\partial_1\phi_1^j, \tag{5.3.16}$$

where $j = 1, 2$. Evaluating the right-hand sides for the different regions and substituting in the spectral ansätze

$$\phi_1^j(X_0, T_0) = \widetilde{\phi}_1^j(X_0)e^{i\omega_1 T_0}, \quad \phi_2^j(X_0, T_0) = \widetilde{\phi}_2^j(X_0)e^{i\omega_2 T_0},$$

we obtain a set of two ordinary differential equations corresponding to the frequencies ω_1, ω_2. To find bounded solutions for equations (5.3.15)–(5.3.16), we apply the Fredholm theorem, which implies that B_i are independent of the first slow time scale T_1, since

$$D_1B_1 = 0, \quad D_1B_2 = 0. \tag{5.3.17}$$

As $\partial_1 B$, as well as $\partial_n B$, do not appear in the final amplitude equations, so we conclude that

$$\partial_n B = 0, \quad n = 1, 2, 3, \ldots, \tag{5.3.18}$$

which implies that there is no dependence on the longer space scales $X_1, X_2, \ldots$.

By putting the solvability conditions (5.3.17) together with (5.3.18) in (5.3.15)–(5.3.16), we obtain the equations similar to those $\mathcal{O}(\epsilon)$. Due to the uniformity in perturbation expansions, we impose

$$\phi_2^j(X_0, T_0) = 0. \tag{5.3.19}$$

5.3.4 Third correction terms

At $\mathcal{O}(\epsilon^3)$, Equations (5.1.1) and (5.1.2) imply

$$\begin{aligned}\partial_0^2\phi_3^{(1,2)} - D_0^2\phi_3^{(1,2)} - \cos(\theta)\phi_3^{(1,2)} &= 2\,(D_0D_2 - \partial_0\partial_2)\phi_1^{(1,2)} \\ &\quad -\frac{1}{6}{\phi_1^{(1,2)}}^3\cos(\theta) + S\,\partial_0^2\phi_3^{(2,1)}.\end{aligned} \tag{5.3.20}$$

Again assuming that $\phi_1^{(1,2)} = \phi_1^{(2,1)}$ or $\phi_1^{(1,2)} = -\phi_1^{(2,1)}$, and calculating the right hand side of the above equations using the previously calculated functions, we obtain

$$\begin{aligned}&(1-S)\,\partial_0^2\phi_3^{(1,2)} - D_0^2\phi_3^{(1,2)} - \cos(\theta + \phi_0^{(1,2)})\phi_3^{(1,2)} \\ &= 2i\omega_1 D_2B_1\Phi_1 e^{i\omega_1 T_0} - \Big[\frac{1}{2}B_1\left(|B_1|^2\,\Phi_1^2 + 2\,|B_2|^2\,\Phi_2^2\right)\Phi_1 e^{i\omega_1 T_0} + \frac{1}{6}B_1^3\Phi_1^3 e^{3i\omega_1 T_0} \\ &+\frac{1}{2}B_1B_2^2\Phi_1\Phi_2^2 e^{i(2\omega_2+\omega_1)T_0} + \frac{1}{2}\overline{B_1}B_2^2\Phi_1\Phi_2^2 e^{i(2\omega_2-\omega_1)T_0}\Big]\cos\theta + c.c.,\end{aligned} \tag{5.3.21}$$

$$
\begin{aligned}
&(1+S)\,\partial_0^2\phi_3^{(1,2)} - D_0^2\phi_3^{(1,2)} - \cos(\theta+\phi_0)\phi_3^{(1,2)} \\
&= 2i\omega_2 D_2 B_2 \Phi_2 e^{i\omega_2 T_0} - \Big[\frac{1}{2}B_2\left(|B_2|^2\Phi_2^2 + 2\,|B_1|^2\,\Phi_1^2\right)\Phi_2 e^{i\omega_2 T_0} + \frac{1}{6}B_2^3\Phi_2^3 e^{3i\omega_2 T_0} \\
&+\frac{1}{2}B_1^2 B_2\Phi_1^2\Phi_2 e^{i(2\omega_1+\omega_2)T_0} + \frac{1}{2}B_1^2\overline{B_2}\Phi_1^2\Phi_2 e^{i(2\omega_1-\omega_2)T_0}\Big]\cos\theta + c.c.. \qquad (5.3.22)
\end{aligned}
$$

As the above equations are linear, their solutions can be written as a linear combination of solutions with frequencies present in the forcing terms, i.e.

$$
\begin{aligned}
\phi_3^{(1,2)} \;=\;& \phi_{3(0,0)}^{(1,2)} + c.c. + \phi_{3\,(1,1)}^{(1,2)} e^{i\omega_1 T_0} + c.c. + \phi_{3\,(1,2)}^{(1,2)} e^{i\omega_2 T_0} + c.c. + \phi_{3\,(22,1)}^{(1,2)} e^{i(2\omega_2+\omega_1)T_0} \\
&+c.c. + \phi_{3\,(22,2)}^{(1,2)} e^{i(2\omega_2-\omega_1)T_0} + c.c. + \phi_{3\,(21,1)}^{(1,2)} e^{i(2\omega_1+\omega_2)T_0} + c.c. \\
&+\phi_{3(22,2)}^{(1,2)} e^{i(2\omega_1-\omega_2)T_0} + c.c. + \phi_{3(3,1)}^{(1,2)} e^{3i\omega_1 T_0} + c.c. + \phi_{3(3,2)}^{(1,2)} e^{3i\omega_2 T_0} + c.c.. \qquad (5.3.23)
\end{aligned}
$$

Having evaluated the right hand side and splitting the solutions into components proportional to simple harmonics, we obtain the solvability condition for the first harmonics

$$
\begin{aligned}
D_2 B_1 &= \psi_1 B_1\,|B_1|^2\,i + \psi_2 B_1\,|B_2|^2\,i, \qquad (5.3.24)\\
D_2 B_2 &= \psi_3 B_2\,|B_2|^2\,i + \psi_4 B_2\,|B_1|^2\,i, \qquad (5.3.25)
\end{aligned}
$$

where $\psi_i, i = 1,2,3,4$ are given in 5.5, and the bounded solutions for the first harmonics are

$$
\phi_{3\,(1,1)}^{(1,2)} = \begin{cases} |B_1|^2 R_{(1,1)} + |B_2|^2 R_{(1,2)}, & X_0 < -a, \\ |B_1|^2 R_{(2,1)} + |B_2|^2 R_{(2,2)}, & |X_0| \le a, \\ |B_1|^2 R_{(3,1)} + |B_2|^2 R_{(3,2)}, & X_0 > a, \end{cases} \qquad (5.3.26)
$$

$$
\phi_{3\,(1,2)}^{(1,2)} = \begin{cases} |B_2|^2 S_{(1,1)} + |B_1|^2 S_{(1,2)}, & X_0 < -a, \\ |B_2|^2 S_{(2,1)} + |B_1|^2 S_{(2,2)}, & |X_0| \le a, \\ |B_2|^2 S_{(3,1)} + |B_1|^2 S_{(3,2)}, & X_0 > a, \end{cases} \qquad (5.3.27)
$$

where $R_{(j,k)}$, $S_{(j,k)}$ will be given in Appendix 5.A.2.

At this stage, we assume that

$$
(3\omega_1)^2 > 1, \quad (3\omega_2)^2 > 1, \qquad (5.3.28)
$$

that is, the third harmonics lie in the continuous spectrum. The solutions for the third harmonics are

$$
\phi_{3\,(3,1)}^{(1,2)} = \begin{cases} W_1, & X_0 < -a, \\ W_2, & |X_0| < a, \\ W_3, & X_0 > a, \end{cases} \qquad (5.3.29)
$$

$$\phi^{(1,2)}_{3\,(3,2)} = \begin{cases} W_4, & X_0 < -a, \\ W_5, & |X_0| < a, \\ W_6, & X_0 > a, \end{cases} \tag{5.3.30}$$

where $W_1, .., W_6$ are also given in Appendix 5.A.2.

The assumptions (5.3.28) imply that $\phi^{(1,2)}_{3\,(22,1)} + c.c.$, $\phi^{(1,2)}_{3\,(21,1)} + c.c.$, $\phi^{(1,2)}_{3\,(3,1)} + c.c.$ and $\phi^{(1,2)}_{3\,(3,2)} + c.c.$ represent continuous wave radiation travelling to the left in $X_0 < -a$ and right in $X_0 > a$. Also with given assumptions (5.3.28) and $\omega_2 > \omega_1$ the harmonics $2\omega_2 + \omega_1$, $2\omega_1 + \omega_2$ also lie in the continuous spectrum, and are responsible for continuous wave oscillations in coupled long Josephson junctions. The bounded solutions for the above harmonics appearing in (5.3.23) are

$$\phi^{(1,2)}_{3\,(22,1)} = \begin{cases} U_1, & X_0 < -a, \\ U_2, & |X_0| < a, \\ U_3, & X_0 > a. \end{cases} \tag{5.3.31}$$

$$\phi^{(1,2)}_{3\,(22,2)} = \begin{cases} U_4, & X_0 < -a, \\ U_5, & |X_0| \le a, \\ U_6, & X_0 > a, \end{cases} \tag{5.3.32}$$

$$\phi^{(1,2)}_{3\,(21,1)} = \begin{cases} V_1, & X_0 < -a, \\ V_2, & |X_0| \le a, \\ V_3, & X_0 > a, \end{cases} \tag{5.3.33}$$

$$\phi^{(1,2)}_{3\,(21,2)} = \begin{cases} V_4, & X_0 < -a, \\ V_5, & |X_0| \le a, \\ V_6, & X_0 > a, \end{cases} \tag{5.3.34}$$

where U_i, V_i for $i = 1, 2, ..6$ are given in Appendix 5.A.2.

By combining Equations (5.3.26)–(5.3.34), we obtain solutions for ϕ^1_3, ϕ^2_3 in the form

$$\begin{aligned} \phi^1_3 = {} & B_1\,\phi^{(1,2)}_{3\,(1,1)} e^{i\omega_1 T_0} + c.c. + B_2\,\phi^{(1,2)}_{3\,(1,2)} e^{i\omega_2 T_0} + c.c. + B_1 B_2^2\,\phi^{(1,2)}_{3\,(22,1)} e^{i(2\omega_2+\omega_1)T_0} \\ & + c.c. + \overline{B_1} B_2^2\,\phi^{(1,2)}_{3\,(22,2)} e^{i(2\omega_2-\omega_1)T_0} + c.c. + B_2 B_1^2\,\phi^{(1,2)}_{3\,(21,1)} e^{i(2\omega_1+\omega_2)T_0} + c.c. \\ & + \overline{B_2} B_1^2\,\phi^{(1,2)}_{3\,(22,2)} e^{i(2\omega_1-\omega_2)T_0} + c.c. + B_1^3 \phi^{(1,2)}_{3\,(3,1)} e^{3i\omega_1 T_0} + c.c. \\ & + B_2^3\,\phi^1_{3\,(3,2)} e^{3i\omega_2 T_0} + c.c., \end{aligned} \tag{5.3.35}$$

$$\begin{aligned} \phi^2_3 = {} & B_1\,\phi^{(1,2)}_{3\,(1,1)} e^{i\omega_1 T_0} + c.c. - B_2\,\phi^{(1,2)}_{3\,(1,2)} e^{i\omega_2 T_0} + c.c. + B_1 B_2^2\,\phi^{(1,2)}_{3\,(22,1)} e^{i(2\omega_2+\omega_1)T_0} \\ & + c.c. + \overline{B_1} B_2^2\,\phi^{(1,2)}_{3\,(22,2)} e^{i(2\omega_2-\omega_1)T_0} + c.c. - B_2 B_1^2\,\phi^{(1,2)}_{3\,(21,1)} e^{i(2\omega_1+\omega_2)T_0} + c.c. \\ & - \overline{B_2} B_1^2\,\phi^{(1,2)}_{3\,(22,2)} e^{i(2\omega_1-\omega_2)T_0} + c.c. + B_1^3 \phi^{(1,2)}_{3\,(3,1)} e^{3i\omega_1 T_0} + c.c. \\ & - B_2^3\,\phi^1_{3\,(3,2)} e^{3i\omega_2 T_0} + c.c.. \end{aligned} \tag{5.3.36}$$

Since the above solutions are still purely periodic in time, we continue to higher order to determine whether amplitude of oscillations increases or decreases.

5.3.5 Fourth correction terms

The terms at order $\mathcal{O}(\epsilon^4)$ from (5.1.1), (5.1.2) give

$$\begin{aligned}\partial_0{}^2\phi_4^{(1,2)} - D_0{}^2\phi_4^{(1,2)} - \cos(\theta)\,\phi_4^{(1,2)} &= 2\left(D_1D_2 + D_0D_3 - \partial_1\partial_2 - \partial_0\partial_3\right)\phi_1^{(1,2)} \\ &+ \left(\frac{1}{24}\phi_1^{4(1,2)} - \phi_3^{(1,2)}\phi_1^{(1,2)}\right)\sin\left(\phi_0^{(1,2)} + \theta\right) \\ &+ 2\left(D_0D_1 - \partial_0\partial_1\right)\phi_3^{(1,2)} + S\partial_0^2\phi_4^{(2,1)}, \quad (5.3.37)\end{aligned}$$

The solvability conditions for the above equations are

$$D_3B_1 = 0, \quad D_3B_2 = 0. \quad (5.3.38)$$

From this we impose the condition that $\phi_4^{(1,2)} = 0$, as we did before for $\phi_2^{(1,2)}$, and note that B_j are independent of T_3, that is, $B_j = B_j(T_2, T_4, \dots)$.

5.3.6 Fifth order terms

Equating terms from (5.1.1), (5.1.2) at $\mathcal{O}(\epsilon^5)$ gives the equations

$$\begin{aligned}\partial_0{}^2\phi_5^{(1,2)} - D_0{}^2\phi_5^{(1,2)} - \cos(\theta)\phi_5^{(1,2)} &= 2\left(D_0D_4 - \partial_0\partial_4\right)\phi_1^{(1,2)} + 2\left(D_3D_1 - \partial_3\partial_1\right)\phi_1^{(1,2)} \\ &+ \left(D_2^2 - \partial_2^2\right)\phi_1^{(1,2)} + \left(D_1^2 - \partial_1^2\right)\phi_3^{(1,2)} \\ &+ \left(-\frac{1}{2}\phi_1^{(1,2)^2}\phi_3^{(1,2)} + \frac{1}{120}\phi_1^{(1,2)^5}\right)\cos(\theta) \\ &+ 2\left(D_2D_0 - \partial_2\partial_0\right)\phi_3^{(1,2)} + S\,\partial_0^2\phi_5^{(2,1)}. \quad (5.3.39)\end{aligned}$$

Having evaluated the right hand side and splitting the solutions into components proportional to simple harmonics, as in Equations (5.3.23), we obtain solutions for the first harmonics as

$$\left(1 - S\right)\partial_0^2\phi_{51}^{(1,2)} - \left(\cos(\theta) - \omega_1^2\right)\phi_{51}^{(1,2)} = \begin{cases} P_{11}, & X_0 < -a, \\ P_{12}, & |X_0| \le a, \\ P_{13}, & X_0 > a, \end{cases} \quad (5.3.40)$$

$$\left(1 + S\right)\partial_0^2\phi_{52}^{(1,2)} - \left(\cos(\theta) - \omega_2^2\right)\phi_{52}^{(1,2)} = \begin{cases} Q_{11}, & X_0 < -a, \\ Q_{12}, & |X_0| \le a, \\ Q_{13}, & X_0 > a, \end{cases} \quad (5.3.41)$$

with P_i, Q_i given in Appendix 5.A.2.

The solvability conditions for Equations (5.3.40)–(5.3.41) are

$$D_4 B_1 = \varphi_1 B_1 |B_1|^4 + \varphi_2 B_1 |B_2|^4 + \varphi_3 B_1 |B_1|^2 |B_2|^2, \tag{5.3.42}$$

$$D_4 B_2 = \varphi_4 B_2 |B_2|^4 + \varphi_5 B_2 |B_1|^4 + \varphi_6 B_2 |B_1|^2 |B_2|^2. \tag{5.3.43}$$

where the values of φ_j are given in 5.5. Since the φ_j are not all purely imaginary, the above equations give growth/decay in amplitude of oscillation, so there is no need to go to higher order.

5.3.7 Amplitude equations

We do not calculate other harmonics for Equations (5.3.40) and (5.3.41), as we expect the final amplitude equations at this stage. Combining all the solvability conditions, we obtain the coupled amplitude equations

$$\frac{\partial}{\partial t}|b_1|^2 = 2\,\mathrm{Re}(\varphi_1)|b_1|^6 + 2\,\mathrm{Re}(\varphi_3)|b_1|^4|b_2|^2 + \left(\varphi_2 \overline{b_1} b_2 + \overline{\varphi_2} b_1 \overline{b_2}\right)|b_2|^4, \tag{5.3.44}$$

$$\frac{\partial}{\partial t}|b_2|^2 = 2\,\mathrm{Re}(\varphi_4)|b_2|^6 + 2\,\mathrm{Re}(\varphi_6)|b_2|^4|b_1|^2 + \left(\varphi_5 \overline{b_2} b_1 + \overline{\varphi_5} b_2 \overline{b_1}\right)|b_1|^4. \tag{5.3.45}$$

The Equations (5.3.44)–(5.3.45) are similar to (5.2.54)–(5.2.55) and describe the amplitude of oscillations for the stacked long Josephson junction, and both amplitudes decay with the same algebraic rate, namely $\mathcal{O}(t^{-1/4})$.

5.4 Driven coupled long Josephson junctions with phase-shift

We now consider the coupled sine-Gordon equations describing a stacked pair of $0-\pi-0$ long Josephson junctions in the presence of external driving with frequency near the natural frequency Ω with $h \neq 0$, $\Omega = \omega_1(1+\rho)$ and for some small value of ρ. We assume strong coupling, that is, $S \sim \mathcal{O}(1)$. By rescaling the time by $\Omega t = \omega_1 \tau$, (5.1.1)-(5.1.2), become

$$\phi^1_{xx}(x,\tau) - (1+\rho)^2 \phi^1_{\tau\tau}(x,\tau) = \sin\left(\phi^1 + \theta\right) + S\phi^2_{xx} + \frac{1}{2}h\left(e^{i\omega_1\tau} + c.c.\right), \tag{5.4.1}$$

$$\phi^2_{xx}(x,\tau) - (1+\rho)^2 \phi^2_{\tau\tau}(x,\tau) = \sin\left(\phi^2 + \theta\right) + S\phi^1_{xx} + \frac{1}{2}h\left(e^{i\omega_1\tau} + c.c.\right). \tag{5.4.2}$$

Here, we assume that the driving amplitude is small, that is,

$$h = \epsilon^3 H, \quad \rho = \epsilon^3 R, \tag{5.4.3}$$

with $H, R \sim \mathcal{O}(1)$. Due to the time rescaling above, our slow temporal variables are now defined as

$$X_n = \epsilon^n x, \quad T_n = \epsilon^n \tau, \quad n = 0, 1, 2, ..., \tag{5.4.4}$$

with the boundary conditions given by (5.1.4) and the phase-shift given by (5.1.3).

Performing a perturbation expansion order by order, we obtain the same expansion up to $\mathcal{O}(\epsilon^2)$, as in Sections 5.3.1–5.3.3.

5.4.1 Third correction terms

Our equations at $\mathcal{O}(\epsilon^3)$ are

$$\begin{aligned}\partial_0^2\phi_3^{(1,2)} - D_0^2\phi_3^{(1,2)} - \cos(\theta)\,\phi_3^{(1,2)} &= 2\,(D_0D_2 - \partial_0\partial_2)\phi_1^{(1,2)} - \frac{1}{6}{\phi_1^{(1,2)}}^3\cos(\theta)\\ &\quad + S\,\partial_0^2\phi_3^{(2,1)} + \frac{1}{2}H\mathrm{e}^{i\omega_1\tau} + c.c..\end{aligned} \tag{5.4.5}$$

The only difference from the undriven case is the presence of the harmonic drive. By using the assumption (5.3.6), the first harmonic for the above equations is

$$\begin{aligned}&(1-S)\,\partial_0^2\phi_3^{(1,2)} - D_0^2\phi_3^{(1,2)} - \cos(\theta+\phi_0)\phi_3^{(1,2)} = 2\,i\,\omega_1 D_2 B_1\,\Phi_1\mathrm{e}^{i\omega_1 T_0}\\ &-\frac{1}{2}B_1\left(|B_1|^2\,\Phi_1^2 + 2\,|B_2|^2\,\Phi_2^2\right)\Phi_1\cos(\theta)\;\mathrm{e}^{i\omega_1 T_0} + \frac{1}{2}H\mathrm{e}^{i\omega_1 T_0} + c.c.,\end{aligned} \tag{5.4.6}$$

the other harmonics are the same as in the undriven case 5.3. The solvability condition for the above equation is

$$D_2B_1 \;=\; \psi_1 B_1|B_1|^2\,i + \psi_2 B_1|B_2|^2\,i + \eta_1 H\,i, \tag{5.4.7}$$

where ψ_1, ψ_2, η_1 are given in Section 5.5.

The solvability condition for harmonic having frequency ω_2 (i.e. D_2B_2) is the same as in 5.3. It should be noted that the above solvability condition is for ϕ_3^1 only. The solvability condition for ϕ_3^2 can be obtained by replacing B_2 by $-B_2$.

The bounded solution for the first harmonic is

$$\widetilde{\phi}_{3\,(1,1)}^{(1,2)} \;=\; \begin{cases} B_1|B_1|^2Y_{(1,1)} + B_1|B_2|^2Y_{(1,2)} + HY_{(1,3)}, & X_0 < -a,\\ B_1|B_1|^2Y_{(2,1)} + B_1|B_2|^2Y_{(2,2)} + HY_{(2,3)}, & |X_0| \le a,\\ B_1|B_1|^2Y_{(3,1)} + B_1|B_2|^2Y_{(3,2)} + HY_{(3,3)}, & X_0 > a,\end{cases} \tag{5.4.8}$$

where $Y_{(j,k)}$ are given in Section 5.A.2.

With the above solution, ϕ_3^1, ϕ_3^2 are now given by

$$\begin{aligned}\phi_3^1 \;=\;& B_1\,\widetilde{\phi}_{3\,(1,1)}^{(1,2)}e^{i\omega_1T_0} + c.c. + B_2\,\phi_{3\,(1,2)}^{(1,2)}e^{i\omega_2T_0} + c.c. + B_1B_2^2\,\phi_{3\,(22,1)}^{(1,2)}e^{i(2\omega_2+\omega_1)T_0}\\ &+c.c. + \overline{B_1}B_2^2\,\phi_{3\,(22,2)}^{(1,2)}e^{i(2\omega_2-\omega_1)T_0} + c.c. + B_2B_1^2\,\phi_{3\,(21,1)}^{(1,2)}e^{i(2\omega_1+\omega_2)T_0} + c.c.\\ &+\overline{B_2}B_1^2\,\phi_{3\,(22,2)}^{(1,2)}e^{i(2\omega_1-\omega_2)T_0} + c.c. + B_1^3\phi_{3\,(3,1)}^{(1,2)}e^{3i\omega_1T_0} + c.c.\\ &+B_2^3\,\phi_{3\,(3,2)}^{1}e^{3i\omega_2T_0} + c.c.,\end{aligned} \tag{5.4.9}$$

$$\begin{aligned}\phi_3^2 &= B_1\,\widetilde{\phi}_{3\,(1,1)}^{(1,2)}e^{i\omega_1 T_0}+c.c.-B_2\,\phi_{3\,(1,2)}^{(1,2)}e^{i\omega_2 T_0}+c.c.+B_1B_2^2\,\phi_{3\,(22,1)}^{(1,2)}e^{i(2\,\omega_2+\omega_1)T_0}\\ &+c.c.+\overline{B_1}B_2^2\,\phi_{3\,(22,2)}^{(1,2)}e^{i(2\,\omega_2-\omega_1)T_0}+c.c.-B_2B_1^2\,\phi_{3\,(21,1)}^{(1,2)}e^{i(2\,\omega_1+\omega_2)T_0}+c.c.\\ &-\overline{B_2}B_1^2\,\phi_{3\,(22,2)}^{(1,2)}e^{i(2\,\omega_1-\omega_2)T_0}+c.c.+B_1^3\phi_{3\,(3,1)}^{(1,2)}e^{3i\omega_1 T_0}+c.c.\\ &-B_2^3\,\phi_{3\,(3,2)}^{1}e^{3i\omega_2 T_0}+c.c..\end{aligned}\tag{5.4.10}$$

5.4.2 Fourth correction terms

The terms at order $\mathcal{O}(\epsilon^4)$ give

$$\begin{aligned}{\partial_0}^2\phi_4^{(1,2)}-{D_0}^2\phi_4^{(1,2)}-\cos(\theta)\,\phi_4^{(1,2)} &= 2\,(D_1D_2+D_0D_3-\partial_1\partial_2-\partial_0\partial_3)\,\phi_1^{(1,2)}\\ &+2\,(D_0D_1-\partial_0\partial_1)\,\phi_3^{(1,2)}+2\,RD_0^2\phi_1^{(1,2)}\\ &+\left(\frac{1}{24}\phi_1^{4(1,2)}-\phi_3^{(1,2)}\phi_1^{(1,2)}\right)\sin(\theta)\\ &+S\,\partial_0^2\phi_4^{(2,1)}.\end{aligned}\tag{5.4.11}$$

The solvability conditions for the above equations are

$$D_3B_1=-\omega_1\,B_1\,R\,i,\quad D_3B_2=-\omega_2\,B_2\,R\,i,\tag{5.4.12}$$

solving the remaining terms we obtain

$$\phi_4^{(1,2)}(X_0,T_0) = 0.\tag{5.4.13}$$

5.4.3 Fifth correction terms

Equating terms at $\mathcal{O}(\epsilon^5)$ gives the equations

$$\begin{aligned}{\partial_0}^2\phi_5^{(1,2)}-{D_0}^2\phi_5^{(1,2)}-\cos(\theta)\phi_5^{(1,2)} &= 2\,(D_0D_4-\partial_0\partial_4)\,\phi_1^{(1,2)}+2\,(D_3D_1-\partial_3\partial_1)\,\phi_1^{(1,2)}\\ &+\left(D_2^2-\partial_2^2\right)\phi_1^{(1,2)}+\left(D_1^2-\partial_1^2\right)\phi_3^{(1,2)}\\ &+\left(-\frac{1}{2}\,{\phi_1^{(1,2)}}^2\phi_3^{(1,2)}+\frac{1}{120}{\phi_1^{(1,2)}}^5\right)\cos(\theta)\\ &+2\,(D_2D_0-\partial_2\partial_0)\,\phi_3^{(1,2)}+S\,\partial_0^2\phi_5^{(2,1)}.\end{aligned}\tag{5.4.14}$$

By using the assumption (5.3.6) and evaluating the right-side, we again split the solutions into components proportional to simple harmonics as in Equation (5.3.23). For the first harmonic, we obtain that

$$(1-S)\,\partial_0^2\widetilde{\phi}_{51}^{(1,2)}-\left(\cos(\theta)-\omega_1^2\right)\widetilde{\phi}_{51}^{(1,2)} = \begin{cases}Z_1, & X_0<-a,\\ Z_2, & |X_0|\le a,\\ Z_3, & X_0>a,\end{cases}\tag{5.4.15}$$

where Z_i are given in Appendix 5.A.3.

The solvability condition for Equation (5.4.15) is

$$\begin{aligned} D_4 B_1 &= \xi_1 B_1 |B_1|^4 + \xi_2 B_1 |B_2|^4 + \xi_3 B_1 |B_1|^2 |B_2|^2 \\ &\quad + \left(\xi_4 |B_1|^2 + \xi_5 |B_2|^2 + \xi_6 B_1^2\right) Hi, \end{aligned} \tag{5.4.16}$$

It should be noted that $D_4 B_2$ is the same as Equation (5.3.43). The quantities ξ_i are given in Section 5.5. Since ξ_i is not purely imaginary the above equations determine the rate of increase in amplitude.

5.4.4 Amplitude equations

Combining all the solvability conditions, we obtain the dynamics of the oscillation amplitude equations in the presence of external drive

$$\begin{aligned} \frac{\omega_1}{\Omega}\frac{\partial b_1}{\partial t} &= \psi_1 b_1 |b_1|^2 i + \psi_2 b_1 |b_2|^2 i + \eta_1 h i + -\omega_1 b_1 \rho i + \xi_1 b_1 |b_1|^4 \\ &\quad + \xi_2 b_1 |b_2|^4 + \xi_3 b_1 |b_1|^2 |b_2|^2 + \left(\xi_4 |b_1|^2 + \xi_5 |b_2|^2 + \xi_6 b_1^2\right) h i, \end{aligned} \tag{5.4.17}$$

$$\begin{aligned} \frac{\omega_1}{\Omega}\frac{\partial b_2}{\partial t} &= \psi_3 b_2 |b_2|^2 i + \psi_4 b_2 |b_1|^2 i - \omega_1 b_2 \rho i + \varphi_4 b_2 |b_2|^4 + \varphi_5 b_2 |b_1|^4 \\ &\quad + \varphi_6 b_2 |b_1|^2 |b_2|^2. \end{aligned} \tag{5.4.18}$$

In this case, the two solutions do not decay to zero as $t \to \infty$. Due to the driving terms, there is a steady state solution. From (5.4.17)–(5.4.18), we expect that a nonzero external drive induces a breathing mode oscillation in the stacked long Josephson junctions.

5.5 Approximate values

If we fix the facet length as, $a(\omega) = 0.4$, and the strength of magnetic induction $S = 0.5$ and consider the systems natural frequencies, which we find by solving (5.2.13) and (5.3.11), we obtain

$$\omega = 0.53342, \quad \omega_1 = 0.53342, \quad \omega_2 = 0.81565.$$

For the other parameters, we obtain the coefficients in the analytical approximations (5.2.54)-(5.2.55), (5.3.44)-(5.3.45) and (5.4.17)-(5.4.18) as

ζ_1 = 0.04333,	ζ_2 = 0.22234,	ζ_4 = 0.08625,	ζ_5 = 0.06905,
ζ_6 = 0.00003,	ζ_7 = 0.16418,	ψ_1 = 0.16984,	ψ_2 = 0.26012,
ψ_3 = -0.00251,	ψ_4 = 0.08354,	ξ_4 = -2.50794,	ξ_5 = 4.95644,
ξ_6 = -0.00948,	η_1 = 0.79108,	η_2 = 0.56503,	ρ_4= -1.14557,
ρ_5 = -2.97325,	ρ_6 = 0.01483,		

φ_1 = -0.00643-0.18433 i, φ_2 = -0.05359+0.40965 i, φ_3 = -0.01879-2.38812 i,
φ_4 = -0.00221-0.03199 i, φ_5 = -0.00302-0.12495 i, φ_6 = -0.03442-1.49371 i,
ξ_1 = -0.00643+0.91037 i, ξ_2 = -0.05359+0.40965 i, ξ_3 = -0.01879-1.91557 i,
ρ_1 = -0.00168+0.52454 i, ρ_2 = -0.00302-0.12495 i, ρ_3 = -0.03442-1.51295 i,
ζ_3 = -0.00325- 0.07216 i.

We will use the above calculations to compare the approximate solutions obtained in Sections 5.2, 5.3 and 5.4 with numerics, which is left for future work.

5.6 Conclusions

We have considered a spatially inhomogeneous coupled sine-Gordon equations with a time periodic drive, modelling stacked long Josephson junctions with a phase shift. Using multiscale expansion, we derived coupled amplitude differential equations considering magnetic coupling $S \sim \mathcal{O}(1)$ and $S \sim \mathcal{O}(\epsilon^2)$ in the absence of an ac-drive. The coupling term between the stack Josephson junctions depends on the physical and geometrical parameters of the system. The multiscale expansion is asymptotic, *i.e.* only valid for small initial amplitudes of the breathing modes. In the small amplitude limit the expansion is expected to provide an accurate description of the breather.

The dynamics of the considered coupled sine-Gordon equations has been extensively studied before for weak and strong coupling [170, 181, 182] to investigate different phenomenon in stacked Josephson junctions, such as voltage locking [175, 176] and current locking [177, 178, 179]. However, the coupled sine-Gordon equations in the context of stacked Josephson junctions with phase shift is considered here for the first time.

We have calculated analytical approximations of breathing modes in stacked Josephson junctions in the limit of small initial amplitudes. We obtained coupled amplitude equations, which describe the gradual decrease of the oscillation amplitude, as the modes emit energy in the form of radiation. The emission of radiation has the effect of damping the breathing. The damping is due to the frequency tripling effect of the nonlinearity that have caused breathing mode to become a source of radiation. The radiation emission in long Josephson junction has been investigated before by many others. The radiation caused by motion of solitons in long Josephson junctions was reported by Dueholm *et al.* [183]. More recently, Krasnov [184] has discussed the radiative annihilation in coupled sine-Gordon equations occurring in a time decay of breather. This phenomenon may be useful to achieve superradiant emission from coupled oscillators.

The obtained amplitude equations decay at the same rate, which cause synchronized

oscillation in Josephson junctions. Here, we showed that, the oscillation amplitudes of breathing mode oscillation decay with the same algebraic rate, namely $\mathcal{O}(t^{-1/4})$ for stacked long Josephson junctions with uniform ground state.

We also investigated strong coupling for $S \sim \mathcal{O}(1)$ with time periodic drive in the coupled sine-Gordon equations for stacked long Josephson junctions. In this case, the obtained amplitude equations do not decay to zero as $t \to \infty$. Due to the driving term, there is a steady state solution. We expect that a nonzero external drive induces a breathing mode oscillation in the stacked long Josephson junctions, similar to the investigation discussed in Chapter 2 for single long Josephson junctions with phase shifts.

5.A Appendix: Explicit expressions

5.A.1 Functions in Section 5.2

$$
\begin{aligned}
F_1 &= 2\left(i\omega D_2 B_1 - \sqrt{1-\omega^2}\partial_2 B_1\right)\cos\left(a\sqrt{1+\omega^2}\right)e^{\sqrt{1-\omega^2}(a+X_0)+i\omega T_0} \\
&\quad + \left(1-\omega^2\right)B_2\cos\left(a\sqrt{1+\omega^2}\right)e^{\sqrt{1-\omega^2}(a+X_0)+i\omega T_0} \\
&\quad -\frac{1}{2}B_1|B_1|^2\cos^3\left(a\sqrt{1+\omega^2}\right)e^{3\sqrt{1-\omega^2}(a+X_0)+i\omega T_0} \\
&\quad -\frac{1}{6}B_1^3\cos^3(a\sqrt{1+\omega^2})e^{3\sqrt{1-\omega^2}(a+X_0)+3i\omega T_0}, \qquad (5.A.1)
\end{aligned}
$$

$$
\begin{aligned}
F_2 &= \Big[2\,i\omega D_2 B_1\cos\left(\sqrt{1+\omega^2}X_0\right) + 2\partial_2 B_1\sqrt{1+\omega^2}\sin\left(\sqrt{1+\omega^2}X_0\right) \\
&\quad -B_2\left(1+\omega^2\right)\cos\left(\sqrt{1+\omega^2}X_0\right) + \frac{1}{2}B_1|B_1|^2\cos^3\left(\sqrt{1+\omega^2}X_0\right)\Big]e^{i\omega T_0} \\
&\quad +\frac{1}{6}B_1^3\cos^3\left(\sqrt{1+\omega^2}X_0\right)e^{3\,i\omega T_0}, \qquad (5.A.2)
\end{aligned}
$$

$$
\begin{aligned}
F_3 &= 2\left(i\omega D_2 B_1 - \sqrt{1-\omega^2}\partial_2 B_1\right)\cos\left(a\sqrt{1+\omega^2}\right)e^{\sqrt{1-\omega^2}(a-X_0)+i\omega T_0} \\
&\quad + \left(1-\omega^2\right)B_2\cos\left(a\sqrt{1+\omega^2}\right)e^{\sqrt{1-\omega^2}(a-X_0)+i\omega T_0} \\
&\quad -\frac{1}{2}B_1|B_1|^2\cos^3\left(a\sqrt{1+\omega^2}\right)e^{3\sqrt{1-\omega^2}(a-X_0)+i\omega T_0} \\
&\quad -\frac{1}{6}B_1^3\cos^3(a\sqrt{1+\omega^2})e^{3\sqrt{1-\omega^2}(a-X_0)+3i\omega T_0}. \qquad (5.A.3)
\end{aligned}
$$

$$
\begin{aligned}
G_1 &= 2\left(i\omega D_2 B_2 - \sqrt{1-\omega^2}\partial_2 B_2\right)\cos\left(a\sqrt{1+\omega^2}\right)e^{\sqrt{1-\omega^2}(a+X_0)+i\omega T_0} \\
&\quad + \left(1-\omega^2\right)B_1\cos\left(a\sqrt{1+\omega^2}\right)e^{\sqrt{1-\omega^2}(a+X_0)+i\omega T_0} \\
&\quad -\frac{1}{2}B_2|B_2|^2\cos^3\left(a\sqrt{1+\omega^2}\right)e^{3\sqrt{1-\omega^2}(a+X_0)+i\omega T_0} \\
&\quad -\frac{1}{6}B_2^3\cos^3(a\sqrt{1+\omega^2})e^{3\sqrt{1-\omega^2}(a+X_0)+3i\omega T_0}, \qquad (5.A.4)
\end{aligned}
$$

$$
\begin{aligned}
G_2 &= \Big[2\,i\omega D_2 B_2\cos\left(\sqrt{1+\omega^2}X_0\right) + 2\partial_2 B_2\sqrt{1+\omega^2}\sin\left(\sqrt{1+\omega^2}X_0\right) \\
&\quad -B_1\left(1+\omega^2\right)\cos\left(\sqrt{1+\omega^2}X_0\right) + \frac{1}{2}B_2|B_2|^2\cos^3\left(\sqrt{1+\omega^2}X_0\right)\Big]e^{i\omega T_0} \\
&\quad +\frac{1}{6}B_2^3\cos^3\left(\sqrt{1+\omega^2}X_0\right)e^{3\,i\omega T_0}, \qquad (5.A.5)
\end{aligned}
$$

$$
\begin{aligned}
G_3 &= 2\left(i\omega D_2 B_2 - \sqrt{1-\omega^2}\partial_2 B_2\right)\cos\left(a\sqrt{1+\omega^2}\right)e^{\sqrt{1-\omega^2}(a-X_0)+i\omega T_0} \\
&\quad + \left(1-\omega^2\right)B_1\cos\left(a\sqrt{1+\omega^2}\right)e^{\sqrt{1-\omega^2}(a-X_0)+i\omega T_0} \\
&\quad -\frac{1}{2}B_2|B_2|^2\cos^3\left(a\sqrt{1+\omega^2}\right)e^{3\sqrt{1-\omega^2}(a-X_0)+i\omega T_0} \\
&\quad -\frac{1}{6}B_2^3\cos^3(a\sqrt{1+\omega^2})e^{3\sqrt{1-\omega^2}(a-X_0)+3i\omega T_0}. \qquad (5.A.6)
\end{aligned}
$$

$$\zeta_1 = \frac{\left(3-2\omega^2-2\omega^6+6\sqrt{1-\omega^2}\left(1+\omega^2\right)a-7\omega^4\right)}{32\,\omega\,\left(1+\omega^2+\sqrt{1-\omega^2}\left(1+\omega^2\right)a\right)}, \tag{5.A.7}$$

$$\zeta_2 = \frac{\left(1+\omega^2\right)\sqrt{1-\omega^2}\,a}{2\,\omega\left(1+\sqrt{1-\omega^2}a\right)}, \tag{5.A.8}$$

$$\begin{aligned}\Psi_1 = {} & C_1 e^{\sqrt{1-\omega^2}X_0}+\frac{\sqrt{2}}{16\,u_2}\Big[\frac{\left(1+\omega^2\right)e^{4\sqrt{1-\omega^2}X_0+3\,u_1u_2}}{4\sqrt{1-\omega^2}}+\frac{4\omega\,\zeta_1 e^{2\sqrt{1-\omega^2}X_0+u_1u_2}}{\sqrt{1-\omega^2}}\\ & -\frac{\left(\left(1+\omega^2\right)e^{2\left(u_1+\sqrt{1+\omega^2}X_0\right)u_2}+16\omega\zeta_1X_0\sqrt{1-\omega^2}\right)e^{\left(2\sqrt{1+\omega^2}X_0+u_1\right)u_2}}{2\sqrt{1-\omega^2}}\\ & \Big]e^{-\sqrt{1-\omega^2}X_0},\end{aligned} \tag{5.A.9}$$

$$\begin{aligned}\Psi_2 = {} & C_2 e^{\sqrt{1-\omega^2}X_0}-\frac{\sqrt{1+\omega^2}}{4\sqrt{2}}\Big(\frac{2\,\left(\omega^2X_0-2\,\omega\,X_0\zeta_2-X_0\right)e^{\left(2\sqrt{1+\omega^2}X_0+u_1\right)u_2}}{\sqrt{1-\omega^2}}\\ & +\frac{\left(2\,\omega\,\zeta_2-\omega^2+1\right)e^{2\sqrt{1-\omega^2}X_0+u_1\,u_2}}{1-\omega^2}\Big)e^{-\sqrt{1-\omega^2}X_0},\end{aligned} \tag{5.A.10}$$

$$\begin{aligned}\Psi_3 = {} & C_1\cos\left(\sqrt{1+\omega^2}X_0\right)+\frac{(9-64\omega\zeta_1)\cos(\sqrt{1+\omega^2}X_0)-\cos(3\sqrt{1+\omega^2}X_0)}{64(1+\omega^2)}\\ & +\frac{X_0\,(3-16\omega\zeta_1)\sin(\sqrt{1+\omega^2}X_0)}{16\left(\sqrt{1+\omega^2}\right)},\end{aligned} \tag{5.A.11}$$

$$\begin{aligned}\Psi_4 = {} & C_2\cos\left(\sqrt{1+\omega^2}X_0\right)-\\ & \frac{\left(\omega^2-2\omega\zeta_2+1\right)\left(X_0\sqrt{1+\omega^2}\sin(\sqrt{1+\omega^2}X_0)+\cos(\sqrt{1+\omega^2}X_0)\right)}{2\,(1+\omega^2)},\end{aligned} \tag{5.A.12}$$

$$\begin{aligned}\Psi_5 = {} & C_1e^{-\sqrt{1-\omega^2}X_0}+\frac{e^{-\sqrt{1-\omega^2}X_0}}{8\sqrt{2}u_2}\Big[8\,\omega\,\zeta_1X_0e^{u_1u_2}-\frac{\left(1+\omega^2\right)e^{3\,u_1u_2-2\sqrt{1-\omega^2}X_0}}{2\sqrt{1-\omega^2}}\\ & +\left(\frac{4\omega\zeta_1e^{u_1u_2+4\sqrt{1-\omega^2}X_0}}{\sqrt{1-\omega^2}}+\frac{\left(1+\omega^2\right)e^{3u_1u_2+2\sqrt{1-\omega^2}X_0}}{4\sqrt{1-\omega^2}}\right)e^{-4\sqrt{1-\omega^2}X_0}\Big],\end{aligned} \tag{5.A.13}$$

$$\Psi_6 = C_2e^{-\sqrt{1-\omega^2}X_0}+\frac{(\omega^2-2\omega\zeta_2-1)\left(1+2\sqrt{1-\omega^2}X_0\right)e^{u_1u_2-\sqrt{1-\omega^2}X_0}}{4\sqrt{2}\sqrt{1-\omega^2}u_2}, \tag{5.A.14}$$

$$\begin{aligned}\Psi_7 = {} & C_1e^{\sqrt{1-\omega^2}X_0}+\frac{\sqrt{2}}{16u_2}\Big[\frac{(1+\omega^2)e^{3u_1u_2+4\sqrt{1-\omega^2}X_0}}{4\sqrt{1-\omega^2}}+\frac{4\omega\,\zeta_1e^{2\sqrt{1-\omega^2}X_0+u_1u_2}}{\sqrt{1-\omega^2}}\\ & -\left(8\omega X_0\zeta_1+\frac{\left(1+\omega^2\right)e^{2\left(u_1+\sqrt{1+\omega^2}X_0\right)u_2}}{2\sqrt{1-\omega^2}}\right)e^{\left(2\sqrt{1+\omega^2}X_0+u_1\right)u_2}\\ & \Big]e^{-\sqrt{1-\omega^2}X_0},\end{aligned} \tag{5.A.15}$$

$$\begin{aligned}\Psi_8 = {} & C_2e^{\sqrt{1-\omega^2}X_0}-\frac{\sqrt{2}}{16\,u_2}\Big(\left(4\,\omega^2X_0-8\,\omega\,X_0\zeta_2-4\,X_0\right)e^{\left(2\sqrt{1+\omega^2}X_0+u_1\right)u_2}\\ & -\frac{2\,\left(\omega^2-2\,\omega\,\zeta_2-1\right)e^{u_1u_2+2\sqrt{1-\omega^2}X_0}}{\sqrt{1-\omega^2}}\Big)e^{-\sqrt{1-\omega^2}X_0},\end{aligned} \tag{5.A.16}$$

$$\begin{aligned}
\Psi_9 &= C_1 \cos\left(\sqrt{1+\omega^2}X_0\right) - \frac{\cos(3\sqrt{1+\omega^2}X_0) + (64\omega\,\zeta_1 - 9)\cos(\sqrt{1+\omega^2}X_0)}{64\,(1+\omega^2)} \\
&\quad - \frac{X_0\,(16\,\omega\,\zeta_1 - 3)\sin\left(\sqrt{1+\omega^2}X_0\right)}{16\,\left(\sqrt{1+\omega^2}\right)}, \qquad (5.A.17)\\
\Psi_{10} &= C_2 \cos\left(\sqrt{1+\omega^2}X_0\right) \\
&\quad - \left(\omega^2 - 2\,\omega\,\zeta_2 + 1\right)\left(\frac{X_0 \sin(\sqrt{1+\omega^2}X_0)}{2\sqrt{1+\omega^2}} + \frac{\cos(\sqrt{1+\omega^2}X_0)}{2\,(1+\omega^2)}\right), \qquad (5.A.18)\\
\Psi_{11} &= C_1 \mathrm{e}^{-\sqrt{1-\omega^2}X_0} + \frac{\sqrt{2}}{16\,u_2}\Big(8\,\mathrm{e}^{u_1u_2}\omega\,\zeta_1 X_0 - \frac{\left(1+\omega^2\right)\mathrm{e}^{3\,u_1u_2 - 2\sqrt{1-\omega^2}X_0}}{2\sqrt{1-\omega^2}} \\
&\quad + \frac{4\,\mathrm{e}^{u_1u_2}\omega\,\zeta_1}{\sqrt{1-\omega^2}} + \frac{\left(1+\omega^2\right)\mathrm{e}^{3\,u_1u_2 - 2\sqrt{1-\omega^2}X_0}}{4\sqrt{1-\omega^2}}\Big)\mathrm{e}^{-\sqrt{1-\omega^2}X_0}, \qquad (5.A.19)\\
\Psi_{12} &= C_2 \mathrm{e}^{-\sqrt{1-\omega^2}X_0} + \frac{\left(\omega^2 - 2\omega\zeta_2 - 1\right)\left(1 + 2\sqrt{1-\omega^2}X_0\right)\mathrm{e}^{u_1u_2 - \sqrt{1-\omega^2}X_0}}{4\sqrt{2}u_2\sqrt{1-\omega^2}}, \qquad (5.A.20)\\
\Psi_{13} &= e^{\sqrt{1-9\,\omega^2}X_0}\widetilde{C_{31}} - \frac{1}{48}\cos^3\left(a\sqrt{1+\omega^2}\right)e^{3\sqrt{1-\omega^2}(a+X_0)}, \qquad (5.A.21)\\
\Psi_{14} &= \cos(\sqrt{1+9\,\omega^2}X_0)\widetilde{C_{32}} - \frac{1}{192\,\omega^2}\left(\omega^2 - 3\right)\cos\left(X_0\sqrt{1+\omega^2}\right), \qquad (5.A.22)\\
\Psi_{15} &= e^{-\sqrt{1-9\,\omega^2}X_0}\widetilde{C_{33}} - \frac{1}{48}\cos^3\left(a\sqrt{1+\omega^2}\right)e^{3\sqrt{1-\omega^2}(a-X_0)}, \qquad (5.A.23)
\end{aligned}$$

with

$$u_1 = \arctan\left(u_2\right), \quad u_2 = \sqrt{\frac{1-\omega^2}{1+\omega^2}}.$$

$$\begin{aligned}
P_1 &= 2\,i\omega\,D_4B_1\cos\left(a\sqrt{1+\omega^2}\right)e^{\sqrt{1-\omega^2}(a+X_0)} \\
&\quad - \left(\zeta_1^2\,B_1|B_1|^4 - \zeta_1\zeta_2\,B_2|B_1|^2 - \zeta_1\zeta_2B_2|B_2|^2 + \zeta_2^2B_1\right)\cos\left(a\sqrt{1+\omega^2}\right)e^{\sqrt{1-\omega^2}(a+X_0)} \\
&\quad -2\,\omega\left(\left(\zeta_1B_1|B_1|^4 - \zeta_2B_2|B_1|^2\right)\Psi_1 + \left(\zeta_1B_2|B_2|^2 - \zeta_2B_1\right)\Psi_2\right) \\
&\quad -\frac{1}{2}\left(3\,B_1|B_1|^4\Psi_1 + \left(B_2|B_1|^2 + B_1^2\bar{B}_2\right)\Psi_2 + B_1|B_1|^4\Psi_{13}\right) \\
&\quad \times\cos^2\left(a\sqrt{1+\omega^2}\right)e^{2\sqrt{1-\omega^2}(a+X_0)} + \frac{1}{12}B_1|B_1|^4\cos^5\left(a\sqrt{1+\omega^2}\right)e^{5\sqrt{1-\omega^2}(a+X_0)} \\
&\quad +B_2|B_2|^2\,\partial_0^2\Psi_7\left(X_0\right) + B_1\,\partial_0^2\Psi_8\left(X_0\right), \qquad (5.A.24)
\end{aligned}$$

$$\begin{aligned}
P_2 &= 2\,i\omega\,D_4B_1\cos\left(X_0\sqrt{1+\omega^2}\right) \\
&\quad - \left(\zeta_1^2\,B_1|B_1|^4 - \zeta_1\zeta_2\,B_2|B_1|^2 - \zeta_1\zeta_2B_2|B_2|^2 + \zeta_2^2B_1\right)\cos\left(X_0\sqrt{1+\omega^2}\right) \\
&\quad -2\,\omega\left(\left(\zeta_1B_1|B_1|^4 - \zeta_2B_2|B_1|^2\right)\Psi_3 + \left(\zeta_1B_2|B_2|^2 - \zeta_2B_1\right)\Psi_4\right) \\
&\quad +\frac{1}{2}\left(3\,B_1|B_1|^4\Psi_3 + \left(B_2|B_1|^2 + B_1^2\bar{B}_2\right)\Psi_4 + B_1|B_1|^4\Psi_{14}\right)\cos^2\left(X_0\sqrt{1+\omega^2}\right) \\
&\quad -\frac{1}{12}B_1|B_1|^4\cos^5\left(X_0\sqrt{1+\omega^2}\right) + B_2|B_2|^2\,\partial_0^2\Psi_9\left(X_0\right) + B_1\,\partial_0^2\Psi_{10}\left(X_0\right), \qquad (5.A.25)
\end{aligned}$$

$$
\begin{aligned}
P_3 \;=\;& 2\,i\omega\,D_4 B_1 \cos\left(a\sqrt{1+\omega^2}\right) e^{\sqrt{1-\omega^2}(a-X_0)} \\
& -\left(\zeta_1^2\,B_1|B_1|^4 - \zeta_1\zeta_2\,B_2|B_1|^2 - \zeta_1\zeta_2 B_2|B_2|^2 + \zeta_2^2 B_1\right)\cos\left(a\sqrt{1+\omega^2}\right) e^{\sqrt{1-\omega^2}(a-X_0)} \\
& -2\,\omega\left(\left(\zeta_1 B_1|B_1|^4 - \zeta_2 B_2|B_1|^2\right)\Psi_5 + \left(\zeta_1 B_2|B_2|^2 - \zeta_2 B_1\right)\Psi_6\right) \\
& -\frac{1}{2}\left(3\,B_1|B_1|^4\Psi_5 + \left(B_2|B_1|^2 + B_1^2\bar{B}_2\right)\Psi_6 + B_1|B_1|^4\Psi_{15}\right) \\
& \times\cos^2\left(a\sqrt{1+\omega^2}\right) e^{2\sqrt{1-\omega^2}(a-X_0)} + \frac{1}{12}B_1|B_1|^4\cos^5\left(a\sqrt{1+\omega^2}\right) e^{5\sqrt{1-\omega^2}(a-X_0)} \\
& +B_2|B_2|^2\,\partial_0^2\Psi_{11}\left(X_0\right) + B_1\,\partial_0^2\Psi_{12}\left(X_0\right), \qquad (5.A.26)
\end{aligned}
$$

$$
\begin{aligned}
Q_1 \;=\;& 2\,i\omega\,D_4 B_2 \cos\left(a\sqrt{1+\omega^2}\right) e^{\sqrt{1-\omega^2}(a+X_0)} \\
& -\left(\zeta_1^2\,B_2|B_2|^4 - \zeta_1\zeta_2\,B_1|B_2|^2 - \zeta_1\zeta_2 B_1|B_1|^2 + \zeta_2^2 B_2\right)\cos\left(a\sqrt{1+\omega^2}\right) e^{\sqrt{1-\omega^2}(a+X_0)} \\
& -2\,\omega\left(\left(\zeta_1 B_2|B_2|^4 - \zeta_2 B_1|B_2|^2\right)\Psi_7 + \left(\zeta_1 B_1|B_1|^2 - \zeta_2 B_2\right)\Psi_8\right) \\
& -\frac{1}{2}\left(3\,B_2|B_2|^4\Psi_7 + \left(B_1|B_2|^2 + B_2^2\bar{B}_1\right)\Psi_8 + B_2|B_2|^4\Psi_{13}\right) \\
& \times\cos^2\left(a\sqrt{1+\omega^2}\right) e^{2\sqrt{1-\omega^2}(a+X_0)} + \frac{1}{12}B_2|B_2|^4\cos^5\left(a\sqrt{1+\omega^2}\right) e^{5\sqrt{1-\omega^2}(a+X_0)} \\
& +B_1|B_1|^2\,\partial_0^2\Psi_1\left(X_0\right) + B_2\,\partial_0^2\Psi_2\left(X_0\right), \qquad (5.A.27)
\end{aligned}
$$

$$
\begin{aligned}
Q_2 \;=\;& 2\,i\omega\,D_4 B_2 \cos\left(X_0\sqrt{1+\omega^2}\right) \\
& -\left(\zeta_1^2\,B_2|B_2|^4 - \zeta_1\zeta_2\,B_1|B_2|^2 - \zeta_1\zeta_2 B_1|B_1|^2 + \zeta_2^2 B_2\right)\cos\left(X_0\sqrt{1+\omega^2}\right) \\
& -2\,\omega\left(\left(\zeta_1 B_2|B_2|^4 - \zeta_2 B_1|B_2|^2\right)\Psi_9 + \left(\zeta_1 B_1|B_1|^2 - \zeta_2 B_2\right)\Psi_{10}\right) \\
& +\frac{1}{2}\left(3\,B_2|B_2|^4\Psi_9 + \left(B_1|B_2|^2 + B_2^2\bar{B}_1\right)\Psi_{10} + B_2|B_2|^4\Psi_{14}\right)\cos^2\left(X_0\sqrt{1+\omega^2}\right) \\
& -\frac{1}{12}B_2|B_2|^4\cos^5\left(X_0\sqrt{1+\omega^2}\right) + B_1|B_1|^2\,\partial_0^2\Psi_3\left(X_0\right) + B_2\,\partial_0^2\Psi_4\left(X_0\right), \qquad (5.A.28)
\end{aligned}
$$

$$
\begin{aligned}
Q_3 \;=\;& 2\,i\omega\,D_4 B_2 \cos\left(a\sqrt{1+\omega^2}\right) e^{\sqrt{1-\omega^2}(a-X_0)} \\
& -\left(\zeta_1^2\,B_2|B_2|^4 - \zeta_1\zeta_2\,B_1|B_2|^2 - \zeta_1\zeta_2 B_1|B_1|^2 + \zeta_2^2 B_2\right)\cos\left(a\sqrt{1+\omega^2}\right) e^{\sqrt{1-\omega^2}(a-X_0)} \\
& -2\,\omega\left(\left(\zeta_1 B_2|B_2|^4 - \zeta_2 B_1|B_2|^2\right)\Psi_{11} + \left(\zeta_1 B_1|B_1|^2 - \zeta_2 B_2\right)\Psi_{12}\right) \\
& -\frac{1}{2}\left(3\,B_2|B_2|^4\Psi_{11} + \left(B_1|B_2|^2 + B_2^2\bar{B}_1\right)\Psi_{12} + B_2|B_2|^4\Psi_{15}\right) \\
& \times\cos^2\left(a\sqrt{1+\omega^2}\right) e^{2\sqrt{1-\omega^2}(a-X_0)} + \frac{1}{12}B_2|B_2|^4\cos^5\left(a\sqrt{1+\omega^2}\right) e^{5\sqrt{1-\omega^2}(a-X_0)} \\
& +B_1|B_1|^2\,\partial_0^2\Psi_5\left(X_0\right) + B_2\,\partial_0^2\Psi_6\left(X_0\right). \qquad (5.A.29)
\end{aligned}
$$

5.A.2 Functions in Section 5.3

$$W_1 = C_1 e^{\sqrt{(1-9\,\omega_1^2)/(1-S)}X_0} - \frac{(1+\omega_1^2)^{3/2}}{96\sqrt{2}}\, e^{\frac{\left(3\,v_2\left(\sqrt{(1-S)}v_1+\sqrt{1+\omega_1^2}X_0\right)\right)}{\sqrt{(1-S)}}}, \tag{5.A.30}$$

$$W_2 = C_2 \cos\left(\sqrt{(1+9\,\omega_1^2)/(1-S)}X_0\right) + \frac{1}{48\omega_1^2}\cos\left(\sqrt{(1+\omega_1^2)(1-S)}X_0\right) - \frac{1}{192}\cos\left(3\sqrt{(1+9\omega_1^2)(1-S)}X_0\right), \tag{5.A.31}$$

$$W_3 = C_1 e^{-\sqrt{(1-9\,\omega_1^2)/(1-S)}X_0} - \frac{(1+{\omega_1}^2)^{3/2}}{96\sqrt{2}}\, e^{\frac{\left(3\,v_2\left(\sqrt{(1-S)}v_1-\sqrt{1+\omega_1^2}X_0\right)\right)}{\sqrt{(1-S)}}}, \tag{5.A.32}$$

$$W_4 = C_1 e^{\sqrt{(1-9\,\omega_2^2)/(1+S)}X_0} - \frac{(1+\omega_2^2)^{3/2}}{96\sqrt{2}}\, e^{\frac{\left(3\,v_{22}\left(\sqrt{(1+S)}v_{11}+\sqrt{1+\omega_2^2}X_0\right)\right)}{\sqrt{(1+S)}}}, \tag{5.A.33}$$

$$W_5 = C_2 \cos\left(\sqrt{(1+9\,\omega_2^2)/(1+S)}X_0\right) + \frac{1}{48\omega_2^2}\cos\left(\sqrt{(1+\omega_2^2)(1+S)}X_0\right) - \frac{1}{192}\cos\left(3\sqrt{(1+9\omega_2^2)(1+S)}X_0\right), \tag{5.A.34}$$

$$W_6 = C_1 e^{-\sqrt{(1-9\,\omega_2^2)/(1+S)}X_0} - \frac{(1+\omega_2^2)^{3/2}}{96\sqrt{2}}\, e^{\frac{\left(3\,v_{22}\left(\sqrt{(1+S)}v_{11}-\sqrt{1+\omega_2^2}X_0\right)\right)}{\sqrt{(1+S)}}}, \tag{5.A.35}$$

with

$$v_1 = \arctan(v_2), \quad v_2 = \frac{\sqrt{1-\omega_1^2}}{\sqrt{1+\omega_1^2}}, \quad v_{11} = \arctan(v_{22}), \quad v_{22} = \frac{\sqrt{1-\omega_2^2}}{\sqrt{1+\omega_2^2}}.$$

$$\begin{aligned} P_{11} = {} & 2i\omega_1 D_4 B_1 \Phi_1 - B_1\left(\psi_1 |B_1|^2 + \psi_2 |B_2|^2\right)^2 \Phi_1 + \frac{1}{12} B_1 |B_1|^4 \Phi_1^5 + \frac{1}{4} B_1 |B_2|^4 \Phi_1 \Phi_2^4 \\ & -2\omega_1 \left(B_1 |B_1|^2 \psi_1 + B_1 |B_2|^2 \psi_2\right)\left(|B_1|^2 R_{(1,1)} + |B_2|^2 R_{(1,2)}\right) \\ & + \frac{1}{2} B_1 |B_1|^2 |B_2|^2 \Phi_1^3 \Phi_2^2 - \frac{1}{2} B_1 |B_1|^4 \left(\Phi_1{}^2 W_1 + 3\Phi_1^2 R_{(1,1)}\right) - \frac{1}{2} B_1 |B_1|^2 |B_2|^2 \\ & \times \left(2\,\Phi_2^2 R_{(1,1)} + 4\,\Phi_1 \Phi_2 S_{(1,2)} + 2\,\Phi_1 \Phi_2 V_4 + 2\,\Phi_1 \Phi_2 V_1 + 3\,\Phi_1^2 R_{(1,2)}\right) \\ & - \frac{1}{2} B_1 |B_2|^4 \left(\Phi_2^2 U_4 + \Phi_2^2 U_1 + 4\Phi_1 \Phi_2 S_{(1,1)} + 2\Phi_2^2 R_{(1,2)}\right), \end{aligned} \tag{5.A.36}$$

$$\begin{aligned} P_{12} = {} & 2\,i\omega_1 D_4 B_1 \Phi_1 - B_1\left(\psi_1 |B_1|^2 + \psi_2 |B_2|^2\right)^2 \Phi_1 - \frac{1}{12} B_1 |B_1|^4 \Phi_1^5 - \frac{1}{4} B_1 |B_2|^4 \Phi_1 \Phi_2^4 \\ & -2\,\omega_1 \left(B_1 |B_1|^2 \psi_1 + B_1 |B_2|^2 \psi_2\right)\left(|B_1|^2 R_{(2,1)} + |B_2|^2 R_{(2,2)}\right) \\ & - \frac{1}{2} B_1 |B_1|^2 |B_2|^2 \Phi_1^3 \Phi_2^2 + \frac{1}{2} B_1 |B_1|^4 \left(\Phi_1^2 W_2 + 3\Phi_1^2 R_{(2,1)}\right) + \frac{1}{2} B_1 |B_1|^2 |B_2|^2 \\ & \times \left(2\,\Phi_2^2 R_{(2,1)} + 4\,\Phi_1 \Phi_2 S_{(2,2)} + 2\,\Phi_1 \Phi_2 V_5 + 2\,\Phi_1 \Phi_2 V_2 + 3\,\Phi_1^2 R_{(2,2)}\right) \\ & + \frac{1}{2} B_1 |B_2|^4 \left(\Phi_2^2 U_5 + \Phi_2^2 U_2 + 4\,\Phi_1 \Phi_2 S_{(2,1)} + 2\,\Phi_2^2 R_{(2,2)}\right), \end{aligned} \tag{5.A.37}$$

$$
\begin{aligned}
P_{13} &= 2\,i\omega_1 D_4 B_1 \Phi_1 - B_1 \left(\psi_1 \left|B_1\right|^2 + \psi_2 \left|B_2\right|^2\right)^2 \Phi_1 + \frac{1}{12} B_1 \left|B_1\right|^4 \Phi_1^5 + \frac{1}{4} B_1 \left|B_2\right|^4 \Phi_1 \Phi_2^4 \\
&\quad -2\,\omega_1 \left(B_1 \left|B_1\right|^2 \psi_1 + B_1 \left|B_2\right|^2 \psi_2\right) \left(\left|B_1\right|^2 R_{(3,1)} + \left|B_2\right|^2 R_{(3,2)}\right) \\
&\quad + \frac{1}{2} B_1 \left|B_1\right|^2 \left|B_2\right|^2 \Phi_1{}^3 \Phi_2^2 - \frac{1}{2} B_1 |B_1|^4 \left(\Phi_1^2 W_3 + 3\Phi_1^2 R_{(3,1)}\right) - \frac{1}{2} B_1 |B_1|^2 |B_2|^2 \\
&\quad \times \left(2\Phi_2{}^2 R_{(3,1)} + 4\Phi_1 \Phi_2 S_{(3,2)} + 2\Phi_1 \Phi_2 V_6 + 2\Phi_1 \Phi_2 V_3 + 3\Phi_1{}^2 R_{(3,2)}\right) \\
&\quad - \frac{1}{2} B_1 |B_2|^4 \left(\Phi_2^2 U_6 + \Phi_2^2 U_3 + 4\Phi_1 \Phi_2 S_{(3,1)} + 2\Phi_2^2 R_{(3,2)}\right), \qquad (5.A.38)
\end{aligned}
$$

$$
\begin{aligned}
Q_{11} &= 2\,i\omega_2 D_4 B_2 \Phi_2 - B_2 \left(\psi_3 \left|B_2\right|^2 + \psi_4 \left|B_1\right|^2\right)^2 \Phi_2 + \frac{1}{12} B_2 \left|B_2\right|^4 \Phi_2^5 + \frac{1}{4} B_2 \left|B_1\right|^4 \Phi_1^4 \Phi_2 \\
&\quad -2\omega_2 \left(B_2 \left|B_2\right|^2 \psi_3 + B_2 \left|B_1\right|^2 \psi_4\right) \left(\left|B_2\right|^2 S_{(1,1)} + \left|B_1\right|^2 S_{(1,2)}\right) \\
&\quad + \frac{1}{2} B_2 \left|B_2\right|^2 \left|B_1\right|^2 \Phi_1^2 \Phi_2^3 - \frac{1}{2} B_2 \left|B_2\right|^4 \left(\Phi_2^2 W_4 + 3\,\Phi_2^2 S_{(1,1)}\right) - \frac{1}{2} B_2 \left|B_1\right|^2 \left|B_2\right|^2 \\
&\quad \times \left(2\,\Phi_1^2 S_{(1,1)} + 4\,\Phi_1 \Phi_2 R_{(1,2)} + 2\,\Phi_1 \Phi_2 U_4 + 2\,\Phi_1 \Phi_2 U_1 + 3\,\Phi_2^2 S_{(1,2)}\right) \\
&\quad - \frac{1}{2} B_2 \left|B_1\right|^4 \left(\Phi_1^2 V_4 + \Phi_1^2 V_1 + 4\,\Phi_1 \Phi_2 R_{(1,1)} + 2\,\Phi_1^2 S_{(1,2)}\right), \qquad (5.A.39)
\end{aligned}
$$

$$
\begin{aligned}
Q_{12} &= 2\,i\omega_2 D_4 B_2 \Phi_2 - B_2 \left(\psi_3 \left|B_2\right|^2 + \psi_4 \left|B_1\right|^2\right)^2 \Phi_2 - \frac{1}{12} B_2 \left|B_2\right|^4 \Phi_2^5 - \frac{1}{4} B_2 \left|B_1\right|^4 \Phi_1^4 \Phi_2 \\
&\quad -2\,\omega_2 \left(B_2 \left|B_2\right|^2 \psi_3 + B_2 \left|B_1\right|^2 \psi_4\right) \left(\left|B_2\right|^2 S_{(2,1)} + \left|B_1\right|^2 S_{(2,2)}\right) \\
&\quad - \frac{1}{2} B_2 \left|B_2\right|^2 \left|B_1\right|^2 \Phi_1^2 \Phi_2^3 + \frac{1}{2} B_2 \left|B_2\right|^4 \left(\Phi_2{}^2 W_5 + 3\,\Phi_2{}^2 S_{(2,1)}\right) + \frac{1}{2} B_2 \left|B_1\right|^2 \left|B_2\right|^2 \\
&\quad \times \left(2\,\Phi_1^2 S_{(2,1)} + 4\,\Phi_1 \Phi_2 R_{(2,2)} + 2\,\Phi_1 \Phi_2 U_5 + 2\,\Phi_1 \Phi_2 U_2 + 3\,\Phi_2^2 S_{(2,2)}\right) \\
&\quad + \frac{1}{2} B_2 \left|B_1\right|^4 \left(\Phi_1^2 V_5 + \Phi_1^2 V_2 + 4\,\Phi_1 \Phi_2 R_{(2,1)} + 2\,\Phi_1^2 S_{(2,2)}\right), \qquad (5.A.40)
\end{aligned}
$$

$$
\begin{aligned}
Q_{13} &= 2\,i\omega_2 D_4 B_2 \Phi_2 - B_2 \left(\psi_3 \left|B_2\right|^2 + \psi_4 \left|B_1\right|^2\right)^2 \Phi_2 + \frac{1}{12} B_2 \left|B_2\right|^4 \Phi_2^5 + \frac{1}{4} B_2 \left|B_1\right|^4 \Phi_1^4 \Phi_2 \\
&\quad -2\,\omega_2 \left(B_2 \left|B_2\right|^2 \psi_3 + B_2 \left|B_1\right|^2 \psi_4\right) \left(\left|B_2\right|^2 S_{(3,1)} + \left|B_1\right|^2 S_{(3,2)}\right) \\
&\quad + \frac{1}{2} B_2 \left|B_2\right|^2 \left|B_1\right|^2 \Phi_1^2 \Phi_2^3 - \frac{1}{2} B_2 \left|B_2\right|^4 \left(\Phi_2^2 W_6 + 3\,\Phi_2^2 S_{(3,1)}\right) - \frac{1}{2} B_2 \left|B_1\right|^2 \left|B_2\right|^2 \\
&\quad \times \left(2\,\Phi_1^2 S_{(3,1)} + 4\,\Phi_1 \Phi_2 R_{(3,2)} + 2\,\Phi_1 \Phi_2 U_6 + 2\,\Phi_1 \Phi_2 U_3 + 3\,\Phi_2^2 S_{(3,2)}\right) \\
&\quad - \frac{1}{2} B_2 \left|B_1\right|^4 \left(\Phi_1^2 V_6 + \Phi_1^2 V_3 + 4\,\Phi_1 \Phi_2 R_{(3,1)} + 2\,\Phi_1^2 S_{(3,2)}\right). \qquad (5.A.41)
\end{aligned}
$$

5.A.3 Functions in Section 5.4

$$
\begin{aligned}
Z_1 \;=\;& 2i\omega_1 D_4 B_1 \Phi_1 - \left(\psi_1 |B_1|^2 + \psi_2 |B_2|^2\right)\left(\psi_1 B_1 |B_1|^2 + \psi_2 B_1 |B_2|^2 + \eta_1 H\right)\Phi_1 \\
& -2\omega_1\left(\psi_1 B_1 |B_1|^2 + \psi_2 B_1 |B_2|^2 + \eta_1 H\right)\left(|B_1|^2 Y_{(1,1)} + |B_2|^2 Y_{(1,2)}\right) \\
& +\frac{1}{4} B_1 |B_2|^4 \Phi_1 \Phi_2^4 + \frac{1}{2} B_1 |B_1|^2 |B_2|^2 \Phi_1^3 \Phi_2^2 - \frac{1}{2}\left(W_1 + 3\,Y_{(1,1)}\right)\Phi_1^2 B_1 |B_1|^4 \\
& -\frac{1}{2}\left(2\,\Phi_2 Y_{(1,2)} + \Phi_2 U_4 + \Phi_2 U_1 + 4\,\Phi_1 S_{(1,1)}\right)\Phi_2 B_1 |B_2|^4 + \frac{1}{12} B_1 |B_1|^4 \Phi_1^5 \\
& -\frac{1}{2}\left(2\,Y_{(1,1)}\Phi_2^2 + 3\,Y_{(1,2)}\Phi_1^2 + 2\,\Phi_1\Phi_2 V_4 + 4\,\Phi_1\Phi_2 S_{(1,2)} + 2\,\Phi_1\Phi_2 V_1\right) \\
& \times B_1 |B_1|^2 |B_2|^2 - \frac{1}{2}\left({B_1}^2\Phi_1{}^2 + 2\,|B_1|^2\Phi_1^2 + 2\,|B_2|^2\Phi_2^2\right) H\,Y_{(1,3)}, \qquad \text{(5.A.42)}
\end{aligned}
$$

$$
\begin{aligned}
Z_2 \;=\;& 2i\omega_1 D_4 B_1 \Phi_1 - \left(\psi_1 |B_1|^2 + \psi_2 |B_2|^2\right)\left(\psi_1 B_1 |B_1|^2 + \psi_2 B_1 |B_2|^2 + \eta_1 H\right)\Phi_1 \\
& -2\omega_1\left(\psi_1 B_1 |B_1|^2 + \psi_2 B_1 |B_2|^2 + \eta_1 H\right)\left(|B_1|^2 Y_{(2,1)} + |B_2|^2 Y_{(2,2)}\right) \\
& -\frac{1}{4} B_1 |B_2|^4 \Phi_1 \Phi_2^4 - \frac{1}{2} B_1 |B_1|^2 |B_2|^2 \Phi_1^3 \Phi_2^2 + \frac{1}{2}\left(W_2 + 3\,Y_{(2,1)}\right)\Phi_1^2 B_1 |B_1|^4 \\
& +\frac{1}{2}\left(2\,\Phi_2 Y_{(2,2)} + \Phi_2 U_5 + \Phi_2 U_2 + 4\,\Phi_1 S_{(2,1)}\right)\Phi_2 B_1 |B_2|^4 - \frac{1}{12} B_1 |B_1|^4 \Phi_1^5 \\
& +\frac{1}{2}\left(2\,Y_{(2,1)}{\Phi_2}^2 + 3\,Y_{(2,2)}{\Phi_1}^2 + 2\,\Phi_1\Phi_2 V_5 + 4\,\Phi_1\Phi_2 S_{(2,2)} + 2\,\Phi_1\Phi_2 V_2\right) \\
& \times B_1 |B_1|^2 |B_2|^2 + \frac{1}{2}\left({B_1}^2\Phi_1^2 + 2\,|B_1|^2\Phi_1^2 + 2\,|B_2|^2\Phi_2^2\right) H\,Y_{(2,3)}, \qquad \text{(5.A.43)}
\end{aligned}
$$

$$
\begin{aligned}
Z_3 \;=\;& 2i\omega_1 D_4 B_1 \Phi_1 - \left(\psi_1 |B_1|^2 + \psi_2 |B_2|^2\right)\left(\psi_1 B_1 |B_1|^2 + \psi_2 B_1 |B_2|^2 + \eta_1 H\right)\Phi_1 \\
& -2\omega_1\left(\psi_1 B_1 |B_1|^2 + \psi_2 B_1 |B_2|^2 + \eta_1 H\right)\left(|B_1|^2 Y_{(3,1)} + |B_2|^2 Y_{(3,2)}\right) \\
& +\frac{1}{4} B_1 |B_2|^4 \Phi_1 \Phi_2^4 + \frac{1}{2} B_1 |B_1|^2 |B_2|^2 \Phi_1^3 \Phi_2^2 - \frac{1}{2}\left(W_3 + 3\,Y_{(3,1)}\right)\Phi_1^2 B_1 |B_1|^4 \\
& -\frac{1}{2}\left(2\,\Phi_2 Y_{(3,2)} + \Phi_2 U_6 + \Phi_2 U_3 + 4\,\Phi_1 S_{(3,1)}\right)\Phi_2 B_1 |B_2|^4 + \frac{1}{12} B_1 |B_1|^4 \Phi_1^5 \\
& -\frac{1}{2}\left(2\,Y_{(3,1)}\Phi_2^2 + 3\,Y_{(3,2)}\Phi_1^2 + 2\,\Phi_1\Phi_2 V_6 + 4\,\Phi_1\Phi_2 S_{(3,2)} + 2\,\Phi_1\Phi_2 V_3\right) \\
& \times B_1 |B_1|^2 |B_2|^2 - \frac{1}{2}\left({B_1}^2\Phi_1^2 + 2\,|B_1|^2\Phi_1^2 + 2\,|B_2|^2\Phi_2^2\right) H\,Y_{(3,3)}. \qquad \text{(5.A.44)}
\end{aligned}
$$

CHAPTER 6

Conclusions and future work

In this study, we have investigated defect modes of long Josephson junctions with phase shifts. In order to study long Josephson junctions, we have considered a variety of ac-driven, inhomogeneous sine-Gordon equations modelling an infinitely long Josephson junctions with phase shifts, driven by a microwave field. Here, we briefly summarize the main results of the work done throughout this project.

6.1 Summary

To begin with, Chapter 1 presented a brief review of superconductivity, its history, extraordinary features and some recent progress in the topic, followed by description of static and dynamic properties of Josephson junctions. The sine-Gordon equation was derived as a model for long Josephson junctions. Some important applications of Josephson junctions were explained and discussed, namely Josephson junctions with phase shifts, particularly $0-\pi-0$ and $0-\kappa$ long Josephson junctions.

Furthermore, the general theory of solitons and their applications were also explained. We discussed special solutions of the sine-Gordon equation, in particular kinks and breathers, and briefly described various properties and applications of the equation. We also introduced the historical and physical background of asymptotic techniques, and discussed multiple scales expansions and the method of averaging. The chapter was concluded by a brief overview of the thesis.

In Chapter 2, a spatially inhomogeneous sine-Gordon equation with a time-periodic drive was investigated. This modelled a microwave–driven long Josephson junctions with phase-shifts. We constructed a perturbation expansion for small-amplitude oscillations of the breathing mode, and derived differential equations for the slowly varying amplitude of the oscillation for the $0-\pi-0$ and $0-\kappa$ Josephson junctions respectively,

by eliminating secular terms from the expansions.

Our obtained amplitude equations do not predict unbounded or growing amplitude. This shows that the emission of radiation has the effect of damping the wobbling. The damping is present because the breathing mode emits radiation due to frequency tripling effect of the nonlinearity, which causes the breathing mode to become a source of radiation. The predictions of these amplitude equations were found to agree well with numerical simulations of the original sine-Gordon equation.

The solitons in the sine-Gordon equation do not excite radiation waves, when the frequency lies in the discrete spectrum. However, higher harmonics generated by the nonlinearity will certainly be resonant with linear modes, and therefore can be excited and generate a radiative tail which will gradually drain energy from the oscillating hump. The oscillation in the sine-Gordon equation was observed by Peyrard *et al.* [185], but has been shown to be the consequence of the discretization of the equation for numerical simulation rather than a property of the governing equation itself.

In this study, in the absence of an ac-drive, we obtained a breathing mode oscillation which decays with rates of at most $\mathcal{O}(t^{-1/4})$ and $\mathcal{O}(t^{-1/2})$ for junctions with a uniform and nonuniform ground states, respectively. The problem and results presented herein are novel and important from several points of view. Our fractional wobbling kink is in principle different from the "normal" wobbler discussed in [99, 100, 107, 108, 109]. Usually, a wobbler is a periodically expanding and contracting kink, due to the interaction of the kink and its *odd* eigenmode. Because our system is not translationally invariant, our wobbler is composed of a fractional kink and an *even* eigenmode, representing a topological excitation oscillating about the discontinuity point. The coupling of a spatially localized breathing mode to radiation modes via a nonlinearity with the same decay rates has been discussed and obtained before for ϕ^4 wobblers [99, 100] and for sine-Gordon wobblers [107, 108, 109].

Next, we applied the method of multiple scales to detect a resonance in the presence of external driving in the case when the natural frequency of the system is close to the driving frequency for $0-\pi-0$ and $0-\kappa$ junctions. The internal mode excitation by direct or parametric driving has been discussed and obtained before in several context e.g., in [99, 100, 186, 187].

Here, we consider the same form of direct driving and the similar resonant frequencies as discussed by Quintero, Sánchez and Mertens in [186, 187, 188]. The authors used a variational approach which neglects the radiation, by assuming a specific functional dependence of the kink on the collective coordinates. Using asymptotic expansion, we detect a resonance when the kink is directly driven at its natural frequency. Unlike the

variational approach reported by Quintero, Sánchez and Mertens [186, 188] perturbation theory does not neglect radiation, an effect which is confirmed by our results. This suggests that radiation can play a role in the transfer of energy to the internal mode.

In the presence of an external drive, the amplitude equations obtained show that there is a balance of energy input into the breathing mode due to the external drive and the radiative damping. We have discussed whether the breathing mode of a junction with a phase shift can be excited to switch the junction into a resistive state. It was conjectured before by Buckenmaier *et al.* [38] that the driving frequency at which switching from the superconducting to the resistive state occurs is the same as the eigenfrequency of the ground state.

Using multiple scales expansions, it was shown that in an infinitely long Josephson junction, an external drive cannot excite the defect mode of a junction, i.e., a breathing mode, to switch the junction into a resistive state. For a small amplitude drive, there is an energy balance between the input given by the external drive and the energy output due to so-called radiative damping experienced by the mode. We discussed that when the external drive amplitude is large enough, the junction can indeed switch to a resistive state. This is caused by a modulational instability of the continuous wave emitted by the oscillating mode.

In Chapter 3, the dynamics of long Josephson junctions with phase-shifts in the presence of a rapidly varying driving force modelled by a periodically driven sine-Gordon equation were studied. The experimentally relevant case of large driving frequency compared to the system's plasma frequency was considered. The case of small driving frequency has been considered theoretically in [38, 39] and in Chapter 2. An average equation for the slowly-varying dynamics was derived analytically, using multiple scales analysis. The equations obtained take the form of a damped, forced double sine-Gordon equation.

A double sine-Gordon equation describing the slow-time dynamics of a rapidly driven sine-Gordon equation without phase shift was obtained previously through approximating the phase $\phi(x,t)$ by a Fourier series expansion [134, 135] and using a normal form technique [122]. In the normal form technique, several canonical transformations are applied to the Hamiltonian system to move terms with mean-zero to higher order [136, 137]. Kivshar *et al.* [134, 135] decomposed the phase $\phi(x,t)$ into the sum of slowly- and rapidly- varying parts. Their method solely uses asymptotic expansions rather than averaging over the fast oscillation. In both methods, the coefficients of the double sine-Gordon equation are given in terms of Bessel functions.

With the method proposed herein, one has more control over the scales of the driving

parameters and the coefficients of the 'average' equation are given by simple explicit functions. The critical value of the applied constant bias current γ_c for the $0-\kappa$ junctions and the critical facet length in the absence of external constant bias current for the $0-\pi-0$ junctions were obtained analytically from the averaged double sine-Gordon equation.

In the absence of an ac drive, studying the stability of the constant solution in $0-\pi-0$ junction, one finds that there is a critical facet length $a_c = \pi/4$ above which the solution is unstable and the ground state is spatially nonuniform [32], which represents a pair of fractional fluxons of opposite polarities. Here, it was shown analytically and numerically that in the presence of an ac drive the threshold length a_c in $0-\pi-0$ junction increases. We compared our approximation as well as that obtained in [134, 135] with numerics. It was observed that the numerics slightly deviates at a particular driving amplitude. Using our method, it seems that we require a different scaling of an external drive amplitude mentioned in this work. The applicability of the method presented in this work in that case is suggested as future work.

Next, the effect of ac-drive on the critical bias current of a $0-\kappa$ junction was studied. Here, we only considered the case of $\kappa = \pi$, which is representative for this type of junctions as the other values of κ can be calculated similarly.

It is known that in the presence of an applied dc bias current ($\gamma \neq 0$), the fractional fluxon will be deformed. When the current is large enough, the static ground state ceases to exist and the junction switches to a resistive state by alternately releasing travelling fluxons and antifluxons in opposite directions. In the absence of an external ac-drive the minimum current at which the junction switches to such a state is called the critical current $\gamma_c = 2\sin(\kappa/2)/\kappa$ as obtained in [132, 133]. Hence, $0-\pi$ junctions are in a resistive state when $\gamma > 2/\pi$ with fluxons and antifluxons being periodically released from the discontinuity.

Using numerical simulations as well as asymptotic approximations, the critical bias current in the presence of an external ac-drive in $0-\kappa$ junctions was determined. This study showed numerically that in the presence of an ac drive the value of the critical bias current γ_c decreased which confirmed our approximation.

In Chapter 4, a spatially inhomogeneous sine-Gordon equation with time-periodic drive and two regions of π phase shift, modelling $0-\pi-0-\pi-0$ long Josephson junctions was investigated. The internal phase shift formation acts as a double well potential. Due to the type of the inhomogeneities, there is a pair of eigenmodes of different symmetries, *i.e.* symmetric and antisymmetric (or, even and odd). We constructed the perturbation expansion for the coupled modes and obtained differential equations

for the slow time evolution of the oscillation amplitude in the $0-\pi-0-\pi-0$ long Josephson junctions.

In the absence of an ac-drive, the coupled amplitude equations describe a gradual decrease in the amplitude of the coupled mode oscillations which is due to the energy emission in the form of radiation. Similar investigations of the effects of radiation, the resonance of breathing modes at its natural oscillating frequency, and the decay rates of the single mode oscillation for sine-Gordon equation in the context of long Josephson junctions and for the wobbling kinks in ϕ^4 models have been discussed and obtained in [99, 100, 101].

Using multiple scale expansions, we have shown that due to the energy transfer from the discrete to continuous modes, the two mode oscillation decays algebraically in the long time regime. The flow of energy from resonant discrete modes to continuous modes due to the nonlinear coupling has been addressed in [149, 150]. The phenomenon which is responsible for the time decay in the coupled modes due to the energy transfer from the discrete to continuous modes in nonlinear Klein-Gordon equations and for nonlinear Schrödinger equations is analyzed by Soffer, Weinstein, Sigal, and others, in [151, 152, 153, 154].

In this thesis, the resonance conditions were discussed when the antisymmetric mode is excited, while the symmetric mode lies in the discrete spectrum. Interestingly solutions of the coupled amplitude equations still decay in time. This shows that the two modes influence each other in the long time regime. It was also shown that, by exciting one mode only, the decay rate is significantly reduced over the long time compared to the two modes.

Next, we investigated the coupled mode oscillations in the presence of an ac-drive. The modes do not oscillate with an unbounded or growing amplitude. We observed that, for a small drive amplitude, there is a balance between the energy input given by the external drive and the energy output due to the radiative damping experienced by the coupled modes.

Comparing the amplitudes of the two modes, we obtained that the amplitude of the symmetric mode oscillates and slowly tends to a steady state when $t \to \infty$, while the envelope of the antisymmetric mode vanishes. This shows that an ac-drive acts as a damping to antisymmetric mode. In other words, we have a synchronized oscillations of localised modes in the two wells. In a double well potential, it has been found by Jackson *et al.* [189] that asymmetric state localised in one of the wells bifurcates from symmetric one. This bifurcation results in the instability of the symmetric state, leading to the asymmetric wave form becoming the ground state of the system [189, 190].

In this thesis, it was concluded from asymptotic calculations as well as from numerical computations that the regular oscillation of the modes indicates that the junction voltage vanishes, even when the driving frequency is the same as one of the system's eigenfrequency as in the case discussed in Chapter 2, as well as obtained in [38, 39] in the single well of long Josephson junctions.

Lastly, in Chapter 5, we have considered a spatially inhomogeneous coupled sine-Gordon equations with a time periodic drive, modelling stacked long Josephson junctions with a phase shift. Using multiscale expansions, we derived coupled amplitude equations considering strong and weak magnetic coupling, $S \sim \mathcal{O}(1)$ and $S \sim \mathcal{O}(\epsilon^2)$, in the absence of an ac-drive. The coupling term between the stacked Josephson junctions depends on the physical and geometrical parameters of the system. The multiscale expansions are asymptotic, i.e. only valid for small amplitudes of the breathing modes. In the small initial amplitude limit the expansion is expected to provide an accurate description of the breather.

The dynamics of the coupled sine-Gordon equation has been extensively studied before for weak and strong coupling [170, 181, 182] to investigate different phenomenon in stacked Josephson junctions, such as voltage locking [175, 176] and current locking [177, 178, 179] in Josephson junctions. However, the coupled sine-Gordon equation in the context of stacked Josephson junctions with phase shifts is considered here for the first time.

The analytical approximations of breathing modes in stacked Josephson junctions in the limit of small initial amplitudes were calculated. The coupled amplitude equations were obtained, these describe the gradual decrease of the oscillation amplitude, as the modes emits energy in the form of radiation. It was shown that the emission of radiation has the effect of damping the breathing. The damping is present because the breathing mode emits radiation due to the frequency tripling effect of the nonlinearity which caused breather to become a source of radiation. Solutions of the amplitude equations decay at the same rate, which causes the Josephson junctions to synchronize. We showed that, a breathing mode decays with a rate of at most $\mathcal{O}\left(t^{-1/4}\right)$ for the stacked Josephson junctions with a uniform ground state.

The observation of electromagnetic radiation from a Josephson junction has been discussed by many authors. The radiation at Fiske steps was detected by Yanson *e*t al. [191], Langenberg *e*t al. [192] and Dayem *e*t al. [193]. The radiation caused by motion of solitons was reported before by Dueholm *et al.* [183]. The radiative annihilation in coupled sine-Gordon equation which occurs during the decay of breather has been discussed by Krasnov [184]. This phenomena may be useful for achieving superradiant

emission from coupled oscillators.

We also considered strong coupling, $S \sim \mathcal{O}(1)$ with a time periodic drive. In this case, the solutions of the amplitude equations do not decay to zero as $t \to \infty$. Due to the driving terms, there is a steady state solution. We expect that a nonzero external drive induces a breathing mode oscillation in the stacked long Josephson junctions, as in our investigation for single Josephson junctions with phase shift in Chapter 2.

6.2 Future work

In the course of this study, we have left several problems which require further investigation. Despite the agreement with the experiments obtained herein, our analysis in Chapter 2 is based on a simplified model. It is of interest to extend the study to the case of *dc, driven long but finite* Josephson junctions with phase-shifts, as used experimentally in [38, 39]. These papers report that a microwave drive can be used to measure experimentally the eigenfrequency of a junction's ground state. Such microwave spectroscopy is based on the observation that when the frequency of the applied microwave is in the vicinity of the natural frequency of the ground state, the junction can switch to a resistive state, characterized by a non-zero junction voltage.

It was conjectured that the process is analogous to the resonance phenomenon of a simple pendulum driven by a time periodic external force. In the case of long junctions with phase-shifts, it would be resonance between the internal breathing mode of the ground state and the microwave field. Nonetheless, it was also reported that the microwave power needed to switch the junction into a resistive state depends on the magnitude of the eigenfrequency to be measured.

In microwave driven finite junctions, the boundaries can be a major external drive (see, e.g., [114, 115]), an effect which is not present in this study. A constant *dc* bias current, which plays an important role in the measurements reported in [38], is not included in our work, even though the results presented herein should still hold for small constant drive. Another open problem is the interaction of multiple defect modes [116] in Josephson junctions with phase-shifts, which is addressed in Chapter 4. This is experimentally relevant, as so-called zigzag junctions have been successfully fabricated by Hilgenkamp *et al.* [23].

Other future work is to investigate the question of oscillations as discussed in Chapter 4. The resulting dynamical systems become more challenging and interesting as the number of wells is increased. The dynamics of solitary waves in nonlinear optics made of photorefractive media and in Bose-Einstein condensates in the presence of

three wells has been considered by Koyama *et al.* [194] and Kapitula in *et al.* [195]. In particular, we will investigate the problem when one increases the number of wells to infinity.

For, the system of coupled sine-Gordon equations considered in Chapter 5 for long Josephson junctions with phase shifts, the obtained approximate solutions will be analyzed with numerics for synchronized oscillation modes. The synchronized oscillation has been demonstrated experimentally before by Barbara *et al.* [196] for Josephson junctions.

The mechanism for synchronization of a Josephson junction array has been studied, based on the generalized Kuramoto models in many contexts, e.g., in [197, 198, 199, 200]. The model explains how mutually interacting oscillators, each of which has a different natural frequency, can undergo a sharp macroscopic transition from a disordered to a coherent dynamical state when the coupling constant exceeds a critical threshold.

The analysis obtained in Chapter 5 will be extended to multi-stacked long Josephson junctions with phase shift. The development of large stacks is a promising way to integrate radiation sources and perhaps to address the issue of the mechanism of THz emission. Recently, a significant THz emission has been reported for intrinsic Josephson junctions [201, 202]. The method for the synchronization for coherent THz emission in Josephson junctions have been discussed before by Machida and Tachiki in [203, 204]. Numerical simulations by several authors [205, 206, 207] showed that the formation of the dynamical phase variation yields electromagnetic THz radiation.

The effect of external drives in the stacked Josephson junctions will be investigated using the result obtained in Chapter 5. The study will be extended to multi-stacked long Josephson junctions with phase shift. This problem has been previously reported in [38, 39] for single Josephson junctions.

We will also investigate switching from superconducting to a resistive state in stacked Josephson junction, when the driving frequency is the same as the eigenfrequency of the ground state. This problem has been studied numerically in Chapter 2 and experimentally by Buckenmaier *et al.* [38] for single long Josephson junctions.

Bibliography

[1] W. Meissner and R. Ochsenfeld. Ein neuer effekt bei eintritt der supraleitfähigkeit. *Naturwissenschaften*, **21**, (1933).

[2] F. London and H. London. The electromagnetic equations of the supraconductor. *Proc. Roy. Soc. London Ser. A*, **149**:71 – 88, (1935).

[3] R.P. Feynman, R.B. Leighton, and M.L. Sands. *The Feynman Lectures on Physics*. Addison-Wesley, (1965).

[4] S. Fujita, K. Ito, and S. Godoy. *Quantum theory of conducting matter: superconductivity*. Springer, (2009).

[5] S. Fujita and S. Godoy. *Theory of high temperature superconductivity*. Kluwer Academic Publishers, (2001).

[6] M. Sigrist and T. M. Rice. Unusual paramagnetic phenomena in granular high-temperature superconductors–A consequence of *d*- wave pairing? *Rev. Mod. Phys.*, **67**:503–513, (1995).

[7] M. H. S. Amin, A. N. Omelyanchouk, and A. M. Zagoskin. Mechanisms of spontaneous current generation in an inhomogeneous *d* -wave superconductor. *Phys. Rev. B*, **63**:212502, (2001).

[8] E. Goldobin, D. Koelle, and R. Kleiner. Semifluxons in long Josephson $0-\pi$-junctions. *Phys. Rev. B*, **66**:100508, (2002).

[9] K. K. Likharev. *Dynamics of Josephson Junctions and Circuits*. Gordon and Breach Science Publishers, New York, (1986).

[10] M. Weides. *Josephson Tunnel Junctions with Ferromagnetic Interlayer*. Forschungszentrum, Zentralbibliothek, (2006).

[11] M. Tinkham. *Introduction to superconductivity*. Dover Publications, (2004).

[12] T.P. Orlando and K.A. Delin. *Foundations of applied superconductivity*. Addison-Wesley, (1991).

[13] E. Goldobin, D. Koelle, and R. Kleiner. Semifluxons in long Josephson 0-π-junctions. *Phys. Rev. B*, **66**:100508, (2002).

[14] L. N. Bulaevskii, V. V. Kuzii, and A. A. Sobyanin. Superconducting system with weak coupling to the current in the ground state. *JETP Lett.*, **25**:290 – 294, (1977).

[15] L. N. Bulaevskii, V. V. Kuzii, A. A. Sobyanin, and P. N. Lebedev. On possibility of the spontaneous magnetic flux in a Josephson junction containing magnetic impurities. *Solid State Commun.*, **25**:1053 – 1057, (1978).

[16] C. M. Pegrum. Applied physics: Can a fraction of a quantum be better than a whole one? *Science*, **312**:1483 – 1484, (2006).

[17] T. Ortlepp, Ariando, O. Mielke, C. J. M. Verwijs, K. F. K. Foo, H. Rogalla, F. H. Uhlmann, and H. Hilgenkamp. Flip-flopping fractional flux quanta. *Science*, **312**: 1495 – 1497, (2006).

[18] H. Hilgenkamp. π-phase shift Josephson structures. *Supercond. Sci. Tech.*, **21**: 034011, (2008).

[19] C. Gürlich, E. Goldobin, R. Straub, D. Doenitz, Ariando, H. H. Smilde, H. Hilgenkamp, R. Kleiner, and D. Koelle. Imaging of order parameter induced π phase shifts in cuprate superconductors by low-temperature scanning electron microscopy. *Phys. Rev. Lett.*, **103**:067011, (2009).

[20] C. C. Tsuei and J. R. Kirtley. Pairing symmetry in cuprate superconductors. *Rev. Mod. Phys.*, **72**:969 – 1016, (2000).

[21] H. J. H. Smilde, Ariando, D. H. A. Blank, G. J. Gerritsma, H. Hilgenkamp, and H. Rogalla. D-wave-induced Josephson current counterflow in $YBa_2Cu_3O_7/Nb$ zigzag junctions. *Phys. Rev. Lett.*, **88**:057004 – 1, (2002).

[22] D. J. Van Harlingen. Phase-sensitive tests of the symmetry of the pairing state in the high-temperature superconductors—evidence for $d_{x^2-y^2}$ symmetry. *Rev. Mod. Phys.*, **67**:515 – 535, (1995).

[23] H. Hilgenkamp, Ariando, H. J. H. Smilde, D. H. A. Blank, G. Rijnders, H. Rogalla, J. R. Kirtley, and C. C. Tsuei. Ordering and manipulation of the magnetic moments in large-scale superconducting π-loop arrays. *Nature*, **422**:50, (2003).

[24] F. Lombardi, F. Tafuri, F. Ricci, F. Miletto Granozio, A. Barone, G. Testa, E . Sarnelli, J. R. Kirtley, and C. C. Tsuei. Intrinsic d-wave effects in $YBa_2Cu_3O_{7-\delta}$ grain boundary Josephson junctions. *Phys. Rev. Lett.*, **89**:207001, (2002).

[25] M. Weides, H. Kohlstedt, R. Waser, M. Kemmler, J. Pfeiffer, D. Koelle, R. Kleiner, and E. Goldobin. Ferromagnetic $0-\pi$ Josephson junctions. *Appl. Phys. A*, **89**:613 – 617, (2007).

[26] S. M. Frolov, D. J. Van Harlingen, V. V. Bolginov, V. A. Oboznov, and V. V. Ryazanov. Josephson interferometry and Shapiro step measurements of superconductor-ferromagnet-superconductor $0-\pi$ junctions. *Phys. Rev. B*, **74**: 020503, (2006).

[27] H. Susanto and S. A. van Gils. Instability of a lattice semifluxon in a current-biased $0-\pi$ array of Josephson junctions. *Phys. Rev. B*, **69**:092507, (2004).

[28] E. Berg, E. Fradkin, and S. A. Kivelson. Theory of the striped superconductor. *Phys. Rev. B*, **79**:064515, (2009).

[29] E. Goldobin, A. Sterck, T. Gaber, D. Koelle, and R. Kleiner. Dynamics of semifluxons in Nb long Josephson $0-\pi$ junctions. *Phys. Rev. Lett.*, **92**:057005, (2004).

[30] B. A. Malomed and A. V. Ustinov. Creation of classical and quantum fluxons by a current dipole in a long Josephson junction. *Phys. Rev. B*, **69**:064502, (2004).

[31] E. Goldobin, D. Koelle, and R. Kleiner. Ground states of one and two fractional vortices in long Josephson $0-\kappa$ junctions. *Phys. Rev. B*, **70**:174519, (2004).

[32] T. Kato and M. Imada. Vortices and quantum tunneling in current-biased $0-\pi-0$ Josephson junctions of d-wave superconductors. *J. Phys. Soc. Jpn.*, **66**:1445 – 1449, (1997).

[33] E. Goldobin, H. Susanto, D. Koelle, R. Kleiner, and S. A. van Gils. Oscillatory eigenmodes and stability of one and two arbitrary fractional vortices in long Josephson $0-\kappa$ junctions. *Phys. Rev. B*, **71**:104518, (2005).

[34] S. Ahmad, H. Susanto, and J. A. D. Wattis. Existence and stability analysis of finite $0-\pi-0$ Josephson junctions. *Phys. Rev. B*, **80**:064515, (2009).

[35] G. Derks, A. Doelman, S. A. van Gils, and H. Susanto. Stability analysis of π-kinks in a $0-\pi$ Josephson junction. *SIAM J. Appl. Dyn. Syst.*, **6**:99 – 141, (2007).

[36] K. Vogel, W. P. Schleich, T. Kato, D. Koelle, R. Kleiner, and E. Goldobin. Theory of fractional vortex escape in a long Josephson junction. *Phys. Rev. B*, **80**:134515, (2009).

[37] E. Goldobin, K. Vogel, O. Crasser, R. Walser, W. P. Schleich, D. Koelle, and R. Kleiner. Quantum tunneling of semifluxons in a $0-\pi-0$ long Josephson junction. *Phys. Rev. B*, **72**:054527, (2005).

[38] K. Buckenmaier, T. Gaber, M. Siegel, D. Koelle, R. Kleiner, and E. Goldobin. Spectroscopy of the fractional vortex eigenfrequency in a long Josephson $0-\kappa$ junction. *Phys. Rev. Lett.*, **98**:117006, (2007).

[39] J. Pfeiffer, T. Gaber, D. Koelle, R. Kleiner, E. Goldobin, M. Weides, H. Kohlstedt, J. Lisenfeld, A. K. Feofanov, and A. V. Ustinov. Escape rate measurements and microwave spectroscopy of 0, π, and $0-\pi$ ferromagnetic Josephson tunnel junctions. *arXiv:0903.1046*, (2009).

[40] P. D. Shaju and V. C. Kuriakose. Logic gates using stacked Josephson junctions. *Physica C*, **322**:163 – 168, (1999).

[41] K. Nakajima, Y. Onodera, and Y. Ogawa. Logic design of Josephson network. *J. Appl. Phys.*, **47**:1620 – 1627, (1976).

[42] K. Nakajima and Y. Onodera. Logic design of Josephson network. II. *J. Appl. Phys.*, **49**:2958 – 2963, (1978).

[43] J. R. Kirtley, C. C. Tsuei, and K. A. Moler. Temperature dependence of the half-integer magnetic flux quantum. *Science*, **285**:1373 – 1375, (1999).

[44] J. R. Kirtley, C. C. Tsuei, Martin Rupp, J. Z. Sun, Lock See Yu-Jahnes, A. Gupta, M. B. Ketchen, K. A. Moler, and M. Bhushan. Direct imaging of integer and half-integer Josephson vortices in high- T_c grain boundaries. *Phys. Rev. Lett.*, **76**:1336 – 1339, (1996).

[45] A. Barone and G. Paternó. *Physics and Applications of the Josephson Effect*. Wiley, New York, (1982).

[46] M. Beck, E. Goldobin, M. Neuhaus, M. Siegel, R. Kleiner, and D. Koelle. High-efficiency deterministic Josephson vortex ratchet. *Phys. Rev. Lett.*, **95**:090603, (2005).

[47] F. Marchesoni, S. Savel'ev, and F. Nori. Achieving optimal rectification using underdamped rocked ratchets. *Phys. Rev. E*, **73**:021102, (2006).

[48] I. Zapata, R. Bartussek, F. Sols, and P. Hänggi. Voltage rectification by a SQUID ratchet. *Phys. Rev. Lett.*, **77**:2292 – 2295, (1996).

[49] G. Hechtfischer, R. Kleiner, A. V. Ustinov, and P. Müller. Non-Josephson emission from intrinsic junctions in $Bi_2Sr_2CaCu_2O_{8+y}$: Cherenkov radiation by Josephson vortices. *Phys. Rev. Lett.*, **79**:1365 – 1368, (1997).

[50] J. Q. You and F. Nori. Superconducting circuits and quantum information. *Phys. Today*, **58**:42 – 47, (2005).

[51] L. N. Bulaevskii and A. E. Koshelev. Radiation due to Josephson oscillations in layered superconductors. *Phys. Rev. Lett.*, **99**:057002, (2007).

[52] M. H. Bae, H. J. Lee, and J. H. Choi. Josephson-vortex-flow terahertz emission in layered high-T_c superconducting single crystals. *Phys. Rev. Lett.*, **98**:027002, (2007).

[53] E. Goldobin, A. Sterck, and D. Koelle. Josephson vortex in a ratchet potential: theory. *Phys. Rev. E*, **63**:031111, (2001).

[54] G. Carapella. Relativistic flux quantum in a field-induced deterministic ratchet. *Phys. Rev. B*, **63**:054515, (2001).

[55] F. Falo, P. J. Martínez, J. J. Mazo, and S. Cilla. Ratchet potential for fluxons in Josephson-junction arrays. *Europhys. Lett.*, **45**:700, (1999).

[56] E. Trías, J. J. Mazo, F. Falo, and T. P. Orlando. Depinning of kinks in a Josephson-junction ratchet array. *Phys. Rev. E*, **61**:2257 – 2266, (2000).

[57] M. Grifoni, M. S. Ferreira, J. Peguiron, and J. B. Majer. Quantum ratchets with few bands below the barrier. *Phys. Rev. Lett.*, **89**:146801, (2002).

[58] J. B. Majer, J. Peguiron, M. Grifoni, M. Tusveld, and J. E. Mooij. Quantum ratchet effect for vortices. *Phys. Rev. Lett.*, **90**:056802, (2003).

[59] M. O. Magnasco. Forced thermal ratchets. *Phys. Rev. Lett.*, **71**:1477 – 1481, (1993).

[60] A. Davidson, B. Dueholm, B. Kryger, and N. F. Pedersen. Experimental investigation of trapped sine-Gordon solitons. *Phys. Rev. Lett.*, **55**:2059 – 2062, (1985).

[61] A. Davidson, B. Dueholm, and N. F. Pedersen. Experiments on soliton motion in annular Josephson junctions. *J. Appl. Phys.*, **60**:1447 – 1454, (1986).

[62] M. P. Lisitskii, G. Ammendola, D. V. Balashov, A. Barone, R. Cristiano, E. Esposito, L. Frunzio, V. N. Gubankov, C. Nappi, S. Pagano, L. Parlato, G. Peluso, and G. Pepe. Annular Josephson junctions for radiation detection: fabrication and investigation of the magnetic behaviour. *Nucl. Instrum. Methods. Phys. Res.*, **444**:476 – 479, (2000).

[63] A. Wallraff, Yu. Koval, M. Levitchev, M. V. Fistul, and A. V. Ustinov. Annular long Josephson junctions in a magnetic field: Engineering and probing the fluxon interaction potential. *J. Low Temp. Phys.*, **118**:543 – 553, (2000).

[64] A. Kemp, A. Wallraff, and A. V. Ustinov. Josephson vortex qubit: design, preparation and read-out. *Phys. Stat. Sol. B*, **233**:472 – 481, (2002).

[65] A. R. Bishop, K. Fesser, P. S. Lomdahl, and S. E. Trullinger. Influence of solitons in the initial state on chaos in the driven damped sine-Gordon system. *Physica D*, **7**:259 – 279, (1983).

[66] A. Mazor, A. R. Bishop, and D. W. McLaughlin. Phase-pulling and space-time complexity in an ac driven damped one-dimensional sine-Gordon system. *Phys. Lett. A*, **119**:273 – 279, (1986).

[67] P. S. Lomdahl and M. R. Samuelsen. Persistent breather excitations in an ac-driven sine-Gordon system with loss. *Phys. Rev. A*, **34**:664 – 667, (1986).

[68] A. Mazor and A. R. Bishop. Phase-pulling and breather instability in an ac-driven damped one-dimensional sine-Gordon system. *Physica D*, **27**:269 – 293, (1987).

[69] F. C. Frank and J. H. van der Merwe. One-dimensional dislocations. I. static theory. *Proc. Roy. Soc. of Lond. A*, **198**:205 – 216, (1949).

[70] M. J. Rice, A. R. Bishop, J. A. Krumhansl, and S. E. Trullinger. Weakly pinned Fröhlich charge-density-wave condensates: a new, nonlinear, current-carrying elementary excitation. *Phys. Rev. Lett.*, **36**:432 – 435, (1976).

[71] E. Abdalla, B. Maroufi, B. C. Melgar, and M. B. Sedra. Information transport by sine-Gordon solitons in microtubules. *Physica A*, **301**:169 – 173, (2001).

[72] S. L. McCall and E. L. Hahn. Self-induced transparency. *Phys. Rev.*, **183**:457 – 485, (1969).

[73] J. L. Shohet, B. R. Barmish, H. K. Ebraheem, and A. C. Scott. The sine-Gordon equation in reversed-field pinch experiments. *Phys. Plasmas*, **11**:3877 – 3887, (2004).

[74] M. J. Ablowitz, D. J. Kaup, A. C. Newell, and H. Segur. Method for solving the sine-Gordon equation. *Phys. Rev. Lett.*, **30**:1262–1264, (1973).

[75] B. Batiha, M.S.M. Noorani, and I. Hashim. Numerical solution of sine-Gordon equation by variational iteration method. *Phys. Lett. A*, **370**:437 – 440, (2007).

[76] Y. Ugur. Homotopy analysis method for the sine-Gordon equation with initial conditions. *Appl. Math. Comput*, **203**:387 – 395, (2008).

[77] A.C. Scott, F.Y.F. Chu, and D.W. McLaughlin. The soliton: A new concept in applied science. *Proc. of the IEEE*, **61**:1443–1483, (1973).

[78] L. Munteanu and S. Donescu. *Introduction to soliton theory: applications to mechanics*. Kluwer Academic Publishers, (2004).

[79] A.C. Newell. *Solitons in mathematics and physics*. SIAM, (1985).

[80] T. Dauxois and M. Peyrard. *Physics Of Solitons*. Cambridge University Press, (2006).

[81] J. ScottRussell. Report on waves, rep. fourteenth meeting of the British Association for the advancement of science. *John Murray, London*, :311–390, (1844).

[82] D. J. Korteweg and G. de Vries. On the change of form of long waves advancing in a rectangular canal, and on a new type of long stationary waves. *Philosophical Magazine*, **39**:422–443, (1895).

[83] R. Hirota. Exact solution of the korteweg–de vries equation for multiple collisions of solitons. *Phys. Rev. Lett.*, **27**, (1971).

[84] N. J. Zabusky and M. D. Kruskal. Interaction of "solitons" in a collisionless plasma and the recurrence of initial states. *Phys. Rev. Lett.*, **15**:240–243, (1965).

[85] C. S. Gardner, J. M. Greene, M. D. Kruskal, and R. M. Miura. Method for solving the korteweg-devries equation. *Phys. Rev. Lett.*, **19**:1095–1097, (1967).

[86] N. Grønbech-Jensen and Yu. S. Kivshar. Inverted kinks in ac driven damped sine-Gordon chains. *Phys. Lett. A*, **171**:338 – 343, (1992).

[87] B. A. Malomed. Emission from, WKB quantization, and stochastic decay of sine-Gordon solitons in external fields. *Phys. Lett. A*, **120**:28–38, (1987).

[88] B. A. Malomed. Decay of shrinking solitons in multidimensional sine-Gordon equation. *Physica D*, **24**:155 – 171, (1987).

[89] A. V. Ustinov. Solitons in Josephson junctions. *Physica D*, **123**:315 – 329, (1998).

[90] L. Debnath. *Nonlinear partial differential equations for scientists and engineers*. Birkhäuser, (1997).

[91] C. Rogers and W. K. Schief. *Bäcklund and Darboux Transformations: Geometry and Modern Applications in Soliton Theory*. Cambridge University Press, (2002).

[92] P. G. Drazin and R. S. Johnson. *Solitons: An introduction*. Cambridge University Press, (1993).

[93] J.K. Perring and T.H.R. Skyrme. A model unified field equation. *Nuclear Phys.*, **31**:550 – 555, (1962).

[94] N. N. Akhmediev, V. M. Eleonskii, and N. E. Kulagin. Exact first-order solutions of the nonlinear schrödinger equation. *Theor. Math. Phys.*, **72**:809 – 818, (1987).

[95] J. Miles. Directly forced oscillations of an inverted pendulum. *Phys. Lett. A*, **133**: 295 – 297, (1988).

[96] N. Krylov and N. Bogoliubov. The application of methods of nonlinear mechanics to the theory of stationary socillatons. *Publ. 8, Ukranian Acad. Sci. Kiev*, (1934).

[97] M. Lakrib. Time averaging for functional differential equations. *J. Appl. Math.*, **2003**:1 – 16, (2003).

[98] C. Robinson. *Second-Order Averaging of Forced and Coupled Nonlinear Oscillators*. IEEE Trans. Circuits Sys. CAS-**30**, (1983).

[99] I. V. Barashenkov and O. F. Oxtoby. Wobbling kinks in ϕ^4 theory. *Phys. Rev. E*, **80**: 026608, (2009).

[100] O. F. Oxtoby and I. V. Barashenkov. Resonantly driven wobbling kinks. *Phys. Rev. E*, **80**:026609, (2009).

[101] A. Ali, H. Susanto, and J. A. D. Wattis. Breathing modes of long Josephson junctions with phase-shifts. *SIAM J. Appl. Math.*, **71**:242–269, (2011).

[102] A. Seeger, H. Donth, and A. Kochendörfer. Theorie der versetzungen in eindimensionalen atomreihen. *Zeitschrift für Physik A Hadrons and Nuclei*, **134**:173–193, (1953).

[103] N. Grønbech-Jensen, M. G. Castellano, F. Chiarello, M. Cirillo, C. Cosmelli, L. V. Filippenko, R. Russo, and G. Torrioli. Microwave-induced thermal escape in Josephson junctions. *Phys. Rev. Lett.*, **93**:107002, (2004).

[104] N. Grønbech-Jensen and M. Cirillo. ac-induced thermal vortex escape in magnetic-field-embedded long annular Josephson junctions. *Phys. Rev. B*, **70**: 214507, (2004).

[105] S. Guozhu, W. Yiwen, C. Junyu, C. Jian, J. Zhengming, K. Lin, X. Weiwei, Y. Yang, H. Siyuan, and W. Peiheng. Microwave-induced phase escape in a Josephson tunnel junction. *Phys. Rev. B*, **77**:104531, (2008).

[106] S. M. Frolov, M. J .A. Stoutimore, T. A. Crane, D. J. Van Harlingen, V. A. Oboznov, V. V. Ryazanov, A. Ruosi, C. Granata, and M. Russo. Imaging spontaneous currents in superconducting arrays of π-junctions. *Nature Phys.*, **4**:32 – 36, (2008).

[107] H. Segur. Wobbling kinks in ϕ^4 and sine-Gordon theory. *J. Math. Phys.*, **24**:1439, (1983).

[108] G. Kälbermann. The sine-Gordon wobble. *J. Phys. A*, **37**:11603, (2004).

[109] L. A. Ferreira, Bernard Piette, and Wojtek J. Zakrzewski. Wobbles and other kink-breather solutions of the sine-Gordon model. *Phys. Rev. E*, **77**:036613, (2008).

[110] P. G. Kevrekidis and M. I. Weinstein. Dynamics of lattice kinks. *Physica D*, **142**: 113 – 152, 2000.

[111] A. Dewes, T. Gaber, D. Koelle, R. Kleiner, and E. Goldobin. Semifluxon molecule under control. *Phys. Rev. Lett.*, **101**:247001, (2008).

[112] J. A. Boschker. Manipulation and on-chip readout of fractional flux quanta. *Master thesis, University of Twente*, (2006).

[113] E. Goldobin, A. Sterck, T. Gaber, D. Koelle, and R. Kleiner. Dynamics of semifluxons in Nb long Josephson $0 - \pi$ junctions. *Phys. Rev. Lett.*, **92**:057005, (2004).

[114] E. Goldobin, A. M. Klushin, M. Siegel, and N. Klein. Long Josephson junction embedded into a planar resonator at microwave frequencies: Numerical simulation of fluxon dynamics. *J. Appl. Phys.*, **92**:3239 – 3250, (2002).

[115] F. L. Barkov, M. V. Fistul, and A. V. Ustinov. Microwave-induced flow of vortices in long Josephson junctions. *Phys. Rev. B*, **70**:134515, (2004).

[116] D. Bambusi and S. Cuccagna. On dispersion of small energy solutions of the nonlinear Klein–Gordon equation with a potential. *Amer. J. Math.*, **133**:1421–1468, (2011).

[117] S. Shapiro, A. R. Janus, and S. Holly. Effect of microwaves on Josephson currents in superconducting tunneling. *Rev. Mod. Phys.*, **36**:223–225, (1964).

[118] N.R. Quintero and A. Sánchez. AC driven sine-Gordon solitons: dynamics and stability. *Eur. Phys J. B*, **6**:133–142, (1998).

[119] S. Flach, Y. Zolotaryuk, A. E. Miroshnichenko, and M. V. Fistul. Broken symmetries and directed collective energy transport in spatially extended systems. *Phys. Rev. Lett.*, **88**:184101, (2002).

[120] E. Goldobin, B. A. Malomed, and A. V. Ustinov. Progressive motion of an ac-driven kink in an annular damped system. *Phys. Rev. E*, **65**:056613, (2002).

[121] A. V. Ustinov, C. Coqui, A. Kemp, Y. Zolotaryuk, and M. Salerno. Ratchet–like dynamics of fluxons in annular Josephson junctions driven by biharmonic microwave fields. *Phys. Rev. Lett.*, **93**:087001, (2004).

[122] V. Zharnitsky, I. Mitkov, and N. Grønbech-Jensen. π kinks in strongly ac driven sine-Gordon systems. *Phys. Rev. E*, **58**:R52–R55, (1998).

[123] A. P. Itin. Comment on "π kinks in strongly ac driven sine-Gordon systems". *Phys. Rev. E*, **63**:028601, (2001).

[124] J. Pfeiffer, M. Kemmler, D. Koelle, R. Kleiner, E. Goldobin, M. Weides, A. K. Feofanov, J. Lisenfeld, and A. V. Ustinov. Static and dynamic properties of 0, π, and $0-\pi$ ferromagnetic Josephson tunnel junctions. *Phys. Rev. B*, **77**:214506, (2008).

[125] M. Moshe and R. G. Mints. Shapiro steps in Josephson junctions with alternating critical current density. *Phys. Rev. B*, **76**:054518, (2007).

[126] O. Vávra, S. Gaži, D. S. Golubović, I. Vávra, J. Dérer, J. Verbeeck, G. Van Tendeloo, and V. V. Moshchalkov. 0 and π phase Josephson coupling through an insulating barrier with magnetic impurities. *Phys. Rev. B*, **74**:020502, (2006).

[127] T. Golod, A. Rydh, and V. M. Krasnov. Detection of the phase shift from a single Abrikosov vortex. *Phys. Rev. Lett.*, 104:227003, (2010).

[128] V. V. Ryazanov, V. A. Oboznov, A. Yu. Rusanov, A. V. Veretennikov, A. A. Golubov, and J. Aarts. Coupling of two superconductors through a ferromagnet: evidence for a π junction. *Phys. Rev. Lett.*, **86**:2427–2430, (2001).

[129] J. J. A. Baselmans, A. F. Morpurgo, B. J. Van Wees, and T. M. Klapwijk. Reversing the direction of the supercurrent in a controllable Josephson junction. *Nature*, **397**:43 – 45, (1999).

[130] A. Gumann, C. Iniotakis, and N. Schopohl. Geometric π Josephson junction in d-wave superconducting thin films. *Appl. Phys. Lett.*, **91**:192502, (2007).

[131] C. Nappi, E. Sarnelli, M. Adamo, and M. A. Navacerrada. Fiske modes in $0 - \pi$ Josephson junctions. *Phys. Rev. B*, **74**:144504, (2006).

[132] B. A. Malomed and A. V. Ustinov. Creation of classical and quantum fluxons by a current dipole in a long Josephson junction. *Phys. Rev. B*, **69**:064502, (2004).

[133] E. Goldobin, N. Stefanakis, D. Koelle, and R. Kleiner. Fluxon-semifluxon interaction in an annular long Josephson $0 - \pi$ junction. *Phys. Rev. B*, **70**:094520, (2004).

[134] Yu. S. Kivshar, N. Grønbech-Jensen, and R. D. Parmentier. Kinks in the presence of rapidly varying perturbations. *Phys. Rev. E*, **49**:4542 – 4551, (1994).

[135] Yu. S. Kivshar and K. H. Spatschek. Nonlinear dynamics and solitons in the presence of rapidly varying periodic perturbations. *Chaos, Solitons & Fractals*, **5**: 2551–2569, (1995).

[136] L.D. Landau and E.M. Lifshitz. *Mechanics*. Pergamon Press, Oxford, (1976).

[137] V.I. Arnol'd and M. Levi. *Geometrical Methods in the Theory of Ordinary Differential Equations*. Springer-Verlag New York, (1988).

[138] A. B. Kuklov, V. S. Boyko, and J. Malinsky. Instability in the current-biased 0-π Josephson junction. *Phys. Rev. B*, **51**:11965–11968, (1995).

[139] H. Susanto, S. A. van Gils, T. P. P. Visser, Ariando, H. J. H. Smilde, and H. Hilgenkamp. Static semifluxons in a long Josephson junction with π-discontinuity points. *Phys. Rev. B*, **68**:104501, (2003).

[140] B.D. Josephson. Possible new effects in superconductive tunnelling. *Phys. Lett.*, **1**:251 – 253, (1962).

[141] P. W. Anderson and J. M. Rowell. Probable observation of the Josephson superconducting tunneling effect. *Phys. Rev. Lett.*, **10**:230–232, (1963).

[142] G. Hechtfischer, R. Kleiner, A. V. Ustinov, and P. Müller. Non-Josephson emission from intrinsic junctions in $Bi_2Sr_2CaCu_2O_{8+y}$: Cherenkov radiation by Josephson vortices. *Phys. Rev. Lett.*, **79**:1365–1368, (1997).

[143] D. Ananikian and T. Bergeman. Gross-pitaevskii equation for Bose particles in a double-well potential: Two-mode models and beyond. *Phys. Rev. A*, **73**:013604, (2006).

[144] E. A. Ostrovskaya, Y. S. Kivshar, M. Lisak, B. Hall, F. Cattani, and D. Anderson. Coupled-mode theory for Bose-Einstein condensates. *Phys. Rev. A*, **61**:031601, (2000).

[145] A. Smerzi, S. Fantoni, S. Giovanazzi, and S. R. Shenoy. Quantum coherent atomic tunneling between two trapped Bose-Einstein condensates. *Phys. Rev. Lett.*, **79**: 4950–4953, (1997).

[146] H. Susanto and G. Derks. Localized mode interactions in $0 - \pi - 0$ Josephson junctions. *Phys. Rev. B*, **82**:132301, (2010).

[147] P. D. Shaju and V. C. Kuriakose. Double-well potential in annular Josephson junction. *Phys. Lett. A*, **332**:326 – 332, (2004).

[148] H. Susanto, J. Cuevas, and P. Krüger. Josephson tunnelling of dark solitons in a double-well potential. *J. Phys. B*, **44**:095003, (2011).

[149] A. Soffer and M.I. Weinstein. Time dependent resonance theory. *Geom. Funct. Anal.*, **8**:1086–1128, (1998).

[150] A. Soffer and M. I. Weinstein. Selection of the ground state for nonlinear Schrödinger equations. *Rev. Math. Phys.*, **16**:977–1071, (2004).

[151] A. Soffer and M. I. Weinstein. Resonances, radiation damping and instability in Hamiltonian nonlinear wave equations. *Invent. Math.*, **136**:9 – 74, (1999).

[152] I. M. Sigal. Non-linear wave and Schrödinger equations. *Commun. Math. Phys.*, **153**:297–320, (1993).

[153] A. Soffer and M. I. Weinstein. Multichannel nonlinear scattering for nonintegrable equations. *Commun. Math. Phys.*, **133**:119 – 146, (1990).

[154] A. Soffer and M. I. Weinstein. Multichannel nonlinear scattering for nonintegrable equations II. the case of anisotropic potentials and data. *J. Diff. Eq.*, **98**:376 – 390, (1992).

[155] D. W. McLaughlin and A.C. Scott. Perturbation analysis of fluxon dynamics. *Phys. Rev. A*, **18**:1652, (1978).

[156] I. Stakgold. *Green's Functions and Boundary Value Problems*. Wiley, New York, (1979).

[157] R. Kleiner, F. Steinmeyer, G. Kunkel, and P. Müller. Intrinsic Josephson effects in $Bi_2Sr_2CaCu_2O_8$ single crystals. *Phys. Rev. Lett.*, **68**:2394–2397, (1992).

[158] R. Kleiner, T. Gaber, and G. Hechtfischer. Stacked long Josephson junctions in zero magnetic field: A numerical study of coupled one-dimensional sine-Gordon equations. *Phys. Rev. B*, **62**:4086–4095, (2000).

[159] H. B. Wang, P. H. Wu, and T. Yamashita. Terahertz responses of intrinsic Josephson junctions in high T_C superconductors. *Phys. Rev. Lett.*, **87**:107002, (2001).

[160] S. O. Katterwe, A. Rydh, H. Motzkau, A. B. Kulakov, and V. M. Krasnov. Superluminal geometrical resonances observed in $Bi_2Sr_2CaCu_2O_{8+x}$ intrinsic Josephson junctions. *Phys. Rev. B*, **82**:024517, (2010).

[161] A.V. Ustinov, H. Kohlstedt, and C. Heiden. Coherent flux-flow in vertically stacked long Josephson tunnel junctions. *IEEE Trans. Appl. Supercond.*, **5**:2743 – 2746, (1995).

[162] E. Goldobin, A. Wallraff, N. Thyssen, and A. V. Ustinov. Cherenkov radiation in coupled long Josephson junctions. *Phys. Rev. B*, **57**:130–133, (1998).

[163] R. Kleiner. Two-dimensional resonant modes in stacked Josephson junctions. *Phys. Rev. B*, **50**:6919–6922, (1994).

[164] V. P. Koshelets, S. V. Shitov, A. M. Baryshev, I. L. Lapitskaya, L. V. Filippenko, H. van de Stadt, J. Mees, H. Schaeffer, and T. de Graauw. Integrated sub-mm wave receivers. *IEEE Trans. on Appl. Supercon.*, **5**:3057 – 3060, (1995).

[165] V. P. Koshelets, S. V. Shitov, A. V. Shchukin, L. V. Filippenko, and J. Mygind. Linewidth of submillimeter wave flux-flow oscillators. *Appl. Phys. Lett.*, **69**:699–701, (1996).

[166] T. Nagatsuma, K. Enpuku, F. Irie, and K. Yoshida. Flux-flow type Josephson oscillator for millimeter and submillimeter wave region. *J. Appl. Phys.*, **54**:3302–3309, (1983).

[167] T. Nagatsuma, K. Enpuku, K. Yoshida, and F. Irie. Flux-flow-type Josephson oscillator for millimeter and submillimeter wave region. II. modeling. *J. Appl. Phys.*, **56**:3284–3293, (1984).

[168] S. Madsen, N.F. Pedersen, and N. Gronbech-Jensen. Long Josephson junction stack coupled to a cavity. *Appl. Supercond., IEEE Tran.*, **17**:926 –929, (2007).

[169] M. B. Mineev, G. S. Mkrtchyan, and V. V. Schmidt. On some effects in a system of two interacting Josephson junctions. *J. of Low Temp. Phys.*, **45**:497–505, (1981).

[170] S. Sakai, P. Bodin, and N. F. Pedersen. Fluxons in thin-film superconductor-insulator superlattices. *J. Appl. Phys.*, **73**:2411–2418, (1993).

[171] M. Braun, Yu. S. Kivshar, and A. M. Kosevichs. Interaction between kinks in coupled chains of adatoms. *J. Phys. C*, **21**:3881–3900, (1988).

[172] A. Zvezdin and V. Kostyuchenko. Nonlinear domain-wall dynamics in a system of two magnetic layers. *J. Exp. Theor. Phys.*, **89**:734–739, (1999).

[173] S. Sakai, A. V. Ustinov, H. Kohlstedt, A. Petraglia, and N. F. Pedersen. Theory and experiment on electromagnetic-wave-propagation velocities in stacked superconducting tunnel structures. *Phys. Rev. B*, **50**:12905–12914, (1994).

[174] V. M. Krasnov. In-plane fluxon in layered superconductors with arbitrary number of layers. *Phys. Rev. B*, **63**:064519, (2001).

[175] J. B. Hansen and P. E. Lindelof. Static and dynamic interactions between Josephson junctions. *Rev. Mod. Phys.*, **56**:431–459, (1984).

[176] G. Kunkel and R.H. Ono. Mutual phase-locking of ten $YBa_2Cu_3O_7$, step-edge Josephson junctions up to 45 K. *Appl. Phys. Letts.*, **69**:1960, (1996).

[177] D.W. Jillie, J.E. Lukens, Y.H. Kao, and G.J. Dolan. Observation of voltage locking and other interactions in coupled microbridge Josephson junctions. *Phys. Lett. A*, **55**:381 – 382, (1976).

[178] E. Goldobin, H. Kohlstedt, and A. V. Ustinov. Tunable phase locking of stacked Josephson flux-flow oscillators. *Appl. Phys. Lett.*, **68**:250–252, (1996).

[179] L. G. Neumann, Y. D. Dai, and Y. H. Kao. Critical current pulling and differential resistance of two coupled superconducting weak links. *J. Low Temp. Phys.*, **49**: 457–463, (1982).

[180] H.Q. Li, R.H. Ono, L.R. Vale, D.A. Rudman, and S.H. Liou. Interactions between bicrystal Josephson junctions in a multilayer structure. *Appl. Supercond., IEEE Trans.*, **9**:3417 –3420, (1999).

[181] Yu. S. Kivshar. On dynamics of soliton excitations in coupled chains. *J. Phys. Soc. Jpn*, **57**:4232–4241, (1988).

[182] N. Grønbech-Jensen, M. R. Samuelsen, P. S. Lomdahl, and J. A. Blackburn. Bunched soliton states in weakly coupled sine-Gordon systems. *Phys. Rev. B*, **42**:3976–3980, (1990).

[183] B. Dueholm, O. A. Levring, J. Mygind, N. F. Pedersen, O. H. Soerensen, and M. Cirillo. Multisoliton excitations in long Josephson junctions. *Phys. Rev. Lett.*, **46**:1299–1302, (1981).

[184] V. M. Krasnov. Radiative annihilation of a soliton and an antisoliton in the coupled sine-Gordon equation. *Phys. Rev. B*, **85**:134525, (2012).

[185] M. Peyrard and D. K. Campbell. Kink-antikink interactions in a modified sine-Gordon model. *Physica D: Nonlinear Phenomena*, **9**:33 – 51, (1983).

[186] N. R. Quintero, A. Sánchez, and F. G. Mertens. Anomalies of ac driven solitary waves with internal modes: Nonparametric resonances induced by parametric forces. *Phys. Rev. E*, **64**:046601, (2001).

[187] N.R. Quintero, A. Sánchez, and F.G. Mertens. Internal mode dynamics in driven nonlinear Klein-Gordon systems. *Eur. Phys. J. B*, **19**:107–115, (2001).

[188] N. R. Quintero, A. Sánchez, and F. G. Mertens. Anomalous resonance phenomena of solitary waves with internal modes. *Phys. Rev. Lett.*, **84**:871–874, (2000).

[189] R. Jackson and M. Weinstein. Geometric analysis of bifurcation and symmetry breaking in a Gross–Pitaevskii equation. *J. Stat. Phys.*, **116**:881–905, (2004).

[190] T. Kapitula and P. G. Kevrekidis. Bose-Einstein condensates in the presence of a magnetic trap and optical lattice: Two-mode approximation. *Nonlinearity*, **18**: 2491–2512, (2005).

[191] I. K. Yanson and I. M. Svistunov, V. M. abd Dmitrenko. Experimental observation of the tunnel effect for Cooper pairs with the emission of photons. *Soviet Phys. JETP*, **21**:650, (1965).

[192] D. N. Langenberg, D. J. Scalapino, B. N. Taylor, and R. E. Eck. Investigation of microwave radiation emitted by Josephson junctions. *Phys. Rev. Lett.*, **15**:842–842, (1965).

[193] A. H. Dayem and C. C. Grimes. Microwave emission from superconducting point-contacts. *Appl. Phys. Lett.*, **9**:47–49, (1966).

[194] T. Kapitula, P. Kevrekidis, and Z. Chen. Three is a crowd: Solitary waves in photorefractive media with three potential wells. *SIAM J. Appl. Dynam. Syst.*, **5**: 598–633, (2006).

[195] R. Franzosi and V. Penna. Chaotic behavior, collective modes, and self-trapping in the dynamics of three coupled Bose-Einstein condensates. *Phys. Rev. E*, **67**: 046227, (2003).

[196] P. Barbara, A. B. Cawthorne, S. V. Shitov, and C. J. Lobb. Stimulated emission and amplification in Josephson junction arrays. *Phys. Rev. Lett.*, **82**:1963–1966, (1999).

[197] J. A. Acebrón, L. L. Bonilla, C. J. P. Vicente, F. Ritort, and R. Spigler. The Kuramoto model: A simple paradigm for synchronization phenomena. *Rev. Mod. Phys.*, **77**: 137–185, (2005).

[198] G. Filatrella, N. F. Pedersen, and K. Wiesenfeld. High-Q cavity-induced synchronization in oscillator arrays. *Phys. Rev. E*, **61**:2513–2518, (2000).

[199] G. Filatrella, N. F. Pedersen, and K. Wiesenfeld. Generalized coupling in the Kuramoto model. *Phys. Rev. E*, **75**:017201, (2007).

[200] K. Wiesenfeld, P. Colet, and S. H. Strogatz. Synchronization transitions in a disordered Josephson series array. *Phys. Rev. Lett.*, **76**:404–407, (1996).

[201] M. Tsujimoto, K. Yamaki, K. Deguchi, T. Yamamoto, T. Kashiwagi, H. Minami, M. Tachiki, K. Kadowaki, and R. A. Klemm. Geometrical resonance conditions for thz radiation from the intrinsic Josephson junctions in $Bi_2Sr_2CaCu_2O_{8+\delta}$. *Phys. Rev. Lett.*, **105**:037005, (2010).

[202] H. B. Wang, S. Guénon, B. Gross, J. Yuan, Z. G. Jiang, Y. Y. Zhong, M. Grünzweig, A. Iishi, P. H. Wu, T. Hatano, D. Koelle, and R. Kleiner. Coherent terahertz emission of intrinsic Josephson junction stacks in the hot spot regime. *Phys. Rev. Lett.*, **105**:057002, (2010).

[203] M. Machida, T. Koyama, A. Tanaka, and M. Tachiki. Collective dynamics of Josephson vortices in intrinsic Josephson junctions: exploration of in-phase locked superradiant vortex flow states. *Physica C: Superconductivity*, **330**:85 – 93, (2000).

[204] M. Tachiki, M. Iizuka, K. Minami, S. Tejima, and H. Nakamura. Emission of continuous coherent terahertz waves with tunable frequency by intrinsic Josephson junctions. *Phys. Rev. B*, **71**:134515, (2005).

[205] S. Lin and X. Hu. Possible dynamic states in inductively coupled intrinsic Josephson junctions of layered high-T_c superconductors. *Phys. Rev. Lett.*, **100**:247006, (2008).

[206] A. E. Koshelev. Alternating dynamic state self-generated by internal resonance in stacks of intrinsic Josephson junctions. *Phys. Rev. B*, **78**:174509, (2008).

[207] T. Koyama, H. Matsumoto, M. Machida, and K. Kadowaki. In-phase electrodynamics and terahertz wave emission in extended intrinsic Josephson junctions. *Phys. Rev. B*, **79**:104522, (2009).